FACETS

Mathematical aspects of single neuron models

Report Version:

Report Preparation:

Classification:

Contract Start Date: 01/09/2005   Duration: 4 Years

Project Co-ordinator: Karlheinz Meier (Heidelberg)

Partners: U Bordeaux, CNRS (Gif-sur-Yvette, Marseille), U Debrecen, TU Dresden, U Freiburg, TU Graz, U Heidelberg, EPFL Lausanne, Funetics S.a.r.l., U London, U Plymouth, IN-RIA, KTH Stockholm

Jonathan Touboul   Romain Brette   Olivier Faugeras

DELIVERABLE SUMMARY SHEET

Project Number: FP6-2004-IST-FETPI 15879

Project Acronym: FACETS

Title: Fast Analog Computing with Emergent Transient States

Deliverable N^o: D4-5

Due date: 2009/02/28

Delivery Date: 2009/05/20

Short Description:

This report is dedicated to the study of nonlinear bidimensional neuron models, which from a mathematical point of view are hybrid dynamical systems, i.e. whose dynamics is defined by a continuous-time dynamical system modelling the subthreshold behavior of the neuron, coupled with a discrete dynamical system corresponding the spike emission. We first provide an introduction to the various models of neurons that have been studied, in particular within the FACETS project, in chapter 1. The subthreshold dynamics is studied in chapter 2, the spike dynamics related with the discrete dynamical system in chapter 3 and all these results are reviewed in chapter 4 in which we provide an electrophysiological-class description of the model, i.e. a partition of the parameter space corresponding to different neurological behaviors. This report is part of the thesis of Jonathan Touboul (113).

Partner owning: All

Partners contributed: INRIA

Made available to: All

Contents

List of Figures

1

PRINCIPLES OF NEURAL SCIENCE AND MODELING BASICS

OVERVIEW

Neural science is undoubtedly a fascinating field of research. It is aimed to understand the nervous system, and in particular the brain and the spinal cord that govern the way we perceive, move, think, remember, learn, speak and feel. It processes sensory inputs and recognizes danger, good food, identify potential mates. It controls movements, the voluntary ones (via the motor cortex, the cerebellum, and the basal ganglia) as well as the involuntary ones (nuclei in the brain stem control many involuntary muscle functions such as heart rate and breathing). Evidence strongly suggests that developed brains derive consciousness from the complex interactions between numerous systems within the brain. Almost[1] every animal have either a centralized brain, collections of individual ganglia playing the role of distributed brains or a diffuse nervous system. In this chapter we very roughly introduce several elementary notions of neural science and present the basic function of neurons from a biological and electrophysiological viewpoints. Modeling these processes in order to understand their origin and nature in order to reproduce them efficiently and accurately are the main motivation of the present dissertation.

After describing very briefly the brain and its basic organization, we will be interested in the main cells involved in the brain's information processing: the nerve cells, or neurons. We will describe these cells anatomically, explain its function from a biophysical point of view, characterize the signal they produce and convey, and discuss the electrophysiological basis of these processes. Based on these observations, we will introduce what we will call detailed neuron models, mainly based on a precise description of each process involved in the nerve signal generation. We will then turn to a more functional description of the nerve cells, and introduce classical phenomenological model.

The aim of this chapter is clearly not to give a comprehensive introduction to such a complex structure as the brain, nor of such a passionating field as neurobiology, but to provide the reader with the basic concepts we will deal with in the rest of this document. The presentation of the biological background will be therefore highly simplistic, selective and lacunar, but I believe it provides the reader with the minimum of information necessary to appreciate the biological discussions of the theoretical work presented in this dissertation. For more details on the fundamental principles of neural science from a biological point of view, we refer the interested reader to the excellent book of Kandel, Schwartz and Jessell (72) where we got the main information developed here. The reader interested in neuronal modeling is referred to the great books of Koch and colleagues (76; 77), Peter Dayan and Larry Abbott (27). The reader interested in ionic exchanges in play in the nerve cell to the very interesting book of Bertil Hille (51). A review of different neuron models viewed as dynamical systems can be found in the excellent book of Izhikevich (65), and phenomenological models of spiking neurons are discussed in depth in (43).

---

[1]Some animals, such as cnidarians and echinoderms do not have a centralized brain, but present instead a decentralized nervous system. Very few primitive animals such as the poriferans (sponge) lack nervous system entirely.

1.1 BRAIN

1.1.1 General overview

The brain is an unresting assembly of cells that continually receives information, elaborates and perceives it, and makes decision. It is a very complex system. It is composed of an immense number of different cells. Among these cells, the nerve cells, or neurons, are the elementary processing units. Neurons are electrically excitable cells that process and transmit information. There are roughly 100 billion neurons for the human brain ($\approx 10^{11}$ cell bodies), that can be of different types (about forty types of neurons have been identified through the cortex, thousands according to (72)). Besides neurons, the brain is also composed of "supporter" cells, so-called glial (or neuroglial) cells. These cells are divided according to anatomical criteria into (1) neuroglial cells in the brain, further subdivided into oligodentrocytes and astrocytes, and (2) Schwann cells, or neurolemmocytes, in the periphery. Neuroglial cells make up almost one half the volume of the brain and outnumber neurons by about 10 to 1. They play an essential role in the brain function: they provide nutrition and energy, maintain homeostasis (regulates their internal environment), form myelin (electrically-insulating dielectric phospholipid layer that surrounds only the axons of some neurons), participate in signal transmission, ensures structural stabilization of brain tissues, destroy pathogens and remove dead neurons. For years, specialists considered that these cells were not involved in information processing, and this vision seems to be contradicted by some recent studies[2]. The study of these cells and of their influence in the signal processing would be very interesting, but in this dissertation we will concentrate on neuronal cells.

The huge number of nerve cells in the brain is interconnected in a very intricate fashion. In the human brain for instance each neuron is typically connected to 10^4 other. All these cell bodies and connections are packed into a very dense and complex network. To get a grasp of the complexity of the network, in a cubic millimeter of human brain there are more than 10^4 cell bodies and several kilometers of wires. And the high level of structuring of the cerebral cortex makes this system even more complex.

1.1.2 Basic organization of the cerebral cortex

The cortex, superficial part of the encephalon, is mainly composed of grey matter formed by neurons and their unmyelinated fibers. The white matter below the grey matter of the cortex is formed predominantly by myelinated axons interconnecting different regions of the central nervous system. First of all, it has been proved that the grey matter has an horizontal organization in layers (*laminae*) composed of different cell types (see figure 1.1). The number of layers, their cell composition, their thickness and organization are not the same over the whole surface of the cortex. These differences led neuroanatomists to divide the cortex into small regions called *areas* (figure 1.2) where those characteristics are homogeneous and that correspond to different functions, e.g., vision or motion. Generally speaking, most of the cortex is made up of six layers of neurons, from layer I at the surface of the cortex to layer VI, deeper, that lies close of the white matter. For humans, its thickness varies from 3 to 6 mm.

More detailed information about cortical structure and function can be found in (46; 70; 72; 99). The organization of the cortex is not only laminar. It has been observed that neurons tend to be strongly connected in columnar structures perpendicular to the surface of the cortex responding to precise stimulations and having similar activities, called *cortical column*. Several studies provided biological evidence of such small aggregates of about one hundred neurons, 20 up to 50 μm wide, called minicolumns (see e.g. (19; 94)). Larger columnar structures of 300 to 500 μm of diameter displaying similar activities (*macrocolumns*) were studied by Mountcastle in (93).

Let us now zoom further into the brain and describe individual nerve cells.

1.2 NEURONS

The information processing in the brain is mainly accomplished through the nerve cells and the connections between them. The neuron's place as the primary functional unit of the nervous system was first recognized in the late 19th century through the work of the Spanish histologist Santiágo Ramon y Cajal. He

---

[2] Recent studies tend to prove that astrocytes glial cells interact with neurons and affect their ability to communicate with each other. This suggests that they may influence the information processing. For instance Newman in (97) showed that activated glial cells (i.e. excited by focal injections of certain chemical substances) can inhibit neurons by releasing ATP. He proves for instance in the rat retina using this technique a subsequent reduction of the firing rate of those neurons that displayed spontaneous spike activity.
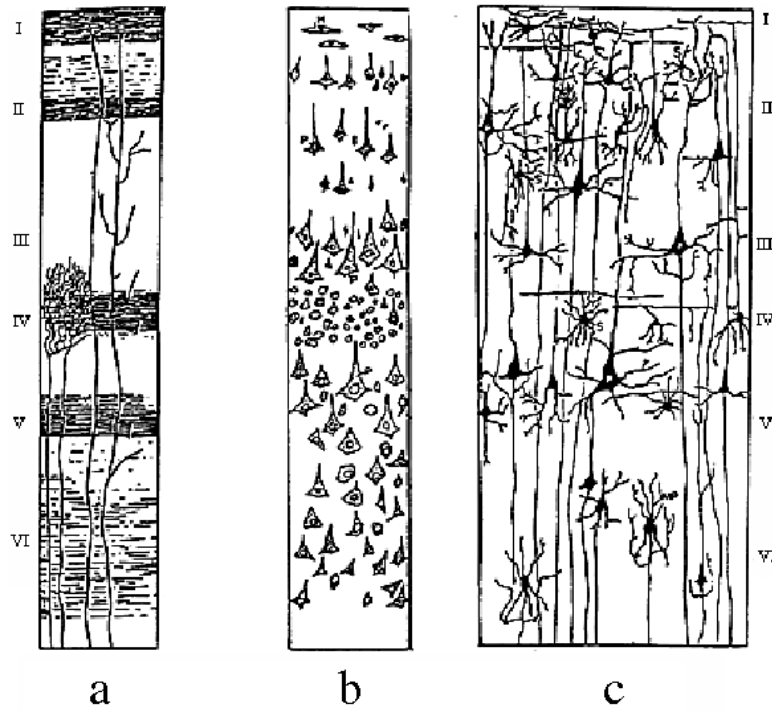
Figure 1.1. Layer organization of the cortex (a) Weigert's coloration shows myelinated fibers (axons) and so the connections inside and between layers, (b) Nissl's coloration only reveals cell bodies (c) Golgi's coloration shows the whole cells (From (98)).
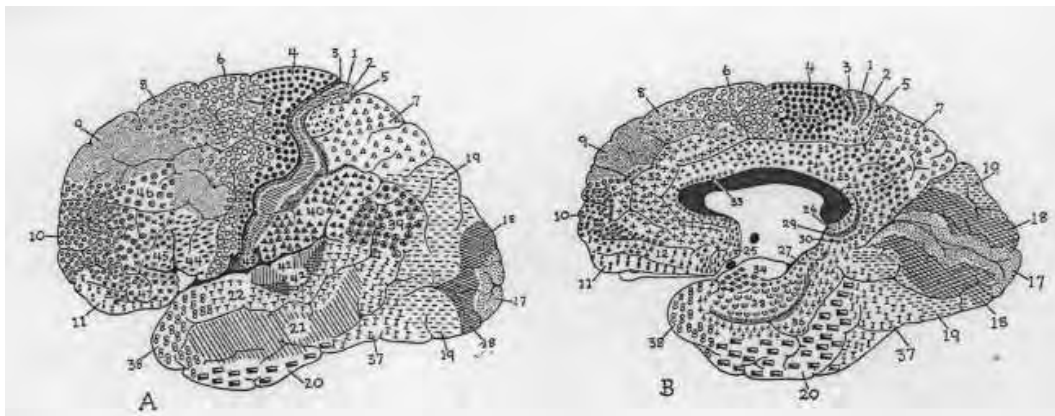
Figure 1.2. In 1909, Brodmann (14) divided the cortex into 52 cytoarchitectonic areas according to the thickness of the cortical layers. For example, layer IV is very thin in the primary motor cortex (area 4) while it is very thick in the primary visual cortex (area 17).

Figure 1.3. The giant axons of the European squid (Loligo vulgaris) were crucial for scientists to understand the action potential (picture: Hans Hillewaert)

proposed that neurons were discrete cells acting as metabolically distinct units communicating via specialized circuits and junctions. This vision, known as the neuron doctrine, is one of the central dogma of modern neuroscience. He was the first to provide a suitable description of the structure nerve cells (101; 102), using Golgi's silver staining method. He showed that all nerve cells share the same basic architecture. Hence the complexity of the brain function depends less on the specialization individual neurons and more on the fact that a great number of these cells form precise and intricate anatomical circuits. The main electrophysiological features of the neurons were obtained by the pioneering works of Hodgkin and Huxley at the same period.

Substantial early knowledge of neuron electrical activity came from experiments on the squid's (see his photo figure 1.3) giant axons. As they are much larger than human neurons, but similar in nature, it was easier to study them with the technology of the first half of the twentieth century. This poor squid suffered pressure, stretch, injections of chemical substances and electrocutions, to record its axon's electrical activity by inserting electrodes into it. The accurate measurements obtained opened the way to the current neural science theory. I solemnly acknowledge the squid 1.3 here for being, to my point of view, a science hero.

1.2.1 Anatomical overview

A typical neuron has four morphologically defined regions: the cell body, dendrites, the axon, and presynaptic terminals. Each of these regions has a distinct role in the communication or generation of signals (see figure 1.4). The cell body (*soma*) is the metabolic center of the cell. It contains the nucleus which stores the genetic information of the cell as well as the endoplasmic reticulum and the whole metabolic apparel for the cell's proteins synthesis. The nucleus ranges from 3 to 18 micrometers in diameter.

The cell body is connected to other nerve cells via cellular extensions called *dendrites*. Dendrites branch out in a tree-like fashion. It is where the majority of input to the neuron occurs. In some few cases, information outflow from dendrites to other neurons can also occur[3].

The information communicated by the nerve cell to other neurons is transmitted by a long tubular structure called the *axon*. An axon can transmit electric signals along distances ranging from 0.1mm to meters. It is a thin structure compared with the cell body. Most neurons have only one axon, but this axon may - and usually will - undergo extensive branching, enabling communication with many target cells. The part of the axon where it emerges from the soma is called the *axon hillock*. Besides being an anatomical structure, the axon hillock is also the part of the neuron that has the greatest density of voltage-dependent sodium channels (see below). This makes it the most easily excited part of the neuron.

Near its ends, the axon divides into branches forming communication sites with other neurons. This structure is referred as the *axon (or presynaptic) terminal*. It contains the *synapses* (see section 1.2.6), specialized structures where neurotransmitter chemicals are released in order to communicate with target neurons. The signal is emitted from the *presynaptic cell* and received by the *postsynaptic cell*. The presynaptic cell transmits signals from the swollen end of its axon. Two communicating cells are generally not in contact anatomically. The small space between these cells is named the *synaptic cleft*. Most presynaptic terminals end on a postsynaptic neuron's dendrite, but terminals may also end on the soma or less often on the axon of the postsynaptic cell.

---

[3]This transmission cannot be held via chemical synapses: there, the backflow of a nerve impulse is impossible since an axon does not possess chemoreceptors and dendrites cannot secrete neurotransmitter chemicals. This unidirectionality of a chemical synapse explains why nerve impulses are conducted only in one direction.
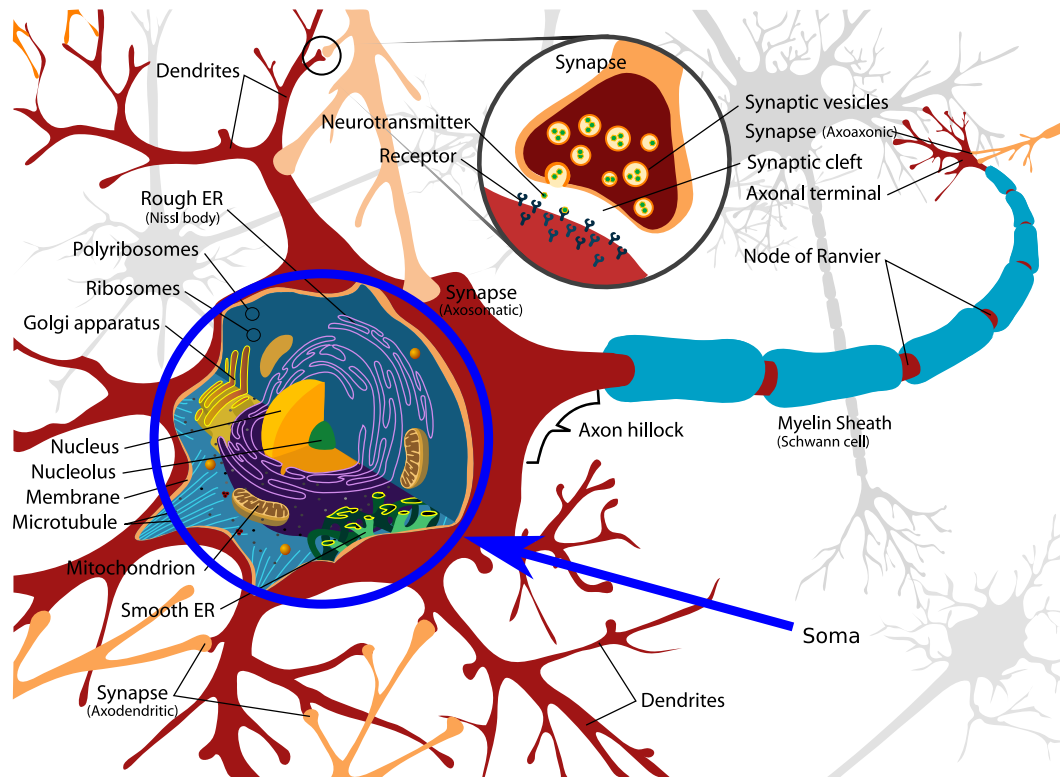
Figure 1.4. Diagram of a typical nerve cell (image: Mariana Ruiz Villarreal, Wikipedia)

Like other cells, neurons are composed and surrounded of a huge number and variety of ions and molecules. A typical cubic micron of cytoplasm might contain, for example, 10^{10} water molecules, 10^8 ions, 10^7 small molecules like amino acids and nucleotides, and 10^5 proteins. Many of these molecules carry charges, either positive or negative. Most of the time there is an excess concentration of negative charge inside the neurons. The nerve cell's membrane is mainly composed of a lipid bilayer 3 to 4 nm thick essentially impermeable to most charged molecules. This bilayer is spanned by highly specialized proteins called *ion channels* (see figure 1.5). These ion channels recognize and select specific ions and conduct them through the membrane. They can be open or closed in response to specific electrical, mechanical or chemical signals. They conduct ions very fast (up to 10^8 ions per second in a single channel) in a very selective way: each type of ion channel allows only one[4] type of ions to pass. Many channels are regulated (or *gated*); they open and close in response to different stimuli: changes in the voltage (*voltage-gated channels*), presence of a chemical transmitter (*ligand-gated channel*) and pressure or stretch (*mechanically gated channels*). Non-gated channels also exist, and are called *resting channels*. The gates can either *activate* (open) or inactivate (close) the channels (see figure 1.6). For a precise description of the structure and function of the ionic channels, we refer to (72, Chapter 6).

1.2.2 The zoo of neurons

Though nerve cell have the same overall organization, many types of nerve cells can distinguished. Eric Kandel in (72, Chapter 2) speaks of at least a thousand of different cells types. Nerve cells can be classified according to different criteria. The first classification that can be performed is a structural classification. More precisely, most of neurons can be characterized by their *polarity* (see figure 1.7). They can be one of three main types:

- *Unipolar or pseudounipolar* when the dendrite and axon emerge from same process.

- *Bipolar* when the axon and a single dendrite emerge on opposite ends of the soma.

- *Multipolar* when it has more than two dendrites. In the multipolar cells there exists a further subdivision in function of the length of the synaptic projections. Neurons with long-projecting axonal processes

---

[4]in some rare case few species are selected.
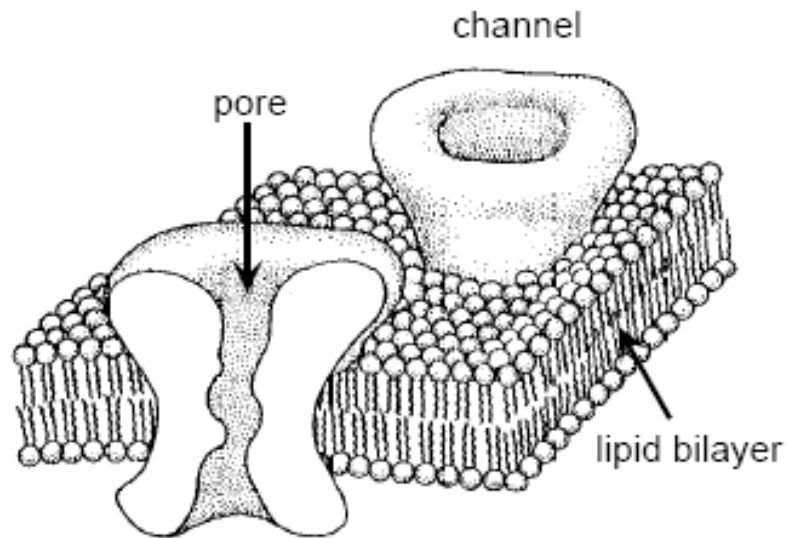
Figure 1.5. Schematic diagram of a section of the nerve cell's membrane with two ion channels embedded in it. The membrane is 3 to 4 nm thick and the ion channels are about 10 nm long. (Adapted in (27) from (51)).
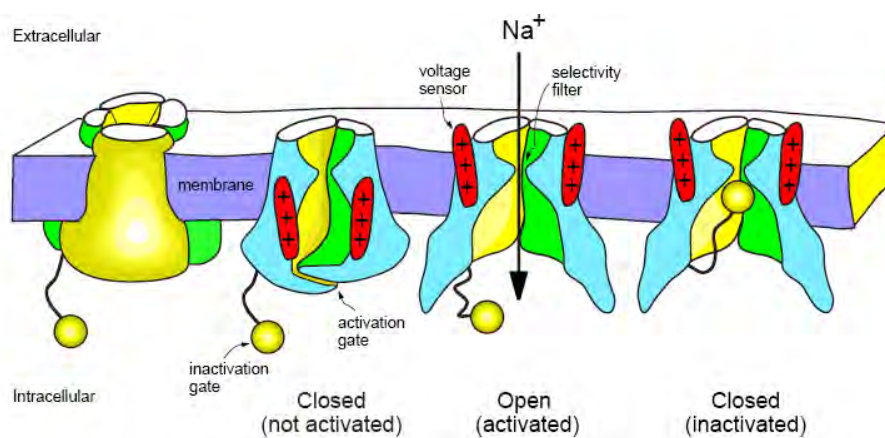
Figure 1.6. Structure of voltage-gated ion channels: voltage sensors open an activation gate and allow selected ions to flow through the channel according to their electrochemical gradients. The inactivation gate blocks the channel. (Taken from (65) where it was modified from (7).)
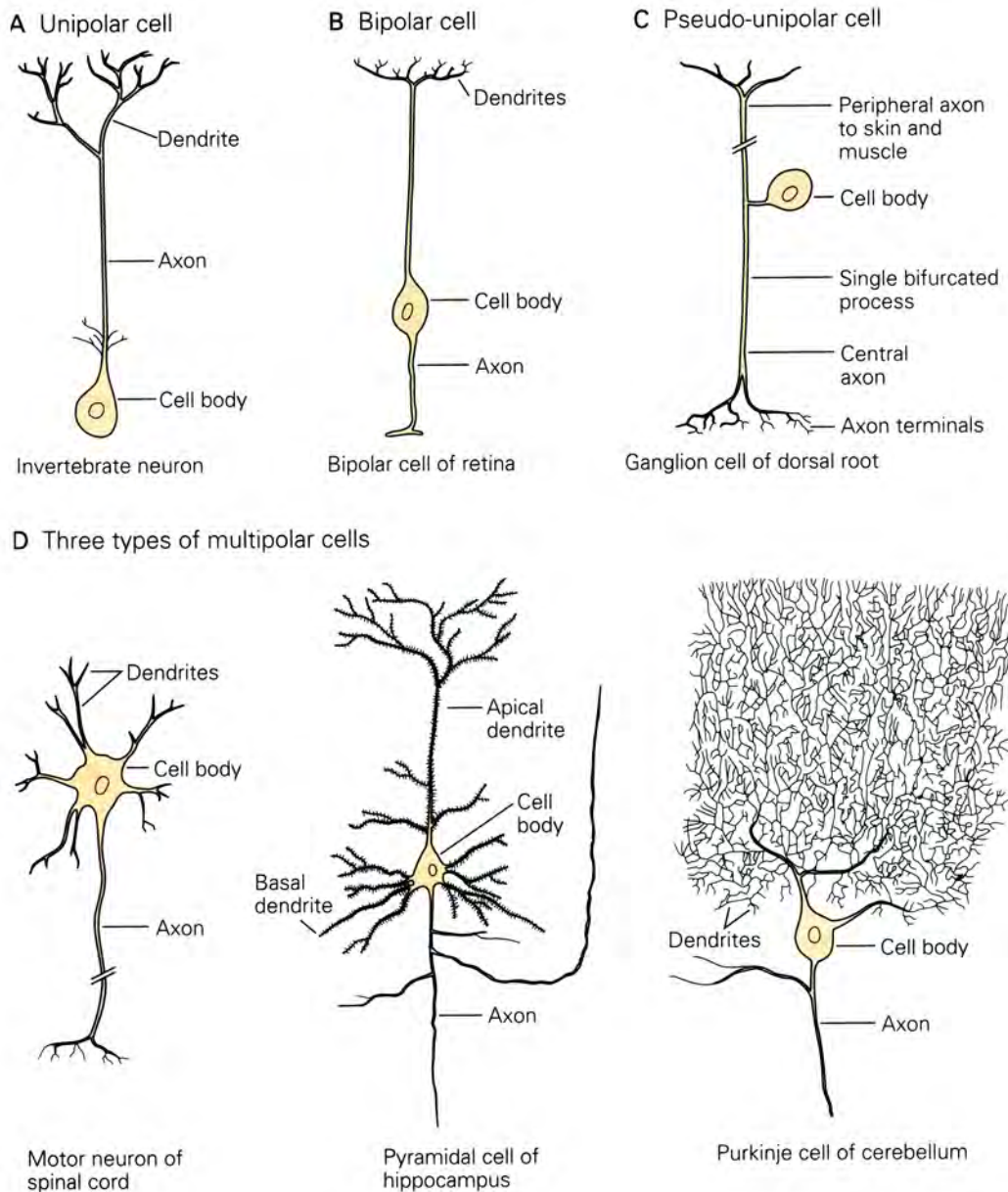
Figure 1.7. Neurons can be classified according to the number of processes that originate from the cell body (their polarity): they can be unipolar, bipolar or multipolar (image taken from (72))

such as the pyramidal cells, Purkinje cells, and anterior horn cells are called *Golgi I* and neurons whose axonal process projects locally such as the granule cell are called *Golgi II*.

Different types of neurons can be distinguished also by the function they play in the nervous system. Neurons conveying informations from tissues and organs to the central nervous system are called *afferent (or sensory) neurons*. The cells transmitting signals from the central nervous system to the effector cells are called *efferent (or motor) neurons*, and the cells connecting neurons within the central nervous system are called *interneurons*.

The action of a neuron on other neurons is also important to understand the role of each individual cell. This role is primarily driven by the type of synapse (see section 1.2.6) and the neurotransmitter used. We distinguish *excitatory* neurons that depolarize their target neurons and *inhibitory* neuron that hyperpolarize their target cell. Nevertheless, this is not a very precise classification, since the action of a presynaptic neuron on a postsynaptic cell does not only depend on the type of neurotransmitter substance released to transmit information, but also the postsynaptic receptor. Eventually *modulatory* neurons evoke more complex effects termed neuromodulation. These neurons use often such neurotransmitters as dopamine,

acetylcholine, serotonin.

Eventually, another classification, which will be specifically used in this dissertation, distinguishes neurons according to their electrophysiological characteristics, i.e. their spiking signature in response to different kinds of stimulations. This classification will be further studied in section 1.4.

1.2.3 Electrophysiology of neurons

The first thing one notice when penetrating into the cell with an intracellular electrode is the existence of an electrical potential across this membrane (this observation dates back to the late 1930's (25; 53)). The difference of electrical potential between the intracellular and the extracellular potential is an essential measurement of the nerve cell's activity.

Passive properties of nerve cells

The neuron as all cells of the body have passive electrical properties which do not depend sensitively on the neuron's activity, and that affect the cell's electrical signaling: the resting membrane resistance and the membrane capacitance. These characteristics can be acquired by intracellular measurements of the membrane potential in response to current inputs.

Membrane resistance   Injecting a negative charge through the an electrode results in most neurons in a subsequent hyperpolarization proportional to the injected current. The slope of this linear relation defines the neuron's input resistance. To compare the membrane properties of neurons of different size, electrophysiologists often use the resistance of a unit area of membrane, the *specific membrane resistance*. This quantity depends on density of resting ion channels and on their conductances.

Membrane capacity   The dynamical properties of the input integration when injecting a negative charge in the cell resembles to the one of capacitor. This property is linked with the structure of the the nerve cell's membrane: it is made of two layers of phospholipid molecules, with their polar head facing the intracellular cytoplasm, and the extracellular space, separating the internal and external conducting solutions by a $35 - 50$ Å thin insulating layer[5]. To understerse how a capacitance slows down the voltage response, we need to recall that the voltage across a capacitor V is proportional to the charge Q stored in it:

$$Q = CV$$

In membrane biophysics, the capacitance is usually specified in terms of the *specific membrane capacitance* C_m expressed in microfarad per square centimeter of membrane area. When the voltage across the capacitance changes, a current will flow, and this current is obtain via the charge equation:

$$I_C = C \frac{\mathrm{d}V_m(t)}{\mathrm{d}t}$$

The capacitance depends on the didelectric constant of a medium and on the geometry of the conductors on either side. In a simple capacitor formed by two parallel plates of area A separated by an insulated of dielectric constant ε_0 and thickness d, the capacitance is:

$$C = \frac{\varepsilon \varepsilon_0 A}{d}$$

where ε is the polarizability of free space universal constant. Cell membranes can be considered as parallel plate capacitors with specific capacitance near $1.0 \mu F/cm^2$ (see (24)), which is just slightly higher than a pure lipid bilayer, $0.8 \mu F/cm^2$. The high electric capacitance of biological membranes appears to be a direct consequence of their molecular dimensions.

Note that these two properties can also be expressed for the axons and the dendrites, and the quantitative differences between the values in the soma and the process plays a role in the propagation properties of the signal (see (72, chapter 8)).

---

[5]It is known from elementary physics that whenever a thin insulator is keeping charges apart, it will act like a capacitance.
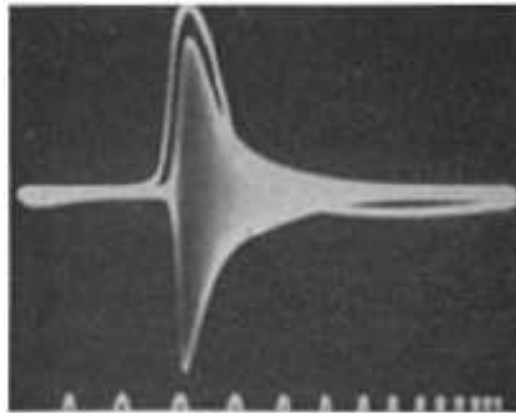
Figure 1.8. Historic oscilloscope record of a net increase of ionic conductance in the membrane of the axon simultaneously to the emission of an action potential by Cole and Curtis (26). The time marks at the bottom are 1 millisecond apart. The uppermost curve is the action potential.

Active properties of the neurons: Ionic exchanges

Neurons are excitable cells, and their specific properties of generating signals and transmitting them are linked with active properties of the cell. From the electrophysiological point of view, we just saw that the nerve cell's membrane acts like a capacitor and can conduct electrical signals with a given conductivity. We are now interested in the ionic exchanges that drive the cell's activity and that lead to the emission of action potentials.

An important clue about how action potentials are generated came from another experiment performed by Kenneth Cole and Howard Curtis(26). While recording from the giant axon of the squid, they found that the ion conductance across the membrane increases dramatically during the emission of action potentials (see figure 1.8). This discovery provided the first evidence that the action potential results from changes in the flux of ions through the channels of the membrane. It raised hence a new question: which ions are responsible for the action potential?

A key to this problem was provided by Alan Hodgkin and Bernard Katz. They found in 1949 (55) that the amplitude of the action potential was reduced when the external Na^+ concentration is lowered, indicating that Na^+ influx is responsible for the rising of phase of the action potential. Their data also suggested that the falling phase of the action potential was caused by a later increase in K^+ permeability. To test this hypothesis, Alan Hodgkin and Andrew Huxley conducted a second series of experiments. They systematically varied the membrane potential of the squid giant axon and measured the resulting changes in the membrane conductance to Na^+ and K^+ (see (54)). It is now understood that four ionic currents are responsible for the electrical activity of the neuron: sodium (Na^+), potassium (K^+), chloride (Cl^-), and calcium (Ca^{2+}). The concentrations of these ions are different on the inside and the outside of a cell. These ionic gradients are the major forces driving neural activity. The extracellular medium has a high concentration of sodium and chloride ions (it is salty medium similar to seawater), and a relatively high concentration of calcium ions. The intracellular medium has high concentrations of potassium and different negatively charged molecules (denote generically A^- for anions) trapped in the intracellular medium (there is no ion channel adapted to send them in the extracellular medium). The flows of sodium and calcium ions appears to be not very significant, at least at rest, while the flows of potassium and chloride ions are quite important. There exist two different kinds of ionic flows through the membrane:

- The *passive redistribution*, linked with the fact that the impermeable anions A^- attract more K^+ into the cell and repel more Cl^- out of the cell, thereby creating concentration gradients.

- The *active transport*, linked with ionic pumps acting on the cell membrane: for example, the Na^+-K^+ pump depicted in figure 1.10 pumps out three Na^+ ions for every two K^+ ions pumped in, thereby maintaining concentration gradients.

Two forces drive each ion species through the membrane channel: the concentration and the electric potential gradients. First, the ions diffuse down the concentration gradient. For example, the K+ ions depicted in figure 1.9.a. diffuse out of the cell because K^+ the internal concentration of potassium is higher than that the external one. While exiting the cell, K^+ ions carry a positive charge and leave a net negative charge
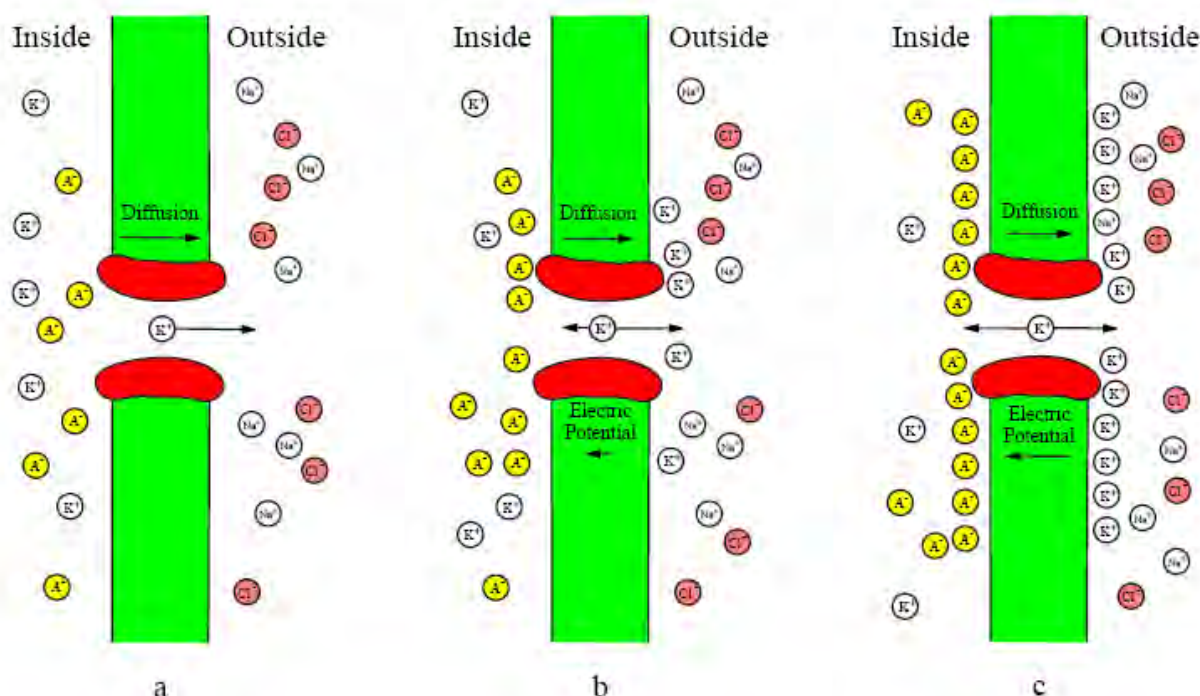
Figure 1.9. Diffusion of K^+ ions through the cell's membrane: (a) creates and electric potential force pointing in the opposite direction, (b) until the diffusion and electrical forces compensate each other (c). The resulting transmembrane potential 1.1 is referred to as the Nernst equilibrium potential for potassium ion (from Izhikevich (65)).

inside the cell, thereby producing an outward current. The positive and negative charges accumulate on the opposite sides of the membrane surface, creating an electric potential gradient across the membrane, which we call the *transmembrane potential or membrane voltage*. This potential slows the diffusion of K^+ since these ions are attracted towards the negatively charged interior and repelled from the positively charged exterior of the cell (figure 1.9.b.). At some point an equilibrium is achieved: the concentration gradient and the electric potential gradient exert equal and opposite forces that counterbalance each other, and the net cross-membrane current is zero, as in figure 1.9.c. The value of such an equilibrium potential depends on the ionic species, and it is given by the *Nernst equation* (see e.g. (51)):

$$E_{ion} = \frac{RT}{zF} \log \frac{[Ion]_{out}}{[Ion]_{in}}, \tag{1.1}$$

where $[Ion]_{out}$ and $[Ion]_{in}$ are the ion concentrations outside and inside the cell, respectively; R is the universal gaz constant ($8.315 mJ/(K° \cdot Mol)$), T is the temperature in degrees Kelvin, F is Faraday's constant ($96,480 coulombs/Mol$) and z is the valence of the ion.

Figure 1.10 shows the different ionic species together with the equilibrium Nernst potential for different ionic species for a typical mammalian neuron.

The Nernst equation gives the equilibrium voltage corresponding to a unique ionic specie only considering the ionic concentrations. It did not take into account the ease with which ions cross the membrane. In terms of electrical current flow, the membrane's conductance provides a convenient measure of how readily the ion crosses the membrane. Another convenient measure is the permeability P of the membrane to a given ion, in velocity unit (cm/s). This quantity measures the rate of solute movement in solution. David Goldman in 1943 published a formula linking of the equilibrium potential, the ionic permeabilities and the intracellular and extracellular ionic concentrations taking into account different ionic species (see (44)):

$$E_m = \frac{RT}{F} \log \left(\frac{P_K [K^+]_{out} + P_{Na} [Na^+]_{out} + P_{Cl} [Cl^-]_{in}}{P_K [K^+]_{in} + P_{Na} [Na^+]_{in} + P_{Cl} [Cl^-]_{out}} \right) \tag{1.2}$$

This equation is known as Goldman, or Goldman-Hodgkin-Katz (GHK) equation. Alan Hodgkin and Bernard Katz used this equation to analyze changes to compute this potential, which is often known as the
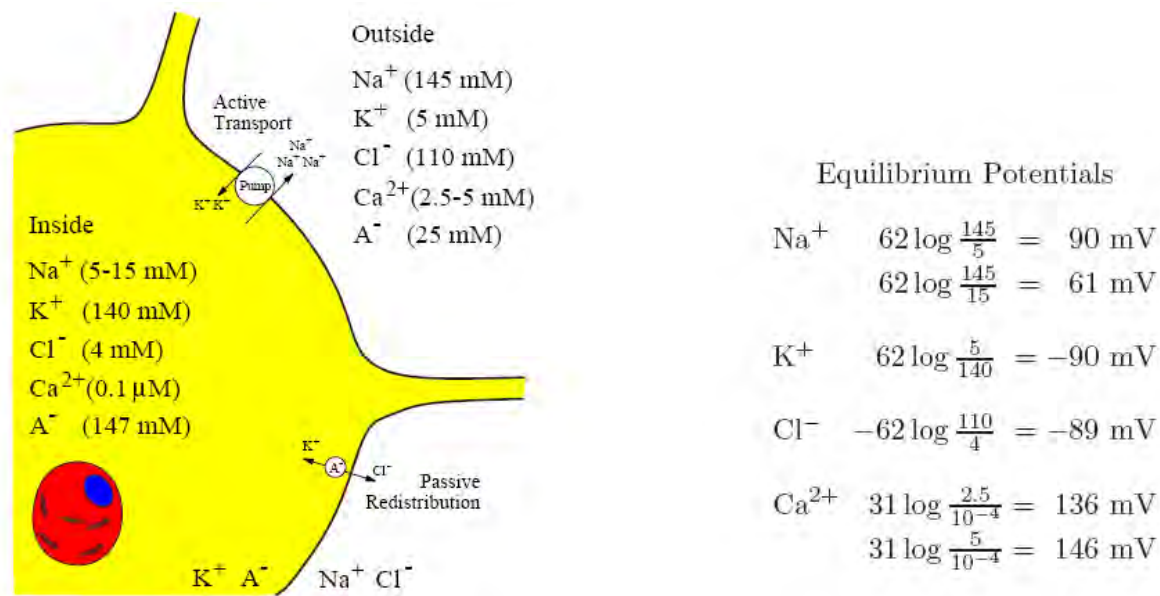
Figure 1.10. Ion concentrations and Nernst equilibrium potentials in a typical mammalian neuron at a temperature of $37°C$ (figure taken from (65) where it was adapted from (68)).

reversal potential (instead of equilibrium potential) because the direction of current flow through the channel switches as the membrane potential passes through this value.

This dynamical equilibrium named the "rest" state is achieved when ionic currents are flowing across the membrane and balance each other so that the net current flowing across the membrane is zero. Maintaining this equilibrium is a major power expenditure for the nervous system. Half the metabolic energy consumed by a mammalian brain is has been estimated to be due to the membrane ionic pumps responsible for the balance of ionic gradients (see (4)), all nerve cell present a quite stable negative potential, ranging from $-70mV$ to $-30mV$. This value is not necessarily fixed and under some condititons where the resting potential dynamically adjusts in function of a network activity (see (27)).

1.2.4 The nerve signal

The signals produced and conveyed by the nerve cell are called *action potentials*, or *spikes*. They are rapid transient nerve electrical impulses with an amplitude of $100mV$ and a duration of about $1ms$ (see figure 1.11). Action potentials are initiated at a specialized trigger region at the origin of the axon, the axon hillock (see section 1.2.1). From this region, the action potential is transported down the axon without failure or distortions at speeds ranging from 1 to 100 meters per second. The amplitude of the action potential travelling along the axon remains almost constant (as we will see in the case of long connections, axons are generally wrapped in a fatty insulating sheath of myelin, which is interrupted at regular intervals by the Ranvier nodes where the action potential is regenerated). The fact that these action potential are highly stereotyped implies that the information conveyed is not in the shape of this signal but rather in the relative times of spike emission and the pathway of the signal through the network.

The course of the action potential can be divided into four parts closely linked with the dynamics of ion channels: the rising phase, the falling phase, the undershoot phase, and the refractory period.

(i) *The spike generation and the rising phase* : A sufficiently strong depolarization of the membrane potential at the axon hillock initiates the action potential. This depolarization is often caused by the injection of extra sodium cations into the cell; these cations can come from a wide variety of sources, such as chemical synapses, sensory neurons or pacemaker potentials. In this phase, the membrane permeability to potassium is low, but much higher than that of other ions, making the resting potential close to E_K.

The depolarization causes the voltage-gated sodium and potassium channels to open, allowing the ions to flow into and out of the axon, respectively. If the depolarization is small, the outward potassium current overwhelms the inward sodium current and the membrane repolarizes back to its normal resting potential around $-70mV$. However, if the depolarization is large enough, the inward sodium current
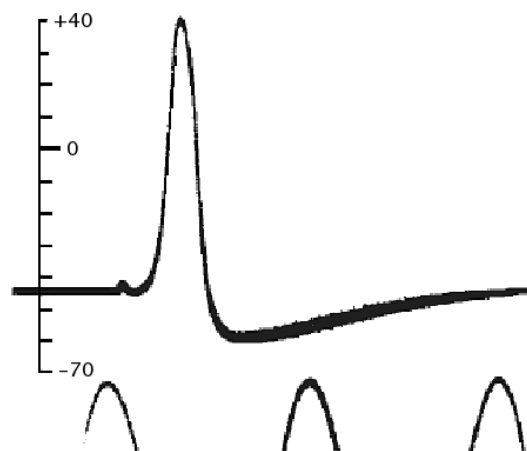
Figure 1.11. First intracellular recording of an action potential obtained in 1939 by Hodgkin and Huxley from the squid giant axon, using glass capillary electrodes filled with sea water. The sinusoid corresponds to a time marker of 500 Hz. The vertical scale indicates the potential in millivolt, the sea water outside being taken as a reference (From (53)).

increases more than the outward potassium current and a positive feedback results: the increasing voltage in turn causes even more sodium channels to open, which pushes V still further towards E_{Na}. This positive feedback continues until the sodium channels are fully open and V is close to E_{Na}.

(ii) The *falling phase* : the same raised voltage that opened the sodium channels initially also slowly shuts them off, by stoppering their pores; the sodium channels become inactivated. This lowers the membrane's permeability to sodium, driving the membrane voltage back down. At the same time, the raised voltage opens voltage-sensitive potassium channels; the increase in the membrane's potassium permeability drives back V towards E_K. Combined, these changes in sodium and potassium permeability cause V to drop quickly, repolarizing the membrane and producing the "falling phase" of the action potential.

(iii) The *hyperpolarizing phase* : The raised voltage opened many more potassium channels than usual, and these do not close right away when the membrane returns to its normal resting voltage. The potassium permeability of the membrane is transiently unusually high, driving the membrane voltage V even closer to the potassium equilibrium voltage E_K. Hence, there is a hyperpolarization persisting until the membrane potassium permeability returns to its usual value.

(iv) The *refractory period* : The opening and closing of the sodium and potassium channels during an action potential may leave some of them in a "refractory" state, in which they are unable to open again until they have recovered. In the absolute refractory period, so many ion channels are refractory that no new action potential can be fired. Significant recovery (desinactivation) requires that the membrane potential remain hyperpolarized for a certain duration. In the relative refractory period, enough channels have recovered that an action potential can be provoked, but only with a stimulus much stronger than usual. These refractory periods ensure that the action potential travels in only one direction along the axon.

Some neurons do not generate action potentials, but instead generate a graded electrical signal, which in turn causes graded neurotransmitter release. Such nonspiking neurons tend to be sensory neurons.

Now that we explained briefly the mechanisms of spike generation, let us present the way the signal propagates along the axons to reach other nerve cells.

1.2.5 Propagation of action potentials

The action potential generated in the soma of the nerve cell propagates as a wave along the axon. Like the soma's membrane, the axon's membrane contains voltage-gated ion channels which allowing propagation of the electrical impulse. These impulses are propagated by charge-carrying ions including the same ionic species as the spike generation, namely the sodium (Na^+), potassium (K^+), chloride (Cl^-), and calcium (Ca^{2+}) ions. The ionic currents flowing towards the intracellular medium at a point on the axon during an action

potential spread out along the axon, and depolarize the adjacent sections of its membrane. If sufficiently strong, this depolarization provokes a similar action potential generation in the neighboring membrane patches. This basic mechanism was demonstrated again by Alan Hodgkin in the late 30's: he inhibited by crushing or cooling nerve segments of the squid giant axon and showed that an action potential arriving on one side of the inhibited zone could provoke another action potential on the other side, provided that the inhibited segment was sufficiently short.

Once an action potential has occurred at a patch of membrane, the membrane patch needs time to recover before it can fire again. At the molecular level, this absolute refractory period corresponds to the time required for its ion channels to return to their normal open or closed states. Hence the absolute refractory period ensures that the action potential moves in only one direction along an axon. The currents flowing in due to an action potential spread out in both directions along the axon. However, only the the part of the axon that has not fired yet an action potential can respond: the part that has just fired is unresponsive until the action potential is safely out of range and cannot restimulate that part. Hence the action potential propagates from the axon hillock towards the axonal terminals[6].

The axons of some neurons are ensheathed in myelin regularly interrupted by myelin gaps (Ranvier's nodes). Myelin prevents ions from entering or leaving the axon along myelinated segments. As a general rule, myelination increases the conduction velocity of action potentials and makes them more energy-efficient. The current passively spreads from one Ranvier's node to another. The myelin inhibits charge leakage, and hence when the current reaches another Ranvier node, the depolarization it provokes is sufficient to generate a new action potential at this node; this "hopping" of the action potential from node to node is known as *saltatory conduction*[7], in contrast with the unmyelinated axons where the action potential is continuously transmitted down the axon like a wave.

Now that the signal has been transported from the soma to the axonal terminal, let us describe the way the signal is transmitted to other neurons, in order to close the loop of neuronal processing.

1.2.6 Synaptic Transmission

For communicating with another cell, the neurons make use of one of two basic forms of synaptic transmission: the electrical and the chemical synapses. The strength of the synaptic transmission can be enhanced or reduced, depending of the history of the cellular activity. This *plasticity* of the nerve cells is crucial to memory, learning and other higher brain functions.

The electrical synapse transmission is rapid and stereotyped, and is mainly used to send simple depolarizing signals for systems requiring the fastest possible response. At the location of an electrical synapse, the separation between two neurons is very small ($\approx 3.5nm$). This narrow gap is bridged by the *gap junction channels*, specialized protein structures that conduct the flow of ionic current from the presynaptic to the postsynaptic cell (see figure 1.12). Electrical synapses thus work by allowing ionic current to flow passively through the gap junction pores from one neuron to another. The usual source of this current is the potential difference generated locally by the action potential. Without the need for receptors to recognize chemical messengers, signaling at electrical synapses is more rapid than that which occurs across chemical synapses, the predominant kind of junctions between neurons. The relative speed of electrical synapses also allows for many neurons to fire synchronously. Because of the speed of transmission, electrical synapses are found in escape mechanisms and other processes that require quick responses, such as the response to danger of the sea hare Aplysia, which quickly releases large quantities of ink to obscure enemies' vision.

This mechanism of electrical transmission, though rapid, is not the most widely used transmission process between neurons. In most of neural connections, the signal transmission is performed via *chemical synapse*, or *synapse* (without qualifier). Chemical synapses transmit information directionally from a presynaptic cell to a postsynaptic cell and are therefore asymmetric in structure and function. In the case of the chemical synapse, there is no structural continuity between pre- and postsynaptic neurons. The region separating these two cells, called the *synaptic cleft*, is usually wider than the mean adjacent intercellular space, and ranges between 20 and 40nm. The chemical synaptic transmission is based on the release by the presynaptic neuron of *neurotransmitter*, a chemical substance that binds to specific receptors on the postsynaptic cell membrane. To this purpose, the presynaptic terminals contain discrete collections of synaptic vesicles, each of which filled with several thousand of transmitter molecules. During the discharge of a presynaptic action potential, Ca^{2+} enters the presynaptic terminal through voltage-gated Ca^{2+} channels at the active zone. The

---

[6]propagation in the opposite direction, known as *antidromic conduction*, exists and is very rare. However, if a laboratory axon is stimulated in its middle, both halves of the axon are unfired, and then two action potentials will be generated, one traveling towards the axon hillock and the other traveling towards the synaptic knobs.

[7]The mechanism of saltatory conduction was suggested in 1925 by Ralph Lillie in his article (84), the first experimental evidence for saltatory conduction came from Ichiji Tasaki, Taiji Takeuchi and from Andrew Huxley and Robert Stämpfli (59; 110; 111; 112).
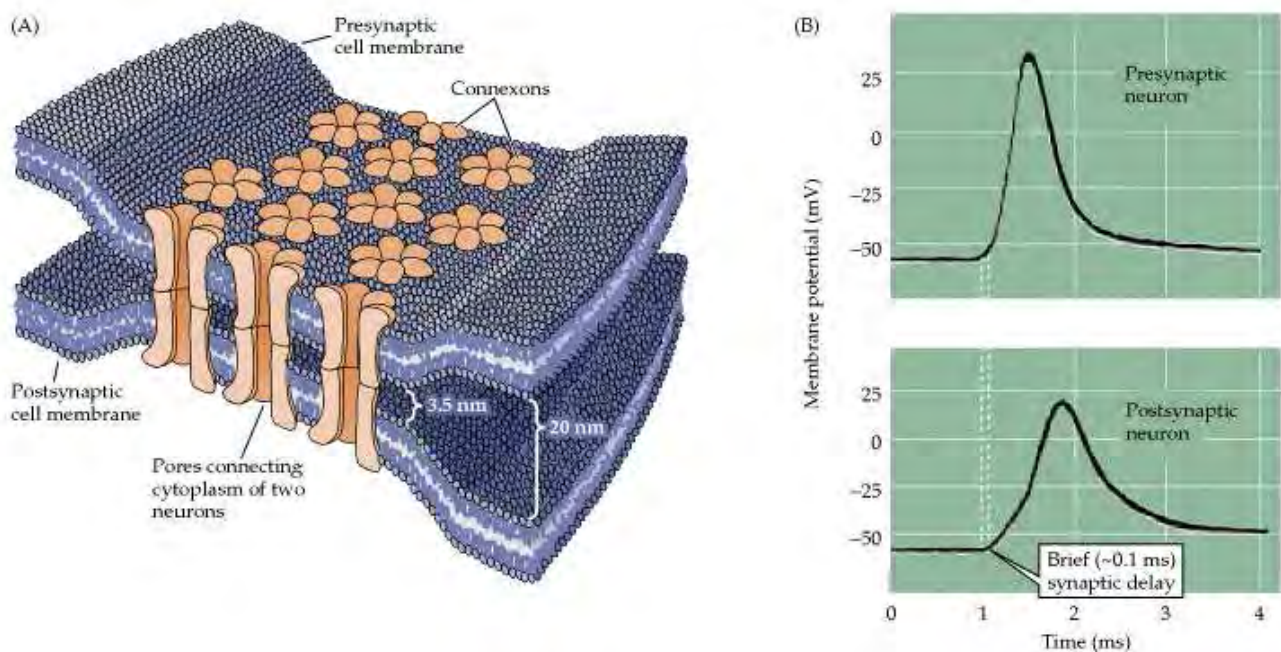
Figure 1.12. Structure and function of gap junctions at electrical synapses. (A) Gap junctions consist of hexameric complexes connecting two similar structure of the pre- and postsynaptic membranes. The pores of the channels connect to one another, creating electrical and chemical continuity between the two cells. (B) Rapid transmission of signals at an electrical synapse in the crayfish (see (42)). An action potential in the presynaptic neuron causes the postsynaptic neuron to be depolarized within a fraction of a millisecond (figure taken from (100)).

rise of Ca^{2+} concentration causes the vesicles to fuse with the presynaptic membrane and thereby release their neurotransmitter into the synaptic cleft (*exocytosis*). The neurotransmitter molecules then diffuse across the synaptic cleft and bind to their receptors on the postsynaptic cell membrane. This in turn activates the receptors, leading to the opening or closing of ion channels. The resulting flux alters the membrane conductance and potential of the postsynaptic cell (see figure 1.13).

These several steps account for the synaptic delay at chemical synapses, which can be as short as 0.3ms, but that often lasts several milliseconds. Hence it lacks the speed of electrical transmission. Nevertheless, it has the important property of amplifying the signal and hence even a small presynaptic nerve terminal generating a weak current can release thousands of transmitter molecules that can depolarize even a large postsynaptic cell.

When the receptors of the postsynaptic cell bind neurotransmitter molecules, they respond by opening nearby ion channels, causing ions to flow in or out and changing the local transmembrane potential of the cell. The resulting change in voltage is called a *postsynaptic potential*. The result of this process can be excitatory in the case of depolarizing currents (this is the more general case), or inhibitory in the case of hyperpolarizing currents. The excitatory or inhibitory nature of a synapse depends on the types of ion channel conduct the postsynaptic current displays, which in turn is a function of both the type of receptors and the type of neurotransmitter employed at the synapse. If a signal is transmitted at an excitatory synapse, then the depolarization of the cell can be strong enough so that an action potential can be initiated in the postsynaptic cell. If the depolarization induced by the excitatory postsynaptic potential is not be sufficient for an action potential initiation, then the effect of the depolarization will be last for some time, and will be progressively attenuated. Therefore, if the neuron receives other signals from the same or other neurons, the postsynaptic potentials (PSP) they provoke will be summed. This phenomenon is known as the *synaptic integration*.

All these phenomena can be modeled independently, and result in what we call the *detailed neuron models*

1.3 ELECTROPHYSIOLOGICAL MODELIZATION OF THE NEURONAL ACTIVITY

In the previous section, we described from a biological point of view the basic mechanisms in play inside
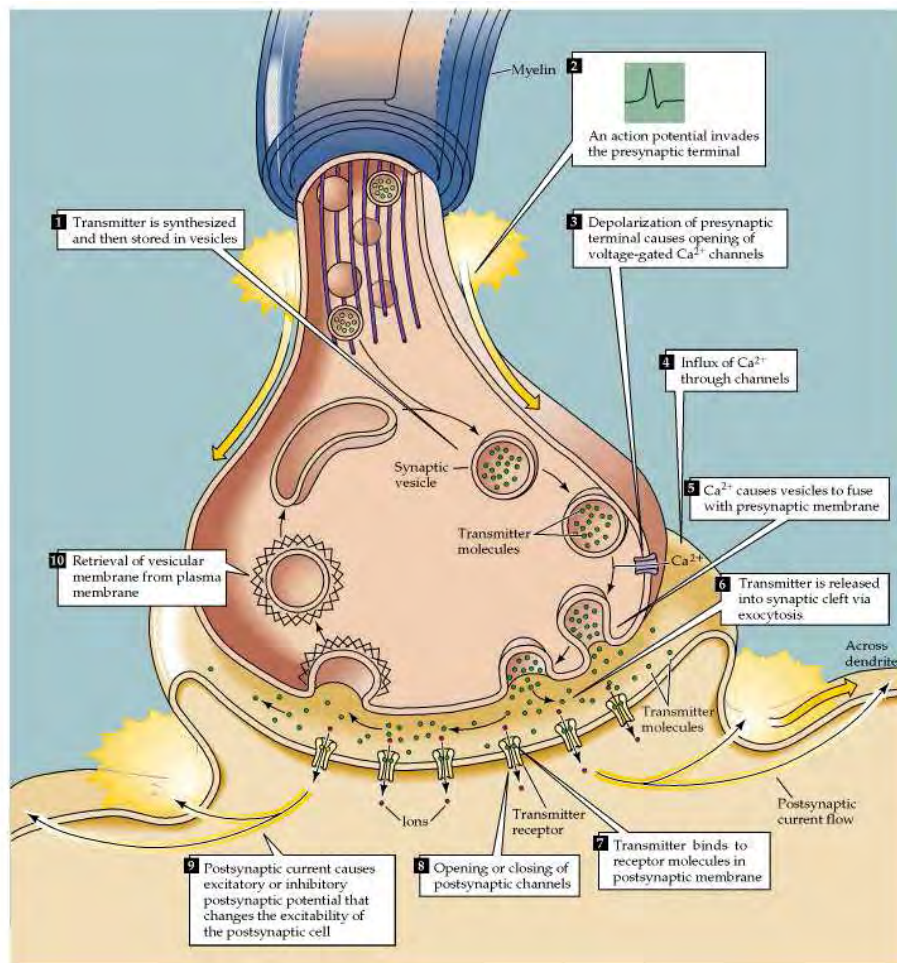
Figure 1.13. Cascade of events involved in the signal transmission at a typical chemical synapse.(from (100)).

the neurons and the transmission mechanisms between neurons. In this section, we present physical and mathematical models for each of these process. The models built upon these considerations will be called *detailed neuron models* since they will be based on a detailed description of the neuron and of each structure's dynamics. We try to keep the presentation intuitive and try to make explicit all the simplifications and their biological origins. This section is only devoted to present models of the neuronal activity itself. Modelizations of synaptic inputs will be presented later.

From a biophysical point of view, action potentials are the result of currents that pass through ion channels in the cell's membrane. In their extensive series of experiments on the giant axon of the squid, Hodgkin and Huxley succeeded in measuring these currents and described their dynamics in terms of differential equations.

1.3.1 Models of ionic currents

The total current flowing across the membrane through all of its ion channels is called the membrane current of the neuron. By convention, the membrane current is defined as positive when positive ions leave the neuron and negative when positive ions enter the neuron. The total membrane current is determined by summing currents due to all of the different types of channels within the cell membrane, including voltage-dependent and synaptic channels. We label the different types of channels in a cell membrane with an index i. As discussed in the last section, the current carried by a set of channels of type i with reversal (Nernst) potential E_i, vanishes when the membrane potential satisfies $V = E_i$. For many types of channels, the current increases or decreases approximately linearly when the membrane potential deviates from this value. The difference $(V - E_i)$ is called the *driving force*, and the membrane current per unit area due to the type i channels is written as $g_i(V - E_i)$ in this linear approximation, where the factor g_i is the conductance per unit area related to the channel. Summing over the different types of channels, we obtain the total membrane current:

$$I_m = \sum_i g_i (V - E_i)$$

In the linear model, it is easy to compute the *resting potential* of the neuron, i.e. the membrane potential corresponding to a null total ionic current. This current reads, considering the 4 ionic species introduced:

$$V_{rest} = \frac{g_{Na} E_{Na} + g_{Ca} E_{Ca} + g_{Cl} E_{Cl} + g_K E_K}{g_{Na} + g_{Ca} + g_{Cl} + g_K}$$

This quite simplistic model is the most commonly used to described ionic currents, and is also chosen in this dissertation. It is valid for small changes of the voltage.

More precise models of voltage-ionic currents relations take into account the ion permeability and the selectivity of membranes. This formalism know as the Goldman-Hodgkin-Katz (GHK) formulation, was developed by Goldman in (44) and used by Hodgkin and Katz (55). The GHK equations involve the membrane permeability to ions, a variable that quantifies the membrane's ability to let ions flow in and out the cell (see (51, Chapter 14)). The GHK current equation says that the current carried by ion S is equal to the related membrane's permeability P_S multiplied by a nonlinear function of the voltage:

$$I_S = P_S z_S \frac{V F^2}{RT} \frac{[S]_{in} - [S]_{out} \exp(-z_S F E / RT)}{1 - \exp(-z_S F E / RT)} \tag{1.3}$$

With this model one can derive of the reversal potential equation (1.2) that we used to explain the spike mechanism. For more details on the GHK equation and its derivation, we refer to (51, Chapter 14).

1.3.2 Models of gated ionic channels

As described in section 1.2.1, many ion channels are voltage-gated and their properties depend on the membrane potential. Gates can *activate* or *inactivate* the channel (i.e. open or close it respectively, see figure 1.6). To model their function, Hodgkin and Huxley introduced two variables: the probability m of an activation gate to be in the open state, and the probability h of an inactivation gate to be in the open state. These variables are probabilities, hence real numbers in $[0, 1]$. When channels are partially open, $m \in (0, 1)$, when the channels are completely activated, $m = 1$, and when it is completely deactivated, $m = 0$. The proportion of open channels in a large population is hence given by:

$$p = m^a h^b; \tag{1.4}$$

where a (resp. b) is the number of activation (resp. inactivation) gates per channel. Some channels do not have inactivation gates ($b = 0$), hence $p = m^a$. Such channels do not inactivate, and they result in persistent currents. In contrast, channels that do inactivate result in transient currents.

The dynamics of the activation variable m is classically described by a general first-order differential equation:

$$\frac{\mathrm{d}m}{\mathrm{d}t} = \frac{m_\infty(V) - m}{\tau(V)} \tag{1.5}$$

where $m_\infty(V)$ is called the *steady-state activation function*, and $\tau(V)$ the *activation time constant*. These two functions can be measured experimentally. The activation function has a sigmoidal shape and the time constant a unimodal shape (see figure 1.14).

The dynamics of the inactivation variable h can also be described by the first-order differential equation

$$\frac{\mathrm{d}h}{\mathrm{d}t} = \frac{h_\infty(V) - h}{\tau(V)} \tag{1.6}$$

Here again we call where $h_\infty(V)$ is called the *steady-state inactivation function*, and $\tau(V)$ the *inactivation time constant*. For the inactivation function, h_∞ is an inverted sigmoidal function (decreasing, tends to 1 at $-\infty$ and to 0 at $+\infty$, see figure 1.14).

1.3.3   The Hodgkin-Huxley model and its reductions

The original Hodgkin-Huxley model

The original Hodgkin-Huxley model is a very classical and widely used detailed neuron model. Though we do not study this model in depth, it is an important model and will be referred to in discussions for being a reference model.

Using pioneering experimental techniques of that time, Hodgkin and Huxley (54) determined that the squid axon curries three major currents: voltage-gated persistent K^+ current with four activation gates, voltage-gated transient Na^+ current with three activation gates and one inactivation gate, and Ohmic leak current, I_L, which is carried mostly by chloride ions Cl^-.

The basic electrical relation between the membrane potential and the currents read:

$$C\frac{\mathrm{d}V}{\mathrm{d}t} = I(t) - I_K - I_{Na} - I_L,$$

This equation, considering the linear model of $I - V$ relations, the model of voltage-gated channels we just introduced and considering the maximal conductance for each ionic specie instead of the real conductance, can be written as follows:

$$\begin{cases} C\dot{V} & = I(t) - \bar{g_K}n^4(V - E_K) - \bar{g_{Na}}m^3 h(V - E_{Na}) - \bar{g_L}(V - E_L) \\ \dot{n} & = \alpha_n(V)(1-n) - \beta_n(V)n \\ \dot{m} & = \alpha_m(V)(1-m) - \beta_m(V)m \\ \dot{h} & = \alpha_h(V)(1-h) - \beta_h(V)h \end{cases} \tag{1.7}$$

In this equation, the we denoted $\dot{x}$ the derivative dx/dt for a variable x. The functions α_i and β_i result of instantiations of the steady-state activation and inactivation functions and of the time constant functions. The equations are presented this way for historical reasons. The related steady-state (in)activation functions of the variable x simply reads $x_\infty = \alpha_x/(\alpha_x + \beta_x)$ and its time constant $\tau_x = 1/(\alpha_x + \beta_x)$. The functions α_x and β_x classically chosen are:

$$\begin{cases} \alpha_n(V) = 0.01\frac{10-V}{\exp(\frac{10-V}{10})-1} & \beta_n(V)) = 0.125\exp\left(-\frac{V}{80}\right) \\ \alpha_m(V) = 0.01\frac{25-V}{\exp(\frac{25-V}{10})-1} & \beta_m(V)) = 4\exp\left(-\frac{V}{18}\right) \\ \alpha_h(V) = 0.07\exp\left(-\frac{V}{80}\right) & \beta_h(V)) = \frac{1}{\exp(\frac{30-V}{10})+1} \end{cases} \tag{1.8}$$

In the original model proposed by Hodgkin and Huxley, these functions and constant are set as in table 1.1.

The related steady state (in)activation function and time constants are plotted in figure 1.14.

This model is widely used in the neuroscience community. It is quite precise, and has the advantage of being based on the main biophysical principles it emulates. It is now quite well understood from a dynamical

ion	E_{ion} (mV)	$\bar{g}_{ion}$ (mS/cm^2)
Na	115	120
K	-12	36
L	10.6	0.3

Table 1.1. Parameters of Hodgkin-Huxley model: (shifted) Nernst potentials and maximal conductances. The membrane capacity is $C = 1\mu F/cm^2$. The voltage scale is shifted so that the resting potential is 0 (i.e. shifted by approximately $+65mV$)
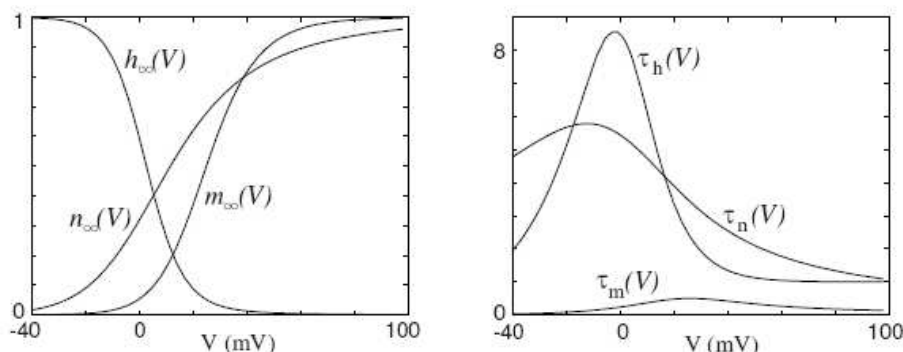
Figure 1.14. Steady state (in)activation functions (left) and time constants (right) in the Hodgkin-Huxley model.

systems point of view. Its bifurcations have been identified numerically, and this model presents a very interesting bifurcation portrait (see e.g. (21)) including an incredible zoology of bifurcations and even chaos. It is able to generate spikes, which are very similar to intracellular recordings, presenting the four phases described in section 1.2.4, bursts, and different other electrophysiological signals, when varying its parameters. Its main drawback is its high complexity and dimensionality that prevent from analytical studies and efficient simulations. The literature about Hodgkin-Huxley model is huge, and this model is still very actively used in the top neuroscience research. Many variants of this model have been proposed (new ion channels considered, different dynamics – (43, Chapter 2.3) – introduction of additional biophysical parameters such as the temperature –see e.g. (40)–).

Many reductions of these models have been proposed in order to be mathematically tractable or more efficient computationally. These reduced models include the famous Fitzhugh–Nagumo and Morris–Lecar models. These two models are bidimensional approximations of the original Hodgkin–Huxley model based on quantitative observations (the m variable, which is the fastest, is here considered as instantaneous, i.e. simply equal to its asymptotic value $m_\infty(V)$, the time constants of h and n are almost the same, and the graphs of the functions $n_\infty(V)$ and $m_\infty(V)$ are very similar, therefore n and $1 - h$ are identified, ...). These two-dimensional models are way more tractable. One of their main advantage is the low dimensionality allowing one to perform a phase plane analysis. This type of models have been extensively studied, from a mathematical and simulation points of view. We will not present here the equations and the results obtained by analyzing these models, and refer to (21; 43; 65; 76).

1.3.4 Models of spike propagation

The models we presented in this section considered only punctual neurons. It is based on the assumption that the membrane potential is constant all along the neuron. Models taking into account the spatial extension of the axon or models of dendrites have been also developed in order to emulate the signal propagation along the axons. These models involve in general reaction-diffusion partial differential equations and models of dendritic tree structures (the interested reader is referred to (27; 43) and mostly to (76)).

1.3.5 Models of synapses

The synaptic signal and its integration will be of particular importance in the study of neuronal networks and noise integration. We will always consider in this dissertation that the contributions of different incoming
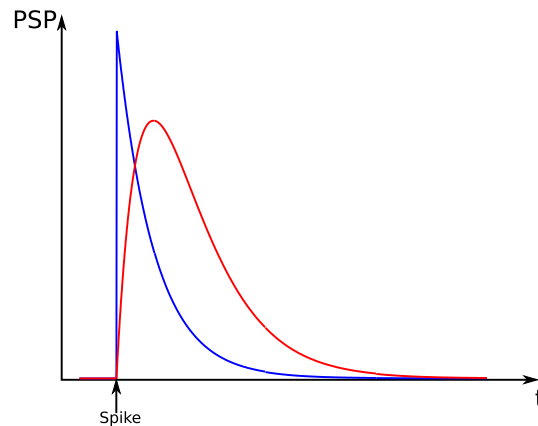
Figure 1.15. Typical postsynaptic (current or conductance) pulses with the same time constant. Blue: exponentially decaying PSP and Red: second-order PSP.

spikes or input current are linearly summed. More precisely, we consider an incoming impulse (Dirac pulse) will generate a typical postsynaptic pulse (PSP) of current or conductivity. The current or conductance at the level of the postsynaptic cell is considered as the convolution of the incoming signal (spike train or continuous firing rate) with the PSP. Different models of PSPs will be considered (see figure 1.15):

- *Instantaneous postsynaptic current (conductance) :* the impulse response of the synapse is a Dirac pulse of current (conductance). This model is described in (113).

- *Exponentially decaying postsynaptic current (conductance):* the inputs received at a given synapse generate an exponentially decaying synaptic current (conductance) of type $\exp(-t/\tau)\mathbb{1}_{t\geq 0}$. For more information see (113).

- *Second-order postsynaptic current (conductance) pulse :* the impulse response is the solution of a second order linear differential equation, taking into account both the rise time and the decay time of real PSPs. This model introduced by Rotterdam et al (119) and is of type $\alpha\beta t e^{-\beta t}\mathbb{1}_{t\geq 0}$. These functions have been successfully applied to neural mass models, see e.g. (113).

- *General postsynaptic current (conductance) pulse :* In (43, section 4.1.3), the authors consider general postsynaptic pulses $\alpha(t)$.

1.4 SPIKE PATTERNS AND NEURONAL EXCITABILITY

In this section we now turn to more phenomenological models, based on spike times description. Spikes are the elementary unit of the neural code, and therefore the neural code can be considered binary (all-or-none). We have seen that neurons are excitable systems, in the sense that they are typically at rest but can fire spikes in response to certain forms of stimulation. The evoked firing pattern, in relation to the type of stimulation, characterize the cell's computational properties. From this point of view, the cell can either simply sum (integrate) the inputs or respond to some precise types of stimulation (resonators), and fire precise spike patterns.

These characteristics will be fundamental throughout this report. Indeed, chapters 2, 3 and 4 are aimed to reproduce spike patterns, excitability and substhreshold behavior with simple formal models.

1.4.1 Excitability

Alan Hodgkin in 1948 (52) studied the spiking behavior of excitable membranes in response to the injection of steps of currents of various amplitudes. His experiments are illustrated in figure 1.16 using recordings of rat neocortical and brainstem neurons. When the injected current amplitude is small, the neurons are quiescent. When it becomes larger, the nerve cell fires spike trains, and depending on the average frequency of these spike trains, Hodgkin identified two major classes of excitability:

- *Class 1 excitability*: action potentials can be generated with arbitrarily low frequency, depending on the strength of the applied current.
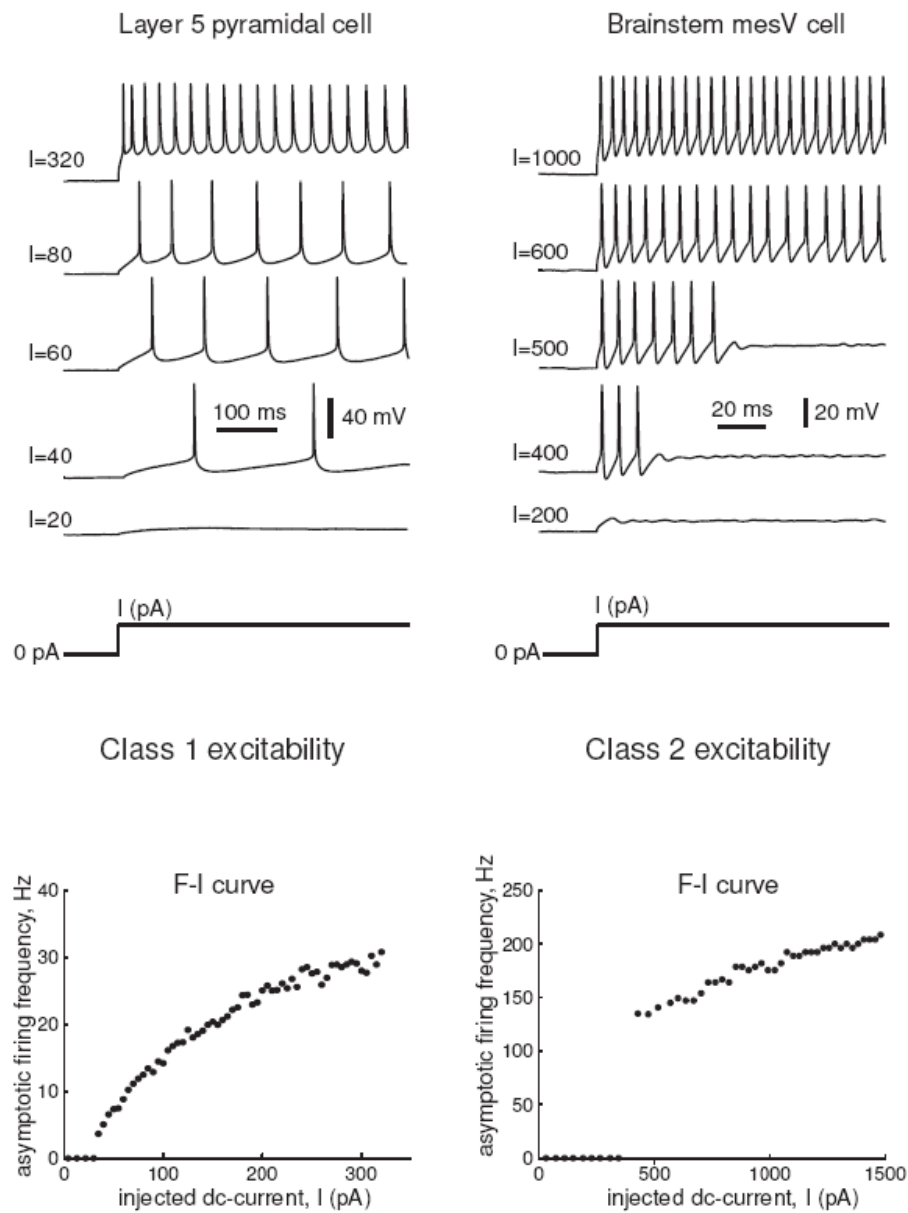
Figure 1.16. (Top) Typical responses of membrane potentials of two neurons to steps of DC-current of various magnitudes. (Bottom) Related frequency-current ($F - I$) curves qualitatively different (recordings of layer 5 pyramidal neurons of the rat's primary visual cortex (left) and mesV neuron from rat brainstem (right)). From Izhikevich 2007 (64)

- *Class 2 excitability*: action potentials are generated in a certain frequency band that is relatively insensitive to changes in the strength of the applied current.

Class 1 neurons, sometimes called type I neurons, fire with a frequency that may vary smoothly over a broad range, starting from 0 Hz to high firing rates as high as 100Hz or even higher. In contrast, the frequency band of class 2 excitable neurons is quite limited, typically ranging from 150 to 200 Hz, but it can vary from neuron to neuron. The qualitative distinction between the classes noticed by Hodgkin is that the frequency-current relation starts from zero and continuously increases for Class 1 neurons, and is discontinuous for class 2 neurons. Obviously, the two classes of excitability have different neuro-computational properties. Class 1 excitable neurons can smoothly encode the amplitude of the stimulation it gets into the frequency of their spiking output, and class 2 neurons act as threshold elements reporting when the strength of input is above a certain value.

1.4.2 Frequency preference and resonance

Some neurons simply integrate the input they get and fire a spike if the inputs where high enough or received consecutively fast. This type of neuron is named integrator. This type of neuron responds to high-frequency inputs, and therefore acts as a coincidence detector because it is most sensitive to the pulses arriving simultaneously.

Some neurons react to pulses when received at a certain frequency, and are named resonators (e.g. mesV neuron). These behaviors have been observed in many in-vitro recordings (see (61; 62) and references herein). The same selectivity exists in vivo as shown by Bryant and Segundo (17): bursts having a precise frequency added to a noisy signal are detected.

Subthreshold PSP oscillations can explain this behavior. Such behaviors have been observed in many cortical cells (2; 3; 5; 9; 71; 85; 86; 87; 89; 90). Assume that a presynaptic pulse evokes an (exponentially decaying) oscillatory postsynaptic behavior. The effect of the second pulse depends on its timing relative to the first pulse: if the interval between the pulses is near the natural period, the second pulse arrives during the rising phase of oscillation and increases the amplitude of oscillation further. In this case the effects of the pulses add up. If the interval between pulses is near half the natural period the second pulse arrives during the falling phase of oscillation, and it leads to decrease the oscillations amplitude.

1.4.3 Thresholds and action potentials

As we will see in section 1.5, a common model of spike emission consists in considering that neurons have firing thresholds: when their membrane potential reaches a given threshold, the neuron fires. Great efforts have been made to determine such thresholds experimentally. Unfortunately, the concept of firing threshold is not well defined, in experimental studies as well as in models. Most of the time, the membrane potential value that separates subthreshold depolarizations from action potentials (if accurately detected) depends on the prior activity of the neuron. For example, if a neuron having transient Na^+ current just fired an action potential, the current is partially inactivated, and a subsequent depolarization above the firing threshold might not evoke another action potential. Conversely, if the neuron was briefly hyperpolarized and then released from hyperpolarization, it could fire a rebound post-inhibitory spike.

1.4.4 Spike latency

An interesting neuronal property is the latency-to-first-spike. A barely superthreshold stimulation can evoke action potentials with a significant delay, which could be as large as a second in some cortical neurons. Usually, such a delay is attributed to slow charging of the dendritic tree or to the action of the A-current, which is a voltage-gated transient K+ current with fast activation and slow inactivation. The current activates quickly in response to a depolarization and prevents the neuron from immediate firing. With time, however, the A-current inactivates and eventually allows firing. We see that the existence of long spike latencies is an innate neuro-computational property of integrators. It is still not clear how or when the brain is using it. Two most plausible hypotheses are 1) Neurons encode the strength of input into spiking latency. 2) Neuronal responses become less sensitive to noise, since only prolong inputs can cause spikes. Interestingly, resonators do not exhibit long latencies

1.4.5 Subthreshold oscillation

Interactions between fast and slow conductances can result in low-frequency subthreshold oscillation of membrane potential, such as the one in figure 1.17, The oscillation is caused by the interplay between
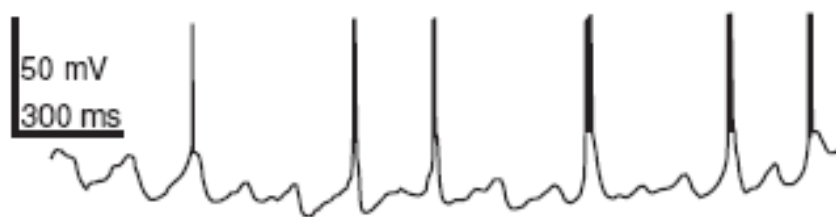
Figure 1.17. Slow subthreshold oscillation of membrane potential of cat thalamocortical neuron evoked by slow hyperpolarization (modified from Roy et al. 1984).

activation and inactivation of the slow Ca^{2+} current and inward h-current. Subtreshold oscillations are discussed further in chapter 2.

1.4.6 Firing patterns of cortical neurons

Cortical neurons exhibit numerous firing patterns, i.e. characteristic trains of action potentials in response to stimulation by current injections (usually depolarizing pulses). Three main notions will be discussed in order to distinguish different spike patterns (see figure 1.18):
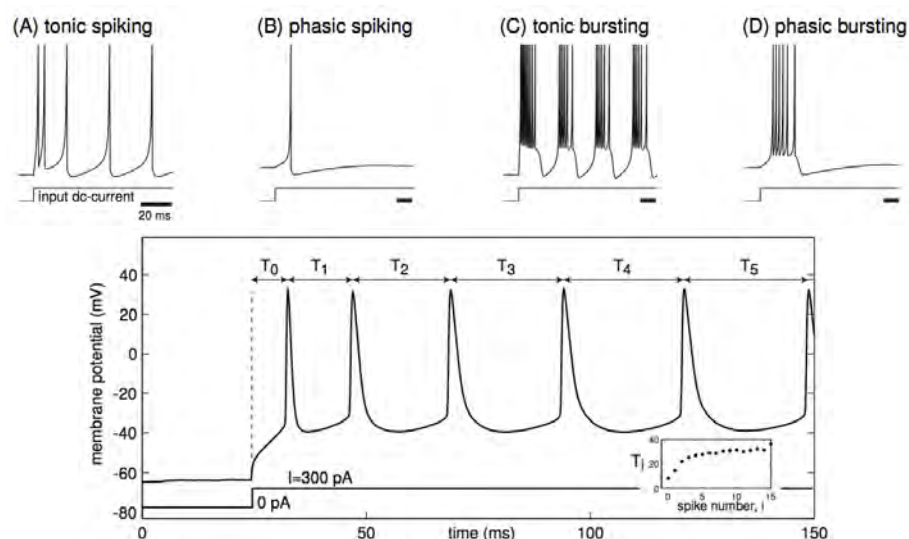
Figure 1.18. Various firing behaviors in response to a sustained depolarizing pulse. Upper panel. Phasic patterns (B,D), tonic patterns (A,C), spiking patterns (A,B) and bursting patterns (C,D). Lower panel. Accommodation of the discharge pattern: interspike intervals increase (From (64)).

- *Tonic and phasic spiking:* Tonically spiking cells fire continuous trains of action potentials for the duration of the depolarizing pulse of injected current (see figure 1.18-B/D). On the contrary, phasically spiking cells respond to a sustained depolarizing current pulse with a very brief train of action potentials followed by no further firing (see figure 1.18-A/C).

- *Bursting:* Sometimes neurons use rapid clusters of two or more action potentials, called *bursts*, as basic signaling events instead of simple spikes (see figure 1.18-C/D).

- *Accommodation:* Neurons sometimes show spike frequency adaptation, i.e. a decrease of firing frequency in response to a sustained depolarizing pulse. They are said to be *accommodating* (see figure 1.18). In contrast, non-accommodating neurons keep a constant discharge frequency to such current injections.

As explained in (64), cortical neurons exhibit six major discharge patterns.

- *Regular spiking (RS)* is a tonic spiking with possible adapting frequency that present a stationary firing rate in response to a sustained depolarizing pulse. This firing pattern is the most spread among excitatory neurons (see figure 1.19).

- *Chattering (CH)* corresponds to high frequency bursts with a relatively short interburst period. This behavior has mainly been observed in layer III Purkinje cell but also concerns excitatory cells in layers II and IV (see figure 1.19).
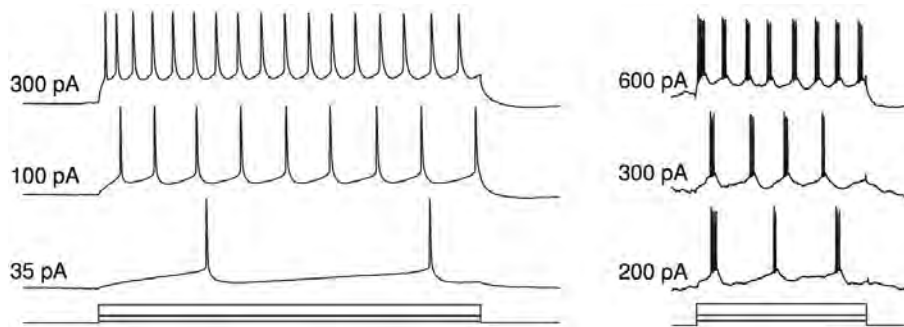
Figure 1.19. Regular spiking (left) and chattering (right) in response to sustained depolarizing pulses of various amplitudes (shown at the bottom of the recordings) (From (64)).

- *Intrinsically bursting (IB)* neurons respond with bursts of action potential at the beginning of a strong depolarizing injection, followed by tonic spiking. The main representatives of this firing pattern are found among layer V PCs (see figure 1.20).
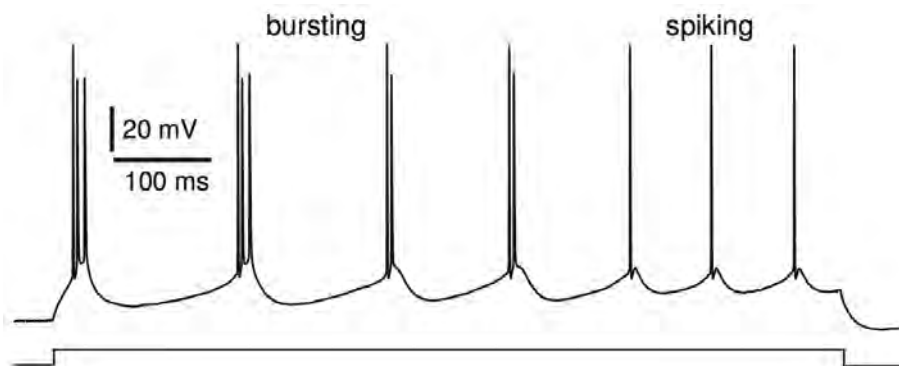
Figure 1.20. Intrinsic bursting in response to a sustained depolarizing pulse. Initial bursting is followed by tonic spiking (From (64)).

- *Fast spiking (FS)* is a high frequency tonic spiking with little adaptation, observed in inhibitory cells (mostly basket and chandelier cells). Fast spiking cells show irregular spiking when injected with weak currents (see figure 1.21).

- *Low-threshold spiking (LTS)* neurons have a tonic firing pattern with strong accommodation. Their name comes from their tendency to exhibit post inhibitory rebounds (spontaneous emission of spikes consecutive to an hyperpolarizing current injection). They can show low frequency firing and phasic responses to weak stimulations (see figure 1.21). LTS neurons are inhibitory interneurons (mostly Martinotti, double bouquet and bitufted cells).

- *Late spiking (LS)* neurons respond to a depolarizing pulse with a slow increase of membrane potential followed, after a delay possibly as long as one second, by low frequency tonic spiking. Late spiking mainly concerns neurogliaform inhibitory interneurons (see figure 1.21).

It appears from the above description that excitatory and inhibitory cells can both be divided into three electrophysiological classes (RS, CH and IB for excitatory neurons, and FS, LTS and LS for inhibitory interneurons). Actually, the firing patterns displayed by inhibitory cells are way more diversified and an alternative
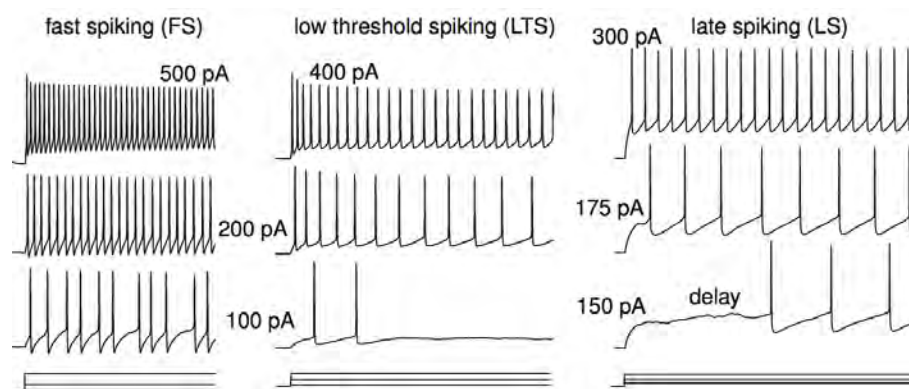
Figure 1.21. Fast spiking (left), low-threshold spiking (center) and late spiking (right) in response to sustained depolarizing pulses of various amplitudes (From (64)).

classification has been proposed for them.

In (92), the authors propose the following electrophysiological classes and subclasses to characterize interneurons firing patterns (see figure 1.22).

- *Non-accommodating (NAC)* neurons show tonic firing without spike frequency adaptation in response to a wide range of depolarizing current injections. Many FS and LS neurons exhibit this behavior. This class of discharge patterns has three subclasses: *c* (classic discharge), *b* (discharge with initial burst) and *d* (discharge with initial delay).

- *Accommodating (AC)* neurons fire tonically with spike adaptation. Hence they do not reach as high discharge frequencies as NAC cells do. While FS and LS interneurons can exhibit this behavior, most cells of this type are LTS neurons. This class admits the same subclasses as NAC discharges (c,b and d).

- *Stuttering (STUT)* can be displayed by some FS and LS cells. It consists in the firing of high frequency clusters of spikes (which are not bursts) separated by unpredictable periods of quiescence. The three subclasses c, b and d are also represented in stuttering patterns.

- *Bursting (BST):* Large basket cells are the only interneurons using bursting (BST) as their main signaling event. They fire bursts of spikes after a slow depolarizing wave, followed by strong slow hyperpolarization. This class has three subclasses: *i* (initial burst followed by regular spike emissions) , *r* (repetitive bursting) and *t* (transient, i.e. phasic burst).

- *Irregular spiking (IS)* cells fire single spikes, in a random fashion, and show strong accommodation. c and b subclasses are represented among irregular firing patterns.

1.5 PHENOMENOLOGICAL NEURON MODELS

The models presented in section 1.3 are based on a precise description of the neuronal basis of spike emission and are able to reproduce a wide class of neuronal behaviors, but are quite complex to handle mathematically and numerically. The aim of this section is to present simpler models aimed to reproduce the "pertinent information" of a neural code: the spike times. *Phenomenological neuron models* consist in modeling the times of emission of the action potential rather than the precise value of the membrane potential for any time.

1.5.1 Linear integrate-and-fire neuron models

Integrate-and-fire (IF) models are based on the assumption that a spike is emitted as soon a cell's membrane potential reaches a certain potential *threshold*. These models were first investigated by Lapicque (79; 80) who introduced those models before any substantial knowledge on the impulse generation mechanisms was acquired. These models have been widely studied and they keep very popular for their simplicity and their ability to reproduce many neuronal behaviors (67; 75; 108; 109; 118). The simplest integrate-and-fire model
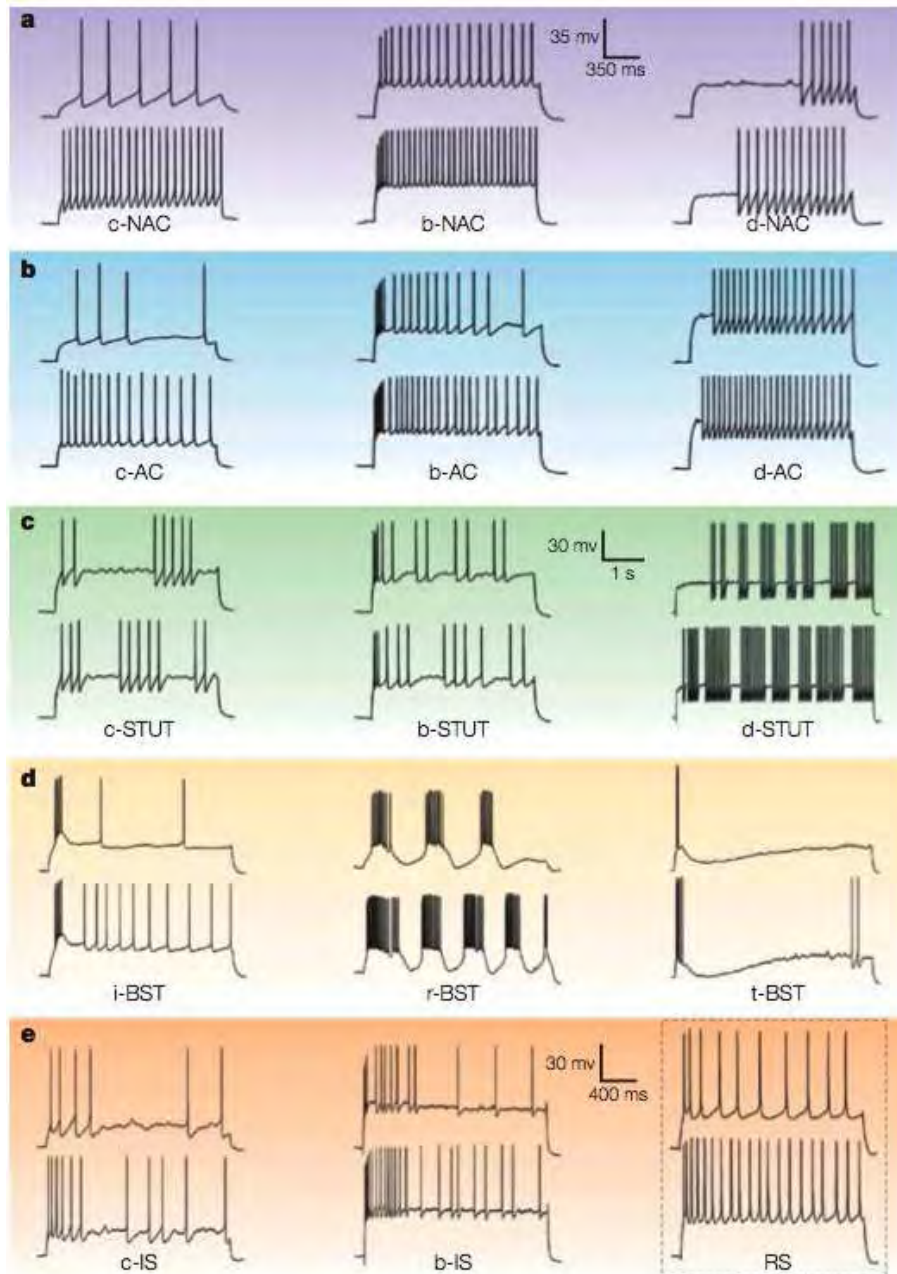
Figure 1.22. The five electrophysiological classes of interneurons (top to bottom) with their subclasses (left to right, see text). In the dashed-lined square at the bottom right corner of the table, examples of regular spiking from excitatory cells are shown for comparison (From (92)).

passively integrates the input. When the membrane potential reaches a threshold, a spike is emitted and the membrane potential is reset. From a biophysical point of view, the existence of a threshold is not clear. Platkiewitz and Brette currently try to define a threshold in a precise model such as the Hodgkin and Huxley model, and they showed that a certain separatrix curve in the phase plane can be considered as a spike threshold. We will see that we can get rid of this threshold by considering nonlinear models.

The Perfect Integrate-and-Fire model

The perfect integrate-and-fire model is the simplest model of this class. In this model, the membrane potential basically integrates the input current, fires when it reaches a constant threshold value θ and is subsequently reset a fixed value V_{reset}.

$$\begin{cases} C\frac{dV}{dt} & = I(t) \\ V(t_0^-) & = \theta \end{cases} \Rightarrow V(t_0) = V_{reset} \quad \oplus \quad \text{spike emitted} \tag{1.9}$$

This model is highly simplistic and unrealistic. Assume that the membrane potential is reset at time t_0. The next spike time for a general input current $I(\cdot)$ is given by

$$t_1 \stackrel{\text{def}}{=} \inf\{t > t_0, V_{reset} + \int_{t_0}^t I(s)\,ds \geq \theta)\}.$$

For a constant positive input current I, spikes are emitted at regular intervals of time, at a frequency $I/(C(\theta - V_{reset}))$, and therefore has type I excitability. Nevertheless, the fact that the input–frequency relation is linear is quite unrealistic. Moreover, we observe that second arbitrary small positive input current elicit spikes and spike trains generated by a constant input are perfectly regular.

The Leaky Integrate-and-Fire neuron

Incorporating the leak resistance of the membrane yields to the famous leaky integrate-and-fire model. The standard equation governing the membrane potential of a LIF neuron is given by:

$$C\frac{dV}{dt} + \frac{V}{R} = I(t) \tag{1.10}$$

If the membrane potential reaches a threshold value θ at time t_0 (i.e. $V(t_0^-) = \theta$) then a spike is emitted and the membrane potential is instantaneously reset to a constant value ($V(t_0) = V_{reset}$).

In its general version, the leaky integrate-and-fire model may incorporate an absolute refractory period. In this case, if V reaches θ at time t_0, the dynamics of V is frozen during a period of time Δ^{abs}. The classical integration (1.10) starts afresh at time $t_0 + \Delta^{\text{abs}}$ with the new initial condition V_{reset}.

This equation is linear, the related Green's function reads $e^{-t/RC}$, and $V(t)$ is determined in a closed form in function of the input current $I(t)$. For constant inputs one can readily prove that the neuron will spike only for inputs greater than $(\theta - V_{reset})/R$, and in that case, the time of the first spike reads:

$$T_{th} = -\tau_m \log\left(1 - \frac{\theta - V_{reset}}{RI}\right)$$

which gives the input-spike frequency relation. In the case where an absolute refractory is considered, the spike frequency f satisfies for subthreshold inputs:

$$f = \frac{1}{\Delta^{\text{abs}} - \tau_m \log\left(1 - \frac{\theta - V_{reset}}{RI}\right)}$$

In that case again, the neuron has type I excitability. This input–frequency is more realistic than the one of the perfect integrate-and-fire. Indeed, for currents below I_{th} no spike is triggered, at $I = I_{th}$, the slope of the f–I curve is infinite. For large currents, the firing rate saturates to the inverse of the refractory period, which means that the neuron spikes almost immediately after the refractory period. In the case where there is no refractory period, the frequency is unbounded, and has a linear asymptote of slope $\frac{1}{V_{th}C}$ (identical to the slope of the nonleaky unit).

Adaptation

In order to better account for the adaptation, Wehmeier and colleagues (120) introduced a time dependent shunting conductance g_{adapt} with reversal potential equal to the resting potential set at zero. Each spike increases the conductance by a fixed amount G_{spike}, and between the spikes, g_{adapt} decreases exponentially with a time constant τ_{adapt}. Such a variable emulates both the absolute and the relative refractory periods, and is referred in general as an *adaptation parameter*:

$$\begin{cases} C\frac{\mathrm{d}V}{\mathrm{d}t} = -\frac{V}{R} - g_{adapt}V + I \\ \tau_{adapt}\frac{\mathrm{d}g_{adapt}}{\mathrm{d}t} = -g_{adapt} \end{cases}$$

When V reaches the threshold θ at time t^*, a spike is generated and subsequently: g_{adapt} is increased by a fixed value G_{spike} (i.e. $g_{adapt}(t^*) = g_{adapt}(t^{*-}) + G_{spike}$) and V is reset to a constant value V_{reset}.

Time-dependent threshold

An alternative to these models is to consider a varying voltage threshold (see e.g. (20; 56)). A usual way to take it into account is to consider the threshold function $\theta(1 + \alpha e^{-(t-t')/\tau_{adapt}})$.

Resonate-and-fire neuron

The simplest model presenting type II excitability is called the resonate-and-fire (or Young) model (see (39; 123)). It is a two-dimensional extension of the integrate-and-fire model incorporating a second variable often interpreted as accounting for the low threshold persistant potassium current. Let W denote the magnitude of this current. The equation of the linear resonate-and-fire model reads:

$$\begin{cases} C\frac{\mathrm{d}V}{\mathrm{d}t} = I - g_{leak}(V - V_{leak}) - W \\ \dot{W} = (V - V_{1/2}) \end{cases}$$

In this model again, when the potential reaches a threshold, a spike is elicited and both the variables V and W are reset to constant values.

Random variability is often added to the parameters of these models (reset voltage, threshold, ...) in order to reproduce the variability observed in intracellular recordings. Nevertheless, all these models fail in reproducing some behaviors which are fundamentally nonlinear. This is what motivated some authors to introduce and study nonlinear integrate and fire neurons.

1.5.2 The nonlinear integrate-and-fire neuron models

Unidimensional models

These models were developed mainly to take into account the nonlinearities observed in the spike generation mechanisms. The most general *nonlinear* unidimensional integrate-and-fire model is governed by the equation:

$$\tau_m \frac{dV}{dt} = F(V) + G(V)I \tag{1.11}$$

As before, when the solution of this equation reaches the threshold θ, V is reset to a fixed value V_{reset} and a spike is emitted. $G(\cdot)$ can be interpreted as a voltage-dependant input resistance and $-F(V)/(V - V_{\mathrm{rest}})$ correspond to a voltage-dependant decay constant. The simplest of these models features a quadratic nonlinearity (16; 81; 82) given by the equation (1.12):

$$\frac{dV}{dt} = V^2 + I \tag{1.12}$$

This equation can blow up in finite time, i.e. the solution of this equation diverges to infinite for a finite time value. This explosion time is often considered as the spike time. Indeed, the solution of this equation with initial condition $V(t_0) = V_0$ reads:

$$V(t) = -\sqrt{A}\tan\left(-(t - t_0)\sqrt{A} - \arctan\left(\frac{V_0}{\sqrt{A}}\right)\right)$$

and since the tangent function diverges when its argument is $k\frac{\pi}{2}$ for $k \in \mathbb{Z}$.

Notice that $\dot{x} = b + x^2$ is a topological normal form for the saddle-node bifurcation. The properties of the bifurcation will drive the properties of the system when considering constant inputs. The right-hand side of the model is strictly greater than b, and hence if $b > 0$, the neuron will fire a periodic train of action potentials with a period

$$T = \frac{1}{\sqrt{b}}(\text{Arctan}\frac{\theta}{\sqrt{b}} - \text{Arctan}\frac{V_{\text{reset}}}{\sqrt{b}})$$

where θ is the spike threshold which can be possibly infinite. Hence the frequency scales as $\sqrt{b}$, as in the typical class 1 excitable systems. When $b < 0$, the system presents two equilibria, one of which being stable and corresponding to the neuron's resting state, and the other unstable and corresponding to the spike threshold. Unlike its linear predecessor, the quadratic integrate-and-fire neuron is a genuine integrator. It exhibits saddle-node bifurcation, it has a soft threshold, and it generates spikes with latencies, like many mammalian cells do. Besides, the model is canonical as proved by Ermentrout and Kopell (35) in the sense that the entire class of neuronal models near saddle-node on invariant circle bifurcation can be transformed into this model by a piecewise continuous change of variables

Nicolas Fourcaud-Trocmé and colleagues (41) proposed a similar model based on a modelization of the dynamic of the sodium activation variable which yields the exponential integrate-and-fire neuron, as an approximation of conductance based models, and show that this model reproduces the dynamics of simple conductance-based models and also intrinsic neuronal properties. The equation of the membrane potential in that case reads:

$$C\frac{du}{dt} = -g_l(u - E_l) + g_l\Delta_t e^{\frac{u-V_t}{\Delta_t}} + I \tag{1.13}$$

Romain Brette studied in (11) the general integrate-and-fire models. In this paper he models the spike map (i.e. the map giving the next interspike interval in function of the current one) and finds that, under conditions satisfied in particular by the periodically and aperiodically driven leaky integrator as well as some of its variants, the spike map is increasing on its range, which leaves no room for chaotic behavior, derives a rigorous expression of the Lyapunov exponent, and analyzes the periodically driven perfect integrator. He shows that the restriction of the phase map to its range is always conjugate to a rotation, and provides an explicit expression of the invariant measure.

Some of these models, complemented with adaptation, are presented in the next sections, together with a precise subthreshold potential and spikes mathematical studies.

Bidimensional Nonlinear IF models

Bidimensional nonlinear neuron models feature both the nonlinearity of the spike generation and a additional recovery variable. This type of phenomenological models will be discussed in depth in the following chapter.

One of these models is quite extensively studied by Eugene Izhikevich in his book (65). This model is called the quadratic integrate-and-fire model (or Izhikevich' model). In this book Izhikevich explains how to derive these equations from more detailed neuron models. The principle of his derivation consist in considering that the decision for spiking or not is made at the resting state, and fully depends on the shape of the nullclines around this point (see figure 1.23). To model the subthreshold behavior of such neurons and the initial segment of the up-stroke of an action potential, the principle is to consider only a small neighborhood of the rest state confined to the shaded square in figure 1.23, since the rest of the phase space is considered to encode only the peak and the down-stroke of the action potential. Since the shape of the action potential is stereotyped, it is less important than the subthreshold dynamics leading to this action potential, then we can retain detailed information about the left knee and its neighborhood and simplify the vector field outside the neighborhood.

Quadratic Adaptive Integrate-and-fire (Izhikevich') model   Eugene Izhikevich (62) proposed a model combining both Latham's quadratic nonlinearity and an adaptation variable. Because of the quadratic term, the membrane potential variable can escape to infinity in finite time. This corresponds to the upstroke corresponding to the firing of an action potential. The modeling of the downstroke is quite sharp: it is considered as an instantaneous reset for the membrane potential variable V, while the adaptation variable w is augmented by a fixed amount w_{reset} modeling the spike-triggered adaptation. Appropriate rescalings lead to the more classical minimal quadratic model:

$$\begin{cases} \dot{v} &= v^2 - w + I \\ \dot{w} &= a(bv - w) \end{cases}$$
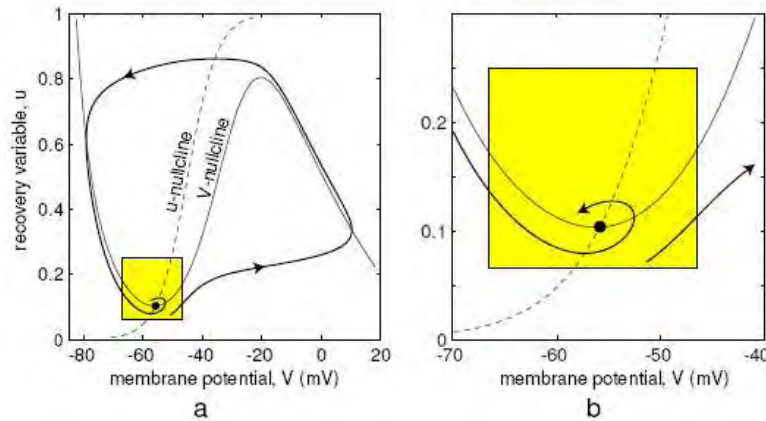
Figure 1.23. Phase portrait for a model having a potential variable V and a recovery variable u. The principle of the approximation is to focus on the dynamics around the fixed point (from (64)).
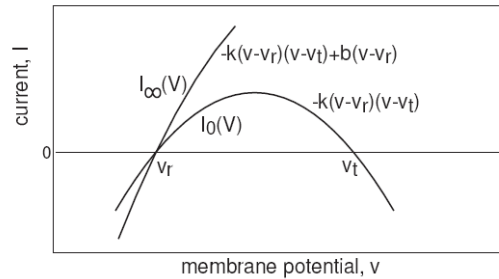
Figure 1.24. The relationship between the parameters of the simple model and instantaneous and steady state I–V relations, $I_0(V)$ and $I_\infty(V)$

This model can be also derived via the analysis of I–V relationships. This point of view allows one to derive the parameters of the simple model using instantaneous (peak) and steady-state I-V relations. More precisely, let us write the system in the following equivalent form:

$$\begin{cases} C\dot{v} = k(v-v_r)(v-v_t) - w + I & \text{if } v \geq v_{peak} \text{ then} \\ u = a\{b(v-v+r) - w\} & v \leftarrow c;\ u \leftarrow u+d \end{cases}$$

where v is the membrane potential, w is the recovery current, and C is the membrane capacitance. The quadratic polynomial $k(v-v_r)(v-v_t)$ approximates the subthreshold part of the instantaneous I–V relation $I_0(V)$. Here, v_r is the resting membrane potential, and v_t is the instantaneous threshold potential, as in Fig. 1.24. That is, instantaneous depolarizations above v_t result in spike response. The polynomial $k(v-v_r)(v-v_t) + b(v-v_r)$ approximates the subthreshold part of the steady-state I–V relation $I_1(V)$. When $b < 0$, its maximum approximates the rheobase current of the neuron, i.e., the minimal amplitude of a DC-current needed to fire a cell. Its derivative with respect to v at $v = v_r$, i.e., $b - k(v_r - v_t)$s, corresponds to the resting input conductance, which is the inverse of the input resistance. Knowing both the rheobase and the input resistance of a neuron, one could determine the parameters k and b.

This model nevertheless loses the good property of having a soft threshold, as discussed in chapter 5.

Adaptive exponential integrate-and-fire model Following the ideas of Izhikevich, Romain Brette and Wulfram Gerstner (13) used the exponential nonlinearity proposed by Fourcaud-Trocme and collaborators (41) together with an adaptation variable. This model is interesting because its parameters can be easily related to physiological quantities, and the model has been successfully fit to a biophysical model of a regular spiking pyramidal cell and to real recordings of pyramidal cells (23; 69).

1.6 CONCLUSION

In this chapter we briefly presented the functioning of nerve cells and the overall structure of the brain. Related to these phenomena, we presented some models to emulate the processes in play, from detailed models emulating the behaviors of each component of the nerve cell to the phenomenological models aimed to reproduce globally the behavior of nerve cells. We also discussed the origin of noise and different types of modelizations for noisy synaptic inputs. Phenomenological models such as the adaptive nonlinear models will be studied in depth in the next chapters.

2

SUBTHRESHOLD DYNAMICS OF BIDIMENSIONAL NONLINEAR INTEGRATE-AND-FIRE NEURONS

OVERVIEW

In this chapter we define a new class of bidimensional integrate-and-fire neuron models being computationally efficient and biologically plausible, i.e., able to reproduce a wide range of behaviors observed in in vivo or in vitro recordings of cortical neurons. This class includes, for instance, two models widely used in computational neuroscience, the Izhikevich' quadratic integrate-and-fire model and the Brette–Gerstner's adaptive exponential models we introduced in section 1.5.2. These models are hybrid dynamical systems defined both by a continuous dynamics, the subthreshold behavior, and a discrete dynamics, the spike and reset process. This chapter is devoted to the study of the subthreshold system. We provide the full local subthreshold bifurcation diagram of the members of this class and show that they all present the same bifurcations: an Andronov-Hopf bifurcation manifold, a saddle-node bifurcation manifold, a Bogdanov-Takens bifurcation, and possibly a Bautin bifurcation, i.e., all codimension two local bifurcations in a two-dimensional phase space except the cusp. Among other global bifurcations, this system shows a saddle homoclinic bifurcation curve. We show how this bifurcation diagram generates the most prominent cortical neuron behaviors. This very general study will lead us to introduce a new neuron model, the *quartic model*, able to reproduce all the behaviors of the Izhikevich and Brette-Gerstner models and also self-sustained subthreshold oscillations, which are of great interest in neuroscience and that the two classical models cannot reproduce. This work was published in SIAM Journal on Applied Mathematics (114), and is the first part of the full study of this class of models. The next chapter will be devoted to the study of the spiking mechanism and will provide a better understanding of the spike patterns generated. The full study of these models will eventually lead us to define electrophysiological classes of neurons, i.e. sets of parameters for which the model behaves the same way in response to different kinds of stimulations. We deal with classifying the models with respect to their electrophysiological class in chapter 4.

INTRODUCTION

During the past few years, in the neurocomputing community, the problem of finding a computationally simple and biologically realistic model of neuron has been widely studied, in order to be able to compare experimental recordings with numerical simulations of large-scale brain models. The key problem is to find a model of neuron realizing a compromise between its simulation efficiency and its ability to reproduce what is observed at the cell level, often considering in-vitro experiments (63; 77; 104).

Among the numerous neuron models, from the detailed Hodgkin–Huxley model (54) still considered as the reference, but unfortunately computationally intractable when considering neuronal networks, down to the simplest integrate-and-fire model (43) very effective computationally, but unrealistically simple and unable to reproduce many behaviors observed, two models seem to stand out (63): the adaptive quadratic (Izhikevich (62) and related models such as the theta model with adaptation (34; 50)) and exponential (Brette and Gerstner (13)) neuron models. These two models are computationally almost as efficient as the integrate-and-fire model. The Brette–Gerstner model involves an exponential function, which needs to be tabulated if we want the algorithm to be efficient. They are also biologically plausible, and reproduce several important neuronal regimes with a good adequacy with biological data, especially in high-conductance states, typical of cortical in vivo activity. Nevertheless, they fail in reproducing deterministic self-sustained subthreshold oscillations, a behavior of particular interest in cortical neurons for the precision and robustness of spike generation patterns, for instance in the inferior olive nucleus (9; 89; 90), in the stellate cells of the entorhinal cortex (2; 3; 71), and in the dorsal root ganglia (DRG) (5; 85; 86). Some models have been introduced to study from a theoretical point of view the currents involved in the generation of self-sustained subthreshold oscillations (121), but the model failed in reproducing lots of other neuronal behaviors.

The aim of this chapter is to define and study a general class of neuron models, containing the Izhikevich and Brette–Gerstner models, from a dynamical systems point of view. We characterize the local bifurcations of these models and show how their bifurcations are linked with different biological behaviors observed in the cortex. This formal study will lead us to define a new model of neuron, whose behaviors include those of the Izhikevich–Brette–Gerstner (IBG) models but also self-sustained subthreshold oscillations.

In the first section, we introduce a general class of nonlinear neuron models which contains the IBG models. We study the fixed-point bifurcation diagram of the elements of this class, and show that they present the same local bifurcation diagram, with a saddle-node bifurcation curve, an Andronov–Hopf bifurcation curve, a Bogdanov–Takens bifurcation point, and possibly a Bautin bifurcation, i.e., all codimension two bifurcations in dimension two except the cusp. This analysis is applied in the second section to the Izhikevich and the Brette–Gerstner models. We derive their bifurcation diagrams and prove that none of them shows the Bautin bifurcation. In the third section, we introduce a new simple model—the *quartic model*—presenting, in addition to common properties of the dynamical system of this class, a Bautin bifurcation, which can produce self-sustained oscillations. Last, the fourth section is dedicated to numerical experiments. We show that the quartic model is able to reproduce some of the prominent features of biological spiking neurons. We give qualitative interpretations of those different neuronal regimes from the dynamical systems point of view, in order to give a grasp of how the bifurcations generate biologically plausible behaviors. We also show that the new quartic model, presenting supercritical Hopf bifurcations, is able to reproduce the oscillatory/spiking behavior presented, for instance, in the DRG. Finally, we show that numerical simulation results of the quartic model show a good agreement with biological intracellular recordings in the DRG.

2.1 BIFURCATION ANALYSIS OF A CLASS OF NONLINEAR NEURON MODELS

In this section we introduce a large class of formal neurons which are able to reproduce a wide range of neuronal behaviors observed in cortical neurons. This class of models is inspired by the review made by Izhikevich (63). He found that the quadratic adaptive integrate-and-fire model was able to simulate efficiently a lot of interesting behaviors. Brette and Gerstner (13) defined a similar model of neuron which presented a good adequacy between simulations and biological recordings.

We generalize these models, and define a new class of neuron models, wide but specific enough to keep the diversity of behaviors of the IBG models.

2.1.1   The general class of nonlinear models

In this chapter, we are interested in neurons defined by a dynamical system of the type

$$\begin{cases} \frac{\mathrm{d}v}{\mathrm{d}t} = F(v) - w + I, \\ \frac{\mathrm{d}w}{\mathrm{d}t} = a(bv - w), \end{cases}$$

where a, b, and I are real parameters and F is a real function.[1]

In this equation, v represents the membrane potential of the neuron, w is the adaptation variable, I represents the input intensity of the neuron, $1/a$ is the characteristic time of the adaptation variable, and b accounts for the interaction between the membrane potential and the adaptation variable.[2]

This equation is a very general model of neuron. For instance when F is a polynomial of degree three, we obtain a FitzHugh–Nagumo model, when F is a polynomial of degree two the Izhikevich neuron model (62), and when F is an exponential function the Brette–Gerstner model (13). However, in contrast with continuous models like the FitzHugh–Nagumo model (43), the two latter cases diverge when spiking, and an external reset mechanism is used after a spike is emitted.

In this chapter, we want this class of models to have common properties with the IBG neuron models. To this purpose, let us make some assumptions on the function F. The first assumption is a regularity assumption.

Assumption 2.1.1. F is at least three times continuously differentiable.

A second assumption is necessary to ensure us that the system would have the same number of fixed points as the IBG models.

Assumption 2.1.2. The function F is strictly convex.

Definition 2.1.1 (convex neuron model). We consider the two-dimensional model defined by the equations

$$\begin{cases} \frac{\mathrm{d}v}{\mathrm{d}t} = F(v) - w + I, \\ \frac{\mathrm{d}w}{\mathrm{d}t} = a(bv - w), \end{cases} \tag{2.1}$$

where F satisfies Assumptions 2.1.1 and 2.1.2 and characterizes the passive properties of the membrane potential.

Many neurons of this class blow up in finite time. These neurons are the ones we are interested in.

Remark 1. Note that all the neurons of this class do not blow up in finite time. For instance if $F(v) = v\log(v)$, it will not. For F functions such that $F(v) = (v^{1+\alpha})R(v)$ for some $\alpha > 0$, where $\lim_{v \to \infty} R(v) > 0$ (possibly ∞), the dynamical system will possibly blow up in finite time. We prove this property in chapter 3, and we will further prove that if $F(v) = (v^{2-\alpha})R(v)$ for some $\alpha > 0$ where $R(v)$ tends to a finite limit, the adaptation value at the explosion time of v also blows up whereas if $F(v) = (v^{2+\alpha})R(v)$ for some $\alpha > 0$, where $\lim_{v \to \infty} R(v) > 0$ (possibly ∞), then the adaptation at the explosion times of the spike will have finite limits.

If the solution blows up at time t^* or reaches a finite cutoff value, a spike is emitted, and subsequently we have the following reset process:

$$\begin{cases} v(t^*) = v_r, \\ w(t^*) = w(t^{*-}) + d, \end{cases} \tag{2.2}$$

where v_r is the reset membrane potential and $d > 0$ a real parameter. Equations (2.1) and (2.2), together with initial conditions (v_0, w_0), give us the existence and uniqueness of a solution on $\mathbb{R}^+$.

The two parameters v_r and d are important to understand the repetitive spiking properties of the system, and will be studied in depth in chapter 3. In the present chapter we focus on the bifurcations of the subthreshold dynamical system with respect to (a, b, I), in order to characterize the behavior of the neuron before spiking (and blowing up).

---

[1]The same study can be done for a parameter-dependent function. More precisely, let $E \subset \mathbb{R}^n$ be a parameter space (for a given n) and $F : E \times \mathbb{R} \to \mathbb{R}$ a parameter-dependent real function. All the properties shown in this section are valid for any fixed value of the parameter p. Further p-bifurcations studies can be done for specific $F(p, \cdot)$. The first equation can be derived from the general I-V relation in neuronal models: $C\frac{\mathrm{d}V}{\mathrm{d}t} = I - I_0(V) - g(V - E_K)$, where $I_0(V)$ is the instantaneous I-V curve.

[2]See, for instance, section 2.2.2, where the parameters of the initial equation (2.26) are related to biological constants and where we proceed to a dimensionless reduction.

2.1.2 Fixed points of the system

To understand the qualitative behavior of the dynamical system defined by (2.1) before the blow up (i.e., between two spikes), we begin by studying the fixed points and analyze their stability. The linear stability of a fixed point is governed by the Jacobian matrix of the system, which we define in the following proposition.

Proposition 2.1.1. The Jacobian of the dynamical system (2.1) can be written

$$L := v \mapsto \begin{pmatrix} F'(v) & -1 \\ ab & -a \end{pmatrix}. \tag{2.3}$$

The fixed points of the system satisfy the equations

$$\begin{cases} F(v) - bv + I = 0, \\ bv = w. \end{cases} \tag{2.4}$$

Let $G_b(v) := F(v) - bv$. From 2.1.1 and 2.1.2, we know that the function G_b is strictly convex and has the same regularity as F. To have the same behavior as the IBG models, we want the system to have the same number of fixed points. To this purpose, it is necessary that G_b has a minimum for all $b > 0$. Otherwise, the *convex* function G_b would have no more than one fixed point, since a fixed point of the system is the intersection of an horizontal curve and G_b.

This means for the function F that $\inf_{x \in \mathbb{R}} F'(x) \leq 0$ and $\sup_{x \in \mathbb{R}} F'(x) = +\infty$. Using the monotony property of F', we write Assumption 2.1.3.

Assumption 2.1.3.

$$\begin{cases} \lim_{x \to -\infty} F'(x) \leq 0, \\ \lim_{x \to +\infty} F'(x) = +\infty. \end{cases}$$

Assumptions 2.1.1, 2.1.2, and 2.1.3 ensure us that for all $b \in \mathbb{R}_+^*$, G_b has a unique minimum, denoted $m(b)$, which is reached. Let $v^*(b)$ be the point where this minimum is reached.

This point is the solution of the equation

$$F'(v^*(b)) = b. \tag{2.5}$$

Proposition 2.1.2. The point $v^*(b)$ and the value $m(b)$ are continuously differentiable with respect to b.

Proof. We know that F' is a bijection. The point $v^*(b)$ is defined implicitly by the equation $H(b,v) = 0$, where $H(b,v) = F'(v) - b$. H is a C^1-diffeomorphism with respect to b, and the differential with respect to b never vanishes. The implicit function theorem (see, for instance, (37, Annex C.6)) ensures us that $v^*(b)$ solution of $H(b,v^*(b)) = 0$ is continuously differentiable with respect to b, and so does $m(b) = F(v^*(b)) - bv^*(b)$. □

Theorem 2.1.3. *The parameter curve defined by $\{(I,b); I = -m(b)\}$ separates three behaviors of the system (see Figure 2.1):*

(i) *If $I > -m(b)$, then the system has no fixed point.*

(ii) *If $I = -m(b)$, then the system has a unique fixed point, $(v^*(b), w^*(b))$, which is nonhyperbolic. It is unstable if $b > a$.*

(iii) *If $I < -m(b)$, then the dynamical system has two fixed points $(v_-(I,b), v_+(I,b))$ such that*

$$v_-(I,b) < v^*(b) < v_+(I,b).$$

The fixed point $v_+(I,b)$ is a saddle fixed point, and the stability of the fixed point $v_-(I,b)$ depends on I and on the sign of $(b-a)$:

(a) *If $b < a$, the fixed point $v_-(I,b)$ is attractive.*

(b) *If $b > a$, there is a unique smooth curve $I^*(a,b)$ defined by the implicit equation $F'(v_-(I^*(a,b),b)) = a$. This curve reads $I^*(a,b) = bv^*(a) - F(v^*(a))$, where $v^*(a)$ is the unique solution of $F'(v^*(a)) = a$.*

    (b.1) *If $I < I^*(a,b)$, the fixed point is attractive.*

    (b.2) *If $I > I^*(a,b)$, the fixed point is repulsive.*

Proof.
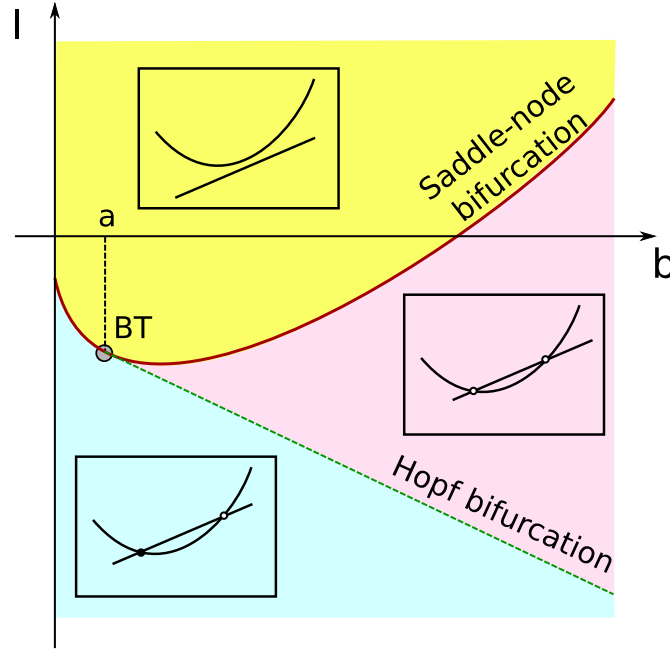
Figure 2.1. Number of fixed points and their stability in the plane (I, b) for the exponential adaptive model.

(i) We have $F(v) - bv \geq m(b)$ by definition of $m(b)$. If $I > -m(b)$, then for all $v \in \mathbb{R}$ we have $F(v) - bv + I > 0$ and the system has no fixed point.

(ii) Let $I = -m(b)$. We have already seen that G_b is strictly convex and continuously differentiable and for $b > 0$ reaches its unique minimum at the point $v^*(b)$. This point is such that $G_b(v^*(b)) = m(b)$, and so it is the only point satisfying $F(v^*(b)) - bv^*(b) - m(b) = 0$.

Furthermore, this point satisfies $F'(v^*(b)) = b$. The Jacobian of the system at this point reads

$$L(v^*(b)) = \begin{pmatrix} b & -1 \\ ab & -a \end{pmatrix}.$$

Its determinant is 0, and so the fixed point is nonhyperbolic (0 is eigenvalue of the Jacobian matrix). The trace of this matrix is $b - a$. So the fixed point $v^*(b)$ is attractive when $b > a$ and repulsive when $b > a$. The case $a = b$, $I = -m(b)$ is a degenerate case which we will study more precisely in section 2.1.3.

(iii) Let $I < -m(b)$. By the strict convexity assumption, Assumption 2.1.2, of the function G together with Assumption 2.1.3, we know that there are only two intersections of the curve G to a level $-I$ higher than its minimum. These two intersections define our two fixed points. At the point v^* the function is strictly lower than $-I$, and so the two solutions satisfy $v_-(I, b) < v^*(b) < v_+(I, b)$.

Let us now study the stability of these two fixed points. To this end, we have to characterize the eigenvalues of the Jacobian matrix of the system at these points.

We can see from formula (2.3) and the convexity assumption, Assumption 2.1.2, that the Jacobian determinant, equal to $-aF'(v) + ab$, is a decreasing function of v and vanishes at $v^*(b)$, and so $\det(L(v_+(I, b))) < 0$ and the fixed point is a saddle point (the Jacobian matrix has a positive and a negative eigenvalue).

For the other fixed point $v_-(I, b)$, the determinant of the Jacobian matrix is strictly positive. So the stability of the fixed point depends on the trace of the Jacobian. This trace reads $F'\big(v_-(I, b)\big) - a$.

  (a) When $b < a$, we have a stable fixed point. Indeed, the function F' is an increasing function equal to b at $v^*(b)$, and so $\text{Trace}\big(L(v_-(I, b))\big) \leq F'(v^*(b)) - a = b - a < 0$ and the fixed point is attractive.

  (b) If $b > a$, then the type of dynamics around the fixed point v_- depends on the input current (parameter I). Indeed, the trace reads

$$T(I, b, a) := F'\big(v_-(I, b)\big) - a,$$

which is continuous and continuously differentiable with respect to I and b, and which is defined for $I < -m(b)$. We have

$$\begin{cases} \lim_{I \to -m(b)} T(I,b,a) = b - a > 0, \\ \lim_{I \to -\infty} T(I,b,a) = \lim_{x \to -\infty} F'(x) - a < 0. \end{cases}$$

So there exists a curve $I^*(a,b)$ defined by $T(I,b,a) = 0$ and such that

- for $I^*(b) < I < -m(b)$, the fixed point $v_-(I,b)$ is repulsive;
- for $I < I^*(b)$, the fixed point v_- is attractive.

To compute the equation of this curve, we use the fact that point $v_-(I^*(b),b)$ is such that $F'(v_-(I^*(b),b)) = a$. We know from the properties of F that there is a unique point $v^*(a)$ satisfying this equation. Since $F'(v^*(b)) = b$, $a < b$, and F' is increasing, the condition $a < b$ implies that $v^*(a) < v^*(b)$.

The associated input current satisfies fixed points equation $F(v^*(a)) - bv^*(a) + I^*(a,b) = 0$, or equivalently

$$I^*(a,b) = bv^*(a) - F(v^*(a)).$$

The point $I = I^*(a,b)$ will be studied in detail in the next section, since it is a bifurcation point of the system.

$\square$

Figure 2.1 represents the different zones enumerated in Theorem 2.1.3 and their stability in the parameter plane (I,b).

Remark 2. In this proof, we used the fact that F' is invertible on $[0,\infty)$. Assumption 2.1.3 is the weakest possible to ensure that this will be the case and that F has a unique minimum.

2.1.3 Bifurcations of the system

In the study of the fixed points and their stability, we identified two bifurcation curves where the stability of the fixed points changes. The first curve $I = -m(b)$ corresponds to a saddle-node bifurcation and the curve $I = I^*(a,b)$ to an Andronov–Hopf bifurcation. These two curves meet in a specific point, $b = a$ and $I = -m(a)$. This point has a double 0 eigenvalue (a nilpotent Jacobian matrix), and we show that it is a Bogdanov–Takens bifurcation point.

Let us show that the system undergoes these bifurcations with no other assumption than 2.1.1, 2.1.2, and 2.1.3 on F. We also prove that the system can undergo only one other codimension two bifurcation, a Bautin bifurcation, and that there is no other bifurcation of codimension two or three.

Saddle-node bifurcation curve

In this section we characterize the behavior of the dynamical system along the curve of equation $I = -m(b)$, and we prove the following theorem.

Theorem 2.1.4. *The dynamical system* (2.1) *undergoes a saddle-node bifurcation along the parameter curve:*

$$(SN) : \{(b,I)\,;\, I = -m(b)\}, \tag{2.6}$$

when $F''(v^*(b)) \neq 0$.

Proof. We derive the normal form of the system at this bifurcation point. Following the works of Guckenheimer and Holmes (48) and Kuznetsov (78), we check the genericity conditions to ensure that the normal form at the bifurcation point will have the expected form.

Let $b \in \mathbb{R}^+$ and $I = -m(b)$. Let $v^*(b)$ be the unique fixed point of the system for these parameters. The point $v^*(b)$ is the unique solution of $F'(v^*(b)) = b$. At this point, the Jacobian matrix (2.3) reads

$$L(v^*(b)) = \begin{pmatrix} b & -1 \\ ab & -a \end{pmatrix}.$$

This matrix has two eigenvalues 0 and $b - a$. The pairs of right eigenvalues and right eigenvectors are

$$0, U := \begin{pmatrix} 1/b \\ 1 \end{pmatrix} \quad \text{and} \quad b - a, \begin{pmatrix} 1/a \\ 1 \end{pmatrix}.$$

Its pairs of left eigenvalues and left eigenvectors are

$$0, V := (-a, 1) \quad \text{and} \quad b - a, (-b, 1).$$

Let $f_{b,I}$ be the vector field

$$f_{b,I}(v, w) = \begin{pmatrix} F(v) - w + I \\ a(bv - w) \end{pmatrix}.$$

The vector field satisfies

$$V \left(\frac{\partial}{\partial I} f_{b,I}(v^*(b), w^*(b)) \right) = (-a, 1) \cdot \begin{pmatrix} 1 \\ 0 \end{pmatrix}$$
$$= -a < 0.$$

So the coefficient of the normal form corresponding to the Taylor expansion along the parameter I does not vanish.

Finally, let us show that the quadratic terms of the Taylor expansion in the normal form does not vanish. With our notations, this condition reads

$$V \left(D_x^2 f_{b,-m(b)}(v^*(b), w^*(b))(U, U) \right) \neq 0.$$

This property is satisfied in our framework. Indeed,

$$V \left(D_x^2 f_{b,-m(b)}(v^*(b), w^*(b))(U, U) \right) = V \left(\begin{pmatrix} U_1^2 \frac{\partial^2 f_1}{\partial v^2} + 2U_1 U_2 \frac{\partial^2 f_1}{\partial v \partial w} + U_2^2 \frac{\partial^2 f_1}{\partial w^2} \\ U_1^2 \frac{\partial^2 f_2}{\partial v^2} + 2U_1 U_2 \frac{\partial^2 f_2}{\partial v \partial w} + U_2^2 \frac{\partial^2 f_2}{\partial w^2} \end{pmatrix} \right)$$
$$= V \left(\begin{pmatrix} \frac{1}{b^2} F''(v^*) \\ 0 \end{pmatrix} \right)$$
$$= (-a, 1) \cdot \begin{pmatrix} \frac{1}{b^2} F''(v^*) \\ 0 \end{pmatrix}$$
$$= -\frac{a}{b^2} F''(v^*) < 0.$$

So the system undergoes a saddle-node bifurcation along the manifold $I = -m(b)$. $\qquad\square$

Remark 3. Note that $F''(v^*(b))$ can vanish only countably many times since F is strictly convex.

Andronov–Hopf bifurcation curve

In this section we consider the behavior of the dynamical system along the parameter curve $I = I^*(b)$, and we consider the fixed point v_-.

Theorem 2.1.5. *Let $b > a$, $v^*(a)$ be the unique point such that $F'(v^*(a)) = a$ and $A(a,b)$ be defined by the formula*

$$A(a,b) := F'''(v^*(a)) + \frac{1}{b-a} \left(F''(v^*(a)) \right)^2. \tag{2.7}$$

If $F''(v^*(a)) \neq 0$ and $A(a,b) \neq 0$, then the system undergoes an Andronov–Hopf bifurcation at the point $v^*(a)$, along the parameter line

$$(AH) := \left\{ (b, I) \; ; \; b > a \text{ and } I = bv^*(a) - F(v^*(a)) \right\}. \tag{2.8}$$

This bifurcation is subcritical if $A(a,b) > 0$ and supercritical if $A(a,b) < 0$.

Proof. The Jacobian matrix at the point $v^*(a)$ reads

$$L(v^*(a)) = \begin{pmatrix} a & -1 \\ ab & -a \end{pmatrix}.$$

Its trace is 0 and its determinant is $a(b-a) > 0$, and so the matrix at this point has a pair of pure imaginary eigenvalues $(i\omega, -i\omega)$, where $\omega = \sqrt{a(b-a)}$. Along the curve of equilibria when I varies, the eigenvalues are complex conjugates with real part $\mu(I) = \frac{1}{2} \text{Tr}\big(L(v_-(I, b))\big)$ which vanishes at $I = I^*(a, b)$.

We recall that from Proposition 2.1.2, this trace varies smoothly with I. Indeed, $v_-(b,I)$ satisfies $F(v_-(I,b)) - bv_-(I,b) + I = 0$ and is differentiable with respect to I. We have

$$\frac{\partial v_-(I,b)}{\partial I}(F'(v_-(I,b)) - b) = -1.$$

At the point $v_-(I^*(b),b) = v^*(a)$, we have $F'(v^*(a)) = a < b$, and so for I close to this equilibrium point, we have

$$\frac{\partial v_-(I,b)}{\partial I} > 0.$$

Now let us check that the transversality condition of an Andronov–Hopf bifurcation is satisfied (see (48, Theorem 3.4.2)). There are two conditions to be satisfied: the transversality condition $\frac{d\mu(I)}{dI} \neq 0$ and the nondegeneracy condition $l_1 \neq 0$, where l_1 is the first Lyapunov coefficient at the bifurcation point.

First of all, we prove that the transversality condition is satisfied:

$$\mu(I) = \frac{1}{2}\mathrm{Tr}(L(v_-(I,b)))$$
$$= \frac{1}{2}(F'(v_-(I,b)) - a),$$
$$\frac{d\mu(I)}{dI} = \frac{1}{2}F''(v_-(I,b))\frac{dv_-(I,b)}{dI}$$
$$> 0.$$

Let us now write the normal form at this point. To this purpose, we change variables:

$$\begin{cases} v - v^*(a) = x, \\ w - w_a = ax + \omega y. \end{cases}$$

The (x,y) equation reads

$$\begin{cases} \dot{x} = -\omega y + (F(x + v^*(a)) - ax - w_a) =: -\omega y + f(x), \\ \dot{y} = \omega x + \frac{a}{\omega}(ax - F(x + v^*(a)) + w_a - I) =: \omega x + g(x). \end{cases} \tag{2.9}$$

According to Guckenheimer in (48), we state that the Lyapunov coefficient of the system at this point has the same sign as B, where B is defined by

$$B := \frac{1}{16}[f_{xxx} + f_{xyy} + g_{xxy} + g_{yyy}] + \frac{1}{16\omega}[f_{xy}(f_{xx} + f_{yy}) - g_{xy}(g_{xx} + g_{yy}) - f_{xx}g_{xx} + f_{yy}g_{yy}].$$

Replacing f and g by the expressions found in (2.9), we obtain the expression of A:

$$B = \frac{1}{16}F'''(v^*(a)) + \frac{a}{16\omega^2}(F''(v^*(a)))^2$$
$$= \frac{1}{16}F'''(v^*(a)) + \frac{1}{16(b-a)}(F''(v^*(a)))^2$$
$$= \frac{1}{16}A(a,b).$$

Hence when $A(a,b) \neq 0$, the system undergoes an Andronov–Hopf bifurcation. When $A(a,b) > 0$, the bifurcation is subcritical and the periodic orbits generated by the Hopf bifurcation are repelling, and when $A(a,b) < 0$, the bifurcation is supercritical and the periodic orbits are attractive (the formula of A has also been introduced by Izhikevich in (65, eq. (15), p. 213)). $\qquad\square$

Remark 4. The case $A(a,b) = 0$ is not treated in the theorem and is a little bit more intricate. We fully treat it in section 2.1.3 and show that a Bautin (generalized Hopf) bifurcation can occur if the A-coefficient vanishes. Since the third derivative is a priori unconstrained, this case can occur, and we prove in section 2.3 that this is the case for a simple (quartic) model.

Bogdanov–Takens bifurcation

We have seen in the study that this formal model presents an interesting point in the parameter space, corresponding to the intersection of the saddle-node bifurcation curve and the Andronov–Hopf bifurcation curve. At this point, we show that the system undergoes a Bogdanov–Takens bifurcation.

Theorem 2.1.6. *Let F be a real function satisfying Assumptions* 2.1.1, 2.1.2, *and* 2.1.3. *Let $a \in \mathbb{R}_+^*$ and $b = a$, and let $v^*(a)$ be the only point such that $F'(v^*(a)) = a$. Assume again that $F''(v^*(a)) \neq 0$.*

Then at this point and with these parameters, the dynamical system (2.1) *undergoes a subcritical Bogdanov–Takens bifurcation of normal form:*

$$\begin{cases} \dot{\eta}_1 = \eta_2, \\ \dot{\eta}_2 = \left(\frac{8F''(v^*(a))aI_1}{(a+b_1)^3} \right) - \left(\frac{2(2b_1 a + I_1 F''(v^*(a)))}{(a+b_1)^2} \right) \eta_1 + \eta_1^2 + \eta_1 \eta_2 + \mathscr{O}(\|\eta\|^3), \end{cases} \tag{2.10}$$

where $b_1 := b - a$ and $I_1 = I + m(a)$.

Proof. The Jacobian matrix (2.3) at this point reads

$$L(v^*(a)) = \begin{pmatrix} a & -1 \\ a^2 & -a \end{pmatrix}.$$

This matrix is nonzero and has two 0 eigenvalues (its determinant and trace are 0). The matrix $Q := \begin{pmatrix} a & 1 \\ a^2 & -a \end{pmatrix}$ is the passage matrix to the Jordan form of the Jacobian matrix:

$$Q^{-1} \cdot L(v^*(a)) \cdot Q = \begin{pmatrix} 0 & 1 \\ 0 & 0 \end{pmatrix}.$$

To prove that the system undergoes a Bogdanov–Takens bifurcation, we show that the normal form reads

$$\begin{cases} \dot{\eta}_1 = \eta_2, \\ \dot{\eta}_2 = \beta_1 + \beta_2 \eta_1 + \eta_1^2 + \sigma \eta_1 \eta_2 + \mathscr{O}(\|\eta\|^3) \end{cases} \tag{2.11}$$

with $\sigma = \pm 1$. The proof of this theorem consists of (i) proving that the system undergoes a Bogdanov–Takens bifurcation, (ii) finding a closed-form expression for the variables β_1 and β_2, and (iii) proving that $\sigma = 1$.

First of all, let us prove that the normal form can be written in the form of (2.11). This is equivalent to showing some transversality conditions on the system (see, for instance, (78, Theorem 8.4)).

To this end, we center the equation at this point and write the system in the coordinates given by the Jordan form of the matrix. Let $\begin{pmatrix} y_1 \\ y_2 \end{pmatrix} = Q^{-1} \begin{pmatrix} v - v^*(a) \\ w - w_a \end{pmatrix}$ at the point $b = a + b_1$, $I = -m(a) + I_1$. We get

$$\begin{cases} \dot{y}_1 = y_2 + \frac{b_1}{a}(ay_1 + y_2), \\ \dot{y}_2 = F(ay_1 + y_2 + v^*(a)) - w_a - m(a) + I_1 - a^2 y_1 - a y_2 - b_1(ay_1 + y_2). \end{cases} \tag{2.12}$$

Let us denote $v_1 = ay_1 + y_2$. The Taylor expansion on the second equation gives us

$$\begin{aligned} \dot{y}_2 &= F(v_1 + v^*(a)) - w_a - m(a) + I_1 - a^2 y_1 - a y_2 - b_1(ay_1 + y_2) \\ &= F(v^*(a)) + F'(v^*(a))v_1 + \frac{1}{2}F''(v^*(a))v_1^2 - w_a - m(a) \\ &\quad + I_1 - a^2 y_1 - a y_2 - b_1(ay_1 + y_2) + \mathscr{O}(\|v_1\|^3) \\ &= (F(v^*(a)) - w_a - m(a)) + I_1 + (F'(v^*(a)) - a)v_1 - b_1 v_1 + \frac{1}{2}F''(v^*(a))v_1^2 \\ &\quad + \mathscr{O}(\|v_1\|^3) \\ &= I_1 - b_1(ay_1 + y_2) + \frac{1}{2}F''(v^*(a))(ay_1 + y_2)^2 + \mathscr{O}(\|y\|^3). \end{aligned} \tag{2.13}$$

Let us denote for the sake of clarity $\alpha = (b_1, I_1)$ and write (2.12) as

$$\begin{cases} \dot{y}_1 = y_2 + a_{00}(\alpha) + a_{10}(\alpha)y_1 + a_{01}(\alpha)y_2, \\ \dot{y}_2 = b_{00}(\alpha) + b_{10}(\alpha)y_1 + b_{01}(\alpha)y_2 + \frac{1}{2}b_{20}(\alpha)y_1^2 + b_{11}(\alpha)y_1 y_2 + \frac{1}{2}b_{02}(\alpha)y_2^2 + \mathscr{O}(\|y\|^3). \end{cases} \tag{2.14}$$

From (2.12) and (2.13), it is straightforward to identify the expressions for the coefficients $a_{ij}(\alpha)$ and $b_{ij}(\alpha)$.

Let us now use the change of variables:

$$\begin{cases} u_1 = y_1, \\ u_2 = y_2 + \frac{b_1}{a}(ay_1 + y_2). \end{cases}$$

The dynamical system governing (u_1, u_2) reads

$$\begin{cases} \dot{u}_1 = u_2, \\ \dot{u}_2 = (1 + \frac{b_1}{a}) - b_1\,a\,u_1 + \frac{1}{2}\frac{a^3 F''(v^*(a))}{a+b_1}u_1^2 + \frac{a^2 F''(v^*(a))}{a+b_1}u_1\,u_2 + \frac{1}{2}\frac{aF''(v^*(a))}{a+b_1}u_2^2. \end{cases}$$

The transversality conditions of a Bogdanov–Takens bifurcation (48; 78) can easily be verified from this expression:

(BT.1) The Jacobian matrix is not 0.

(BT.2) With the notations of (2.14), we have $a_{20} = 0$ and $b_{11}(0) = aF''(v^*(a)) > 0$, and so $a_{20}(0) + b_{11}(0) = aF''(v^*(a)) > 0$.

(BT.3) $b_{20} = a^2 F''(v^*(a)) > 0$.

(BT.4) We show that the map

$$\left(x := \begin{pmatrix} y_1 \\ y_2 \end{pmatrix}, \ \alpha := \begin{pmatrix} I_1 \\ b_1 \end{pmatrix} \right) \mapsto \left[f(x,\alpha), \operatorname{Tr}(D_x f(x,\alpha)), \operatorname{Det}(Dxf(x,\alpha)) \right]$$

is regular at the point of interest.

From the two first assumptions, we know that the system can be put in the form of (2.11). Guckenheimer in (48) proves that this condition can be reduced to the nondegeneracy of the differential with respect to (I_1, b_1) of the vector $\binom{\beta_1}{\beta_2}$ of (2.11).

In our case, we can compute these variables β_1 and β_2 following the calculation steps of (78), and we get

$$\begin{cases} \beta_1 = \frac{8F''(v^*(a))\,a I_1}{(a+b_1)^3}, \\ \beta_2 = -\frac{2(2b_1\,a + I_1\,F''(v^*(a)))}{(a+b_1)^2}. \end{cases} \tag{2.15}$$

Hence the differential of the vector $\binom{\beta_1}{\beta_2}$ with respect to the parameters (I_1, b_1) at the point $(0,0)$ reads

$$D_\alpha \beta|_{(0,0)} = \begin{pmatrix} \frac{8F''(v^*(a))}{a^2} & 0 \\ -2\frac{F''(v^*(a))}{a^2} & -4/a \end{pmatrix}.$$

This matrix has a nonzero determinant if and only if $F''(v^*(a)) \neq 0$.

Therefore we have proved the existence of a Bogdanov–Takens bifurcation under the condition $F''(v^*(a)) \neq 0$.

Let us now show that $\sigma = 1$. Indeed, this coefficient is given by the sign of $b_{20}(0)(a_{20}(0) + b_{11}(0))$ which in our case is equal to $a^3 F''(v^*(a))^2 > 0$, and so the bifurcation is always of the type (2.10) (generation of an unstable limit cycle) for all the members of our class of models. $\square$

The existence of a Bogdanov–Takens bifurcation point implies the existence of a smooth curve corresponding to a saddle homoclinic bifurcation in the system (see (78, Lemma 8.7)).

Corollary 2.1.7. There is a unique smooth curve (P) corresponding to a saddle homoclinic bifurcation in the system (2.1) originating at the parameter point $b = a$ and $I = -m(a)$ defined by the implicit equation:

$$(P) := \left\{ I = -m(a) - \frac{12}{25\,F''(v^*(a))}(b - a)^2; \ b > a \right\}. \tag{2.16}$$

Moreover, for (b, I) in a neighborhood of $(a, -m(a))$, the system has a unique and hyperbolic unstable cycle for parameter values inside the region bounded by the Hopf bifurcation curve and the homoclinic bifurcation curve (P), and it has no cycle outside this region.

Proof. As noticed, from the Bogdanov–Takens bifurcation point, we have the existence of this saddle homoclinic bifurcation curve. Let us now compute the equation of this curve in the neighborhood of the Bogdanov–Takens point. To this purpose we use the normal form we derived in Theorem 2.1.6 and use the local characterization given, for instance, in (78, Lemma 8.7) for the saddle homoclinic curve:

$$(P) := \left\{ (\beta_1, \beta_2) ; \beta_1 = -\frac{6}{25}\beta_2^2 + o(\beta_2^2),\ \beta_2 < 0 \right\}.$$

Using the expressions (2.15) yields

$$(P) := \left\{ (I = -m(a) + I_1,\ b = a + b_1) ; \right.$$

$$\frac{8F''(v^*(a))aI_1}{(a+b_1)^3} = \frac{24}{25}\frac{(2b_1a + I_1F''(v^*(a)))^2}{(a+b_1)^4} + o(|b_1| + |I_1|)$$

$$\left. \text{and } b_1 > -\frac{I_1F''(v^*(a))}{2a} \right\}.$$

We can solve this equation. There are two solutions but only one satisfying $I_1 = 0$ when $b_1 = 0$. This solution is the curve of saddle homoclinic bifurcations, and reads:

$$(P) := \left\{ I = -m(a) + I_1,\ b = a + b_1) ; \right.$$

$$I_1 = \frac{\left(-\frac{25}{6}a - \frac{37}{6}b_1 + \frac{5}{6}\sqrt{25a^2 + 74b_1a + 49b_1^2}\right)a}{F''(v^*(a))} + o(|b_1| + |I_1|)$$

$$\left. \text{and } b_1 > -\frac{I_1F''(v^*(a))}{2a} \right\}.$$

which is equivalent to formula (2.16) $\qquad\square$

Bautin bifurcation

In the study of the Andronov–Hopf bifurcation, we showed that the sub- or supercritical type of bifurcation depended on the variable $A(a,b)$ defined by (2.7). If this variable changes sign when b varies, then the stability of the limit cycle along Hopf bifurcation changes stability. This can occur if the point $v^*(a)$ satisfies the following condition.

Assumption 2.1.4. For $v^*(a)$ such that $F'(v^*(a)) = a$, we have

$$F'''(v^*(a)) < 0.$$

Indeed, if this happens, the type of Andronov–Hopf bifurcation changes, since we have

$$\begin{cases} \lim_{b \to a^-} A(a,b) = +\infty, \\ \lim_{b \to +\infty} A(a,b) = F'''(v^*(a)) < 0. \end{cases}$$

In this case the first Lyapunov exponent vanishes for

$$b = a - \frac{(F''(v^*(a)))^2}{F'''(v^*(a))}.$$

At this point, the system has the characteristics of a Bautin (generalized Hopf) bifurcation. Nevertheless, we still have to check two nondegeneracy conditions to ensure that the system actually undergoes a Bautin bifurcation:

(BGH.1) The second Lyapunov coefficient of the dynamical system l_2 does not vanish at this equilibrium point.

(BGH.2) Let $l_1(I,b)$ be the first Lyapunov exponent of this system and $\mu(I,b)$ the real part of the eigenvalues of the Jacobian matrix. The map

$$(I,b) \mapsto (\mu(I,b), l_1(I,b))$$

is regular at this point.

In this case the system would be locally topologically equivalent to the normal form:

$$\begin{cases} \dot{y}_1 = \beta_1 y_1 - y_2 + \beta_2 y_1 (y_1^2 + y_2^2) + \sigma y_1 (y_1^2 + y_2^2)^2, \\ \dot{y}_2 = \beta_1 y_2 - y_1 + \beta_2 y_2 (y_1^2 + y_2^2) + \sigma y_2 (y_1^2 + y_2^2)^2. \end{cases}$$

We reduce the problem to the point that checking the two conditions of a BGH bifurcation becomes straightforward.

Let $(v^*(a), w_a)$ be the point where the system undergoes the Bautin bifurcation (when it exists). Since we already computed the eigenvalues and eigenvectors of the Jacobian matrix along the Andronov–Hopf bifurcation curve, we can use it to reduce the problem. The basis where we express the system is given by

$$\begin{cases} Q := \begin{pmatrix} \frac{1}{b} & \frac{\omega}{ab} \\ 1 & 0 \end{pmatrix}, \\ \begin{pmatrix} x \\ y \end{pmatrix} := Q^{-1} \begin{pmatrix} v - v^*(a) \\ w - w_a \end{pmatrix}. \end{cases}$$

Let us write the dynamical equations satisfied by (x, y):

$$\begin{cases} \dot{x} = \omega y, \\ \dot{y} = \frac{ab}{\omega} \left(F\left(v^*(a) + \frac{1}{b}x + \frac{\omega}{ab}y \right) - w_a - x + I_a - ay \right). \end{cases}$$

To ensure that we have a Bautin bifurcation at this point we will need to perform a Taylor expansion up to the fifth order, and so we need to make the following assumption.

Assumption 2.1.5. The function F is six times continuously differentiable at $(v^*(a), w_a)$.

First, let us denote $v_1(x, y) = \frac{1}{b}x + \frac{\omega}{ab}y$; the Taylor expansion reads

$$\begin{aligned} \dot{y} = {} & \frac{ab}{\omega} \left(F(v^*(a)) - w_a + I \right) + \frac{ab}{\omega} \left[F'(v^*(a)) v_1(x, y) - ay \right] + \frac{1}{2} \frac{ab}{\omega} \left[F''(v^*(a)) v_1(x, y)^2 \right] \\ & + \frac{1}{6} \frac{ab}{\omega} F'''(v^*(a)) v_1(x, y)^3 + \frac{1}{4!} \frac{ab}{\omega} F^{(4)}(v^*(a)) v_1(x, y)^4 \\ & + \frac{1}{5!} \frac{ab}{\omega} F^{(5)}(v^*(a)) v_1(x, y)^5 + \mathscr{O}\left(\left\| \begin{pmatrix} x \\ y \end{pmatrix} \right\|^6 \right). \end{aligned}$$

This expression, together with the complex left and right eigenvectors of the Jacobian matrix, allows us to compute the first and second Lyapunov coefficients and to check the existence of a Bautin bifurcation.

Nevertheless, we cannot push the computation any further at this level of generality, but, for a given function F presenting a change in the sign of $A(a, b)$, this can easily be done through the use of a symbolic computation package. In the following proof we show that the quartic model undergoes a Bautin bifurcation.

Proof. To prove that the quartic model undergoes a Bautin bifurcation at the point

$$\begin{cases} b = \frac{5}{2} a, \\ I = -3 \left(\frac{a}{4} \right)^{4/3} (2a - 1), \\ v^*(a) = -\left(\frac{a}{4} \right)^{1/3}. \end{cases} \tag{2.17}$$

we compute the first and second lyapunov exponents and prove that the conditions given to characterize Bautin bifurcations are satisfied.

The first Lyapunov exponent: Using a suitable affine change of coordinates having for origin the point (2.17), we can readily write the dynamical system in the form:

$$\begin{cases} \dot{x} = \omega y, \\ \dot{y} = \frac{ab}{\omega} \left(6v^*(a)^2 v_1(x, y)^2 + 4v^*(a) v_1(x, y)^3 + v_1(x, y)^4 \right) \\ \phantom{\dot{y}} = \frac{1}{2} F_2 \left(\binom{x}{y}, \binom{x}{y} \right) + \frac{1}{6} F_3 \left(\binom{x}{y}, \binom{x}{y}, \binom{x}{y} \right) + \frac{1}{24} F_3 \left(\binom{x}{y}, \binom{x}{y}, \binom{x}{y}, \binom{x}{y} \right), \end{cases} \tag{2.18}$$

where $v_1(x, y) = \frac{1}{b}x + \frac{\omega}{ab}y$. Let us denote $F_2(X, Y)$, $F_3(X, Y, Z)$, and $F_4(X, Y, Z, T)$ the multilinear symmetric vector functions of (2.18) $(X, Y, Z, T \in \mathbb{R}^2)$:

$$\begin{cases} F_2 \left(\binom{x}{y}, \binom{z}{t} \right) = \begin{pmatrix} 0 \\ 12 \frac{ab}{\omega} v^*(a)^2 v_1(x, y) v_1(z, t) \end{pmatrix}, \\ \dots \end{cases}$$

To compute the two first Lyapunov exponents of the system, we follow Kuznetsov's method (78). In this method we need to compute some specific right and left complex eigenvectors, which can be chosen in our case to be

$$
\begin{cases}
p = \begin{pmatrix} \frac{1}{-i\sqrt{ab-a^2}+a} \\ 1 \end{pmatrix}, \\[3mm]
q = \begin{pmatrix} \frac{1}{2}\frac{(i\sqrt{a(b-a)}+a)b}{b-a-i\sqrt{a(b-a)}} \\[2mm] 1/2\frac{(i\sqrt{a(b-a)}+a)^2}{a(b-a-i\sqrt{a(b-a)})} \end{pmatrix}.
\end{cases}
$$

(2.19)

We now put the system in a complex form letting $z = x + iy$.
We can now compute the complex Taylor coefficients g_{ij}:

$$
\begin{cases}
g_{20} = \langle p, F_2(q,q) \rangle, \\
g_{11} = \langle p, F_2(q,\bar{q}) \rangle, \\
g_{02} = \langle p, F_2(\bar{q},\bar{q}) \rangle, \\[2mm]
g_{30} = \langle p, F_3(q,q,q) \rangle, \\
g_{21} = \langle p, F_3(q,q,\bar{q}) \rangle, \\
g_{12} = \langle p, F_3(\bar{q},\bar{q},\bar{q}) \rangle, \\
g_{03} = \langle p, F_3(\bar{q},\bar{q},\bar{q}) \rangle, \\
\dots
\end{cases}
$$

(2.20)

So the Taylor coefficients (2.20) read

$$
\begin{cases}
g_{20} = 12\frac{ab}{\omega}v^*(a)^2 v_1\left(\frac{1}{2}\frac{(i\sqrt{a(b-a)}+a)b}{b-a-i\sqrt{a(b-a)}}, \frac{1}{2}\frac{(i\sqrt{a(b-a)}+a)^2}{a(b-a-i\sqrt{a(b-a)})}\right)^2, \\
g_{11} = 12\frac{ab}{\omega}v^*(a)^2 v_1(q)v_1(\bar{q}), \\
g_{02} = 12\frac{ab}{\omega}v^*(a)^2 v_1(\bar{q})v_1(\bar{q}), \\[2mm]
\dots
\end{cases}
$$

(2.21)

Now let $S(I,b) := F'(v_-(I,b))$ be the value of the derivative of the function F, defined around the bifurcation point we are interested in.

The Jacobian matrix in the neighborhood of the point (2.17) reads

$$
L(v) = \begin{pmatrix} S(I,b) & 1 \\ ab & -a \end{pmatrix}.
$$

Let us denote $\alpha = \binom{I}{b}$ the parameter vector and $\lambda(\alpha) = \mu(\alpha) \pm i\omega(\alpha)$ the eigenvalues of the Jacobian matrix. We have

$$
\begin{cases}
\mu(\alpha) = \frac{1}{2}\left(S(\alpha) - a\right), \\
\omega(\alpha) = \frac{1}{2}\sqrt{-(S(\alpha) - a)^2 + 4ab}.
\end{cases}
$$

With these notations, let $c_1(\alpha)$ be the complex defined by

$$
c_1(\alpha) = \frac{g_{20}g_{11}(2\lambda + \bar{\lambda})}{2|\lambda|^2} + \frac{|g_{11}|^2}{\lambda} + \frac{|g_{02}|^2}{2(2\lambda - \bar{\lambda})} + \frac{g_{21}}{2}
$$

(in this formula we omit the dependence in α of λ for the sake of clarity).
The first Lyapunov exponent $l_1(\alpha)$ eventually reads

$$
\boxed{l_1(\alpha) = \frac{Re(c_1(\alpha))}{\omega(\alpha)} - \frac{\mu(\alpha)}{\omega(\alpha)^2}Im(c_1(\alpha))}
$$

(2.22)

The second Lyapunov exponent : The method to compute the second Lyapunov exponent is the same as the one we described in the previous section. The expression is given by the following formula:

$$2l_2(0) = \frac{1}{\omega(0)}\,\mathrm{Re}[g_{32}]$$

$$+ \frac{1}{\omega(0)^2}\,\mathrm{Im}\left[g_{20}\,\bar{g}_{31} - g_{11}\left(4\,g_{31} + 3\,\bar{g}_{22}\right) - \frac{1}{3}g_{02}\left(g_{40} + \bar{g}_{13}\right) - g_{30}\,g_{12}\right]$$

$$+ \frac{1}{\omega(0)^3}\left\{\mathrm{Re}\left[g_{20}\left(\bar{g}_{11}\left(3\,g_{12} - \bar{g}_{30}\right) + g_{02}\left(\bar{g}_{12} - 1/3\,g_{30}\right) + \frac{1}{3}\bar{g}_{02}g_{03}\right)\right.\right.$$

$$\left.\left. + g_{11}\left(\bar{g}_{02}\left(\frac{5}{3}\bar{g}_{30} + 3\,g_{12}\right) + \frac{1}{3}g_{02}\,\bar{g}_{03} - 4\,g_{11}\,g_{30}\right)\right]\right.$$

$$\left. + 3\,\mathrm{Im}[g_{20}\,g_{11}]\,\mathrm{Im}[g_{21}]\right\}$$

$$+ \frac{1}{\omega(0)^4}\left\{\mathrm{Im}\left[g_{11}\bar{g}_{02}\left(\bar{g}_{20}^{\,2} - 3\,\bar{g}_{20}g_{11} - 4\,g_{11}^2\right)\right]\right.$$

$$\left. + \mathrm{Im}[g_{20}\,g_{11}]\left(3\,\mathrm{Re}(g_{20}\,g_{11}) - 2\,|g_{02}|^2\right)\right\}.$$

This expression is quite intricate in our case. Nevertheless, we have a closed-form expression depending on the parameter a, vanishing for two values of the parameter a. We evaluate numerically this second Lyapunov exponent. We get the following expression:

$$l_2(a) \approx -0.003165\,a^{-\frac{28}{3}} - 0.1898\,a^{-\frac{22}{3}} + 0.3194\,a^{-16/3}$$

$$- 0.05392\,a^{-\frac{25}{3}} + 0.1400\,a^{-\frac{19}{3}} - 0.3880\,a^{-7/3} + 0.5530\,a^{-10/3} \tag{2.23}$$

$$+ 0.7450\,a^{-13/3}.$$

We can see that this numerical exponent vanishes only for two values of the parameter a which are

$$\{0.5304, 2.385\}.$$

The expression of the determinant of the matrix $D_{I,b}(\mu(I,b),l_1(I,b))$ is even more involved, and so we do not reproduce it here (it would take pages to write down its numerical expression!). Nevertheless, we proceed exactly as we did for the second Lyapunov exponent and obtain again the rigorous result that this determinant never vanishes for all $a > 0$. $\qquad\square$

2.1.4   Conclusion: The full bifurcation diagram

We now summarize the results obtained in this section in the two following theorems.

Theorem 2.1.8. *Let us consider the formal dynamical system*

$$\begin{cases} \dot{v} = F(v) - w + I, \\ \dot{w} = a(bv - w), \end{cases} \tag{2.24}$$

where a is a fixed real, b and I bifurcation parameters, and $F : \mathbb{R} \mapsto \mathbb{R}$ a real function. If the function F satisfies the assumptions that

(A.1) *the function F is three times continuously differentiable,*

(A.2) *F is strictly convex, and*

(A.3) *F' satisfies the conditions*

$$\begin{cases} \lim_{x \to -\infty} F'(x) \leq 0, \\ \lim_{x \to \infty} F'(x) = \infty, \end{cases}$$

then the dynamical system (2.24) *shows the following bifurcations:*

(B1) *A saddle-node bifurcation curve:*

$$(SN) : \{(b,I)\ ;\ I = -m(b)\},$$

where $m(b)$ is the minimum of the function $F(v) - bv$ (if the second derivative of F does not vanish at this point).

(B2) *An Andronov–Hopf bifurcation line:*

$$(AH) := \left\{ (b,I) \, ; \, b > a \ and \ I = bv^*(a) - F(v^*(a)) \right\},$$

where $v^*(a)$ is the unique solution of $F'(v^*(a)) = a$ (if $F''(v^*(a)) \neq 0$). This type of Andronov–Hopf bifurcation is given by the sign of the variable

$$A(a,b) = F'''(v^*(a)) + \frac{1}{b-a} F''(v^*(a))^2.$$

If $A(a,b) > 0$, then the bifurcation is subcritical, and if $A(a,b) < 0$, then the bifurcation is supercritical.

(B3) *A Bogdanov–Takens bifurcation point at the point $b = a$ and $I = -m(a)$ if $F''(v^*(a)) \neq 0$.*

(B4) *A saddle homoclinic bifurcation curve characterized in the neighborhood of the Bogdanov–Takens point by*

$$(P) := \left\{ I = -m(a) - \frac{12}{25 F''(v^*(a))} (b-a)^2; \, b > a \right\}.$$

Theorem 2.1.9. *Consider the system (2.1), where a is a given real number, b and I are real bifurcation parameters, and $F : E \times \mathbb{R} \mapsto \mathbb{R}$ is a function satisfying the following assumptions:*

(A.5) *The function F is six times continuously differentiable.*

(A.2) *F is strictly convex.*

(A.3) *F' satisfies the conditions*

$$\begin{cases} \lim\limits_{x \to -\infty} F'(x) \leq 0, \\ \lim\limits_{x \to \infty} F'(x) = \infty. \end{cases}$$

(A.4) *Let $v^*(a)$ be the unique real such that $F'(v^*(a)) = a$. We have*

$$F'''(v^*(a)) < 0.$$

Furthermore, consider the following conditions:

(BGH.1) *The second Lyapunov coefficient of the dynamical system $l_2(v^*(a)) \neq 0$.*

(BGH.2) *Let $l_1(v)$ denote the first Lyapunov exponent and $\lambda(I,b) = \mu(I,b) \pm i\omega(I,b)$ the eigenvalues of the Jacobian matrix in the neighborhood of the point of interest. The map $(I,b) \to (\mu(I,b), l_1(I,b))$ is regular at this point.*

Having these, the system undergoes a Bautin bifurcation at the point $v^*(a)$ for the parameters $b = a - \frac{F''(v^*(a))^2}{F'''(v^*(a))}$ and $I = bv^*(a) - F(v^*(a))$.

Remark 5. Theorem (2.1.8) enumerates some of the bifurcations that any dynamical system of the class (2.1) will always undergo. Together with Theorem 2.1.9, they summarize all the local bifurcations the system can undergo, and no other fixed-point bifurcation is possible. In section 2.3 we introduce a model actually showing all these local bifurcations.

2.2 APPLICATIONS: IZHIKEVICH AND BRETTE–GERSTNER MODELS

In this section we show that the neuron models proposed by Izhikevich in (62) and Brette and Gerstner in (13) are part of the class studied in section 2.1. Using the results of the latter section, we derive their bifurcation diagram and obtain that they show exactly the same types of bifurcations.

2.2.1   Adaptive quadratic IF model

We produce here a complete description of the bifurcation diagram of the adaptive quadratic integrate-and-fire model proposed by Izhikevich in (62) and (65, Chapter 8). We use here the dimensionless equivalent version of this model with the fewest parameters:

$$\begin{cases} \dot{v} = v^2 - w + I, \\ \dot{w} = a(bv - w). \end{cases} \tag{2.25}$$

Equation (2.25) is clearly a particular case of (2.1) with

$$F(v) = v^2.$$

F is clearly strictly convex and C^∞. $F'(v) = 2v$, and so it also satisfies Assumption 2.1.3. Furthermore, the second derivative never vanishes, and so the system undergoes the three bifurcations stated in Theorem 2.1.8.

(Izh.B1) A saddle-node bifurcation curve defined by

$$\left\{ (b, I) \; ; \; I = \frac{b^2}{4} \right\}.$$

For $(I, b) \in \mathbb{R}^2$, the fixed point is given by $(v^*(b) = \frac{1}{2}b, \; w^*(b) = \frac{1}{2}b^2)$.

For $I < \frac{b^2}{4}$, the fixed point(s) are

$$v_\pm(b, I) = \frac{1}{2} \left(b \pm \sqrt{b^2 - 4I} \right).$$

(Izh.B2) An Andronov–Hopf bifurcation line:

$$\left\{ (I, b) \; ; \; b > a \text{ and } I = \frac{a}{2} \left(b - \frac{a}{2} \right) \right\},$$

whose type is given by the sign of the variable

$$A(a, b) = \frac{4}{b - a}.$$

This value is always strictly positive, and so the bifurcation is always subcritical.

(Izh.B3) A Bogdanov–Takens bifurcation point for $b = a$ and $I = \frac{a^2}{4}$, $v^*(a) = \frac{a}{2}$.

(Izh.B4) A saddle homoclinic bifurcation curve satisfying the quadratic equation near the Bogdanov–Takens point:

$$(P) := \left\{ I = \frac{a^2}{4} - \frac{6}{25}(b - a)^2 ; \; b > a \right\}.$$

Figure 2.2 represents the fixed points of this dynamical system, and their stability, together with the bifurcation curves.

2.2.2   Adaptive exponential IF model

In this section we study the bifurcation diagram of the adaptive exponential neuron. This model has been introduced by Brette and Gerstner in (13). This model, inspired by the Izhikevich adaptive quadratic model, can be fitted to biological values, takes into account the adaptation phenomenon, and is able to reproduce many behaviors observed in cortical neurons. The bifurcation analysis we derived in section 2.1 allows us to understand how the parameters of the model can affect the behavior of this neuron. We show that this model is part of the general class studied in section 2.1, and we obtain the fixed-point bifurcation diagram of the model.
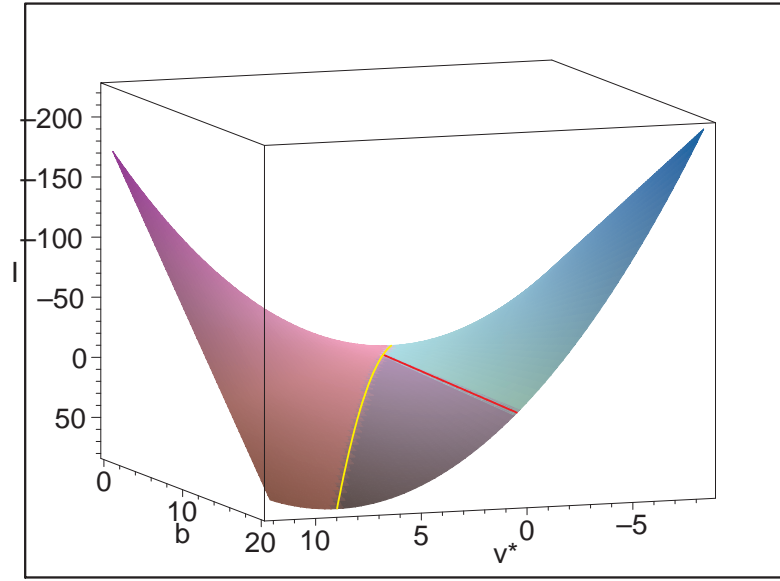
Figure 2.2. Representation of the *v* fixed point with respect to the parameters *I* and *b* in the Izhikevich model. The reddish component is the surface of saddle fixed points, the purplish one corresponds to the repulsive fixed points, and the greenish/bluish one corresponds to the attractive fixed points The yellow curve corresponds to a saddle-node bifurcation and the red one to an Andronov–Hopf bifurcation.

Reduction of the original model

This original model is based on biological constants and is expressed with a lot of parameters. We first reduce this model to a simpler form with the fewest number of parameters.

The basic equations proposed in the original paper (13) read

$$
\begin{cases}
C\dfrac{dV}{dt} = -g_L(V - E_L) + g_L\Delta_T \exp\left(\dfrac{V - V_T}{\Delta_T}\right) \\
\qquad\qquad - g_e(t)(V - E_e) - g_i(t)(V - E_i) - W + I_m, \\
\tau_W\dfrac{dW}{dt} = \kappa(V - E_L) - W.
\end{cases}
\tag{2.26}
$$

First, we do not assume that the reversal potential of the *w* equation is the same as the leakage potential E_L, and we write the equation for the adaptation variable by

$$
\tau_W \frac{dW}{dt} = a(V - \bar{V}) - W.
$$

Next we assume that $g_e(\cdot)$ and $g_i(\cdot)$ are constant (in the original paper it was assumed that the two conductances were null).

After some straightforward algebra, we eventually get the following dimensionless equation equivalent to (2.26):

$$
\begin{cases}
\dot{v} = -v + e^v - w + I, \\
\dot{w} = a(bv - w),
\end{cases}
\tag{2.27}
$$

where we denoted

$$
\begin{cases}
\tilde{g} := g_L + g_e + g_i, \\
\tau_m := \dfrac{C}{\tilde{g}}, \\
B := \dfrac{\kappa}{\tilde{g}}\left(\dfrac{E_L}{\Delta_T} + \log\left(\dfrac{g_L}{\tilde{g}}e^{-V_T/\Delta_T}\right)\right), \\
v(\tau) := \dfrac{V(\tau\tau_m)}{\Delta_T} + \log\left(\dfrac{g_L}{\tilde{g}}e^{-V_T/\Delta_T}\right), \\
w(\tau) := \dfrac{W(\tau\tau_m)}{\tilde{g}\Delta_T} + B, \\
a := \dfrac{\tau_m}{\tau_W}, \\
b := \dfrac{\kappa}{\tilde{g}}, \\
I := \dfrac{I_m + g_L E_L + g_e E_e + g_i E_i}{\tilde{g}\Delta_T} + \log\left(\dfrac{g_l}{\tilde{g}}e^{-V_T/\Delta_T}\right) + B
\end{cases}
\tag{2.28}
$$

and where the dot denotes the derivative with respect to τ.

The differential equations and the parameters have a physiological interpretation. The first equation is the membrane equation, which states that the capacitive current through the membrane (C is the membrane capacitance) is the sum of the injected current I and of the ionic currents. The first term is the leak current (g_L is the leak conductance and E_L is the leak reversal potential), the membrane time constant is $\tau_m = C/g_L$. The second (exponential) term approximates the sodium current, responsible for the generation of action potentials (41). The approximation results from neglecting the inactivation of the sodium channel and assuming that activation is infinitely fast (which is reasonable). Because activation curves are typically Boltzmann functions (6), the approximated current is exponential near spike initiation. The voltage threshold V_T is the maximum voltage that can be reached without generating a spike (without adaptation), and the slope factor Δ_T quantifies the sharpness of spikes. In the limit of zero slope factor, the model becomes an integrate-and-fire model with a fixed threshold V_T. Quantitatively, it is proportional to the slope constant k in the activation function of the sodium current. The second variable w is an adaptation current with time constant τ_w, which includes both spike-triggered adaptation, through the reset $w \to w+d$, and subthreshold adaptation, through the coupling (variable b). It may model ionic channels (e.g. potassium) or a dendritic compartment. Quantitatively, the coupling variable b can result from a linearization of the dynamics of a ionic channel, or from the axial conductance in the case of a dendritic compartment. We generally assume $b > 0$ in this chapter, although the analysis also applies for $b < 0$ when $|b|$ is not too large.

Remark 6. These expressions confirm the qualitative interpretation of the parameters a, b, and I of the model (2.1). Indeed, $a = \frac{\tau_m}{\tau_w}$ accounts for the time scale of the adaptation (with the membrane time scale as reference), and the parameter $b = \frac{\kappa}{\bar{g}}$ is proportional to the interaction between the membrane potential and the adaptation variable and inversely proportional to the total conductivity of the membrane potential. Eventually, I is an affine function of the input current I_m and models the input current of the neurons.

Bifurcation diagram

From (2.27) we can clearly see that the Brette–Gerstner model is included in the formal class studied in the present chapter with

$$F(v) = e^v - v.$$

This function satisfies Assumptions 2.1.1, 2.1.2, and 2.1.3. Furthermore, its second order derivative never vanishes.

Theorem 2.1.8 shows that the system undergoes the following bifurcations:

(BG.B1) A saddle-node bifurcation curve defined by

$$\{(b,I)\,;\,I = (1+b)(1-\log(1+b))\}.$$

So $v^*(b) = \log(1+b)$. For $I \leq (1+b)(1-\log(1+b))$, the system has the fixed points

$$\begin{cases} v_-(I,b) := -W_0\left(-\frac{1}{1+b}e^{\frac{I}{1+b}}\right) + \frac{I}{1+b}, \\ v_+(I,b) := -W_{-1}\left(-\frac{1}{1+b}e^{\frac{I}{1+b}}\right) + \frac{I}{1+b}, \end{cases} \tag{2.29}$$

where W_0 is the principal branch of Lambert's W function[3] and W_{-1} the real branch of Lambert's W function such that $W_{-1}(x) \leq -1$, defined for $-e^{-1} \leq x < 1$.

(BG.B2) An Andronov–Hopf bifurcation line for

$$\{(b,I)\,;\,b > a \text{ and } I = I^*(a,b) = (1+b)\log(1+a) - (1+a)\}$$

at the equilibrium point $(v^*(a) = \log(1+a), w_a = bv^*(a))$. This type of Andronov–Hopf bifurcation is given by the sign of the variable

$$A(a,b) = F'''(v^*(a)) + \frac{1}{b-a}F''(v^*(a))^2 = (1+a) + \frac{4}{b-a}(1+a)^2 > 0.$$

So the bifurcation is always subcritical, and there is not any Bautin bifurcation.

(BG.B3) A Bogdanov–Takens bifurcation point at the point $b = a$ and $I = \log(1+a)$.

---

[3]The Lambert W function is the inverse function of $x \mapsto xe^x$.
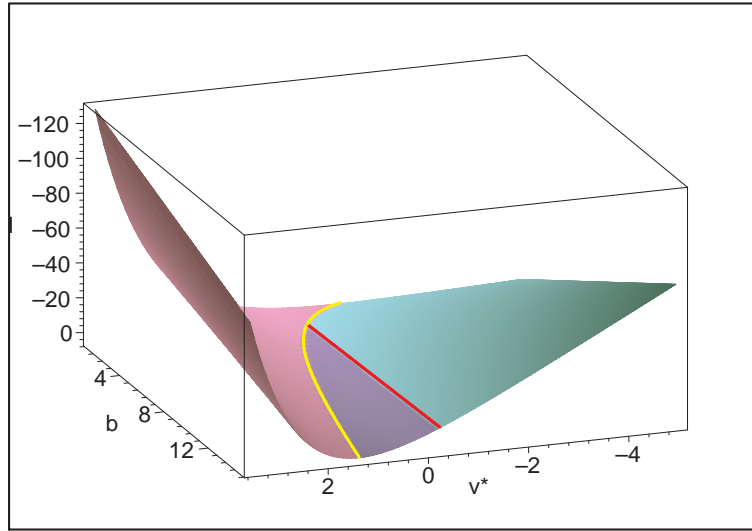
Figure 2.3. Representation of the v fixed point of the Brette–Gerstner model with respect to the parameters I and b. The reddish/pinkish component is the surface of saddle fixed points, the purplish one corresponds to the repulsive fixed points, and the bluish/greenish one corresponds to the attractive fixed points The yellow curve corresponds to a saddle-node bifurcation and the red one to an Andronov–Hopf bifurcation.

(BG.B4) A saddle homoclinic bifurcation curve satisfying, near the Bogdanov–Takens point, the equation

$$(P) := \left\{ I = (1+a)(\log(1+a) - 1) - \frac{12}{25(1+a)}(b-a)^2; \, b > a \right\}.$$

In Figure 2.3 we represent the fixed points of the exponential model and their stability, together with the bifurcation curves, in the space (I, b, v).

2.3 THE RICHER QUARTIC MODEL

In this section, we introduce a new specific model having a richer bifurcation diagram than the two models studied in section 2.2. It is as simple as the two previous models from the mathematical and computational points of view. To this end, we define a model which is part of the class studied in section 2.1 by specifying the function F.

2.3.1 The quartic model: Definition and bifurcation map

Let $a > 0$ be a fixed real and $\alpha > a$. We instantiate the model (2.1) with the function F a quartic polynomial:

$$F(v) = v^4 + 2av.$$

Remark 7. The choice of the function F here is just an example where all the formulas are rather simple. Exactly the same analysis can be done with any F function satisfying $F'''(v^*(a)) < 0$ and the transversality conditions given in Theorem 2.1.9. This would be the case, for instance, for any quartic polynomial $F(v) = v^4 + \alpha v$ for $\alpha > a$.

The function F satisfies Assumptions 2.1.1, 2.1.2, and 2.1.5. $F'(v) = 4v^3 + 2a$ satisfies Assumption 2.1.3. Nevertheless, we have to bear in mind that the second order derivative vanishes at $v = 0$:

$$\begin{cases} \dot{v} = v^4 + 2av - w + I, \\ \dot{w} = a(bv - w). \end{cases} \tag{2.30}$$

Theorem 2.1.8 shows that the quartic model undergoes the following bifurcations:

(B1) A saddle-node bifurcation curve defined by

$$(SN) := \left\{ (b, I) \, ; \, I = 3 \left(\frac{b - 2a}{4} \right)^{(4/3)} \right\}.$$

Proof. Indeed, the function G reads $G(v) = v^4 + (2a-b)v$ and reaches its minimum at the point $v = \left(\frac{b-2a}{4}\right)^{(1/3)}$. So the minimum of G is $m(b) = -3\left(\frac{b-2a}{4}\right)^{(4/3)}$. $\qquad\square$

The point $v^*(b)$ is $\left(\frac{b-2a}{4}\right)^{(1/3)}$, and we have closed-form expressions (but rather complicated) for the two fixed points for $I < 3\left(\frac{b-2a}{4}\right)^{(4/3)}$ since the quartic equation is solvable in radicals. The closed form expression can be obtained using a symbolic computation package like Maple using the command

```
S:=allvalues( solve( x^4 + (2*a - b) * x + I0 = 0,x));
```

(B2) An Andronov–Hopf bifurcation curve for $b > a$ along the straight line

$$(AH) := \left\{ (I,b) \,;\, b > a \text{ and } I = -\left(\frac{a}{4}\right)^{1/3} b - \left(\frac{a}{4}\right)^{4/3} \right\}.$$

The fixed point where the system undergoes this bifurcation is $v^*(a) = -\left(\frac{a}{4}\right)^{1/3}$. The kind of Andronov–Hopf bifurcation we have is governed by the sign of

$$\alpha = -24\left(\frac{a}{4}\right)^{1/3} + \frac{144}{b-a}\left(\frac{a}{4}\right)^{4/3}.$$

Finally, the type of bifurcation changes when b varies.

- When $b < \frac{5}{2}a$, then $\alpha > 0$, hence $l_1 > 0$, and the Andronov–Hopf bifurcation is subcritical.
- When $b > \frac{5}{2}a$, then $\alpha < 0$, hence $l_1 < 0$, and the Andronov–Hopf bifurcation is supercritical.

We prove below that the change in the type of Hopf bifurcation is obtained via a Bautin bifurcation.

(B3) A Bogdanov–Takens bifurcation point is located at $b = a$ and $I = -3\left(\frac{a}{4}\right)^{(4/3)}$.

(B4) A saddle homoclinic bifurcation curve satisfying, near the Bogdanov–Takens point, the equation

$$(P) := \left\{ I = -7\left(\frac{a}{4}\right)^{\frac{4}{3}} - \frac{1}{25}\left(\frac{4}{3}\right)^{\frac{2}{3}}(b-a)^2 ;\, b > a \right\}.$$

(B5) A Bautin bifurcation at the point $\left(b = \frac{5}{2}a, I = -3\left(\frac{a}{4}\right)^{4/3}(2a-1)\right)$ and a saddle node bifurcation of periodic orbits coming along (see section 2.3.2).

Figure 2.4 represents the bifurcation curves and the fixed point of the quartic model in the space (I,b,v).

2.3.2 The Bautin bifurcation

As we have seen in the last section, at the point

$$\begin{cases} v^*(a) = -\left(\frac{a}{4}\right)^{1/3}, \\ I = -3\left(\frac{a}{4}\right)^{4/3}(2a-1), \\ b = \frac{5}{2}a \end{cases} \tag{2.31}$$

the Jacobian matrix of the system has a pair of purely conjugate imaginary eigenvalues and a vanishing first Lyapunov exponent.

The proof that the quartic model undergoes a Bautin bifurcation at this point is provided in section 2.1.3. We prove that the system actually undergoes a Bautin bifurcation except for two particular values of the parameter a. With this same method we obtain a closed-form expression for the second Lyapunov exponent. We show that this second Lyapunov exponent vanishes for two values of a, whose expressions are complicated. These calculations are rigorous, but nevertheless, the interested reader can find numerical expressions of this exponent to get a grasp on its behavior in the appendix (see (2.23)) and of the two numerical values of a such that $l_2(a)$ vanishes.

Things are even more involved when we are interested in the regularity of the map $(I,b) \mapsto (\mu(I,b), l_1(I,b))$. Nevertheless, we obtain that this determinant never vanishes.

Eventually, for all a different from the critical values where the second Lyapunov exponent vanishes, the system undergoes a Bautin bifurcation.

Note finally that the Bautin bifurcation point separates two branches of sub- and supercritical Hopf bifurcations. For nearby parameter values, the system has two coexisting limit cycles, an attractive one and a repelling one, which collide and disappear via a saddle-node bifurcation of periodic orbits.
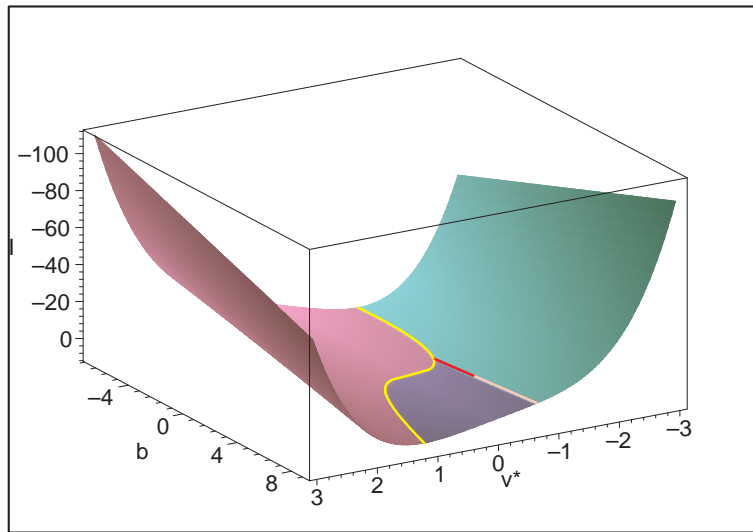
Figure 2.4. *v* fixed points and their stability in function of *I* and *b*. The reddish/pinkish component is the surface of saddle fixed points, the purplish one corresponds to the repulsive fixed points, and the bluish/greenish one corresponds to the attractive fixed points. The yellow curve corresponds to a saddle-node bifurcation, the red curve to a subcritical Andronov–Hopf bifurcation, and the greyish one to the supercritical Andronov–Hopf bifurcation. The intersection point between the yellow and the red curve is the Bogdanov–Takens bifurcation point, and the intersection point of the red and greyish curves is the Bautin bifurcation point.

2.4 ELECTROPHYSIOLOGICAL CLASSES

In the previous sections we emphasized the fact that the class of models we defined in section 2.1 was able to reproduce the behaviors observed by Izhikevich in (63). In this section, first we show that the quartic model indeed reproduces the behaviors observed by Izhikevich and which correspond to cortical neuron behaviors observed experimentally. We also produce some simulations of self-sustained subthreshold oscillations which occur only when the dynamical system has attracting periodic orbits, which is not the case in the other usual models of this class.

Izhikevich in (63) explains the main features we obtain in numerical simulations from the neurocomputational point of view. In chapter 4, we comment on these same features from the dynamical systems point of view mainly for the adaptive exponential model for its physiological relevance in that its parameters can be easily related to physiological quantities. By study different quantities of the model as a dynamical system, we will be able to define electrophyisiological classes, i.e. sets of parameters where the model responds qualitatively the same way to different current inputs.

2.4.1 Simulation results

Simulation results for the quartic model introduced in section 2.3 are provided here. In the simulated model, the spike is not represented by the blow up of the potential membrane *v*, but we consider that the neuron emits a spike when its membrane potential crosses a constant threshold. Note that the numerical simulations are very robust with respect to the choice of the threshold, if taken large enough, since the underlying equation blows up in finite time, and the adaptation variable converges. This issue is specifically discussed in chapter 5 and in the paper (115). This is also the case for the exponential model, but not for the quadratic model (see discussions herein).

Let θ be our threshold. The simulated model considered in this section is the solution of the equations

$$\begin{cases} \dot{v} = v^4 + 2av - w + I, \\ \dot{w} = a(bv - w) \end{cases} \tag{2.32}$$

together with the spike-and-reset condition

$$\text{If } v(t^-) > \theta \Rightarrow \begin{cases} v(t) = v_r, \\ w(t) = w(t^-) + d. \end{cases} \tag{2.33}$$

(i) Tonic Spiking	(ii) Phasic Spiking	(iii) Tonic Bursting
$a=1$; $b=0.49$; $v_r=0$; $I(t)=1.56\,\mathbb{1}_{t>1}(t)$; $d=1$; $T=10$; $dt=0.01$; $\theta=10$;	$a=1$; $b=0.76$; $v_r=0.2$; $I=0.37\,\mathbb{1}_{t>1}(t)$; $d=1$; $T=10$; $dt=0.01$; $\theta=10$;	$a=0.15$; $b=1.68$; $v_r=(-2a+b)^{\frac13}$; $I=4.67\,\mathbb{1}_{t>1}(t)$; $d=1$; $T=30$; $dt=0.01$; $\theta=10$;
(iv) Phasic Bursting	**(v) Mixed Mode**	**(vi) Spike Freq. Adaptation**
$a=1.58$; $b=1.70$; $v_r=-\frac{a}{4}^{\frac13}$; $I(t)=0.73\,\mathbb{1}_{t>1}$; $d=0.01$; $T=50$; $dt=0.01$; $\theta=10$.	$a=0.07$; $b=0.32$; $v_r=0$; $I(t)=3.84\,\mathbb{1}_{t>1}(t)$; $d=1.50$; $T=50$; $dt=0.01$; $\theta=10$.	$a=0.02$; $b=0.74$; $v_r=0$; $I(t)=4.33\,\mathbb{1}_{t>1}(t)$; $d=0.36$; $T=50$; $dt=0.01$; $\theta=10$.
(vii) Class 1 Excitability	**(viii) Class 2 Excitability**	**(ix) Spike Latency**
$a=4$; $b=0.67$; $v_r=-1.3$; $I(t)=-0.1+0.23t$; $d=1$; $T=30$; $dt=0.01$; $\theta=10$.	$a=1$; $b=1.09$; $v_r=-1.2$; $I(t)=0.06t$; $d=5$; $T=50$; $dt=0.01$; $\theta=20$.	$a=0.02$; $b=0.42$; $v_r=0$; $I(t)=5\delta_{7.5}(t)$; $d=1$; $T=15$; $dt=0.01$; $\theta=10$.
(x) Damped Subthr. Oscill.	**(xi) Resonator**	**(xii) Integrator**
$a=2.58$; $b=4.16$; $v_r=0.1$; $I(t)=2\delta_2(t)$; $d=0.05$; $T=20$; $dt=0.01$; $\theta=10$.	$a=5.00$; $b=7.88$; $v_r=-1.28$; $I(t)=\delta_{6,6.8,15,16.5,24,26}(t)$; $d=0.5$; $T=30$; $dt=0.01$; $\theta=10$.	$a=1.00$; $b=1.10$; $v_r=-0.97$; $I(t)=\delta_{2,5.3.3,17.5,19}(t)$; $d=0.5$; $T=25$; $dt=0.01$; $\theta=10$.
(xiii) Rebound Spike	**(xiv) Rebound Burst**	**(xv) Threshold variability**
$a=1$; $b=2$; $v_r=-0.63$; $I(t)=-0.48-5\delta_{2.5}(t)$; $d=1$; $T=50$; $dt=0.1$; $\theta=10$.	$a=1$; $b=2$; $v_r=1.3$; $I(t)=-0.48-30\delta_{6.5}(t)$; $d=1$; $T=20$; $dt=0.01$; $\theta=10$.	$a=1$; $b=1.23$; $v_r=-0.91$; $I(t)=\delta_{2,16.5}-\delta_{15}$; $d=1$; $T=20$; $dt=0.01$; $\theta=10$.
(xvi) Bistability	**(xvii) Depol. after-pot**	**(xviii) Self-sustained oscill.**
$a=1$; $b=1.2$; $v_r=0.8$; $I(t)=-0.47+20*(\delta_{10}-\delta_{30})$; $d=0.5$; $T=50$; $dt=0.01$; $\theta=10$.	$a=1$; $b=1.5$; $v_r=0.06$; $I(t)=2\delta_3$; $d=0.01$; $T=30$; $dt=0.01$; $\theta=10$.	$a=1$; $b=2.5$; $v_r=-0.63$; $I(t)=-0.475+10*\delta_{10}$; $d=1$; $T=100$; $dt=0.01$; $\theta=10$.
(xix) Mixed Chatter/ C^1 exc.	**(xx) Purely oscill.**	
$a=0.89$; $b=3.65$; $v_r=1.12$; $I(t)=0.07t$; $d=1$; $T=50$; $dt=0.01$; $\theta=10$.	$a=1$; $b=2.6$; $v_r=-0.63$; $I(t)=-0.47\,\mathbb{1}_{t>1}$; $d=1$; $T=500$; $dt=0.01$; $\theta=10$.	

Table 2.1. Simulation parameters to produce figure 2.5.

Simulations have been done using an Euler numerical scheme, with a time step ranging from 10^{-1} to 10^{-2} depending on the precision needed, and with time intervals ranging from 10 to 500. This method is very efficient numerically and remains precise. Other integration methods could be used, and the qualitative results we obtained do not depend on the integration scheme, as soon as the time step is small enough.

Remark 8. Note that we did not reproduce the last three behaviors presented by Izhikevich in (63, *Figs.* 1.(R), 1.(S), *and* 1.(T)). Indeed, these behaviors are not in the scope of the present chapter and do not correspond to the model we studied.

More precisely, in the study of the general model (2.1), we considered for phenomenological reasons $a>0$, modelling the leak of the adaptation variable: the adaptation would converge to its rest value if it was not influenced by the membrane potential v. If we considered $a<0$, this adaptation variable would diverge exponentially from this rest value if it was not controlled by the membrane potential v. The inhibition-induced behaviors (63, *Figs.* 1.(S) *and* 1.(T)) require a to be strictly negative, and so we will not comment on these behaviors any further.

Similarly, the accommodation behavior presented by Izhikevich in (63, *Fig.* 1.(R)) is a limit case when w is very slow and the adaptation efficiency b very high. Mathematically speaking, it corresponds to a case where $a\to 0$ and $ab\to\lambda\neq 0$. This case is not taken into account in our study and amounts to replacing (2.1) by an equation of the type

$$\begin{cases} \frac{\mathrm{d}v}{\mathrm{d}t} = F(v) - w + I, \\ \frac{\mathrm{d}w}{\mathrm{d}t} = ab(v-v_0), \end{cases} \tag{2.34}$$

and the study of this equation is not in the scope of the present chapter.

In table 2.1, we provide the numerical values used to obtain the simulations of figure 2.5. In this table, the $\delta_u(t)$ function is defined by

$$\delta_{u_1,\dots,u_N}(t) = \begin{cases} 1 & if\ t\in \bigcup_{k\in\{1,\dots,N\}} [u_k, u_k+0.3], \\ 0 & else. \end{cases}$$

The simulated behaviors we obtained in Figure 2.5 have been obtained playing with the bifurcation parameters in the phase plane. The way the parameters were set was based on a qualitative reasoning on the phase plane and the bifurcation diagram in a way we describe in chapter 4. The simulations presented in the figure 2.5 are done with the quartic model.

2.4.2 Bifurcations and neuronal dynamics

In this section we link the neuronal behaviors shown in Figure 2.5 with the bifurcations of the system. We are first interested in behaviors generated by applied current steps to the neuron. These behaviors consist

(i) Tonic Spiking (ii) Phasic Spiking (iii) Tonic Bursting

(iv) Phasic Bursting (v) Mixed Mode (vi) Spike Freq. Adapt.

(vii) Class I Excitability (viii) Class II Excitability (ix) Spike Latency

(x) Damped Subthr. Oscill. (xi) Resonator (xii) Integrator

(xiii) Rebound Spike (xiv) Rebound Burst (xv) Threshold Variability

(xvi) Bistability (xvii) Depol. After-Pot. (xviii) Self-Sustained Oscill.

(xix) Mixed chatter/C1 exc. (xx) Purely Oscill. mode

Figure 2.5. Different remarkable neurocomputational interesting behaviors of the neuron model (2.32) with the reset condition (2.33) for different choices of the parameters (a,b,I,v_r,d). The higher curve represents the membrane potential v and the lower one the input current I (see table 2.1) for the numerical values of each simulations).
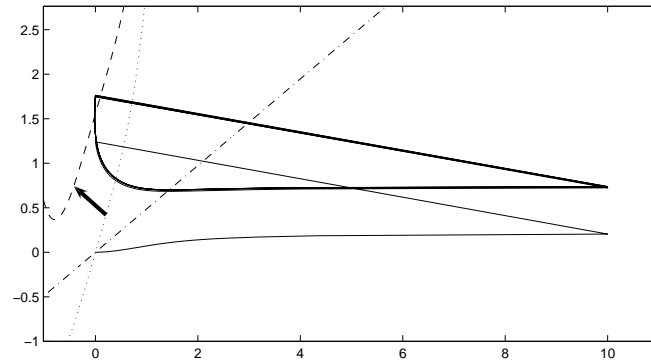
Figure 2.6. Tonic spiking: phase plane trajectory. The dotted curve is the v nullcline at the initial time. It is shifted to the dashed one when applying a constant input current. The new dynamical system has no fixed point and spikes regularly. We can see the spiking cycle appearing.

in studying the effect of the initial condition on the dynamics, as we will see in the following chapters.

- (i), (iii), (v), (vi) *Tonic behaviors* : Tonic behaviors correspond to a sustained destabilization of the resting voltage. In the four cases we discuss here, the voltage of a neuron is at rest for a given value of input current I. Then a current step is applied to the neuron and subsequently, the neuron emits an infinite sequence of spikes (as long as the current step is applied). This behavior hence can correspond to destabilizing on a permanent basis the resting state, which can be achieved either by crossing the saddle-node or the Andronov-Hopf bifurcation, or to be permanently reset outside the attraction basin of the fixed point. When the system does not returns to the attraction basin of the resting state, two cases can occur depending on the parameters: either the system has a stable limit cycle (it is the case when the system undergoes a Bautin bifurcation). In this case, the destabilization can result in the generation of self-sustained subthreshold oscillations, as in the case (xx). If there is no stable limit cycle nor stable non-spiking trajectory, then the neuron will emit infinitely many spikes, as in the cases cited. The different spike patterns observed are a result of the interplay between the subthreshold dynamics and the reset process. It will be studied further in chapter 3. The phase plane orbits give a grasp on the phenomena occurring. We observe that the case of tonic regular spiking is linked with the existence of what we will call a *limit spiking cycle*, i.e. a trajectory including spikes similar to a cycle containing a spike point ($v = \infty$, or $v =$ threshold in the numerical case). In that case the adaptation variable w converges to an attracting stable value w_{spike}. This value satisfies the relation $w_s(t_{\text{spike}}) + b = w_{\text{spike}}$, where $w_s(\cdot)$ is solution of (2.32) with the initial conditions

$$\begin{cases} v(0) = v_r, \\ w(0) = w_{\text{spike}} \end{cases}$$

and where t_{spike} denotes the time of the spike.

The mixed mode (v) and the spike frequency adaptation (vi) are particular cases of tonic spiking differing by the way they converge to this spiking limit cycle. While in the spike frequency adaptation the convergence is smooth, in the mixed mode the convergence happens quite fast, the system sends a burst of few spikes before converging to the spiking cycle.

The case of the tonic bursting is induced by the same mechanism. Nevertheless, in that case (see figure 2.7(a)) the generalized cycle towards which the trajectory converges contains few (≥ 2) spikes. It is interesting to note that in that case if we consider the reset locations, they form a cycle, with at least a point in the zone $\{(v, w); w > F(v) + I\}$. So the system emits quickly a precise number of spikes and then crosses the v nullcline. At this point, the membrane potential decays before spiking. We can see numerically that the system converges to a stable *bursting cycle* (see Figure 2.7(a)) Interestingly enough, the two-dimensional system is able to reproduce the diagrams presented by Izhikevich in (60) in an (at least) three-dimensional space, because of the singularity of the model (explosion or threshold/reinitialization). If the system was regular, this behavior would not have been possible because it would have contradicted the Cauchy–Lipschitz theorem of existence and uniqueness of a solution.

Note that we can choose exactly the number of spikes per burst by changing the adaptation parameter d and that the bursting can be of parabolic or square-wave type as defined in Hoppensteadt and

(a) Phase plane of the tonic bursting (without the transient phase)

(b) Controlling the number of spikes per burst
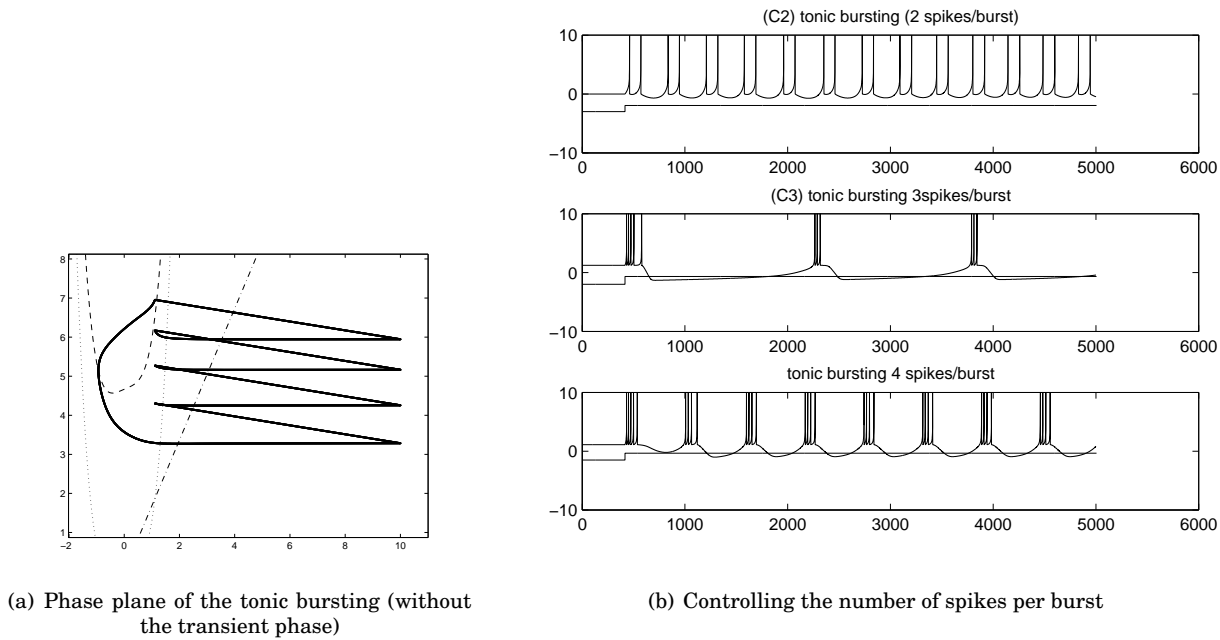
Figure 2.7. Tonic bursting: phase plane trajectory. The dotted curve is the v nullcline at the initial time. It is shifted to the dashed one when applying a constant input current. The new dynamical system has no fixed point. We can see the multiple spike limit cycle here.

Izhikevich (57) (see Figure 2.7(b)).

These tonic behaviors will be studied further in section 3.

- (ii), (iv) *Phasic behaviors*: In these behaviors the current step applied is not high enough to destroy all the stable subthreshold orbits (fixed points or limit cycles). In that case there exists a subthreshold orbit, and the system will fall after emitting a finite number of spikes in the attraction basin of this stable trajectory. If the "initial condition" of the system, i.e. the previous stable fixed point, is inside the attraction basin of the new fixed point, then no spike will be emitted. If it is outside this attraction bass in, then the neuron will elicit spikes. If the trajectory goes back in the attraction basin of the stable fixed point, then we will have a return to equilibrium after the emission of few spikes. This is what we call a phasic behavior. These behaviors will be also studied a little bit more in depth in chapter 3.

- (vii)/(viii) *Excitability types*: The excitability properties of these types of neurons will be discussed in chapter 4. These behaviors are linked with the way the equilibrium loses stability, i.e. either via saddle-node bifurcation (type I) or via Andronov-Hopf bifurcation (type II excitability), and on the parameters of the model.

All the other behaviors are generated using current pulses, and are linked with the local behavior around the destabilized fixed point. These behaviors will mainly be studied in the chapter 4. It corresponds to the integration of perturbations at the stable equilibrium point.

- (ix)/(xvii) *Spike latency/DAP*: It is a particular case of phasic spiking when the equilibrium v^* or the reset point v_r is near a point such that $F(v) = F'(v) = 0$. The membrane potential dynamics is very slow around this point. In the spike latency behavior, the initial point is close to this point, which generates the observed latency. In our case, it is around the minimum of the function F (see Figure 2.9(ix)). In the depolarized after-potential (DAP) case, the reset occurs near this point, which is also in the attraction basin of the stable fixed point.

- (x), (xi), (xii), (xv) *Damped subthreshold oscillations, resonator and integrator, threshold variability* are linked with the imaginary part of the eigenvalues of the Jacobian matrix at the fixed point. When this imaginary part is non null, then a perturbation will result in damped subthreshold oscillations, and multiple excitations will respond stronger to particular frequency inputs (resonator). The oscillations around the fixed point also generate the threshold variability behavior. When this imaginary part is

(a) Bistability: return to equilibrium via the same impulse
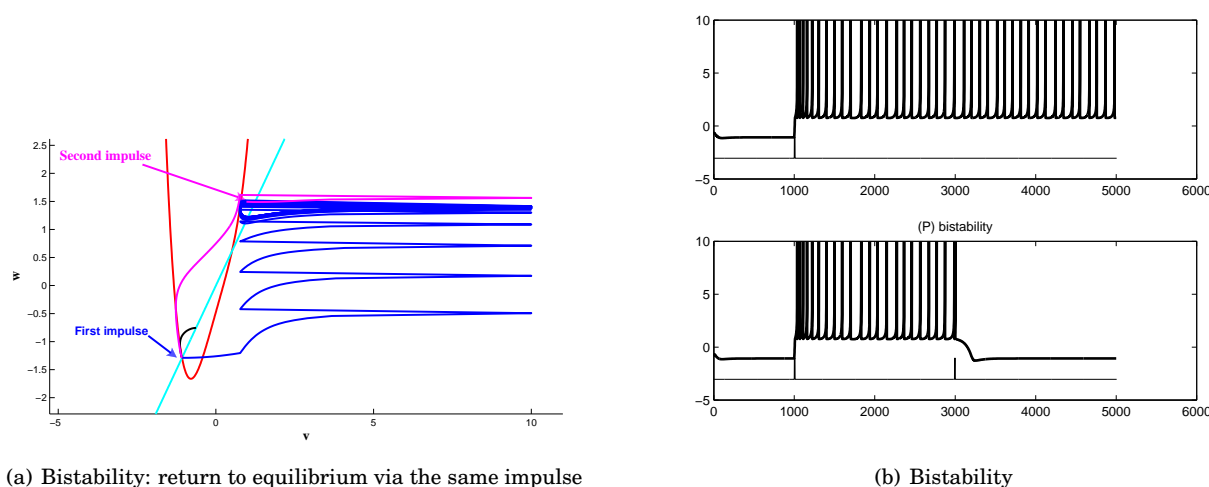
(b) Bistability

Figure 2.8. Bistability phenomenon: The first impulse induces a self-sustained tonic spiking behavior while the system has a stable fixed point. The second impulse perturbs this regular spiking behavior, and the system falls in the attraction basin of the stable fixed point.

null, the neuron will be an integrator: since it returns monotonously to equilibrium, the more two excitations are close the more it will depolarize the neuron.

- (xiii)/(xiv) *Rebound spike or burst*: These behaviors are linked with the topology of the attraction basin of the fixed point as discussed in chapter 4

- (xvi) *Bistability*: The bistability behavior (Figure 2.8) is quite interesting since it presents two stable trajectories: the stable fixed point (stable for the subthreshold dynamics) and a stable tonic spiking trajectory (stable from the spikes point of view).

- (xviii)/(xx) *Self-sustained subthreshold oscillations and purely oscillating mode*: They are linked with the supercritical Hopf bifurcation and its stable periodic orbit. These two behaviors cannot be obtained in the IBG models since the Hopf bifurcations are always subcritical.

2.4.3 Self-sustained subthreshold oscillations in cortical neurons

In this study we gave a set of sufficient conditions to obtain an IBG-like model of neuron. In this framework we proposed a model that displays a Bautin bifurcation the IBG neurons lack; as a consequence our model can produce subthreshold oscillations. In this section, we explain from a biological point of view the origin and the role of those oscillations and reproduce in vivo recordings.

In the IBG models, the Andronov–Hopf bifurcation is always subcritical. The only oscillations created in these models are damped (see Figure 2.10(a)) and correspond in the phase plane to the convergence to a fixed point where the Jacobian matrix has complex eigenvalues. Our quartic model undergoes supercritical Andronov–Hopf bifurcations, and so there are attracting periodic solutions. This means that the neurons can show self-sustained subthreshold oscillations (Figures 2.10(b) and 2.10(c)), which is of particular importance in neuroscience.

Most biological neurons show a sharp transition from silence to a spiking behavior, which is reproduced in all the models of class (2.1). However, experimental studies suggest that some neurons may experience a regime of small oscillations (86). These subthreshold oscillations can facilitate the generation of spike oscillations when the membrane gets depolarized or hyperpolarized (89; 90). They also play an important role in shaping specific forms of rhythmic activity that are vulnerable to the noise in the network dynamics.

For instance, the inferior olive nucleus, a part of the brain that sends sensory information to the cerebellum, is composed of neurons able to support oscillations around the rest potential. It has been shown by Llinás and Yarom (89; 90) that the precision and robustness of these oscillations are important for the precision and the robustness of spike generation patterns. The quartic model is able to reproduce the main features of the inferior olive neuron dynamics:

i. autonomous subthreshold periodic and regular oscillations (see intracellular recordings of inferior olive neurons in brain stem slices in (90)),
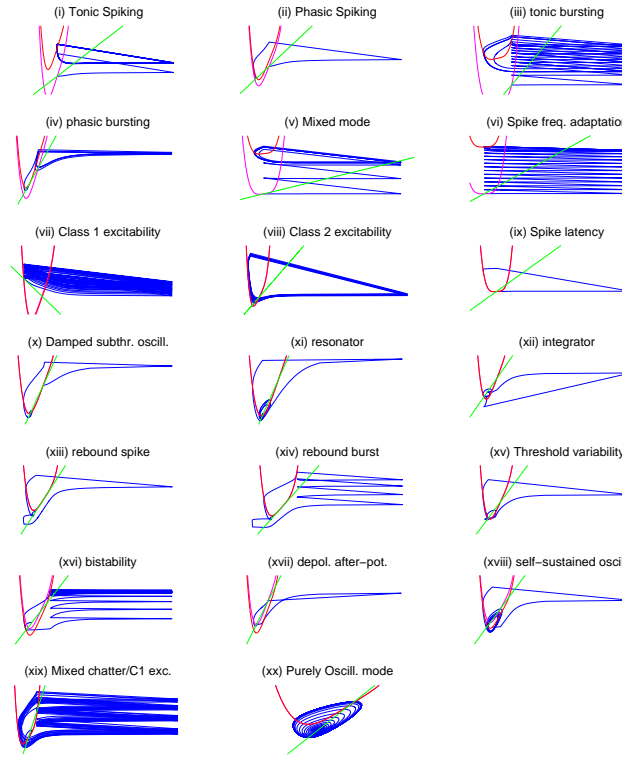
Figure 2.9. Phase diagrams corresponding to the behaviors presented in Figure 2.5.

(a) Damped oscillations

(b) Transient phase towards the self-sustained oscillations

(c) Self-sustained oscillations (stationary state)
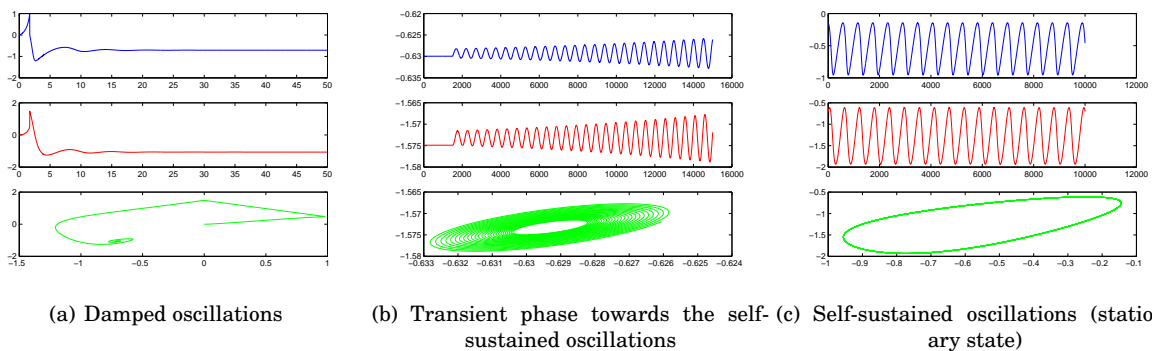
Figure 2.10. The quartic model shows damped subthreshold oscillations like the IBG models (Figure 2.10(a)): the trajectory collapses to a fixed point (parameters: $a = 1$, $b = 1.5$, $I = 0.1$, $T_{max} = 100$, $dt = 0.01$). The upper (blue) curve represents the solution in v, the middle (red) one w, and the lower one (green) the trajectory in the plane (v, w). Self-sustained subthreshold oscillations of the quartic model (Figures 2.10(b) and 2.10(c)): the trajectory is attracted towards a limit cycle (parameters: $a = 1$, $b = 5/2$, $I = -3(a/4)^{4/3}(2a-1)$, $T_{max} = 150000$, $dt = 0.01$, $I = (-3(a/4)^{4/3}(2a-1) + 0.001)$.

(a) Without spiking

(b) With intermittent spiking

(c) With intermittent bursting

(d) Biological recordings
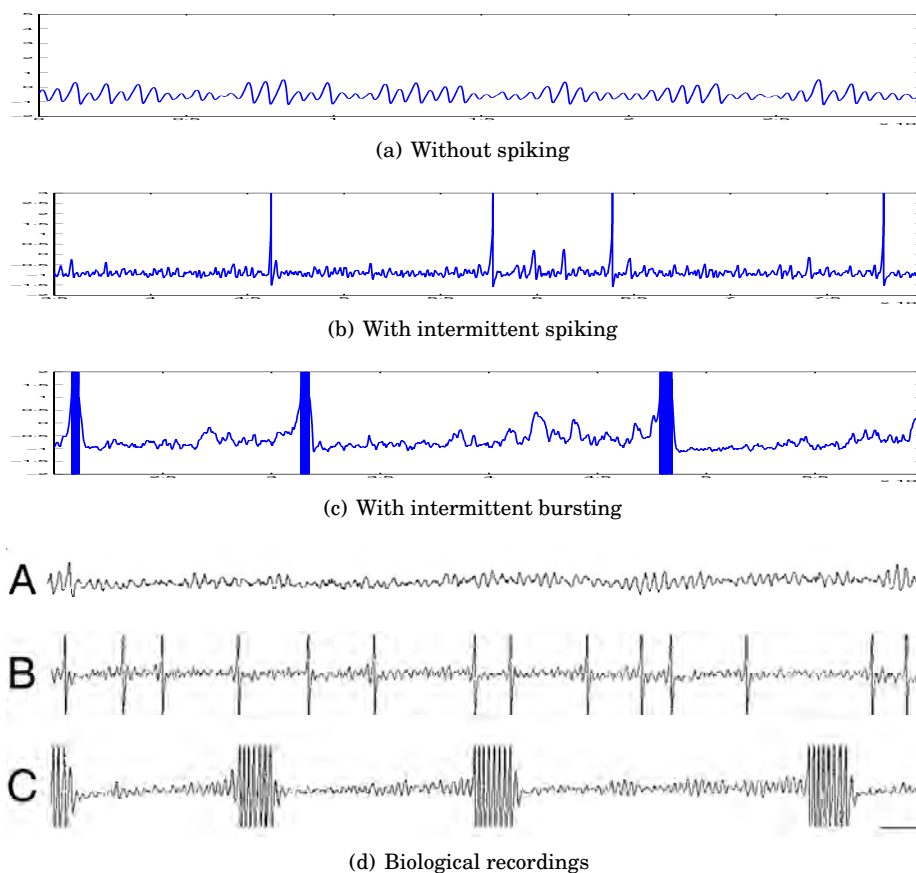
Figure 2.11. Subthreshold membrane oscillations, qualitatively reproducing the recordings from (85) in DRG neurons. Traces illustrate (2.11(a)) oscillations without spiking, (2.11(b)) oscillations with intermittent spiking, and (2.11(c)) oscillations with intermittent bursting (in the figures, spikes are truncated). The noisy input is an Ornstein–Ulhenbeck process. The biological recordings 2.11(d) are reproduced from (85, *Fig. 1)* and used with permission.

ii. rhythmic generation of action potentials.

The robust subthreshold oscillations shown by in vivo recordings (9; 86; 90) correspond in our quartic model to the stable limit cycle coming from the supercritical Hopf bifurcation. The oscillations generated by this cycle are stable, and they have a definite amplitude and frequency. This oscillation occurs at the same time as the rhythmic spike generation in the presence of noisy or varying input. Note that other neuron models such as those studied above, even if they do not undergo a supercritical Hopf bifurcation, can also exhibit oscillations in the presence of noise, for instance near a subcritical Hopf bifurcation. Nevertheless, these oscillations do not have the regularity in the amplitude and the frequency linked with the presence of an attracting limit cycle. The results we obtain simulating the quartic model are very similar to those obtained by in vivo recordings (see Figure 2.11).

But the inferior olive neurons are not the only neurons to present subthreshold membrane potential oscillations. For instance, stellate cells in the enthorhinal cortex demonstrate theta frequency subthreshold oscillations (2; 3; 71), linked with the persistent Na^+ current I_{NaP}.

We now conclude this section on the specific example of subthreshold self-sustained oscillations given by the dorsal root ganglia (DRG) neuron. This neuron presents subthreshold membrane potential oscillations coupled with repetitive spike discharge or burst, for instance in the case of a nerve injury (5; 85). Figure 2.11(d) shows biological in vivo intracellular recordings performed by Liu et al. (85) from a DRG neuron of an adult male rat. The recorded membrane potentials exhibit high frequency subthreshold oscillation in the presence of noise, combined with a repetitive spiking or bursting. These behaviors can be reproduced by the quartic model, as we can see in Figure 2.11, around a point where the system undergoes a supercritical Hopf bifurcation.[4]

---

[4]The amplitude and frequency of the subthreshold oscillations can be controlled choosing a point on the supercritical Hopf bifurcation curve.

CONCLUSION

In this chapter we defined a general class of neuron models able to reproduce a wide range of neuronal behaviors observed in experiments on cortical neurons. This class includes the Izhikevich and the Brette–Gerstner models, which are widely used. We derived the bifurcation diagram of the neurons of this class and proved that they all undergo the same types of bifurcations: a saddle-node bifurcation curve, an Andronov–Hopf bifurcation curve, and a codimension two Bogdanov–Takens bifurcation. We proved that there was only one other possible fixed-point bifurcation, a Bautin bifurcation. Then using those theoretical results we proved that the Izhikevich and the Brette–Gerstner models had the same bifurcation diagram.

This theoretical study allows us to search for interesting models in this class of neurons. Indeed, Theorem 2.1.8 ensures us that the bifurcation diagram will present at least the bifurcations stated. This information is of great interest if we want to control the subthreshold behavior of the neuron of interest.

Following these ideas, we introduced a new neuron model of our global class undergoing the Bautin bifurcation. This model, called the *quartic model*, is computationally and mathematically as simple as the IBG models and able to reproduce some cortical neuron behaviors which the IBG models cannot reproduce.

This study focused on the subthreshold properties of this class of neurons. The adaptative reset of the model is of great interest and is a key parameter in the repetitive spiking properties of the neuron. Its mathematical study is very rich. A new insight of its properties is given in chapter 3. This study also allows us to define new electrophysiological classes of neuron, i.e. sets of parameters for which the neuron has the same qualitative behaviors in response to different stimulations. These results are provided for the general model and in the particular case of the adaptive exponential model (13) in chapter 4, were we explain the origin of different behaviors observed in the neuron.

3

SPIKING DYNAMICS OF BIDIMENSIONAL INTEGRATE-AND-FIRE NEURONS

ABSTRACT

The class of non-linear integrate and fire neuron models introduced in the previous chapter are hybrid dynamical systems combining differential equations and discrete resets, which generate complex dynamics. The dynamical properties of the subthreshold system has studied in chapter 2. This previous study does not account for the spiking properties of the model. We study in this chapter the spike patterns produced by these models. These patterns of activity are the result of an interplay between the continuous subthreshold dynamics and the reset process. Interestingly, the reset induces in bidimensional models behaviors only observed in higher dimensional continuous systems such as bursting and chaos.

This is why in the first section we study in depth the subthreshold dynamical system, and characterize its main dynamical properties. We then introduce a suitable framework in order to study the spike dynamics through the use of a discrete map, called the adaptation map. The relationship between spiking behavior and dynamical properties of the map is then investigated. We show in particular that the system can exhibit a transition to chaos via a cascade of period adding including chaotic transitions, which was previously observed in Hodgkin-Huxley models and in Purkinje cells.

This work was done in collaboration with Romain Brette, has been published as a research report (117) and is still in preparation for publication.

3.1 INTRODUCTION

As stated in chapter 2, finding a computationally simple and biologically realistic model of neuron has been a great endeavor in computational neuroscience, the main interest being to be able to obtain mathematically tractable models in order to understand the nature of the nerve cell activity, and computationaly simple in order to be able to compare experimental recordings with large scale brain models. The class of nonlinear bidimensional spiking neuron models with adaptation defined in section 2 and also studied for instance in (13; 63; 114) seems to present the advantages of being mathematically tractable, efficiently implemented, and able to reproduce a large number of electrophysiological signatures such as bursting or regular spiking. These models emulate the membrane potential of the nerve cell v together with an adaptation variable w, and distinguishes between to phases of the neuronal activity: the *subthreshold* behavior corresponding to the input integration at the level of the cell, and the emission of action potentials (spikes). The subthreshold dynamics is governed by the following ordinary differential equation:

$$\begin{cases} \frac{dv}{dt} = F(v) - w + I \\ \frac{dw}{dt} = a(bv - w) \end{cases} \tag{3.1}$$

where a, b are real parameters accounting respectively for the time constant ratio between the adaptation variable and the membrane potential and to the coupling strength between these two variables, I is a real parameter modeling a DC-input current in the neuron, and F is a real function accounting for the leak and spike initiation currents. Following (114), we assume F to be regular (at least three times continuously differentiable), strictly convex, and its derivative to have a negative limit at $-\infty$ and an infinite limit at $+\infty$. In order to ensure that the neuron will elicit spikes, we add the following assumption:

Assumption 3.1.1. There exists $\varepsilon > 0$ such that $F(v)$ grows faster than $v^{1+\varepsilon}$ when $v \to \infty$ (i.e. there exists $\alpha > 0$ such that $F(v)/v^{1+\varepsilon} \geq \alpha$ when $v \to +\infty$).

We prove in section 3.2.4 that the membrane potential blows up in finite time in these cases. Among these models, the *quadratic adaptive* model (63) corresponds to the case where $F(v) = v^2$, and has been recently used by Eugene Izhikevich and coworkers (66) in very large scale simulations of neural networks. The *adaptive exponential* model (13) corresponds to the case where $F(v) = e^v - v$, is based on an electrophysiological description of the sodium current responsible for the generation of action potentials following the work of (41), has the interest that its parameters can be related to electrophysiological quantities, and has been successfully fit to intracellular recordings of pyramidal cells (23; 69). The *quartic* model (114) corresponds to the case where $F(v) = v^4 + 2av$ and has the advantage of being able to reproduce all the behaviors featured by the other two and also self-sustained subthreshold oscillations which are of particular interest to model certain nerve cells.

As we proved in (115) and in chapter 5, in the case of the quadratic adaptive model (or when the function F diverges slower than v^2 when $v \to \infty$, i.e. when there exists $V_F > 0$ such that $F(v)/v^2$ is bounded for $v \geq V_F$), the adaptation variable blows up at the same time as the membrane potential. In these cases one is led to introduce a hard threshold, the cutoff value θ, which has no biophysical interpretation. A spike is emitted at the time t^* when the membrane potential v reaches a cutoff value θ, and the membrane potential is instantaneously reset to a constant value v_r and the adaptation variable is updated to $w(t^*) + d$ where $w(t^*)$ is the value of the adaptation variable at the time of the spike and $d > 0$ is the spike-triggered adaptation parameter. The spiking properties are highly sensitive to changes in this cutoff parameter (see chapter 5), and therefore constitutes a new bifurcation parameter which artificially adds complexity to the model.

In this chapter, we are interested in models for which the adaptation variable does not blow up. In this case, spikes are emitted when the membrane potential blows up. Therefore we shall consider models with an F function satisfying the following assumption:

Assumption 3.1.2. There exists $\varepsilon > 0$ such that F grows faster than $v^{2+\varepsilon}$ when $v \to \infty$ (i.e. there exists $\alpha > 0$ such that $F(v)/v^{2+\varepsilon} \geq \alpha$ when $v \to \infty$).

In these cases as proved in (115) (see also section 3.2.4), the membrane potential blows up in finite time and at this explosion time the adaptation variable will converge to a finite value. A spike is emitted at the time t^* when the membrane potential blows up. At this time, the adaptation variable converges to the value

$$w(t^{*-}) \overset{\text{def}}{=} \left(\lim_{t \to t^*} w(t) \right).$$

At spike time, the membrane potential is reset to a constant value v_r and the adaptation variable is incre-

mented by a positive quantity, the spike-triggered adaptation parameter:

$$v(t) \xrightarrow[t \to t^*]{} \infty \implies \begin{cases} v(t^*) = v_r \\ w(t^*) = w(t^{*-}) + d \end{cases} \qquad (3.2)$$

In these models, the reset mechanism makes the value of the adaptation variable at the time of the spike critical. Indeed, when a spike is emitted at time t^*, the new initial condition of the system (3.1) is $(v_r, w(t^*) + d)$. Therefore, this value governs the subsequent evolution of the membrane potential, and hence the spike pattern produced.

These models are *hybrid* dynamical systems, in the sense that they are defined by both a continuous and a discrete dynamical system. This structure make these models very interesting. Indeed the addition of the reset to the bidimensional continuous dynamical systems makes possible behaviors which cannot appear in autonomous bidimensional nonlinear ordinary differential equations, such as bursting and chaos (see (13; 62; 114) and figure 2.5). In this chapter we will rigorously study from a mathematical point of view these different behaviors, in order to understand their origin and to get insights about the related parameter ranges.

To this end, we precisely study in section 3.2 the orbits of equation (3.1) in the phase plane (v, w) in order to characterize the value of the adaptation variable at the time of the spike. We will be particularly interested in the attraction basins of the subthreshold attractors (SA), i.e. non spiking (bounded) attractors of the models. We will also introduce an essential tool to study the spike patterns, the adaptation map Φ. We will show that the properties of this map are closely linked with the dynamical properties of the subthreshold system. Section 3.3 will be devoted to the case where the subthreshold system has no fixed point. In that case, the neuron will fire whatever its initial condition. Therefore the study of the iterations of the map Φ will allow us to discriminate between different modes of tonic spiking. Section 3.4 is devoted to the case where there exist non-spiking (subthreshold) orbits. In this case, depending on the initial condition, the system can either fire infinitely many spikes (tonic spiking) or finitely many spikes (phasic spiking). In the last section 3.5 we comment these results from a neurocomputational viewpoint.

3.2 DETAILED STUDY OF THE SUBTHRESHOLD DYNAMICS ─────────

In order to study the spike dynamics, we first need to understand the underlying continuous dynamical system defined by the differential equations. We shall call *subthreshold orbits* the orbits that do not spike (i.e., bounded orbits for positive time). Among these orbits, we will be particularly interested in the *subthreshold attractors* (SA), which are the non spiking (bounded) attractors of the subthreshold system. Since the subthreshold system is a bidimensional continuous dynamical system, these SAs are either fixed points or limit cycles.

3.2.1 Subthreshold Attractors

The number and stability of fixed points were studied in (114), and this study accounts for many excitability properties of these models, as described in (116). The basic local bifurcation structure is given in figure 3.1(a). The parameter a is a scaling parameter, and as a function of b and I the set of fixed points has the following structure: let us denote $v^*(x)$ the unique solution, when it exists, of the equation $F'(v^*(x)) = x$, and by $F'_{-\infty}$ the limit of $F'(x)$ for $x \to -\infty$. This value can be either finite (but nonpositive) or equal to $-\infty$. Note that because of the strict convexity assumption, if there exists a solution, it is unique. Furthermore, $v^*(x)$ is defined for any $x \in (F'_{-\infty}, \infty)$. For x in this interval, we denote $m(x) = F(v^*(x)) - xv^*(x)$ the unique minimum of the application $t \mapsto F(t) - xt$. We have:

i. If $I > -m(b)$, the system has no fixed point.

ii. If $I = -m(b)$, the system has a unique fixed point, $(v^*(b), w^*(b))$, which is nonhyperbolic. It is unstable if $b > a$. Along this curve in the parameter space (I, b), the system undergoes a saddle-node bifurcation provided that $F''(v^*(b)) \neq 0$.

iii. If $I < -m(b)$, then the dynamical system has two fixed points $(v_-(I, b), v_+(I, b))$ such that

$$v_-(I, b) < v^*(b) < v_+(I, b).$$

The fixed point $v_+(I, b)$ is a saddle fixed point, and the stability of the fixed point $v_-(I, b)$ depends on I and on the sign of $(b - a)$:

(a) Fixed Points and Stability   (b) Nullclines and symbolic dynamics
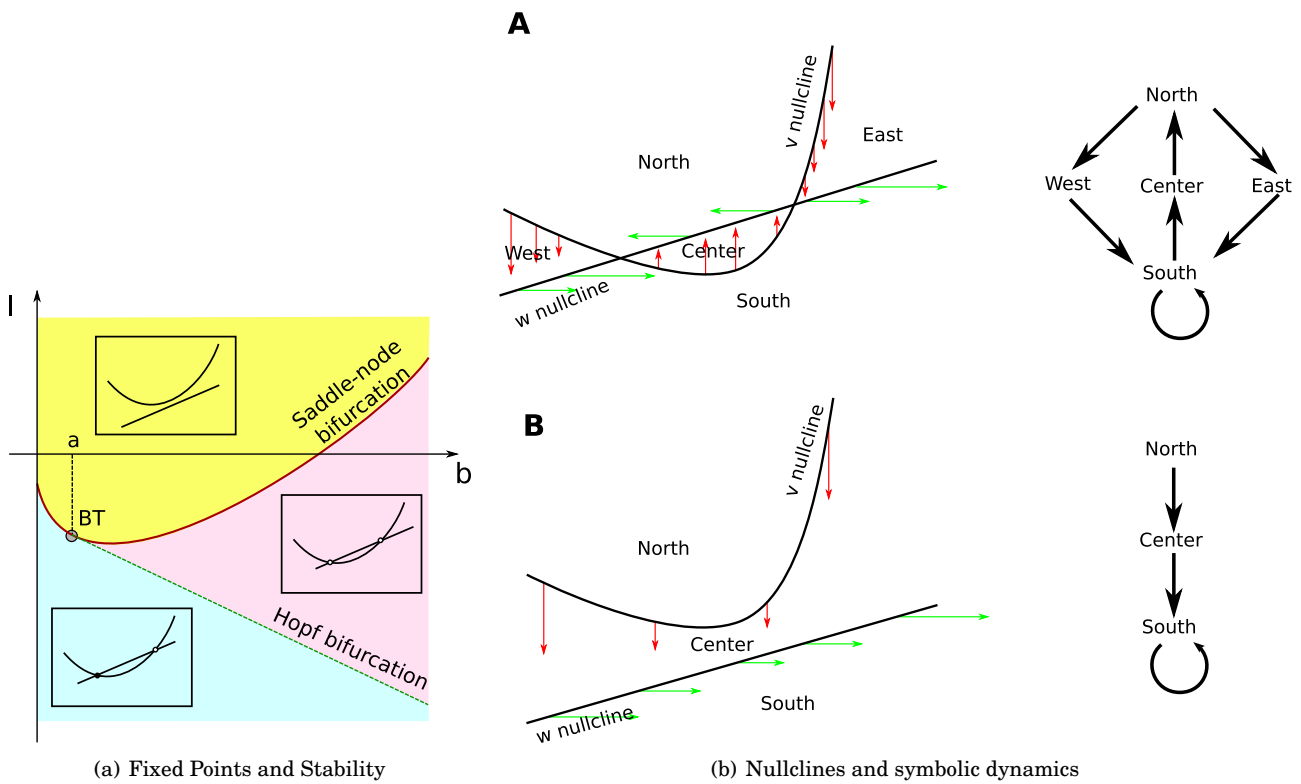
Figure 3.1. (a): Number of fixed points and their stability in the plane (I, b) for the exponential adaptive model. (b): Nullclines of the dynamical system (horizontal axis: v; vertical axis: w). A. The nullclines intersect in two points, and divide the phase space into 5 regions. The potential V increases below the V-nullcline, w increases below the w-nullcline. The direction of the flow along each boundary gives the possible transitions between regions (right). Spiking can only occur in the South region. B. The nullclines do not intersect. All trajectories must enter the South region and spike.
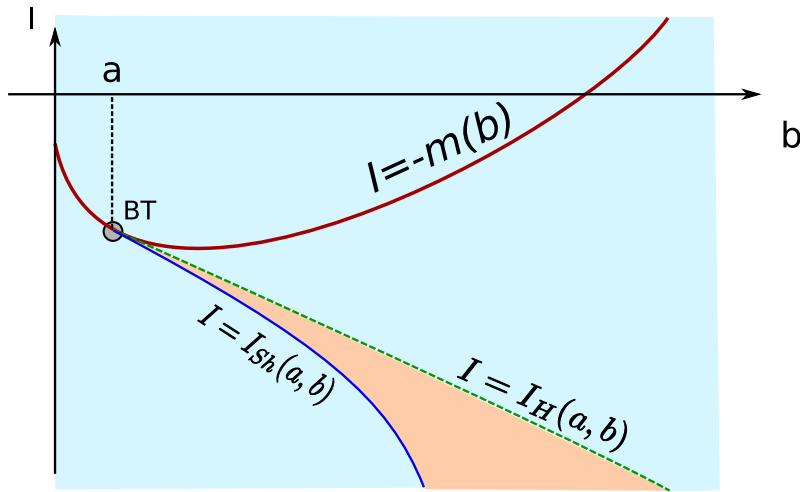
Figure 3.2. Unstable limit cycles in the case where there is no Bautin bifurcation. The system has no periodic orbit in the blue zone, and a unique unstable periodic orbit in the orange zone. For a fixed $b > a$, the family appears via Hopf bifurcation at $I = I_H$ and disappears via saddle-homoclinic bifurcation at $I = I_{Sh}$. BT is the Bogdanov-Takens bifurcation point.

(a) If $b < a$, the fixed point $v_-(I, b)$ is attractive.

(b) If $b > a$, it depends on the input current I with respect to the value $I_H(a, b) = bv^*(a) - F(v^*(a))$.

(c) At the point $b = a$ and $I = -m(a)$, the system undergoes a Bogdanov-Takens bifurcation provided that $F''(v_a) \neq 0$. Therefore, from this point, there is a saddle homoclinic bifurcation curve characterized in the neighborhood of the Bogdanov–Takens point by

$$(P) \stackrel{\text{def}}{=} \left\{ (I, b \geq a) \, ; I_{Sh} = -m(a) + -\frac{12}{25} \frac{(b-a)^2}{F''(v^*(a))} + o(|\,(b-a)^2\,|) \right\}. \tag{3.3}$$

(c.1) If $I < I_H(a, b)$, the fixed point $v_-(I, b)$ is attractive.

(c.2) If $I > I_H(a, b)$, the fixed point $v_-(I, b)$ is repulsive.

(c.3) On the parameter line given by

$$(AH) \stackrel{\text{def}}{=} \left\{ (b, I) \, ; \, b > a \text{ and } I = I_H(a, b) = bv^*(a) - F(v^*(a)) \right\},$$

the system undergoes an Andronov Hopf bifurcation, whose type is given by the sign of the variable

$$A(a, b) = F'''(v^*(a)) + \frac{1}{b-a} F''(v^*(a))^2.$$

If $A(a, b) > 0$, then the bifurcation is subcritical, and if $A(a, b) < 0$, then the bifurcation is supercritical. If furthermore we have $F'''(v^*(a)) < 0$ and some technical conditions fulfilled, then the system undergoes a Bautin bifurcation at the point $v^*(a)$ for $b = a - \frac{F''(v^*(a))^2}{F'''(v^*(a))}$ and $I = bv^*(a) - F(v^*(a))$.

Let us now discuss the number and stability of periodic orbits. First of all, when the subthreshold system has no fixed point, it is clear that no limit cycle can exist, because in planar systems, the existence of a cycle implies the existence of at least one fixed point inside the cycle. In the case where the Hopf bifurcation is always subcritical the system will present unstable cycles originating from the Hopf bifurcation for $b > a$, which will collide with the saddle fixed-point manifold and disappear via saddle-homoclinic bifurcation around the Bogdanov-Takens bifurcation (see figure 3.2). For input currents between the current value corresponding to the Hopf and the saddle-homoclinic bifurcation, there exists an unstable cycle in the system. The saddle-homoclinic bifurcation curve can then be continued, and it either remains finite for all $b > a$, or tend to $-\infty$, in which case cycles would exist for any I smaller than the current associated with the Hopf bifurcation. Because of the structure of the vector field presented in figure 3.1(b).A., cycles necessarily contains the fixed point v_-, and do not include the fixed point v_+, because the intersection of the South zone and the

(a) Bifurcation Diagram (generated with MatCont)   (b) Zoom and Limit Cycles
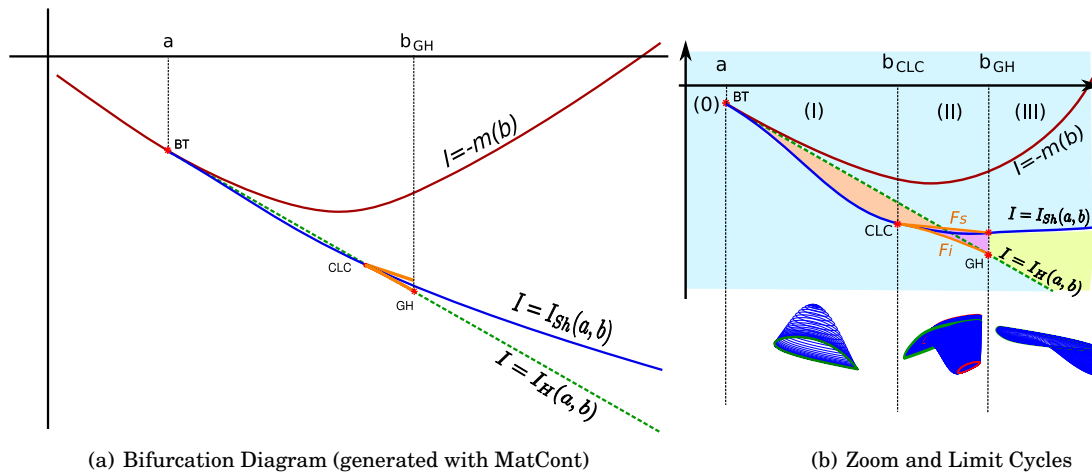
Figure 3.3. Limit cycles in the case where a Bautin bifurcation exist. The saddle-node of limit cycles presents a singular point corresponding to a cusp of limit cycles. From this point emerge two branches of saddle-node of limit cycles. The lower branch of folds of limit cycles connects to the Bautin point, while the upper branch connects with the saddle-homoclinic bifurcation. (a) The orange curve represents the fold of limit cycles, the singular point CLC corresponds to a cusp of limit cycles. In the blue region there is no limit cycle. Zone (0) : No cycle. Zone (I): There exists a unique family of limit cycles in the orange zone, starting from Hopf bifurcation and disappearing via saddle-homoclinic bifurcation. Zone (II) the family of limit cycles undergoes two folds of limit cycles. There are two branches of unstable limit cycles and a branch of stable limit cycles. The family appears via subcritical Hopf bifurcation and disappears via saddle-homoclinic bifurcation. In zone (III) there is a unique family of stable limit cycles in the yellow zone for inputs between the saddle-homoclinic and the supercritical Hopf bifurcation, disappearing via saddle-homoclinic bifurcation. (b) Families of limit cycles in each case. Green cycle = saddle-homoclinic orbit, red cycle= fold of limit cycle.

set $\{v \geq v_+\}$ is stable and therefore no trajectory can escape from this zone. At a subcritical Hopf bifurcation, cycles appear around the fixed point v_-, and inflate when decreasing the input current until reaching the saddle fixed point v_+.

In the cases where the system undergoes a Bautin bifurcation, the structure of the limit cycles is slightly more complex. Indeed, in addition to the subcritical Bogdanov-Takens bifurcation, the system undergoes a Bautin bifurcation. Locally around this point, a family of stable limit cycles and family of unstable ones coexist, collide and disappear via a fold (saddle-node) bifurcation of limit cycles. We numerically computed these two curves in the case of the quartic model using the MatCont toolbox (31; 32) and present the results in figure 3.3. We observe that for $b < a$, there is no limit cycle (zone (0)).

I. For $a < b < b_{CLC}$, there is one family of limit cycles, starting from Hopf bifurcation and disappearing via saddle-homoclinic bifurcation.

II. For $b_{CLC} < b < b_{GH}$ the family of limit cycles undergoes two folds of limit cycles. There are two branches of unstable limit cycles and a branch of stable limit cycles. One of the branches of unstable limit cycles disappears via saddle-homoclinic bifurcation.

III. For $b > b_{GH}$ there is a unique family of stable limit cycles in the green zone emerging from a supercritical Hopf bifurcation and disappearing via saddle-homoclinic bifurcation.

In zones (0),(I) and (III) the structure of limit cycles is quite simple. Case (II) is more complex and needs some attention (see figure 3.4). In this case, the Bautin bifurcation generates a fold of limit cycles bifurcation in its neighborhood. We observe numerically that the curve of fold of limit cycles has a singular point where the system undergoes a cusp of limit cycles. Between the Bautin bifurcation point and the cusp of limit cycles point, the curve of folds of limit cycles can be parameterized as the graph of a function of b: $\{(I, b); I = F_i(b)\}$. The second branch of fold of limit cycles branching to the first one at the cusp point disappears via saddle-homoclinic bifurcation. It can also be characterized as the graph of a function of b: $\{(I, b); I = F_s(b)\}$. For $I_H < I < F_s$ there is a unique unstable limit cycle around the stable fixed point. For $F_s < I < I_{Sh}$ there are three limit cycles, two unstable limit cycles circle a stable limit cycle. For $I_{Sh} < I < F_i$ there are two limit cycles: an unstable around the fixed point, circled by a stable one. Therefore, in that case, the system presents self-sustained subthreshold oscillations before the Bautin bifurcation. Note eventually that zone (II) is relatively small in the parameter space.
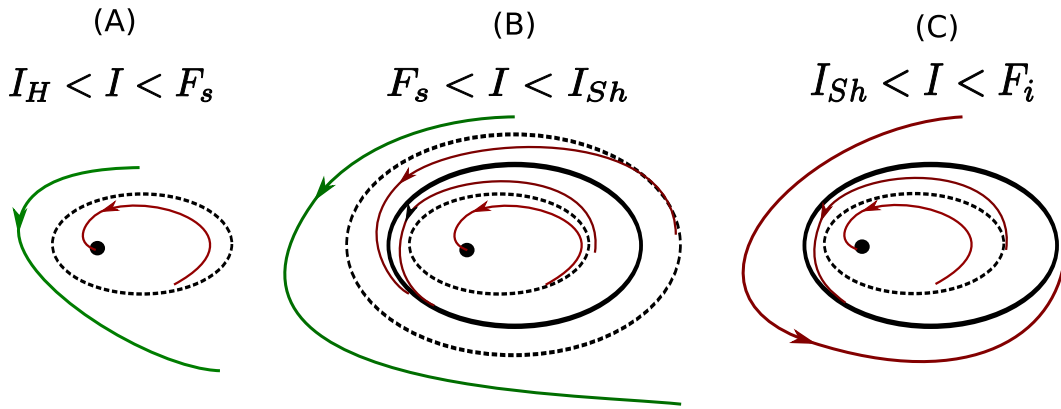
Figure 3.4. Families of limit cycles in zone (II) of the diagram corresponding to $b_{CLC} < b < b_{GH}$. Dashed cycles correspond to unstable periodic orbits, plain cycles to stable periodic orbit, the black dot symbolizes the fixed point. Red orbits are those attracted by the stable limit cycles or fixed point, and green orbits the other ones.

The presence of periodic orbits shapes the structure of the stable manifold of the saddle-fixed point. We describe now the topology of this stable manifold and the shape of the attraction basins of the possible subthreshold attractors.

3.2.2   Stable manifold and attraction basins

We are now interested in the structure of the attraction basins of SAs. A point (v, w) belongs to the attraction basin of a SA if and only if the system (3.1) starting from this point converges towards this attractor. The topology of this set is governed by the subthreshold dynamics, and the problem of identifying in a closed form the attraction basin of the SAs is very hard to handle formally. Nevertheless in our particular case, the structure of these attraction basins can be characterized because the system has the property that the shape of this attraction basin is closely related to the structure of the stable manifold of the saddle fixed point (SMSFP).

The first order expansion of the SMSFP around the saddle fixed point is given by the eigenvalues and eigenvectors of the Jacobian matrix at this point. The SMSFP is composed of two submanifolds: one of them is locally contained in the zone $v \geq v_+$ which we denote Γ^+ and the other in the zone $v \leq v_+$ and will be denoted Γ^-. In all the cases, the submanifold Γ^+ is fully above the v-nullcline (i.e. $w \geq F(v) + I$), because of the direction of the eigenvectors of the Jacobian matrix at this point and of the shape of the vector field. This submanifold stays in the North zone described in figure 3.1(b) and this curve is the graph of an increasing function of v. The shape of the submanifold Γ^- locally in the zone $v \leq v_+$ and below the v-nullcline, depends on finer properties of the vector field, as we discuss in the sequel and in section 3.2.3.

Subcritical case:

We are first interested in the case where the system presents a unique repulsive periodic orbit. The description of the shape of the SMSFP is based on qualitative arguments including Cauchy–Lipschitz and Poincaré–Bendixon theorems. Since this orbit is a trajectory of the dynamical system, no solution can cross it because of the Cauchy-Lipschitz theorem. The attraction basin of the stable fixed point will therefore be delineated by the periodic orbit: any trajectory having its initial condition inside this closed orbit will necessarily converge to the fixed point because of the Poincaré-Bendixon theorem, and no solution starting outside this zone can converge towards this fixed point because it cannot cross the periodic orbit. Therefore, the attraction basin of the stable fixed point is the zone in the phase plane delineated by the unstable limit cycle. In that case, the submanifold Γ^- winds around this cycle. Indeed, this submanifold can be computed using the backward equation related to (3.1). If it is an unbounded orbit, this stable manifold will split the phase plane into two zones, one of which containing the unstable limit cycle and the stable fixed point. Any trajectory starting in the zone containing the stable fixed point will either converge to the fixed point if it is inside the attraction basin of this fixed point delineated by the unstable periodic orbit, or will be trapped inside this zone and will not enter inside the periodic orbit. In the latter case, this trajectory cannot diverge because of the structure of the trajectories and the shape of Γ^+. The Poincaré-Bendixon theorem would imply that there exists a stable fixed point or a stable periodic orbit in this zone which is not the case. Therefore the

(a) Stable Manifold and limit cycle

(b) Fixed point, separatrix crosses both nullcline

(c) Fixed point, separatrix crosses no nullcline

(d) Periodic orbit, separatrix crosses the w-nullcline
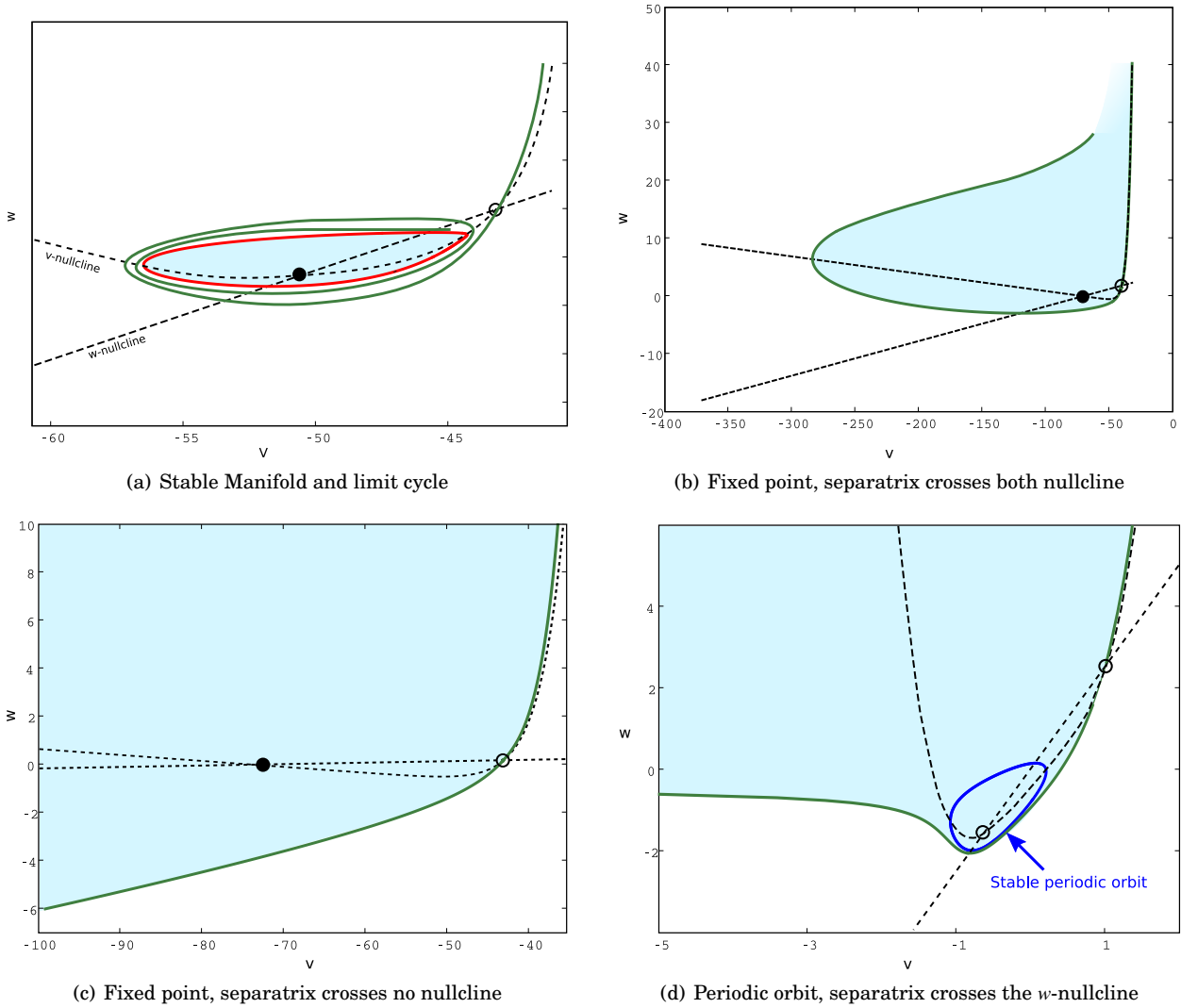
Figure 3.5. Representation of the attraction basin and the stable manifold of the saddle fixed point in different cases. (a): A repulsive limit cycle (red curve) exists around the stable fixed point (black circle), the SMSFP (green line) converges towards the cycle, and the attraction basin (blue zone) is bounded. The black dashed lines corresponds to the nullclines. (b): Case where the separatrix crosses both nullclines (same color code), in the case of the adaptive exponential model with original parameters except $a = 2g_L$ and $\tau_m = \tau_w$; (c): Case where the stable manifold crosses no nullcline: it is the graph of an increasing function of v which delineates the attraction basin of the stable fixed point (case of the dimensioned adaptive exponential model with the original parameters except $a = 2g_L$ and $\tau_w = \tau_m/3$); (d): Case where the stable manifold only crosses the w-nullcline. It was represented in the case where the stable trajectory is a periodic orbit (quartic model, $a = 1$, $b = 2.51 > b_{GH}$, $I = -0.5$).

shape Γ^- will necessarily be bounded, and because of Poincaré-Bendixon's theorem, it will either converge to a fixed point or to a periodic orbit. Since there is no stable fixed point reachable by the stable manifold (the stable fixed point is repulsive for the backwards dynamics, and is trapped in the limit cycle), this orbit will converge to the limit cycle (see figure 3.5(a)).

In the cases where there is no unstable limit cycle around the SA (i.e. for $b < a$, or $b > a$ and $I < I_{Sh}$), the attraction basin of the SA will be unbounded, and its shape will be deduced from the shape of the SMSFP.

For the submanifold Γ^-, several cases can occur, depending on the limit of the derivative of F at $-\infty$, which we denote $F'_{-\infty}$.

- The stable manifold of the saddle fixed point can cross both nullclines (see figure 3.5(b)). As proved in (116), this will be the case when $F'_{-\infty} > -\infty$ and if $b \geq \frac{(F'_{-\infty}+a)^2}{4a}$,

- It can cross the w-nullcline (which will always be the case when $a < -F'_{-\infty}$) but not the v-nullcline. In this

68

case, the SMSFP is the graph of a function of v, that will be decreasing before it crosses the nullcline and increasing after this point (see figure 3.5(d)),

- It can cross no nullcline, and in this case the separatrix is the graph of an increasing function of v (see figure 3.5(c)). This case never occurs when $F'_{-\infty} = -\infty$.

In these cases, the SMSFP is unbounded, and splits the phase plane into two connected components, one of which containing the SA. This component is the attraction basin of the SA.

Hence we conclude that the attraction bassin of the stable fixed point is either bounded and delineated by the unstable limit cycle, or unbounded and delineated by the stable manifold of the saddle fixed point.

Bautin case

This dichotomy also applies in the case where the system undergoes a Bautin bifurcation: if the SA (fixed point or stable periodic orbit) is circled by an unstable limit cycle, then the attraction basin of the SA will be delineated by this cycle, and if not, the attraction basin will be delineated by the SMSFP.

Consider for instance the case of figures 3.3 and 3.4. Using the notations of figure 3.3 we can prove that:

- When there is no fixed point, the system has no SA and there is no saddle fixed point.

- For $b < a$ and $I < -m(b)$, the system has a unique stable fixed point whose attraction basin is unbounded and delineated by the SMSFP.

- For $a < b < b_{CLC}$, the case is very similar to the subcritical case and the behavior depends on the input current:

  - If $I_H < I < -m(b)$ the system has no SA and two unstable fixed points. This case is treated in section 3.2.3.

  - If $I_{Sh} < I < I_H$ where I_{Sh} is the value of the current at the saddle-homoclinic bifurcation, the system has a unique SA which is a stable fixed point, circled by an unstable limit cycle. This periodic orbit delineates the attraction basin of the stable fixed point and the SMSFP winds around it

  - If $I < I_{Sh}$ the system has a unique stable fixed point whose attraction basin is unbounded and delineated by the SMSFP.

- For $b_{CLC} < b < b_{GH}$, we have:

  - For $I_{SN} < I < \max(I_H, F_s)$ there are two unstable fixed points and no periodic orbit, hence no SA.

  - For $\max(I_H, F_s) < I < F_s$, the system has a unique SA which is a stable fixed point, circled by an unstable limit cycle. This periodic orbit delineates the attraction basin of the stable fixed point and the SMSFP winds around it (case of figure 3.5(a)).

  - For $F_s < I < I_{Sh}$ the system has two SAs: a fixed point and a stable limit cycle (see figure 3.4(B)). The stable fixed point is circled by an unstable limit cycle which delineates its attraction basin. The stable periodic orbit is contained in a ring delineated by two unstable limit cycles. This ring is the attraction basin of the stable limit cycle. The submanifold Γ^- of the SMSFP winds around the exterior unstable limit cycle.

  - For $I_{Sh} < I < F_i$ the system has a stable fixed point whose attraction basin is delineated by an unstable periodic orbit circling around it (see figure 3.4(C)). Around this cycle there is a stable limit cycle, whose attraction basin is an unbounded zone with one hole delineated by the unstable limit cycle and the SMSFP which is unbounded.

  - For $I < F_i$ the system has a stable fixed point whose attraction basin is unbounded and delineated by the SMSFP.

- In the case $b > b_{GH}$, we have:

  - if $I_{Sh} < I < -m(b)$ the system has no SA and two unstable fixed points.

  - if $I_H < I < I_{Sh}$ the system has two unstable fixed points and a stable periodic orbit whose attraction basin is unbounded and delineated by the SMSFP.

  - if $I < I_H$ the system has a stable fixed point with an unbounded separatrix.

3.2.3 Heteroclinic orbits

In the case where there are two unstable fixed points, one of which is repulsive and the other saddle, then the component Γ^+ of the SMSFP is the graph of an increasing function of v for $v \geq v_+$ and stays above the v-nullcline. The submanifold Γ^- will connect to the repulsive fixed point, for the same reasons as mentioned in the case of the presence of an unstable limit cycle. Indeed, if we consider the backward equation starting in the neighborhood of the saddle fixed point, the repulsive fixed point of the forward dynamics becomes attractive, and it is the unique bounded trajectory possible. The stable manifold when considering the backward equation will either converge to the fixed point, or will diverge, according to Poincaré-Bendixon's theorem. But assuming that it is unbounded leads to a contradiction: if it was unbounded, it would separate two zones of the phase plane (see figure 3.5), one of which containing the unstable fixed point. A trajectory having its

(a) Monotonous connection to equilibrium

(b) Oscillatory connection to equilibrium
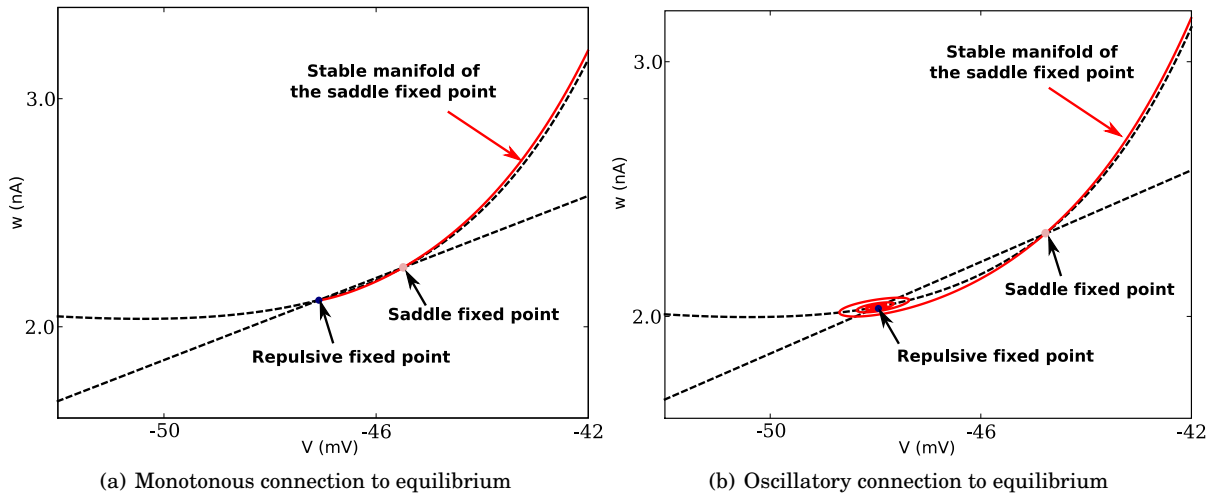
Figure 3.6. Stable manifold of the saddle fixed point in the case of two unstable equilibria. Dashed black curves are the nullclines of the system and the red curve is the stable manifold.

initial condition in this zone will be trapped in it for all $t > 0$. But in this zone, the trajectory will be bounded because of the structure of the vector field, but there is neither fixed point nor stable periodic orbit. Therefore Poincaré-Bendixon's theorem leads to a contradiction, and the stable manifold necessarily connects to the repulsive fixed point. This connection can be one of two types (see figure 3.6): a monotonous connection in the case where the eigenvalues of the Jacobian matrix of the repulsive fixed point are real, and an oscillating connection when the eigenvalues have a non-null imaginary part. This branch of stable manifold is therefore a heteroclinic orbit, connecting a repulsive equilibrium to a saddle equilibrium. It is structurally stable, and disappears at the Hopf bifurcation. In the case where the Hopf bifurcation is subcritical, the heteroclinic orbit connecting the repulsive fixed point and the saddle fixed point converts into a heteroclinic orbit connecting the saddle fixed point with the repulsive limit cycle and we are in the case of figure 3.5(a). In the case where the Hopf bifurcation is supercritical (after the Bautin bifurcation) the heteroclinic orbit will simply disappear. By continuity, the SMSFP will be, after the bifurcation, of type 3.5(b).

3.2.4 Symbolic dynamics and spiking regions

This detailed description of the subthreshold dynamics allows us to get a better insight of the dynamics and to make the diagram 3.1(b) more precise. Indeed, we are now able to provide a Markov partition of the phase plane (see fig.3.7).

- In the case $I > -m(b)$, there is no SA, and the phase plane is partitioned into the *up zone* above the v-nullcline, i.e. defined by $\{(v,w); w \geq F(v)+I\}$, the *center zone* between the two nullclines and the spiking zone below the w-nullcline $\{(v,w); w \leq bv\}$. We observe that any trajectory having its initial condition in the up zone enters in finite time the center zone. Indeed, while the orbit is in the up zone, the derivative of the adaptation variable is strictly inferior to $-d(F(v)+I, bv)$ the distance between the two nullclines. In the center zone, w is decreasing and v is increasing. Because of the vector field along the v-nullcline, we observe that the orbit cannot go back to the up zone. Since in this zone w is a decreasing function of v and the boundary bv an increasing function, it will enter in finite time the spiking zone. In this

spiking zone defined by $w \leq bv$, the trajectory is trapped, and the membrane potential blows up in finite time.

- In the case where there are SAs, we reviewed the different shapes of the related attraction basins. These regions correspond to what we call the *rest* region, in the sense that any orbit starting inside this zone will never fire. This zone is stable under the dynamics, and does not communicate with the other zones (see figures 3.7(b), 3.7(c) and 3.7(d)). We define here again the spiking zone below both the w-nullcline and the SMSFP. This zone is also stable under the dynamics. The *right* zone is the zone above the w-nullcline and below the SMSFP. In this zone, for any initial condition below the v-nullcline, v is increasing and w decreasing. Therefore, the derivative of v increases, and the orbit will enter the spiking zone in finite time, since the orbit is a non-increasing function of v and the boundary is strictly increasing. If the initial condition is in the right zone below the SMSFP and above the v-nullcline, both v and w will be decreasing and therefore the orbit cannot stay above the v-nullcline indefinitely, because of the presence of the unstable manifold of the saddle fixed point, and therefore will be in the right zone below the v nullcline after a finite time, and therefore in the spiking zone in finite time. The *up* zone is the rest of the phase plane. In this zone, orbits do not stay indefinitely, and cannot enter either the rest zone or the right zone, hence enter in finite time the spiking zone.

- In the cases where are two unstable fixed points and no stable limit cycles (Figures 3.7(e) and 3.7(f)), there is no SA except from the SMSFP. We define the *up* zone above both the w-nullcline and the SMSFP, the right zone the zone between the SMSFP and the w-nullcline and the *spiking* zone below both the w-nullcline and the SMSFP. In the spiking zone, as we will see, the system will fire. For any initial condition in the right zone, since the orbit will not cross the SMSFP, it will necessarily enter the spiking zone in finite time.

This is very important in terms of spikes. Indeed, we can prove that for any initial condition in the spiking region, the membrane potential v will blow up in finite time, and therefore a spike will be emitted. Indeed, let (v_0, w_0) be a given initial condition in the bottom region at time t_0. According to the shape of the vector field, as presented in our Markov partition, the whole trajectory will be trapped in this zone. But in this zone, we always have $w \leq v$ and therefore for all $t \geq t_0$ we have $w(t) \leq bv(t)$. According to Gronwall's theorem, the membrane potential at time $t \geq t_S$ will be greater than or equal to the solution of:

$$\begin{cases} \dot{\tilde{v}} & = F(\tilde{v}) - b\tilde{v} + I \\ \tilde{v}(t_S) & = v(t_S) \end{cases}$$

which blows up in finite time by the virtue of assumption 3.1.1.

Therefore any trajectory entering the bottom region will spike, and furthermore any trajectory having its initial condition outside the rest region will enter the bottom region in finite time, and elicit a spike. As we have seen, the dynamics of the reset after a spike depends on the value of the adaptation variable at the times of the spikes, which we describe in the following section.

3.2.5 Behavior of the adaptation variable at spike times

In the spiking zone, we saw that the membrane potential blew up in finite time. This zone does not intersect the v-nullcline. Therefore, in this zone, the orbit (v, w) with initial condition (v_0, w_0) at time t_0 inside the spiking zone can be written as the graph of a function of v for all $t \geq t_0$, i.e. $w(t) = W(v(t))$ where the function W is the solution of the differential equation:

$$\begin{cases} \frac{dW}{dv} = \frac{a(bv - w)}{F(v) - w + I} \\ W(v_0) = w_0 \end{cases} \tag{3.4}$$

Proof. Let $\delta(t) = W(v(t)) - w(t)$. We have $\delta(t_0) = 0$ and furthermore, since the value of $F(v) - w + I > 0$, $\frac{d\delta}{dt} = \frac{dW}{dv}\frac{dv}{dt} - \frac{dw}{dt} = 0$, and hence $\delta(t) \equiv 0$. $\square$

To study the value of the adaptation variable at the explosion time of the membrane potential, we simply study the limit of the equation of the orbits when $v \to \infty$. Here we prove that this value is finite under assumption 3.1.2, and that if $F(v)/v^2$ is asymptotically bounded, the adaptation value tends to infinity. This theorem justifies the introduction of this assumption.

Theorem 3.2.1. *Under assumption 3.1.2, the adaptation variable is finite at the times of the spikes. If $F(v)/v^2$ is bounded when $v \to \infty$, the adaptation variable at the times of the spikes tends to infinity.*

(a) No fixed point case

(b) Unstable limit cycle

(c) Unbounded attraction basin crossing both nullclines

(d) Unbounded attraction basin crossing no nullcline

(e) Monotonous heteroclinic orbit

(f) Oscillatory heteroclinic orbit
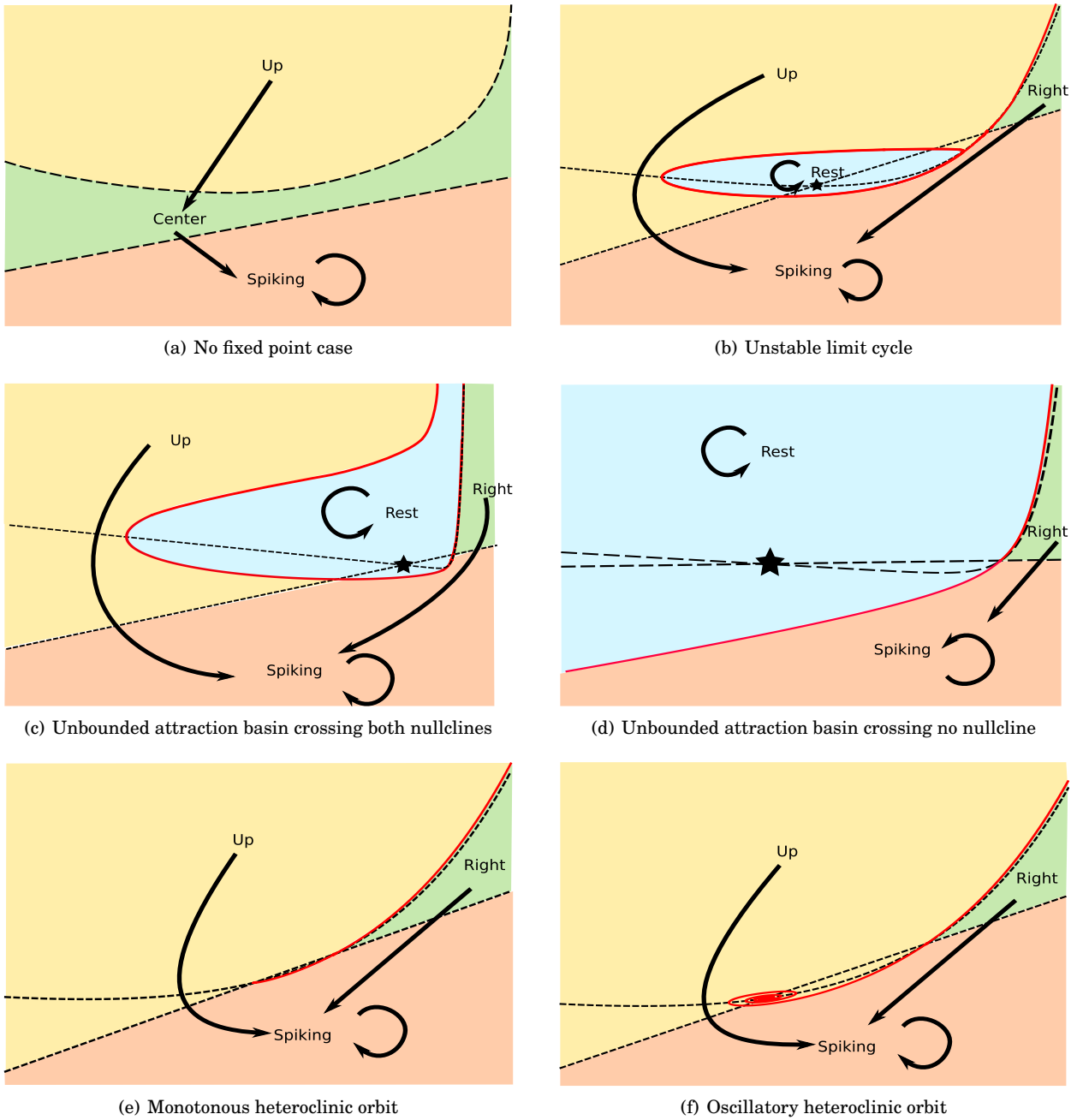
Figure 3.7. Markov partition of the dynamics: the bottom region is a stable region where each trajectory starting from the up or right region will end up in finite time. The rest region composed of the attraction basin of the possible stable trajectory is an isolated region.

Proof. In section 3.2.4, we proved that all the orbits of the system that are not in the attraction basin of the (possible) stable fixed point enter after a finite time the *spiking zone* where they are trapped. This spiking zone is fully included in the half space $\{w < bv\}$, and in this zone the membrane potential blows up in finite time.

The value of the adaptation variable at the time of the spike can therefore be computed using the orbital equation (3.4). We consider $(v(t), w(t))$ an orbit of the differential system (3.1) such that the membrane potential blows up at time t^*. Let $(v_1 = v(t_1), w_1 = w(t_1))$ be a point of the orbit inside the spiking zone. We recall that in the spiking zone, we have $w(t) \leq bv(t)$ and $w(t)$ is non-decreasing. Hence we have

$$\frac{\mathrm{d}W}{\mathrm{d}v} \leq \frac{a(bv - w_1)}{F(v) - bv + I} \tag{3.5}$$

and therefore

$$W(v) \leq w_1 + \int_{v_1}^{v} \frac{a(bu - w_1)}{F(u) - bu + I}\, du$$

If F satisfies assumption 3.1.2, this integral converges when $v \to \infty$. Therefore, $W(v)$ (resp. $w(t)$) is an upperbounded nondecreasing function of v (resp. time), and therefore has a finite value when $v \to \infty$ (resp. $t \to t^*$).

In the case where $F(v)/v^2$ is bounded, this integral does not converge. Using the same technique, we lowerbound this value:

$$\frac{\mathrm{d}W}{\mathrm{d}v} \geq \frac{a(b - W)}{F(v) - w_1 + I}. \tag{3.6}$$

Gronwall's theorem (47) ensures us that the solution of equation (3.4) will be lowerbounded for $v \geq v_1$ by the solution of the linear ordinary differential equation:

$$\begin{cases} \frac{\mathrm{d}z}{\mathrm{d}v} = \frac{a(b-z)}{F(v) - w_1 + I} \\ z(v_1) = w_1 \end{cases} \tag{3.7}$$

that reads:

$$z(v) = \left(\int_{v_1}^{v} \frac{abu}{F(u) - w_1 + I} e^{-g(u)}\, du + w_1 \right) e^{g(v)}$$

where $g(v) = \int_{v_1}^{v} -\frac{a\,du}{F(u) - w_1 + I}$. Because of assumption 3.1.1, the integrand is integrable, and the function g has a finite limit $g(\infty)$ when $v \to \infty$. The exponential terms will hence converge when $v \to \infty$. But the integral involved in the particular solution diverges in the case where $F(v)$ grows slower than v^2, since the integrand is equivalent when $u \to \infty$ to

$$\frac{abu}{F(u)} e^{-g(\infty)}$$

When $F(u)$ grows slower than v^2 there exists $\alpha > 0$ such that $F(v) \leq \alpha v^2$ asymptotically and therefore the solution of the linear differential equation (3.7) tends to infinity when $v \to \infty$ faster than a logarithmic function of v, and so does $W(v)$, and hence $w(t)$ blows up at the time when $v(t)$ blows up. In the case where $F(v)$ grows slower than $v^{2-\varepsilon}$, the solution of the differential equation diverges faster than v^{ε}. □

We conclude that in the case of the quadratic adaptive model, the adaptation variable blows up at the explosion time of the membrane potential variable v, and in the case of the quartic and exponential models, the adaptation variable remains bounded.

For the quadratic model, and models such that the nonlinear function $F(v)$ grows slower than a quadratic function when $v \to \infty$, the system can only be defined using a cutoff value for the spikes. The value of the adaptation variable at the cutoff θ will be given by $W(\theta)$, and therefore will heavily depend on the cutoff value, in a very sensitive way as discussed in (115).

In the quartic and exponential models, and for any model such that $F(v)$ grows faster than $v^{2+\varepsilon}$ for a given $\varepsilon > 0$, the adaptation variable converges, and hence the model can be defined with an infinite threshold.

In these cases, for technical reasons we will use a transformed version of the orbital equation (3.4) obtained by changing variables. For (v_0, w_0) in the spiking zone, we consider $u = (v - v_0 + 1)^{-\varepsilon/2}$ where $\varepsilon > 0$ is given by assumption 3.1.2. When $v(t)$ blows up, $u(t)$ tends to zero, and the orbit in the plane (v, u) satisfies the equation:

$$\begin{cases} \frac{\mathrm{d}\tilde{W}}{\mathrm{d}u} = -\frac{2a(bu^{-2/\varepsilon} - \tilde{W} + \beta)}{\varepsilon u^{1+2/\varepsilon}(F(u^{-2/\varepsilon} + v_0 - 1) - \tilde{W} + I)} \stackrel{\text{def}}{=} g(u, \tilde{W}) \\ \tilde{W}(1) = w_0 \end{cases} \tag{3.8}$$

where $\beta = b(v_0 - 1)$

As we can see in equation (3.1), at the times where the membrane potential blows up and since the adaptation variable remains bounded, the derivative of the adaptation variable tends to infinity when v blows up. For this reason, accurate numerical simulations are quite hard to perform. But since in the phase plane the orbit has a regular equation, an accurate algorithm based on the simulation of the orbital equation as soon as the orbit enters the spiking zone provides a precise and stable evaluation of the adaptation value at the time of the spike using standard simulation algorithms (Runge-Kutta, Euler, ...). This method was implemented in order to produce our numerical simulations.

3.2.6 Existence and uniqueness of a solution

We first discuss the well-posedness of these equations. Mathematically, the problem is well-posed if the system defined by equations (3.1) and (3.2) together with an initial condition (v_0, w_0) at time t_0 has a unique solution defined for all $t \geq t_0$. The precise study we just performed gives us a better understanding of the dynamics of the subthreshold system. In particular, we saw that the solutions of the subthreshold equation (3.1) blew up in finite time, and under assumption 3.1.2, the adaptation variable at these times has a finite value. The solutions of the subthreshold equations are hence not defined for all time. The reset condition is therefore essential to have a forward solution to the problem defined for all $t \geq t_0$. The reset condition is sufficient for the problem to be well posed, as we prove in the following:

Proposition 3.2.2. The equations (3.1) and (3.2), together with initial conditions (v_0, w_0) at time t_0 have a unique solution defined for $t \geq t_0$.

Proof. Because of the regularity assumption on F, Cauchy-Lipschitz theorem of existence and uniqueness of solution applies for equation (3.1) up to the explosion time. If the solution of (3.1) does not blow up in finite time, we have existence and uniqueness of solutions for the problem. If the solution blows up at time t^*, then we are reset to a unique point, defined by the reset condition (3.2), and we are again in the case we already treated starting from $(v_r, w(t^*) + d)$ at time t^*. We can apply this mechanism again provided since the value of $w(t^*)$ is finite. Furthermore, to be able to prove the existence and uniqueness of solution for all $t \geq t_0$, we need to ensure that the interspike interval does not tend to 0 (i.e. spikes do not accumulate at a given time). The spike time decreases when the value of the adaptation on the reset line decreases. Therefore we have to ensure that the adaptation value at the times of the spike do not tend to $-\infty$. But for w_0 in the spiking zone, the value of the adaptation variable is increasing all along the trajectory and therefore the new adaptation value after a spike is emitted will be greater than the former value plus d, and hence it is impossible that this reset value tends to $-\infty$. We conclude that the interspike interval has a lower bound on this trajectory, and between two spike times, there is a unique solution. Therefore we have existence and uniqueness of a solution starting from (v_0, w_0) which is defined for all $t \geq t_0$. □

Another interesting question from the mathematical and neural coding points of view would be to solve the related Cauchy problem. This problem consists in proving that there exists a unique solution defined for all $t \in \mathbb{R}$. The Cauchy problem was addressed by Romain Brette in (12) in the case of spiking models defined by a one dimensional ODE with a finite spiking threshold and a reset condition. He found that the reset introduced a countable and ordered set of backward solutions for a given initial condition, and that this structure of solutions had important implications in terms of neural coding. The case of the system given by (3.1) and (3.2) can be treated in the same fashion as done in (12) and one obtains the same results as Brette in (12). It is done in appendix A.

3.2.7 The adaptation map

Now that we are ensured that there exists a unique solution to the forward problem given by equations (3.1) and (3.2), we are interested in characterizing the spike patterns fired by a neuron of this type. These patterns are governed by the initial condition of the system after each spike, and this is why we now introduce an essential element of our work, a discrete map called the adaptation map.

Definition 3.2.1 (The adaptation map). We denote by $\mathscr{D}$ the domain of adaptation values w_0 such that the solution of (3.1) with initial condition (v_r, w_0) blows up in finite time. Let $w_0 \in \mathscr{D}$, and denote $(v(t), w(t))$ the solution of (3.1) with initial condition (v_r, w_0) and t^* the blowing time of v. The adaptation map Φ is the unique function such that

$$\Phi(w_0) = w(t^*) + d$$

The adaptation map gives the next reset location of a spiking orbit with initial condition on the *reset line* $v = v_r$. If we are interested in the spike patterns generated from an initial condition (v_0, w_0) where $v_0 \neq v_r$, the analysis will be valid after the first spike is emitted. More precisely, if (v_0, w_0) is in the attraction basin of a bounded trajectory or on the stable manifold of the saddle fixed point, then it will not elicit a spike. If it is not, then it will fire in finite time and be reset on the line $v = v_r$ at a given value w_1. From this point, the study of the iterations of the map Φ will be valid.

Moreover, assume that in the dynamical system defined by (3.1) starting from the initial condition (v_r, w_0) is in a tonic spiking behavior (i.e. fires infinitely many spikes). Then let $(t_n)_{n \geq 0}$ be the sequence of spike times, and define the sequence of adaptation reset points by $w_n \stackrel{\text{def}}{=} w(t_n) = w(t_n^-) + d$. The adaptation map of this dynamical system is the function Φ such that

$$\Phi(w_n) = w_{n+1}$$

Hence we will be able to apply techniques of nonlinear analysis of iterations of maps to study the spiking location sequences and the spiking times.

For these reasons, we will be interested in the sequel in the dynamics of the iterations of the map Φ which corresponds to a trajectory starting from an initial condition on the reset line. The intersections of the nullclines with the reset lines are of particular interest in the study of Φ. We define:

$$\begin{cases} w^* & = F(v_r) + I \\ w^{**} & = bv_r \end{cases} \tag{3.9}$$

Both points depend on the reset voltage v_r. Interestingly enough, besides v_r, the point w^* only depends on the input current and the nonlinearity, while the point w^{**} only depends on the parameter b. The figure Fig.3.8 represents bundles of trajectories for $w_0 < w^*$ or $w_0 > w^*$ in the case where the nullclines do not intersect. It illustrates the qualitative distinctions linked with the relative location of w with respect to w^*.

(a) Phase plane for $w_0 < w^*$ (b) Phase plane for $w_0 > w^*$
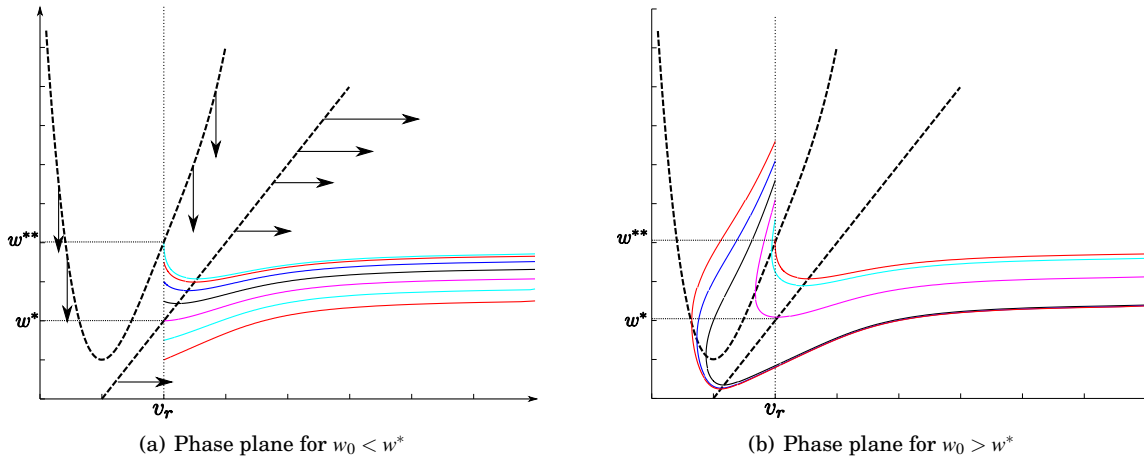
Figure 3.8. Phase plane and trajectories for the quartic model in the no-fixed point case. The trajectories starting from $w < w^{**}$ have an increasing w all along the trajectory, which is not the case for $w > w^{**}$. For $w > w^*$, we observe that the trajectory turns around the point (v_r, w^*) and crosses again the line $v = v_r$ before spiking.

The sequence of interspike intervals is the image of the orbit under Φ by the application $\mathscr{T} : w \in \mathscr{D} \mapsto t^*(w)$, where $t^*(w)$ is the spike time if the membrane potential starts at (v_r, w) at time $t = 0$. Although this map is not always injective, the spike patterns are qualitatively governed by the adaptation map.

Now that we introduced the main framework of our study, we will study more precisely the properties of the adaptation map Φ and its links with the spike patterns produced. The different spike patterns are linked with the topology of the domain $\mathscr{D}$ and with properties of the map Φ. We chose here to present our results in function of the subthreshold dynamical properties, since it will make our mathematical analysis clearer. We will summarize the different regions of parameters for which a given spike pattern is produced in section 3.5.2.

3.3 NO FIXED POINT CASE

In this section we consider the case where there is no fixed point in for the subthreshold dynamical system. This case corresponds to the case where $I > -m(b)$. In that case the system has neither stable fixed point nor limit cycle, and hence no bounded trajectory, and the neuron will fire whatever its initial condition, which means that the definition domain $\mathscr{D}$ of the adaptation map Φ is $\mathbb{R}$.

3.3.1 Description of the adaptation map

We prove the following theorem.

Theorem 3.3.1. *In the case $I > -m(b)$ and under the condition 3.1.2, the adaptation map satisfies the following properties (see figure Fig.3.9):*

- *It is increasing on $(-\infty, w^*]$ and decreasing on $[w^*, \infty)$,*
- *For all $w < w^{**}$ we have $\Phi(w) \geq w + d \geq w$,*
- *Φ is regular (at least continuously differentiable),*
- *It is concave for $w < w^*$,*
- *It has a unique fixed point in $\mathbb{R}$,*
- *It has a horizontal asymptote (plateau) when $w \to +\infty$*

This theorem is important to understand the main properties of the *adaptation sequence* $(w_n)_{n \geq 0}$ starting from a given initial condition $w_0 \in \mathscr{D}$ defined by:

$$w_{n+1} = \Phi(w_n) \qquad n \geq 0 \tag{3.10}$$

These properties would be straightforward if we had a spiking threshold, the only technical intricacy is the fact that the spike occurs when the membrane potential blows up.
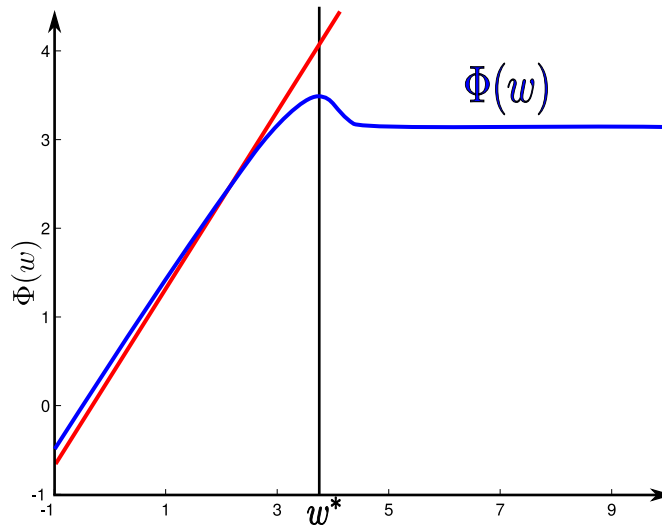
Figure 3.9. The adaptation map Φ in the case of the quartic model for $I > -m(b)$ (no-fixed point). The blue line corresponds to the map Φ, the red line to the identity map and the black line localizes w^*. We represent on this diagram the main properties of Φ stated in theorem 3.3.1 (w^{**} is smaller than -1 in this case and does not appear in this plot.)

Proof. The proof of this theorem is mainly based on a characterization of the orbits in the phase plane, given by equations (3.4) and (3.8). Using these equations, the orbit of the system with initial condition (v_r, w_0) in the spiking zone (i.e. $w_0 \leq w^*$) can be written as:

$$\tilde{W}(u; w_0) = w_0 - \int_u^1 g(s, \tilde{W}(s, w_0)) \, ds. \tag{3.11}$$

We have in particular

$$\Phi(w_0) = \lim_{u \to 0} \tilde{W}(u, w_0) + d. \tag{3.12}$$

- *Monotony:* Let $w_1(0) < w_2(0) \leq w^*$. The orbits $(v_1(t), w_1(t))$ having initial condition $(v_r, w_1(0))$ at time $t = 0$ and $(v_2(t), w_2(t))$ having initial condition $(v_r, w_2(0))$ at time $t = 0$ will never cross because of Cauchy-Lipschitz theorem. Since they both are in the center or in the spiking zone of diagram 3.7(a), they satisfy equation (3.4) and since they do not cross, we will always have $\tilde{W}_1(v) \leq \tilde{W}_2(v)$, and thus $\Phi(w_1(0)) \leq \Phi(w_2(0))$.

  Let us now assume that $w^* \leq w_1(0) < w_2(0)$. In that case, the initial condition is in the up zone of diagram 3.7(a). In this zone, we have seen that both variables v and w decrease. The orbit enters in finite time the center zone where v increases and w keeps decreasing. The orbits will therefore cross one time the reset line before spiking. This reset line is a Jordan section, and Jordan's theorem (see for instance (33, Chap. 9, appendix, p. 246)) implies that the solutions are always ordered on this section, and the order of the adaptation value at the two new crossing positions w_1^1 and w_2^1 is inverted, i.e. $w_2^1 < w_1^1$. By application of the previous case, we obtain

  $$\Phi(w_1(0)) = \Phi(w_1^1) \geq \Phi(w_2^1) = \Phi(w_2(0)).$$

  We conclude that the map Φ is increasing on $(-\infty, w^*]$ and decreasing on $[w^*, \infty)$.

- *Behavior for $w < w^{**}$:* If $w < w^{**}$, then w will increase all along the trajectory, and hence for all t smaller than the spike time t_s, we have $w(t) \geq w$ and therefore $w(t_s) \geq w$ and hence $\Phi(w) \geq w + d$.

- *Regularity:* The regularity of Φ for $w < w^*$ comes from the theorem of regularity of the solution of an ordinary differential equation with respect to its initial condition. Since in the region $w < w^*$ (center and spiking regions of diagram 3.7(a)) the value of $F(v) - w + I$ never vanishes, the orbit starting from the initial condition (v_r, w_0) satisfies equations (3.4) in the plane (v, w) and equation (3.8) in the plane (u, w). In order to apply the regularity theorem with respect to the initial condition, we consider here equation (3.8) and check the regularity conditions.

  The function g is C^∞ with respect to its two variables on $(0, 1] \times \mathbb{R}$. We prove that it is regular at the point $u = 0$. First, the map g tends to 0 when $u \to 0$ because of condition 3.1.2, since it is equivalent when $u \to 0$ to $-2ab/(\varepsilon u^{1+4/\varepsilon} F(u^{-2/\varepsilon} + v_r - 1))$ which tends to 0 ($F(u^{-2/\varepsilon} + v_r - 1) \leq \alpha u^{-4/\varepsilon - 2}$). Furthermore it is Lipschitz on $[0, 1]$ with respect to $\tilde{W}$ since the partial derivative of this function reads:

  $$\frac{\partial g}{\partial \tilde{W}} = \frac{2a}{\varepsilon u^{1+2/\varepsilon}} \frac{(F(u^{-2/\varepsilon} + v_r - 1) - b(u^{-2/\varepsilon} + v_r - 1) + I)}{(F(u^{-2/\varepsilon} + v_r - 1) - \tilde{W} + I)^2}$$

  This derivative is therefore positive, and because of assumption 3.1.2 tends to zero when $u \to 0^+$. Therefore, this function can be extended as a continuously differentiable function in the neighborhood of 0 and using the theorem of Cauchy-Lipschitz with parameters, we conclude that the map $\tilde{W}$ is continuous with respect to the initial condition.

  We can obtain even more regularity, provided that we prove that the map g has limits for its partial derivatives of higher order. The higher order partial derivatives of g with respect to $\tilde{W}$ will converge to zero when $u \to 0^+$ using the same argument, and by induction, we can prove that this is true for all the derivatives with respect to $\tilde{W}$ at $u = 0^+$. The partial derivative with respect to u are slightly more intricate in the general case, but in the case of the quartic and exponential model, we can readily prove that g is C^∞ in $(u, \tilde{W})$ and therefore the theorem of Cauchy-Lipschitz with parameters implies that the map $\tilde{W}(\cdot, \cdot)$ and $\Phi(\cdot)$ are C^∞.

  For $w \geq w^*$, the orbit will turn around the point (v_r, w^*). Hence Φ is the composition of the application giving the first crossing location of the orbit with the curve $\{v = v_r\}$ and Φ for $w < w^*$. The second is continuously differentiable or even more regular because of the latter argument, and the first one is C^∞ because of the standard theory of Poincaré applications (Cauchy-Lipschitz theorem with parameters for the system 3.1).

- *Concavity:* As already stated, for $w < w^*$, the solution of equation (3.1) will never cross the v nullcline, and the equation of the orbits in the phase plane $(u, \tilde{W})$ is given by equation (3.8), whose solution can be formally written using equation (3.11). We have:

$$\begin{cases} \frac{\partial g}{\partial \tilde{W}} = \frac{2a}{\varepsilon u^{1+2/\varepsilon}} \frac{F(u^{-2/\varepsilon} + v_r - 1) - b(u^{-2/\varepsilon} + v_r - 1) + I}{(F(u^{-2/\varepsilon} + v_r - 1) - \tilde{W} + I)^2} > 0 \\ \frac{\partial^2 g}{\partial \tilde{W}^2} = \frac{4ab}{\varepsilon u^{1+2/\varepsilon}} \frac{F(u^{-2/\varepsilon} + v_r - 1) - b(u^{-2/\varepsilon} + v_r - 1) + I}{(F(u^{-2/\varepsilon} + v_r - 1) - \tilde{W} + I)^3} > 0 \end{cases} \tag{3.13}$$

using the fact that $F(v) - w + I > 0$ and $w < bv$. Because of (3.8) the following formula for the second derivative of Φ with respect to w_0.

$$\frac{\partial^2 \tilde{W}}{\partial w_0^2} = - \int_u^1 \frac{\partial^2 g}{\partial \tilde{W}^2} \left(\frac{\partial \tilde{W}}{\partial w_0} \right)^2 + \frac{\partial g}{\partial \tilde{W}} \frac{\partial^2 \tilde{W}}{\partial w_0^2},$$

Because of the second inequality (3.13) we have $\frac{\partial^2 \tilde{W}}{\partial w_0^2} \leq - \int_u^1 \frac{\partial g}{\partial \tilde{W}} \frac{\partial^2 \tilde{W}}{\partial w_0^2}$, and furthermore $\frac{\partial^2 \tilde{W}}{\partial w_0^2}(1, w_0) = 0$. Thus using Gronwall's theorem we obtain the convexity of the function $\tilde{W}(u, \cdot)$ for all u.

The adaptation map Φ is defined by

$$\Phi(\cdot) = \lim_{u \to 0} \tilde{W}(u, \cdot) + d$$

Since g is at least C^2 in the second variable, so is the flow (Cauchy-Lipschitz theorem with parameters) and hence Φ has the same convexity property for $w < w^*$.

- *Existence and uniqueness of fixed point:* Since $\Phi(w) \geq w + d$ for all $w < w^{**}$ and $\Phi(w)$ is a non-increasing function for $w > w^*$, we have existence of at least one fixed point. If $\Phi(w^*) < w^*$, then there exists a fixed point $w_{fp} \leq w^*$. Because of the concavity property of Φ, there is no other fixed point in $(-\infty, w^*)$, and since Φ is decreasing on (w^*, ∞), it has no fixed point for $w > w^*$. If $\Phi(w^*) > w^*$, the map Φ has no fixed point for $w \leq w^*$ because of the concavity of Φ and has a unique fixed point for $w > w^*$ since Φ is non-increasing for $w > w^*$.

- *Horizontal asymptote (plateau):* The principle of the proof is to show that there exists a solution whose membrane potential diverges to $-\infty$ when integrating the backward equation (i.e. changing t by $-t$), so that the solution separates the phase plane into two subdomains, and the orbits are trapped in one of the two domains. In the zone above this solution, the map Φ will be decreasing and lowerbounded, hence will converge when $w \to +\infty$.

To prove the existence of such a solution, we search for an invariant subspace of the phase plane for the backwards dynamics (i.e for the dynamical system $(v_b(t) = v(-t), w_b(t) = w(-t))$) below the v-nullcline $\mathcal{N}$ (i.e. included in the center or spiking zones).

It is sufficient to consider domains bounded by two lines, of type:

$$\mathscr{B} \stackrel{\text{def}}{=} \{(v, w) \mid v \leq v_0, w \leq w_0 + \alpha(v - v_0)\}$$

where the real parameters α, v_0, w_0 are free.

We show that we can find real parameters (v_0, w_0, α) such that this domain is invariant by the backwards dynamics and does not cross $\mathcal{N}$. We will search for non positive values of α.

First of all, for the boundary $\{v = v_0, w \leq w_0\}$, we want $\frac{dv_b}{dt} \leq 0$, which only means $w_b \leq w^*(v_0) = F(v_0) + I$.

Now we have to characterize both v_0, w_0 and α such that the vector field is flowing out of the affine boundary $\mathscr{B}$. This means that $\langle \binom{\dot{v}}{\dot{w}} | \binom{\alpha}{-1} \rangle \leq 0$ where $\langle \cdot | \cdot \rangle$ denotes the Euclidean dot product. This condition simply reads $\alpha \dot{v} - \dot{w} \leq 0$ and has to be fulfilled on each point of the boundary, which is equivalent to:

$$\begin{cases} H_\alpha(v) & \stackrel{\text{def}}{=} \alpha(F(v) - w + I) - a(bv - w) \leq 0 \text{ with} \\ w & = w_0 + \alpha(v - v_0) \end{cases} \tag{3.14}$$

We first fix α and v_0 so that $\mathscr{B}$ is fully included in the center or spiking zones. This condition is achieved by taking $v_0 < v^*(0)$, the value where F achieves its minimum, and $\lim_{v \to -\infty} F'(v) < \alpha < F'(v_0) < 0$. Because of the convexity assumption and the fact that the limit of the derivative of F at $-\infty$ is strictly negative, there exists $F_{\min}$ such that for all $v \in \mathbb{R}$ we have $F(v) \geq F_{\min}$. We have on the boundary of the domain:

$$\begin{aligned} H_\alpha(v) &\leq \alpha\left(F_{\min} - w + I\right) - a\left(bv - w\right) \\ &\leq \alpha(F_{\min} - \alpha(v - v_0) - w_0 + I) - a(b(v - v_0) - \alpha(v - v_0) + bv_0 - w_0) \\ &\leq (v - v_0)\{-\alpha^2 - ab + \alpha a\} + \{-\alpha w_0 + \alpha I + \alpha F_{\min} - abv_0 + aw_0\} \end{aligned}$$

Therefore the lefthand term of condition (3.14) is bounded by an affine function of v. The slope coefficient is negative. Therefore a sufficient condition for (3.14) to be satisfied is that the second term is negative. This affine term reads:

$$(a - \alpha)w_0 + \alpha I + \alpha F_{\min} - a b v_0$$

and hence involves a term proportional to w_0 with a positive coefficient, and w_0 is the last free parameter of the boundary. Choosing a large negative value for w_0 solves the problem.

We have defined a domain $\mathscr{B}$ on the boundary of which the vector field flows outwards, and hence the backward equation's vector field flows inwards this zone. Therefore, $\mathscr{B}$ is flow invariant for the backward solution, and every solution having its initial condition in this zone does not cross the nullcline, hence goes to infinity with a speed lowerbounded by the minimal distance between le nullcline and $\mathscr{B}$.

We have proved that there is an orbit such that the membrane potential of the backward solution goes to $-\infty$, and whose forward solution spikes (since the initial condition in the spiking zone). This solution necessarily crosses the line $\{v = v_r\}$; denote w_L the value of w at this intersection. This solution splits the phase space in two subspaces which do not communicate: every orbit starting in one of the two subspaces will stay in this subspace by application of Cauchy-Lipschitz theorem. Hence for all $w > w^*$, $\Phi(w) \geq \Phi(w_L)$, hence Φ is decreasing and lowerbounded, hence converges to a finite value when $w \to +\infty$ and its graph presents an horizontal asymptote.

$\square$

We characterized the shape of the adaptation map in the case where the subthreshold system has no fixed point. In this case, the spiking will necessarily be of *tonic* type, i.e. the neuron will fire infinitely many spikes (this will be the case whenever $\Phi(\mathscr{D}) \subset \mathscr{D}$). Since the system has a tonic spiking behavior, the study of the adaptation sequence of iterations of Φ provides a good way to understand the different tonic spiking patterns observed in these models.

3.3.2 Regular spiking

As observed numerically in the previous chapter, and as we can see in figure 3.10, the regular spiking is linked with the presence in the hybrid system of a generalized limit cycle, the *regular spiking limit cycle*, virtually containing one point having an infinite value of the membrane potential. From a mathematical point of view, this property simply corresponds to the convergence of the adaptation sequence (3.10). Indeed,
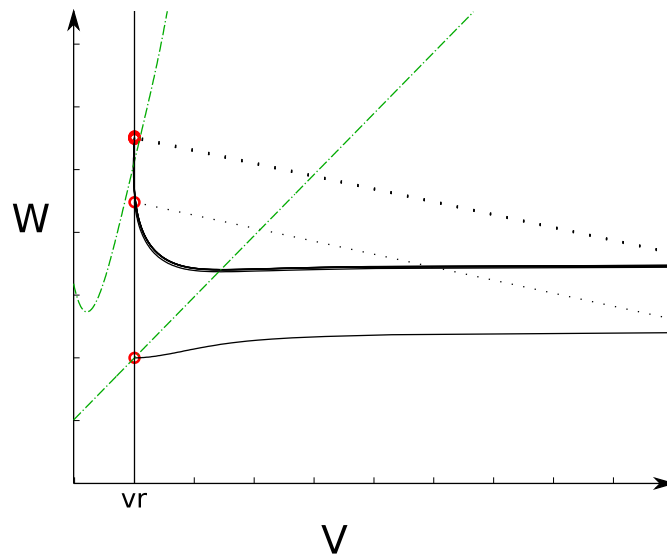
Figure 3.10. Spiking generalized limit cycle, case of the quartic model. In the simulation, we have cut the trajectories to a given threshold. Threshold has been taken large enough to ensure we simulate the intrinsic system. Green dotted curves represent the nullclines, the red circles the sequence of reset positions, the solid black curves the orbit of the solution of the differential equation and the dotted lines the reset.

if this sequence converges, then the frequency of the spikes will also converge[1].

Since we do not have closed form expressions for the map Φ, we provide here sufficient conditions on the dynamics of Φ leading to a regular spiking behavior.

Theorem 3.3.2. *Assume that* $\Phi(w^*) \leq w^*$. *Then the adaptation sequence* (3.10) *converges for any initial condition.*

Proof. First of all we note that the interval $(-\infty, w^*]$ is stable under Φ. Indeed, Φ is increasing on this interval, therefore for all $w \in (-\infty, w^*]$, $\Phi(w) \leq \Phi(w^*) \leq w^*$. Similarly, we necessarily have $w^{**} < w^*$, since theorem 3.3.1 ensures us that for all $w < w^{**}$ we have $\Phi(w) > w$, and the interval $[w^{**}, w^*]$ is invariant under Φ since $w^{**} \leq \Phi(w^{**}) \leq \Phi(w^*) \leq w^*$. Therefore, the fixed point of Φ is contained in this interval.

Moreover Φ maps the interval $[w^*, \infty)$ on the interval $(-\infty, \Phi(w^*)]$ since Φ is decreasing on this interval, and therefore for all $w \in [w^*, \infty)$, we have $\Phi(w) \leq \Phi(w^*) \leq w^*$. Therefore, is is sufficient to prove that the sequence of iterates of Φ converges on $(-\infty, w^*]$.

For $w_0 \in [w^{**}, w^*]$, the sequence $(w_n)_{n \geq 0}$ is a monotonous sequence (since Φ is increasing on this interval) in a compact set, and hence will necessarily converge to the unique fixed point of Φ.

If $w_0 < w^{**}$ then $\Phi(w_n) \geq w_n + d$ while $w_n \leq w^{**}$ and hence there exists an index N such that $w^{**} \leq w_N \leq w^*$, and the previous result applies and gives us the convergence of the sequence.

We conclude therefore that for any initial condition $w \leq w^*$ the sequence converges to the unique fixed point of Φ, and since Φ maps the interval $[w^*, \infty)$ on $(-\infty, w^*]$, for any initial condition in this interval, the sequence (3.10) will converge to the fixed point of Φ. □

The following theorem provides a sufficient condition on the map Φ to get regular spiking or bursts of period two.

Theorem 3.3.3. *Assume that* $\Phi(w^*) \geq w^*$ *and* $\Phi^2(w^*) \geq w^*$. *Then the adaptation sequence either converges to the fixed point of* Φ *or to a period two cycle.*

Proof. Let w_0 be a given initial condition for the sequence (3.10). Necessarily this sequence (w_n) will enter the interval $[w^*, \Phi(w^*)]$ after a finite number of iterations. Indeed, assume that $w_0 < w^*$. Since there is no fixed point in $(-\infty, w^*)$, Φ is increasing and $\Phi(w) \geq w$ in this interval, the sequence cannot be upperbounded by w^*. Hence there will be an integer p such that $\Phi^p(w_0) \leq w^*$ and $\Phi^{p+1}(w_0) \geq w^*$. Then because of the monotony of Φ on $(-\infty, w^*)$ we have $\Phi^{p+1}(w_0) \leq \Phi(w^*)$. Thus $w_{p+1} \in [w^*, \Phi(w^*)]$. If $w_0 > w^*$, because of the monotony of Φ on (w^*, ∞) we have $\Phi(w_0) \leq \Phi(w^*)$ and hence the sequence will enter the interval $[w^*, \Phi(w^*)]$ after a finite number of iterations.

Moreover, the interval $[w^*, \Phi(w^*)]$ is stable under Φ, since Φ is decreasing on this interval, and

$$\Phi([w^*, \Phi(w^*)]) = [\Phi^2(w^*), \Phi(w^*)] \subset [w^*, \Phi(w^*)].$$

Let $w \in [w^*, \Phi(w^*)]$ and $w_n = \Phi^n(w)$ the related adaptation sequence. Since Φ^2 is increasing on this invariant bounded interval, the sequences (w_{2n}) and (w_{2n+1}) are monotonous and both converge to a fixed point of Φ^2, hence (w_n) either converges to a fixed point of Φ or to a periodic orbit of period two depending on the stability of the fixed point. □

We have identified two simple sufficient conditions on Φ to obtain a regular spiking behavior. These criteria are not directly related to the parameters of the model, but they will be useful in order to describe mathematically the dependency with respect to the parameters as done in section 3.3.4. They can also be used in numerical simulations to compute the zones of parameters corresponding to this regular spiking behavior, as we do in section 3.5.2.

This analysis accounts for the stationary spiking behavior as well as for the transient phase, i.e. before the convergence of the sequence. In the spike patterns analysis, we generally distinguish between two types of regular spiking: the spike frequency adaptation that corresponds to the case where the spike frequency smoothly converges to its stationary value, and initial bursting mode (or mixed mode) where the neuron transiently fires a burst before spiking regularly. From the biological point of view, the distinction between these behaviors is not so clear, and we can continuously go from one behavior to the other. Mathematically, the difference between these two behaviors corresponds to the value of the fixed point of the adaptation map. Indeed, assume that the fixed point of the map Φ is smaller than w^*. In this case, when the sequence will

---

[1]If the adaptation sequence does not converge, the only way for the neuron to fire spikes regularly corresponds to the case where the sequence jumps between points corresponding to the same spike time. This occurs when the ISI map $\mathscr{T}$ is not one-to-one. In that particular case, there is necessarily a point lower than w^* which corresponds to a sharp after-potential and the a point greater than w^* corresponding to a broad after potential, and the sequence will then be considered as a regular bursting from a biophysical point of view as well as from our mathematical point of view.

(a) Spike Frequency Adaptation

(b) Initially Bursting
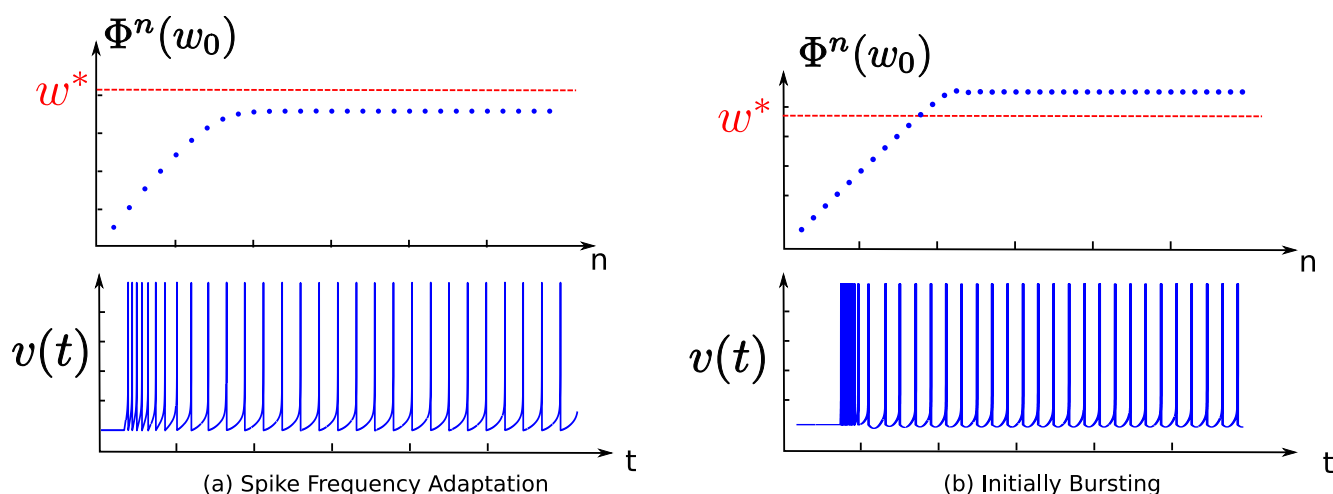
Figure 3.11. Regular spiking. The different transient phases (initially bursting, spike frequency adaptation) are linked with the relative position of the fixed point with respect to w^*.
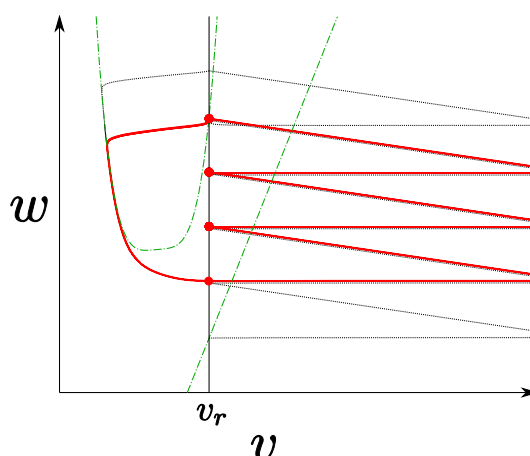
Figure 3.12. Bursting generalized limit cycle. Trajectories are cut to a given threshold high enough to approximate the behavior of the system with explosion. The red curve corresponds to the bursting limit cycle, and the red circles the reset locations on this cycle. The black trajectory is the transient phase, and the green dotted curves correspond to the nullclines of the system.

converge towards the fixed point, the value of the adaptation sequence will always be smaller than w^*, and the orbit will present a sharp after potential. The interspike interval in this zone is quite smooth and therefore the convergence towards the fixed point will result in the smooth adaptation of the spike frequency. If the fixed point is greater than w^*, when we apply a current step to the system, it will fire spikes with a sharp after-potential before converging to the fixed point where the system will present a broad after potential, therefore the system will present a typical transient phase corresponding to the initial bursting mode.

We conclude that if the neuron satisfies theorem 3.3.2, it will be in an adapting mode, and if not, it will be in an initial bursting mode. This criterion predicts the results numerically obtained by Naud and collaborators (95), as discussed in more details in section 3.5.2.

3.3.3 Tonic Bursting

As observed numerically in the previous chapter and as we can see in figure 3.12, the bursting activity is linked with the existence of a generalized limit cycle of the hybrid system, the *bursting limit cycle*, virtually containing a few points having an infinite membrane potential. The regular bursting behavior, whatever the transient behavior, is related to the presence of such a cycle, and this cycle corresponds exactly to periodic orbits for the adaptation map Φ.

We can provide a condition for having cycles of any period. Indeed, one of the simplest application of Sarkovskii's theorem (see e.g. (30)) is that if there exists a periodic point of period 3, then there exist periodic points of any period, hence bursts with any number of spikes per burst. Theorem 3.3.4 provides a simple criterion on Φ to have a period 3 cycle.

Theorem 3.3.4 (Cycles of any period). *Let $w_1 \stackrel{\text{def}}{=} \min\{\Phi^{-1}(w^*)\}$. Assume that:*

$$\begin{cases} \Phi(w^*) > w^* \\ \Phi^2(w^*) < w_1 \\ \Phi^3(w^*) > w^* \end{cases} \tag{3.15}$$

Then there exists a non-trivial period 3 cycle, hence the reset process has cycles of any period.

Proof. The only thing to prove is that there exists a point $x \in \mathbb{R}$ such that

$$\begin{cases} \Phi^3(x) = x \\ \Phi(x) \neq x \end{cases}$$

We know that there exists a unique fixed point of Φ, which we denote w_{fp} and which lies in the interval $[w^*, \Phi(w^*)]$. Here we prove that there exists another solution of $\Phi^3(x) = x$. Indeed, let us describe the function Φ^3:

- It is increasing on $(-\infty, w_2)$ where $w_2 = \min\{\Phi^{-2}(w^*)\}$, and $\Phi^3(w) > w$ on this interval by concavity

- decreasing on (w_2, w_1) and $\Phi^3(w_1) = \Phi^2(w^*) < w_1$ hence the curve crosses once the curve $y = x$, at a point strictly lower than w^*.

Hence we proved that there exists a period 3 cycle. Sarkovskii's theorem (see e.g. (30)) ensures us that there are cycles of any period for the map Φ . $\qquad\square$

Remark 9. This theorem gives us a simple condition on Φ to get period 3 cycles. This implies that the system has periodic points of any period, but also that it has an uncountable number of non asymptotically periodic points, which is referred as chaos in the paper of Li and Yorke (83). Nevertheless this property can be rather defined as *topological* chaos, and does not correspond to the usual definition of chaos in mathematics and in neuroscience where it is understood as sensitive dependency on the initial condition.

Simple sufficient conditions such as the ones given in theorem 3.3.4 in the case of periodic points of period three can be provided to for cycles of any given period. The difficulty is to prove that these conditions are satisfied, since we have no closed form expression for the map Φ, and in this case numerical simulation is helpful. As we will see in section 3.3.4, the system will undergo a period-adding bifurcation structure with respect to the reset value of the membrane potential, and therefore bursts of many periods will be observed.

3.3.4 Dependency on the parameters

We have seen that in the case where the subthreshold dynamics has no fixed point, the spike patterns produced can correspond to tonic spiking or tonic bursting depending on the parameters of the system. The question we address in this section is to characterize the dependency of the spike patterns with respect to the parameters of the model, and the bifurcations from one behavior to the other.

Bifurcations with respect to the spike-triggered adaptation parameter

The parameter having the simplest effect on the dynamics is the spike-triggered adaptation parameter d: it simply shifts vertically (i.e. along the y-axis) the adaptation map, and does not modify its shape. This simple behavior allows us to understand qualitatively the changes in the behavior of the adaptation sequence.

First of all, note that the unique fixed point of the map Φ is an increasing function of the spike-triggered adaptation d. We denote it $w_{fp}(d)$.

If the adaptation map is globally contracting (i.e. $\max_{v \in \mathbb{R}} |\Phi'(v)| < 1$), we will not observe bifurcations in the parameter d, and the sequence will always converge to the unique fixed point.

If the map is not globally contracting, bifurcations can appear with respect to the parameter d. Denote by $\mathscr{I}_1$ the set of $w \in \mathbb{R}$ such that $|\Phi'(w)| > 1$. This set is a bounded closed set included in $[w^*, \infty)$, because of the

(a) Bursting, three spikes per burst

(b) Bursting, two spikes per burst
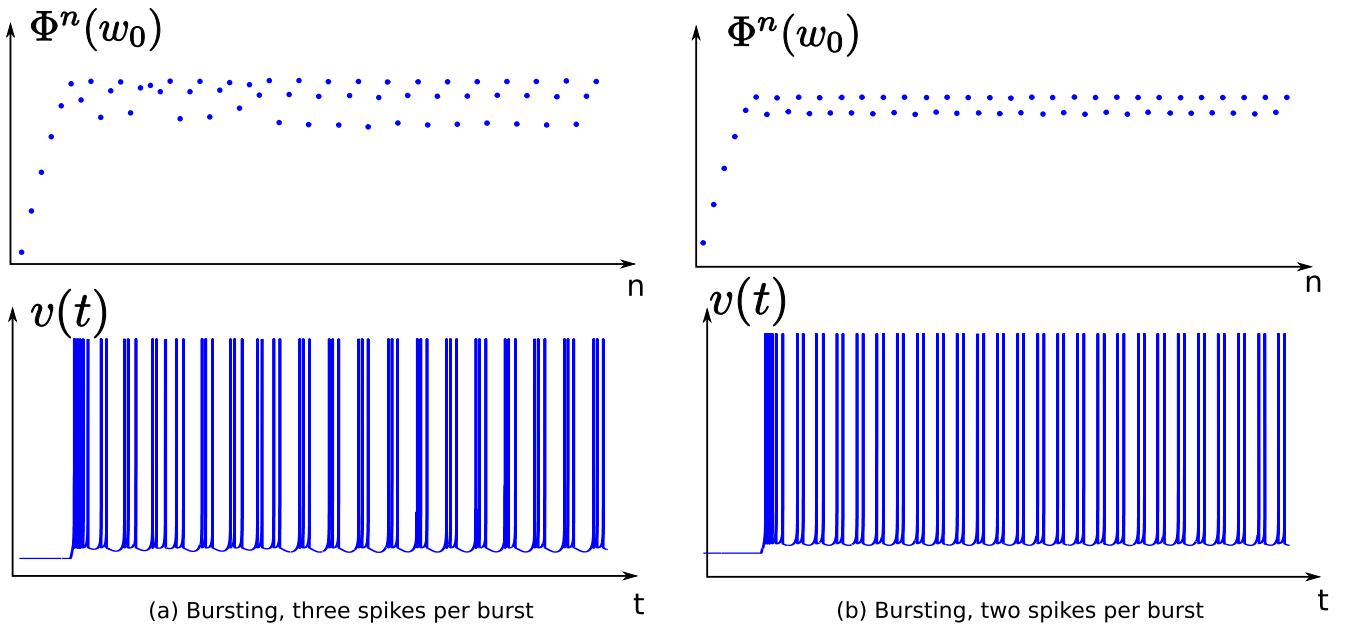
Figure 3.13. Bursting in the quartic model: bursts with different number of spike per bursts and related periodic orbit of Φ.

convexity property of Φ and the presence of the plateau. Indeed, if $w_{fp} < w^*$, then since Φ is increasing we would have $0 < \Phi'(w_{fp}) < 1$. Furthermore, because of the plateau region, we have $\Phi'(w_{fp}(d)) \to 0$ when $d \to \infty$. As stated, since the shape of Φ does not depend on d, neither does $\mathscr{I}_1$.

If $w_{fp}(0) > \max\{\mathscr{I}_1\}$, then the fixed point of the system is always stable for all $d > 0$ and there is no bifurcation in d.

If $w_{fp}(0) \in \mathscr{I}_1$, we denote by $d_1 = \inf\{d > 0; w_{fp}(d) \notin \mathscr{I}_1\}$. The fixed point will be unstable and the neuron will be bursting or chaotically spiking while $d < d_1$, and for $d > d_1$, the fixed point becomes stable and the neuron will fire regularly. At the point where $d = d_1$, the fixed point has a multiplier equal to -1 because of the negativity and continuity of the derivative, and the map undergoes a non-generic doubling bifurcation. The transversality condition (see e.g. (78, section 4.5)) is never satisfied since we have $\frac{\partial \Phi}{\partial d} \equiv 1$ (see equation (3.12)) and hence $\frac{\partial^2 \Phi}{\partial w \partial d} \equiv 0$.

If $w_{fp}(0) < \min\{\mathscr{I}_1\}$, we similarly define $d_1 = \inf\{d > 0, w_{fp}(d) \in \mathscr{I}_1\}$ and $d_2 = \sup\{d \geq d_1, w_{fp}(d) \in \mathscr{I}_1\}$. The system will undergo a degenerate period doubling bifurcation at the point $w_{fp}(d_1)$ for $d = d_1$ and a period doubling bifurcation at the point $w_{fp}(d_2)$ for $d = d_2$. For $d \in (d_1, d_2)$, the system does not have a stable fixed point. It can emit bursts, or even have a chaotic behavior in this zone (see figure 3.14).

Stabilization by the input current

The input current is a very interesting parameter, since it can be related to a biophysical value that can be controlled in *in vitro* experiments. Moreover, the set of input currents such that the system has no fixed point has a very simple shape, corresponding to the semi-infinite interval $(-m(b), \infty)$.

Interestingly, we prove that increasing the input current has a stabilizing effect on the behavior of the neuron: we prove in theorem 3.3.5 that for I large enough the adaptation sequence always converges to a fixed point.

Theorem 3.3.5. *Let the parameters a, b, v_r, d be fixed. There exists I_s such that for all $I > I_s$ all orbits under Φ converges.*

Proof. The proof of this theorem is based on the changes induced by increasing the current around the point (v_r, w^*). We prove that increasing I enough will make the system satisfy the hypothesis of theorem 3.3.2.

The point w^* depends on I, and therefore we denote it $w^*(I)$ in this proof for the sake of clarity. We change variables and consider $\hat{w} = w - I$. The change of variables maps w^* to $\hat{w}^* = F(v_r)$. The equations satisfied by $(v, \hat{w})$ are readily deduced from the original system, the new adaptation map can be written as:

$$\hat{\Phi}(\hat{w}) = \Phi(\hat{w} + I) - I,$$

(a) $v_r = -48.2mV$

(b) $v_r = -47.7mV$
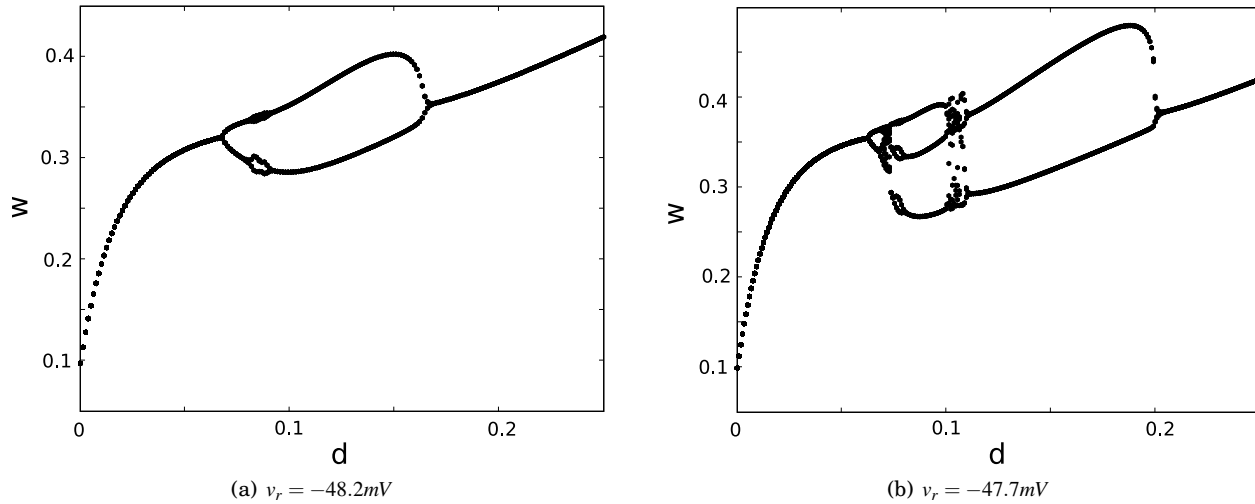
Figure 3.14. Orbits under Φ for different initial conditions, varying the spike-triggered adaptation parameter d, in the case of the dimensioned Adaptive Exponential model. We can observe that for d small enough the system converges towards the fixed point of Φ. When increasing d, as described in the text, the fixed point loses stability via a period doubling bifurcation and a cycle of period 2 appears. In the case (a) the system presents another period doubling bifurcation for $d \approx 0.8$, and then returns to equilibrium via an inverted period doubling bifurcation. In the second simulation for a larger value of v_r, the system involves chaotic spiking patterns.

and the condition of theorem 3.3.2 simply reads $\hat{\Phi}(\hat{w}^*) \leq \hat{w}^*$.

The equation of the trajectory in the phase plane $(v, \hat{w})$ for any initial condition in the spiking zone can be parametrized as a function of v: $\hat{w}(t) = \hat{W}(v(t), v_0, w_0, I)$, where $\hat{W}$ satisfies the equation:

$$\begin{cases} \frac{\partial \hat{W}}{\partial v} = \frac{a(bv - \hat{W})}{F(v) - \hat{W}} - \frac{aI}{F(v) - \hat{W}} \stackrel{\text{def}}{=} \hat{g}(v, \hat{W}, I) \\ \hat{W}(v_0, v_0, w_0, I) = w_0 \end{cases}$$

Let $I_0 > -m(b)$ a fixed current, $\delta > 0$ a given real and $\Delta = d + 1$ where d is the spike-triggered adaptation parameter. Because of the shape of the vector field, the trajectories with initial condition (v_r, w^*) can be parameterized as a function of v with a singularity at $v = v_r$. We consider the trajectories on the interval $[v_r, v_r + \delta]$, and we prove that the infimum of the variable $\hat{W}$ with initial condition $(v_r, \hat{w}^*)$, for $I \geq I_0$ and $v \in [v_r, v_r + \delta]$ is smaller than $F(v_r) - \Delta$.

To this end, let us characterize the orbits starting from this point $(v_r, \hat{w}^*)$ as a function of the input current I. First of all, it is clear using Gronwall's theorem that $I \mapsto \hat{W}(v, v_r, \hat{w}^*, I)$ is decreasing. Therefore we have $\hat{W}(v_r + \frac{\delta}{2}, v_r, \hat{w}^*, I) \leq \hat{W}(v_r + \frac{\delta}{2}, v_r, \hat{w}^*, I_0) \stackrel{\text{def}}{=} \hat{w}_0$ and hence $\hat{W}(v_r + \delta, v_r, \hat{w}^*, I) \leq \hat{W}(v_r + \delta, v_r + \frac{\delta}{2}, \hat{w}_0, I)$.

Assume now that the infimum of $\hat{W}$ for all $v \in [v_r + \frac{\delta}{2}, v_r + \delta]$ is greater than $F(v_r) - \Delta$. We have:

$$\hat{g}(v, \hat{W}, I) - \hat{g}(v, \hat{W}, I_0) = -\frac{a(I - I_0)}{F(v) - \hat{W}}$$

and hence:

$$\hat{W} \geq F(v_r) - \Delta$$

$$F(v) \leq \max_{v \in [v_r, vr + \delta]} F(v)$$

$$F(v) - \hat{W} \leq \max_{v \in [v_r, vr + \delta]} F(v) - F(v_r) + \Delta$$

$$\frac{1}{F(v) - \hat{W}} \geq \frac{1}{\max_{v \in [v_r, vr + \delta]} F(v) - F(v_r) + \Delta}$$

$$-\frac{a(I - I_0)}{F(v) - \hat{W}} \leq -\frac{a(I - I_0)}{\max_{v \in [v_r, vr + \delta]} F(v) - F(v_r) + \Delta}$$

which is constant and strictly negative. Therefore, using Gronwall's theorem, we have

$$\hat{W}(v_r+\delta,v_r,\hat{w}^*,I)-\hat{W}(v_r+\delta,v_r,\hat{w}^*,I_0) \leq -\frac{a(I-I_0)\delta}{\max_{v\in[v_r,vr+\delta]}F(v)-F(v_r)-\Delta}$$

Therefore there exists I_1 such that for all $I > I_1$, we have $\min_{v\in[v_r,v_r+\delta]}\hat{W}(v) < F(v_r)-\Delta$. This contradicts the assumption that the infimum of $\hat{W}$ for all $v\in[v_r+\frac{\delta}{2},v_r+\delta]$ is greater than $F(v_r)-\Delta$. Hence there exists I_1 such that for all $I > I_1$, we have $\min_{v\in[v_r,v_r+\delta]}\hat{W}(v) < F(v_r)-\Delta$, which means in particular $\min_v W(v) < F(v_r)+I-\Delta$. This minimal value is reached when the trajectory crosses the w-nullcline, and denote by v_1 the value of the variable v at this crossing time. We have, for all $I > I_1$:

$$\Phi(w^*(I)) = \lim_{v\to\infty} W(v)+d$$

$$= W(v_1)+\int_{v_1}^{\infty}\frac{a(bv-W)}{F(v)-W+I}dv+d$$

Moreover, we have $W(v) \geq bv_r$ for all v and $W(v) \leq bv$ for $v \geq v_1$. Therefore, we have:

$$\int_{v_1}^{\infty}\frac{a(bv-W)}{F(v)-W+I}dv \leq \int_{v_1}^{\infty}\frac{ab(v-v_r)}{F(v)-bv+I}dv.$$

The integrand is positive between v_r and v_1, hence we have in particular:

$$\Phi(w^*(I)) \leq F(v_r)+I-\Delta+d+\int_{v_r}^{\infty}\frac{ab(v-v_r)}{F(v)-bv+I}dv$$

$$= F(v_r)+I-1+\int_{v_r}^{\infty}\frac{ab(v-v_r)}{F(v)-bv+I}dv$$

The integrand tends to zero when $I \to \infty$ and is bounded by an integrable function (for instance the same function with $I = I_0$), hence by Lebesgue's theorem tends to 0 when $I \to \infty$. Therefore, there exists $I_s > I_0$ such that for all $I > I_s$, the integral is strictly smaller than 1, and therefore:

$$\Phi(w^*(I)) \leq F(v_r)+I = w^*(I).$$

Hence theorem 3.3.2 applies, which ends the proof. □

Therefore, we can see that increasing the input current has a stabilizing effect on the dynamics. We present in figure 3.15 some numerical results illustrating this stabilization effect in the case of the exponential integrate-and-fire model. We observe for two different values of v_r that the system undergoes bifurcations with respect to the input current, sometimes involving chaotic spiking, but above a given value of the input current, the system spikes regularly, and the adaptation sequence converges towards its fixed point. Moreover, we have seen in the proof that when $I \geq I_s$, theorem 3.3.2 applies. Hence for I large enough, the system will present a spike frequency adaptation transient phase. Decreasing it will make the system switch to the case where there are two fixed points treated in section 3.4.

Cascade of period adding bifurcations and chaos with respect to v_r

Another parameter preserving the number of fixed point is the reset value of membrane potential v_r. The dependency of the adaptation map with respect to this parameter is very intricate. The effect of increasing the reset value sharpens the adaptation map, and therefore can destabilize the possible stable fixed point or stable cycles. This qualitative observation is confirmed by numerical simulations. In the case of the exponential model, for v_r small enough, the adaptation map is smooth, because the slope of the exponential function for small v values tends to zero. But in the case of the quartic model, decreasing v_r also sharpens F because of the fast divergence of the quartic function.

We provide in figure 3.16 a graph of the stationary adaptation sequence (i.e. removing the transient phase) as a function of the reset voltage v_r corresponding to the quartic model. A similar diagram was given in the case of the adaptive exponential model in (116). We observe that the system present sharp transitions from rest (regular spiking) to cycles of period two (bursts with two spikes per burst) via a period doubling bifurcation, and from cycles of period n to cycles of period $n+1$ for $n \geq 2$ via period adding bifurcations involving chaotic spiking regions.

(a) $d = 0.1nA$

(b) $d = 0.5nA$
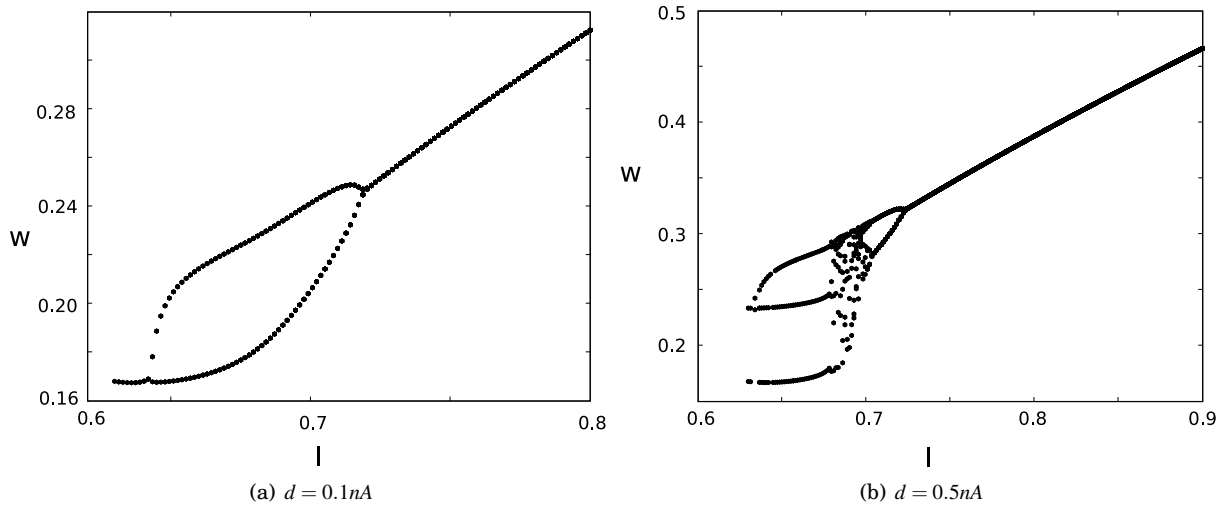
Figure 3.15. Orbits under Φ when varying the input current I in the case of the dimensioned Adaptive Exponential model. (a): Small v_r, the dynamics only presents a loss of stability via period doubling and then returns to equilibrium. (b): greater value of v_r: a period two cycle appears at the saddle-node current, immediately followed by a period 3 cycle, then via period-adding bifurcation the system returns to a period two cycle, and then by period doubling bifurcation to regular spiking. The transition from period three to period two shows a chaotic behavior.
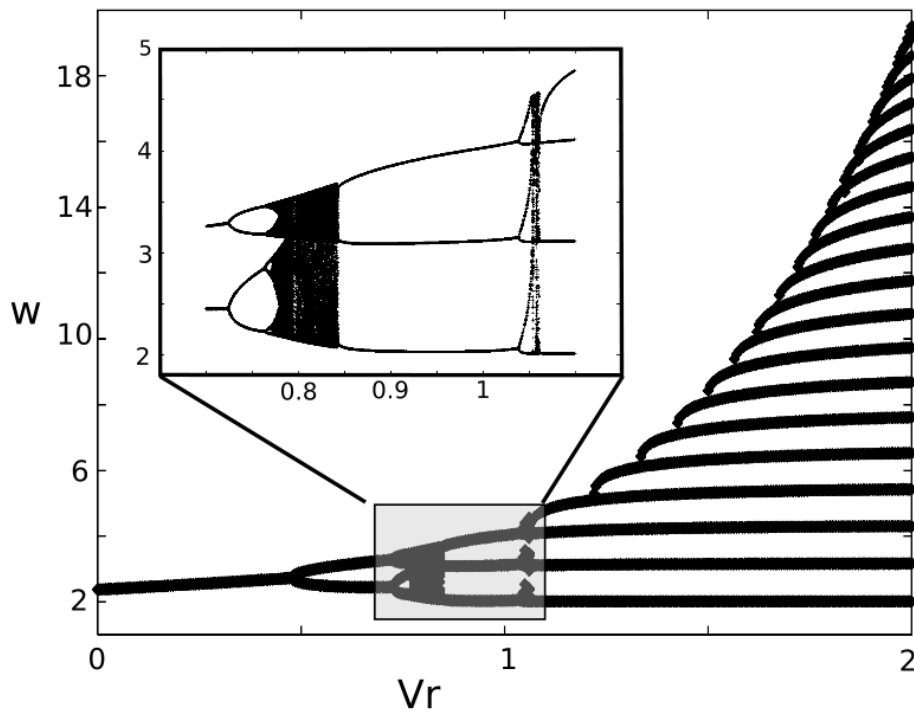
Figure 3.16. The period adding bifurcation cascade in the adaptation sequence for the quartic model, $a = 0.03$, $b = 0.7$, $d = 1.15$, and $v_r \in [0,2]$, and a zoom on the transitions from period 2 to period 3 and period 3 to period 4. The same phenomenon appears in the adaptive exponential model, see (116).

3.3.5 Multistability

In section 3.3.2, we gave a sufficient condition on the map Φ for the convergence of the sequence (3.10) to the fixed point of Φ whatever the initial condition, which implies that the fixed point of Φ is stable and that its attraction basin is equal to $\mathbb{R}$. Nevertheless, in the case where the map Φ is not globally contracting, multistable behaviors could appear, corresponding to the coexistence of stable spiking orbits.

The study of periodic orbits is quite intricate in general systems, and this study in our case is even more complex since we do not have a closed form for the map Φ. We nevertheless observe numerically that cases of this type do not seem to occur: the stationary behavior of the adaptation sequence is the same whatever the initial condition.

3.4 EXISTENCE OF FIXED POINTS

In the case where $I < -m(b)$, the system has two fixed points, one of which is always a saddle fixed point. We already studied in section 3.2 the stable manifold of this saddle fixed point (SMSFP) and explained in the cases where there exist SAs (fixed points or periodic orbit) how this manifold shaped the related attraction basin.

This stable manifold is essential for characterizing the definition domain and the the dynamics of Φ. The map Φ will only be defined for values of w such that (v_r, w) is neither in the attraction basin of the possible SA nor on the SMSFP. We will study different cases in function of the topology of the intersection of the reset line with these sets, and mainly distinguish the cases where there is no intersection, finitely or countably many intersections or a continuous uncountable set of intersections.

3.4.1 Unconditional tonic behaviors

We are first interested in the cases where the reset line $\{v = v_r\}$ neither crosses the SMSFP nor the attraction basin of the possible SA. We know that the SMSFP is the graph of an unbounded increasing function of v for $v \geq v_+$ where v_+ is the greatest fixed point of the system. The cases where the SMSFP do not cross the reset line necessarily correspond to the cases where the stable manifold is included in a half plane $\{v \geq v_{\min}\}$. This corresponds to the cases where:

- the subthreshold system has two unstable fixed points and no stable limit cycle (Figs. 3.6(a) and 3.6(b)).

- an unstable limit cycle circles the stable fixed point (Fig. 3.5(a))

- the stable manifold crosses both nullclines (Fig. 3.5(b)).

In these cases, for all $v_r \leq v_{\min}$, the reset line does not intersect the SMSFP nor any possible attraction basin. Therefore, the adaptation map Φ is defined on $\mathbb{R}$ and the proof of theorem 3.3.1 readily extends to this case. Hence in these cases Φ is a regular map increasing and concave on $(-\infty, w^*]$ and decreasing on $[w^*, \infty)$, having a unique fixed point, a horizontal asymptote at infinity and such that $\Phi(w) \geq w + d$ for all $w \leq w^{**}$. Since the map Φ is defined on $\mathbb{R}$ (and therefore $\Phi(\mathscr{D}) \subset \mathscr{D}$), if the neuron fires a spike, then it will fire infinitely many spikes. In that case, the map satisfies the same properties as when the subthreshold system has no fixed point, and theorems 3.3.2, 3.3.3 and 3.3.4 apply.

3.4.2 Phasic behaviors

In this section, we consider the cases where the reset line intersects the attraction basin $\mathscr{B}$ of SA and denote by $\mathscr{C}$ the SMSFP. The set of adaptation values on the reset line that do not lead the system to fire is given by:

$$\mathscr{A} = \left\{ w \in \mathbb{R} \; ; \; (v_r, w) \in \mathscr{B} \text{ or } (v_r, w) \in \mathscr{C} \right\}.$$

The definition domain of the adaptation map in this case is

$$\mathscr{D} = \mathbb{R} \setminus \mathscr{A},$$

the set of initial conditions corresponding to a phasic spiking (i.e. emission of a finite number of spikes) is given by

$$P = \bigcup_{n=0}^{\infty} \Phi^{-n}(\mathscr{A})$$

and the complement of this set corresponds to the tonic spiking cases.

To study further the behavior of the system in this case, we discuss different cases depending on the shape of the stable manifold and the position of v_r with respect to the fixed point v_+. Interestingly, the shape of the stable manifold only depends on the parameters of the subthreshold system.

3.4.3 The stable manifold Γ^- does not cross the v-nullcline

We first consider the case where the manifold Γ^- does not cross the v-nullcline. We distinguish two cases depending on wether $v_r \leq v_+$ or not.

Proposition 3.4.1. If the manifold Γ^- does not cross the v-nullcline and $v_r > v_+$, the manifold Γ^+ separating the spiking and non-spiking regions is the graph of an increasing function of v, and is above the two nullclines. The definition domain $\mathscr{D}$ of the adaptation map Φ is an open interval $(-\infty, w_{\max}(v_r))$ with $w_{\max}(v_r) > w^* (> w^{**})$. We denote $\Phi(w_{\max}(v_r)^-) \overset{\text{def}}{=} \lim\limits_{w \to w_{\max}(v_r)} \Phi(w)$ the left limit of Φ at the point $w_{\max}(v_r)$. We have:

- If $\Phi(w_{\max}(v_r)^-) > w_{\max}(v_r)$ the system fires finitely many spikes whatever the initial condition in $\mathscr{D}$,

- If $\Phi(w_{\max}(v_r)^-) < w_{\max}(v_r)$ and $\Phi(w^*) < w_{\max}(v_r)$ the system fires infinitely many spikes whatever the initial condition in $\mathscr{D}$,

- Else, the system will either fire finitely or inifinitely many spikes depending on the initial condition.

Proof. First of all, we note that Φ satisfies the same properties on $\mathscr{D}$ as the one given in theorem 3.3.1. The shape of the domain $\mathscr{D}$ is readily deduced from the shape of the separatrix.

- In the case where $\Phi(w_{\max}(v_r)^-) > w_{\max}(v_r)$ (see figure 3.18(d)) there exists a real $\varepsilon > 0$ such that $\Phi(w) - w \geq \varepsilon$ for all $w \in \mathscr{D}$. Indeed, because of the monotony of Φ on $(w^*, w_{\max}(v_r))$ we have for all w in this interval $\Phi(w) \geq \Phi(w_{\max}(v_r)^-) > w_{\max}(v_r) \geq w$ and because of the convexity property of Φ and the fact that $\Phi(w) \geq w + d$ for all $w \leq w^{**}$, the distance between Φ and the identity map is lowerbounded. Hence $\Phi(w) \geq w + \varepsilon$, and there exists $N > 0$ such that $\Phi^N(w) \geq w_{\max}(v_r)$, thus the system has a phasic spiking behavior (see figure 3.18(g)).

- In the case where $\Phi(w_{\max}(v_r)^-) < w_{\max}(v_r)$ and $\Phi(w^*) < w_{\max}(v_r)$ (see figure 3.18(c)), then we have $\Phi(\mathscr{D}) \subset \mathscr{D}$, since the maximum of the map Φ is reached at w^*, and therefore the system will fire infinitely many spikes. Depending on the properties of the map Φ and of its fixed point, the system can either spike regularly (when the fixed point is stable), generate bursting or chaotic spike patterns. Figure 3.18(g) corresponds to this case when the fixed point is stable and generates a regular spiking behavior.

- In the case where $\Phi(w^*) \geq w_{\max}(v_r)$, we do not have $\Phi(\mathscr{D}) \subset \mathscr{D}$. In this case, $\mathscr{D}$ can be split into two different sets that can have quite intricate shapes: a set of values of the adaptation variable where the neuron fires finite many spikes and a set where the neuron fires infinitely many spikes. To study these sets, we define
$$P_1 = \{w \in \mathscr{D} \,;\, \Phi(w) \geq w_{\max}(v_r)\}$$
This set corresponds to the set of adaptation values w such that $\Phi(w) \notin \mathscr{D}$ and hence that will fire one spike and then return to a subthreshold stable orbit. We then define recursively the set $P_{n+1} = \Phi^{-1}(P_n)$ of initial conditions such that the neuron will fire exactly $n+1$ spikes before being attracted by the stable subthreshold orbit. The set of phasic spiking initial conditions is therefore defined by
$$P = \bigcup_{n=1}^{\infty} P_n,$$
and the set of tonic spiking is $\mathscr{D} \setminus P$. In figure 3.17 we represented the construction of these two sets until T_3, and we observe the complexity of the set we will obtain. If the fixed point is stable, both the tonic spiking and the phasic spiking sets will be a countable union of non-empty intervals, and the adaptation sequence will jump from one interval to the other until reaching the attraction basin of the fixed point of Φ, where they keep trapped. If the fixed point is unstable, the tonic spiking set will be countable, defined by the union of the consecutive reciprocal images of the unstable fixed point under Φ. Therefore the neuron will not present cycles. In this case, the behavior of Φ strongly depends on the initial condition.

$\square$
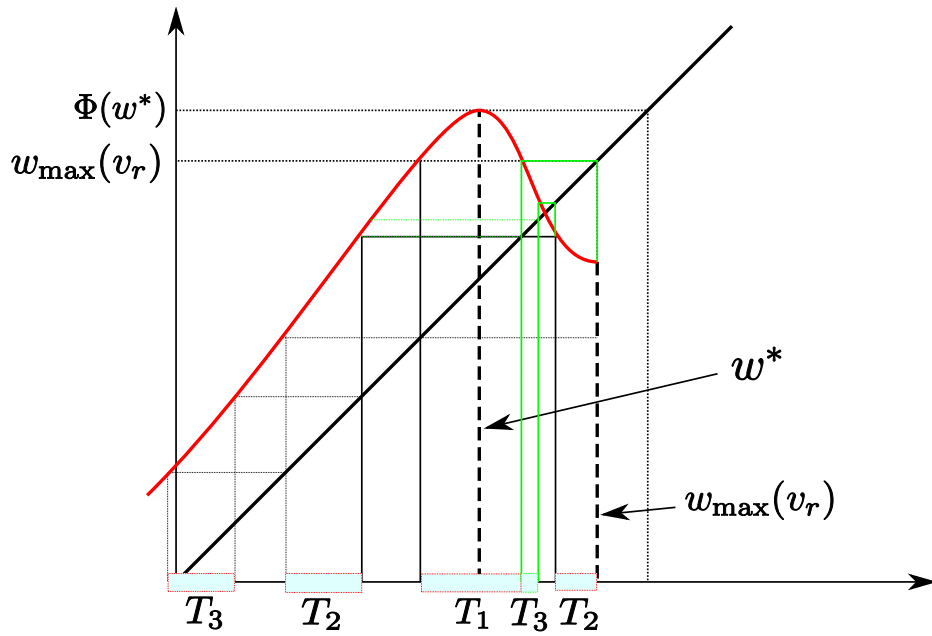
Figure 3.17. Construction of the phasic spiking set in the case of an unbounded separatrix when $\Phi(w^*) > w_{\max}$, for three iterations. The red curve is the map Φ and the black line the first bissector. The green construction line correspond to the contribution of the set T_2 for $w > w^*$ to T_3.

Proposition 3.4.2. If $v_r \leq v_+$ and Γ^- does not cross the v-nullcline, the definition domain $\mathscr{D}$ is an open interval $(-\infty, w_{\max}(v_r))$ with $w_{\max}(v_r) \leq w^*$. The neuron fires infinitely many spikes if and only if $\Phi(w_{\max}(v_r)^-) \leq w_{\max}(v_r)$. In this case the neuron is in a regular spiking mode with spike frequency adaptation.

Proof. If $v_r \leq v_+$ and Γ^- does not cross the v-nullcline, it is clear that the definition domain $\mathscr{D}$ of the adaptation map Φ an open interval $(-\infty, w_{\max}(v_r))$ where $w_{\max}(v_r) \leq w^*$ is the value of the adaptation variable at the intersection point of the reset line with Γ^-. The maximal value of Φ on its definition domain is given by $\Phi(w_{\max}(v_r)^-)$.

- if $\Phi(w_{\max}(v_r)^-) \leq w_{\max}(v_r)$, then we have $\Phi(\mathscr{D}) \subset \mathscr{D}$ and hence the system is always in a regular spiking mode if it fires one spike. Moreover, the proof of theorem 3.3.2 readily extends to the present case and therefore the system will be in a regular spiking mode with spike frequency adaptation.

- If $\Phi(w_{\max}(v_r)^-) > w_{\max}$, because of the convexity property (which can be proved in exactly the same way as in theorem 3.3.1), there exists $\varepsilon > 0$ such that $\Phi(w) - w \geq \varepsilon$ and therefore the system will return to rest after firing finitely many spikes.

$\square$

In the case where Γ^- intersects no nullcline (e.g. in the case of figure 3.18(a)), we will have $w_{\max}(v_r) \leq w^{**}$ and hence $\Phi(w_{\max}(v_r)^-) \geq w_{\max}(v_r) + d$, hence the system will always be in a phasic spiking mode. In the tonic spiking cases of propositions 3.4.1 and 3.4.2 the system presents a bistable behavior: a stable subthreshold behavior and a stable spiking one coexist.

The stable manifold Γ^- crosses the v-nullcline

If the stable manifold crosses the v-nullcline as in figure 3.5(b), then there exists $v_{\min} \leq v_-$ such that the SMSFP is included in the half plane $\{v \geq v_{\min}\}$. For each $v \leq v_{\min}$, we have $\mathscr{D} = \mathbb{R}$ and the results of section 3.4.1 apply. For $v \geq v_{\min}$, the spiking behavior of the system satisfies the following:

Proposition 3.4.3. For $v \geq v_{\min}$, the reset line intersects the attraction basin on a bounded interval $(w_{\min}(v_r), w_{\max}(v_r))$ and the definition domain of the adaptation map is the union of two semi-infinite intervals:

$$\mathscr{D} = (-\infty, w_{\min}(v_r)) \cup (w_{\max}(v_r), \infty) \overset{\text{def}}{=} \mathscr{I}_1 \cup \mathscr{I}_2.$$

The spiking pattern satisfies the following classification (see figure 3.19):

(a) Unbounded separatrix crossing no nullcline

(b) Adaptation map for $v_r = v_{r1}$

(c) Adaptation map for $v_r = v_{r2}$ and $d = d_1$

(d) Adaptation map for $v_r = v_{r2}$ and $d = d_2$

(e) Trace of v for $v = v_{r1}$

(f) Trace of v for $v = v_{r2}$ and $d = d_1$

(g) Trace of v for $v = v_{r2}$ and $d = d_2$
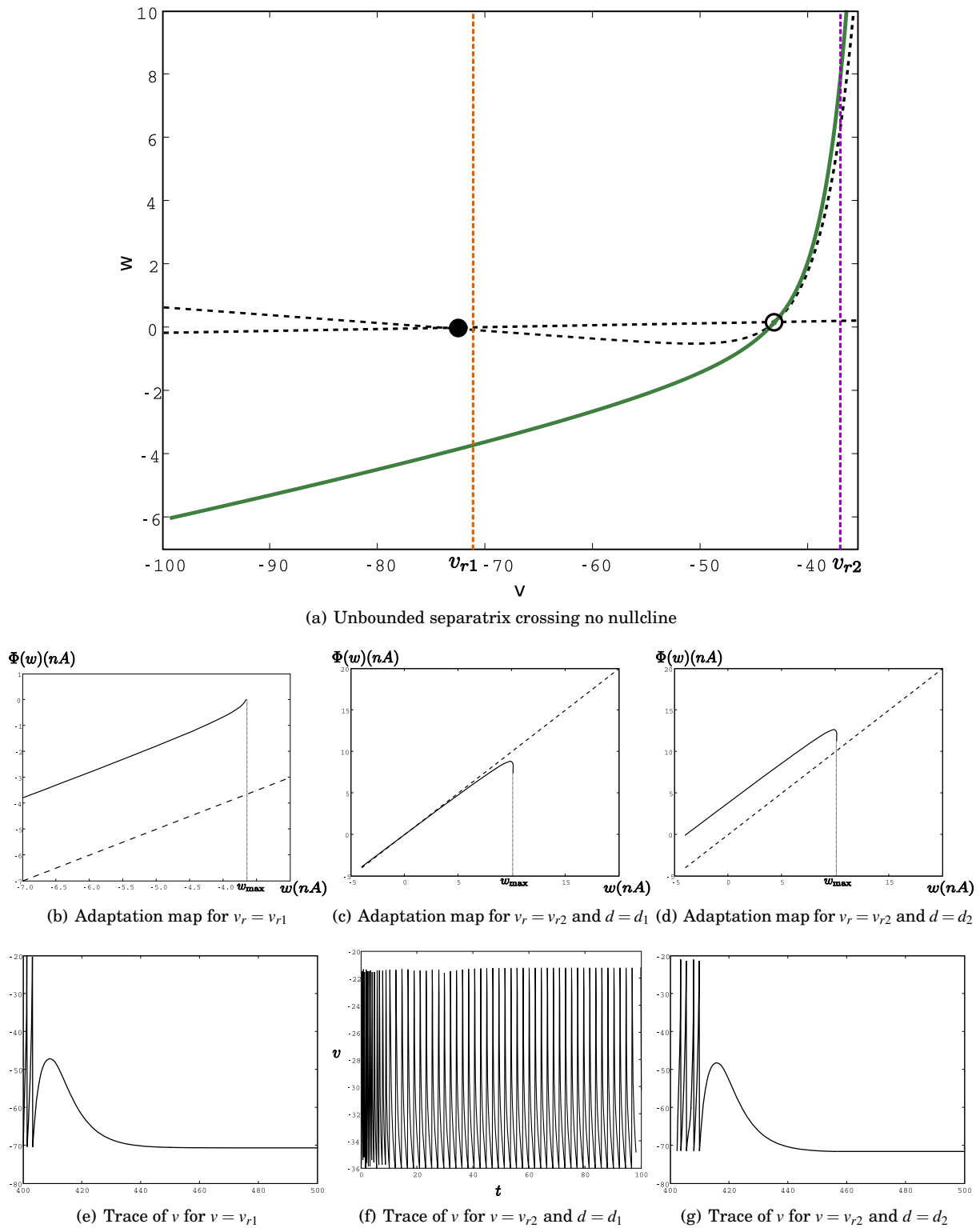
Figure 3.18. Case of an unbounded separatrix: unconditional phasic behavior for $v < v_-$. In the case $v > v_+$, the behavior can either be phasic or tonic depending on the parameters of the system. It can also depend on the initial condition. Case of the adaptive exponential model, original parameters, $a = .2g_L$ and $\tau_w = \tau_m/3$, $d_1 = 0.01nA$ and $d_2 = 3nA$. We chose $v_{r1} = -70.6mV$ (value of the original model) and $v_{r2} = -36mV$ which is unrealistically high for biological applications, and results in very fast spiking behaviors as in the case of figure (f).

- If $\sup_{w \in \mathscr{I}_1} \Phi(w) \in [w_{\min}(v_r), w_{\max}(v_r)]$, the system fires finitely many spikes

(a) Tonic spiking case

(b) Phasic spiking case

(c) Dependency on initial condition
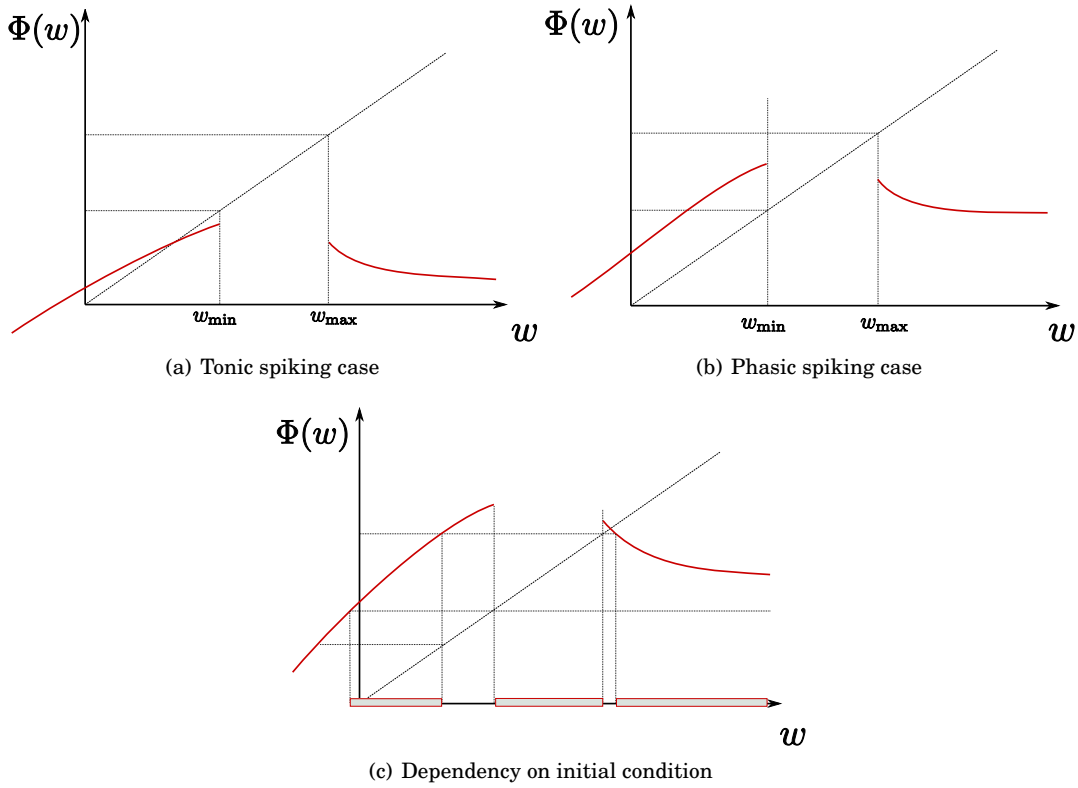
Figure 3.19. Case where the SMSFP crosses the v-nullcline, in the case of the quartic model, $a = 1$, $b = 2.5$, $I = -0.5$, $v_r = 0$ and different values of d. (a): Tonic spiking mode, the adaptation sequence converges towards the fixed point of Φ. (b): Phasic spiking mode: for any initial condition the adaptation sequence will enter the zone $[w_{\min}, w_{\max}]$ and the neuron stops firing. (c): the spiking behavior is tonic or phasic depending on the initial condition. The blue boxes represent the zones of initial conditions related to a phasic behavior with zero or one spikes emitted.

- If $\sup_{w \in \mathscr{I}_1} \Phi(w) < w_{\min}(v_r)$, the system fires infinitely many spikes. If $v_r \leq v_+$, the system presents regular spiking with spike frequency adaptation.

- If $\sup_{w \in \mathscr{I}_1} \Phi(w) > w_{\max}(v_r)$, the system fires finitely or infinitely many spikes depending on the initial condition.

Proof. The shape of the domain $\mathscr{D}$ is a direct consequence of the assumption on Γ^-. First of all, we note that any orbit starting from (v_r, w) with $w \in \mathscr{I}_2$ will cross the reset line on $\mathscr{I}_1$ after a finite time, and therefore we have $\Phi(\mathscr{I}_2) \subset \Phi(\mathscr{I}_1)$.

- If $\sup_{w \in \mathscr{I}_1} \Phi(w) \in [w_{\min}(v_r), w_{\max}(v_r)]$ (see figure 3.19(a)), then there exists $\varepsilon > 0$ such that $\sup_{w \in \mathscr{I}_1} \Phi(w) - w \geq \varepsilon$ and therefore any orbit will exit $\mathscr{D}$ and enter the subthreshold orbits set after firing few spikes. For any initial condition $w \in \mathscr{I}_2$ we have $\Phi(w) \subset \Phi(\mathscr{I}_1)$ and therefore either $\Phi(w)$ is in the attraction basin of the subthreshold equilibrium, or it is in $\mathscr{I}_1$ and the above analysis applies and the system is in a phasic spiking mode.

- If $\sup_{w \in \mathscr{I}_1} \Phi(w) < w_{\min}(v_r)$ (see figure 3.19(b)), then necessarily $\Phi(\mathscr{I}_1) \subset \mathscr{I}_1$ and the map Φ has a fixed point in $\mathscr{I}_1$. Furthermore, we have $\Phi(\mathscr{D}) \subset \mathscr{I}_1$ and therefore the system will be in a tonic spiking behavior. If $v_r \leq v_+$, we have $w_{\min} < w^*$, the fixed point is attracting and for any initial condition the adaptation sequences converge to this fixed point (see proof of theorem 3.3.2). Moreover in that case the transient phase is characterized by spike frequency adaptation.

  If $v_r > v_+$, the type of tonic spiking depends on the properties of the map, the system is in a regular spiking mode with initial bursting, a bursting mode or a chaotic spiking mode.

- If $\sup_{w \in \mathscr{I}_1} \Phi(w) > w_{\max}(v_r)$ (see figure 3.19(c)), then there exists an interval $J \subset \mathscr{D}$ such that all the trajectory with initial condition (v_r, w) with $w \in J$ will stop firing after one spike. We can build the

phasic and the tonic subspaces of $\mathscr{D}$ recursively as done in the previous case. The shape of this set can be quite complex, and the behavior of the adaptation sequence depends on the initial condition on this set.

$\square$

Bounded attraction basin

In the case where the attraction basin of the SA is delineated by a periodic orbit, we denote by $v_{\min}$ the minimal value of the membrane voltage on the cycle and by $v_{\max}$ its maximal value. The behavior of the system for $v_r \in (v_{\min}, v_{\max})$ is very complex. Indeed, the reset line will cross the attraction basin on an interval of values for the adaptation $(w_{\min}, w_{\max})$, but since the stable manifold spirals around the orbit and converges to it, there is a countable sequence of intersection points of the reset line with the stable manifold: $(m_i, i \in \mathbb{N})$ converging to $w_{\min}$ and $(M_i, i \in \mathbb{N})$ converging to $w_{\max}$. At each of these points the map Φ is undefined and there is a jump of the values of the map Φ. Hence the definition domain of the map Φ has a complex shape, and Φ an intricate discontinuous dynamics on it.

For $v_r > v_{\max}$ the reset line will cross the stable manifold on a finite set of adaptation values, and at these points the map Φ is undefined and has a unique discontinuity, case we now generalize and study.

3.4.4 Case $\mathscr{D} = \mathbb{R} \setminus \mathscr{A}$ where $\mathscr{A}$ is a finite or countable set

The case where the reset line crosses the SMSFP but not any attraction basin of SA is more intricate (see figure 3.20). It corresponds to the cases where:

- the subthreshold system has two unstable fixed points and no stable limit cycle, and $v_r \geq v_{\min}$ (cases of Figures 3.6(a) and 3.6(b)). When the stable manifold oscillates around the fixed point, there is a countably many intersection points.

- the subthreshold system has a stable fixed point and an unstable periodic orbit. In that case let us denote by $v_{p,\max}$ (respectively $v_{p,\min}$) the maximal (respectively minimal) value of the variable v or the periodic orbit. The line $\{v = v_r\}$ crosses the SMSFP but not the attraction basin when $v_{\min} \leq v_r < v_{p,\min}$ or $v_r \geq v_{p,\max}$.

In these two cases, the reset line $\{v = v_r\}$ has finitely many intersections with the stable manifold (except if $v_r = v_-$), and we denote by $\mathscr{A}$ the set of intersection points. The map Φ is defined on $\mathbb{R} \setminus \mathscr{A}$. This set is a finite union of open intervals. On each interval, the map Φ satisfies the properties given in theorem 3.3.1 for the same reasons as the ones given in the related proof. At the intersection points of the reset line with the SMSFP, the shape of the orbits of the differential system (3.1) changes, and this implies that at these points the map Φ is discontinuous.

If $v_r > v_+$ then the map Φ will have a unique discontinuity point where the map is undefined (see figure 3.20(e)). For $v_{\min} < v_r < v_-$ it will have an odd number of such points (figures 3.20(c) and 3.20(d)) and for $v_r > v_-$, an even number. In the case where the Jacobian matrix has complex eigenvalues at the equilibrium v_-, the Poincaré map will have an infinite countable set of discontinuity points for $v_r = v_-$. The dynamics of Φ in this region of parameters will therefore be very complex. It can have multiple fixed points, no fixed point, and the map is discontinuous.

The set of adaptation values such that the system stops firing after a finite number of spikes emitted (phasic spiking regime) is given by:

$$\bigcup_{n=0}^{\infty} \Phi^{-n}(\mathscr{A})$$

It is the set of initial conditions such that the orbits are exactly on the SMSFP after a finite number of iterations.

Therefore, the topology and the dynamics of Φ on these sets is quite complex. The related spiking sequence is also extremely complex in these cases:

- If the map Φ has not fixed point, regular spiking is impossible, and the system will either present bursts or irregular spiking.

- If there is a unique fixed point, then regular spiking and bursts can coexist depending on the initial condition on the reset line.
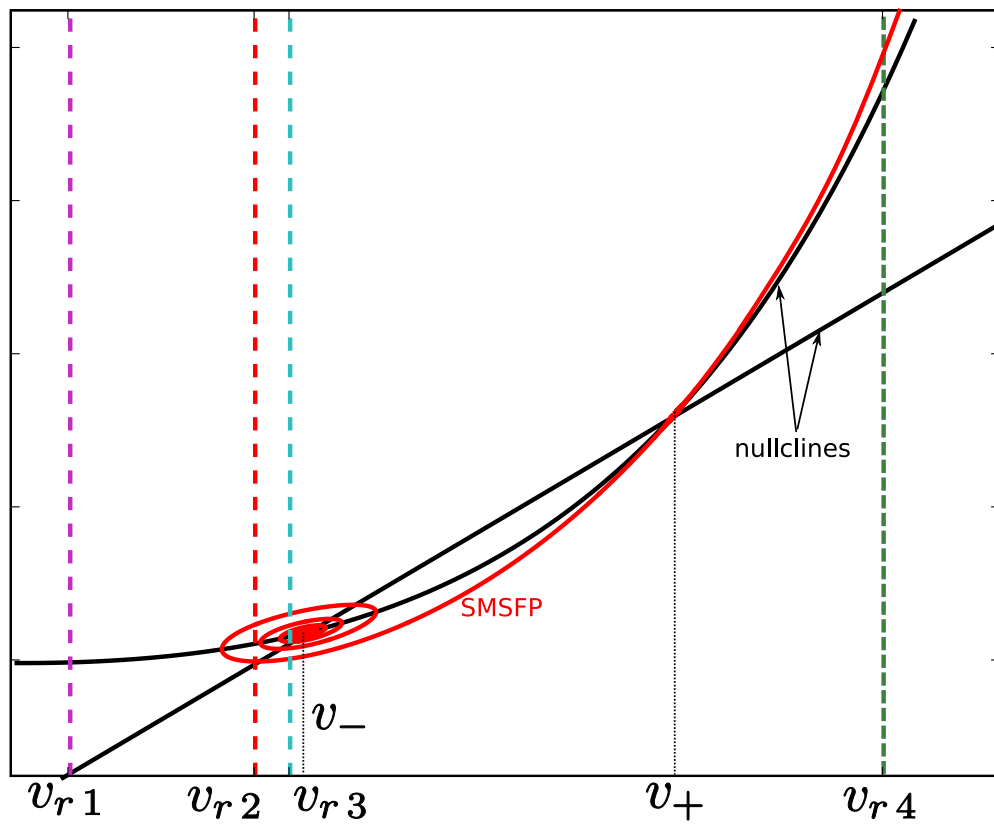
(a) Nullclines and different reset locations v_{r1}, v_{r2}, v_{r3}, v_{r4} corresponding to different qualitative behaviors for the map Φ.
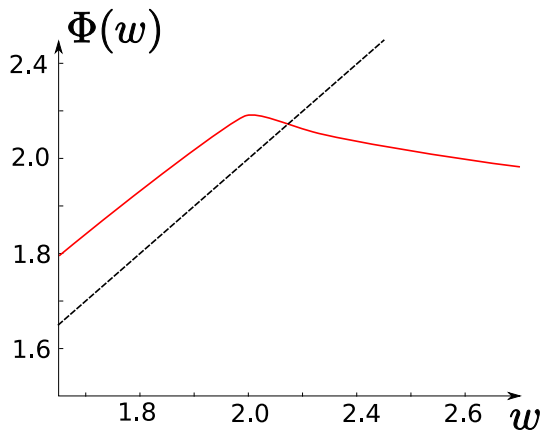
(b) $v_r = v_{r1}$: Φ is continuous
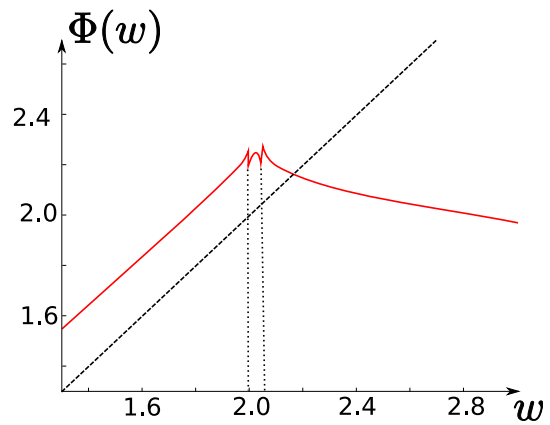
(c) $v_r = v_{r2}$: 2 discontinuity points
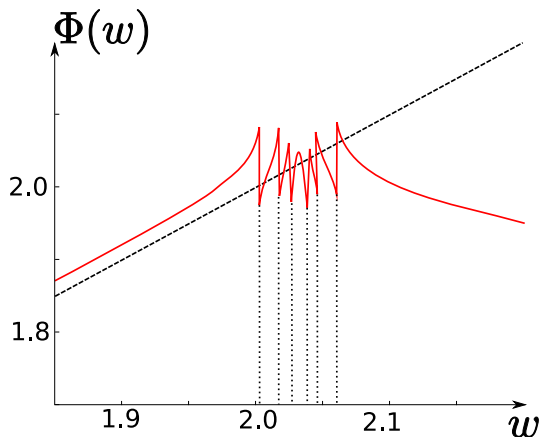
(d) $v_r = v_{r3}$: 6 discontinuity points, 7 fixed points
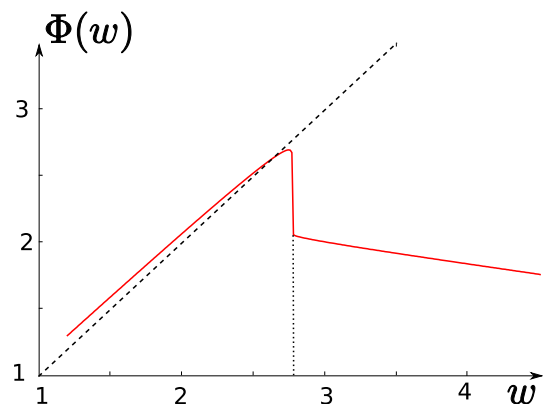
(e) $v_r = v_{r4}$: 1 discontinuity point

Figure 3.20. Case of two unstable fixed points for the classical adaptive exponential model. Phase plane and graph of the map Φ for different values of v_r, for the same set of parameters.

- The case where there are many fixed points (see figure 3.20(d)) is even more complex. In this case the system could have different regular spiking frequencies, depending on the initial condition. In this case of multiple attractors, the system could switch between these attractors, be chaotic, present hysteresis and its sensitivity increases.

3.5 DISCUSSION

3.5.1 Physiological relevance

The first two-dimensional spiking neuron model with diverging spiking dynamics was introduced by Izhikevich (62), who showed that these models could qualitatively reproduce many different electrophysiological features of real neurons, such as spike-frequency adaptation, bursting, resonance, rebound spiking... A variation of that model, the adaptive exponential integrate-and-fire model (13), includes an exponential spike initiation current (41), which is a realistic approximation of the sodium current (whose activation function is a Boltzmann function). That model (and variants) is able to quantitatively predict the responses of real neurons to injected currents in terms of spike times, with a millisecond precision (8; 23; 69). The quartic model (114) is another variant which can exhibit sustained subthreshold oscillations. Thus, a mathematical analysis of those models has direct biological relevance. That analysis was first addressed in (114; 116), mainly in terms of subthreshold dynamics. Here we studied the patterns of spikes, which correspond to orbits under the adaptation map.

Dynamical properties of that map can be related to electrophysiological features of the neuron model. When the differential system has a stable fixed point, orbits are generally finite, i.e., a finite number of spikes are emitted, which is called *phasic spiking* (one spike) or *phasic bursting* (several spikes). In some situations, typically when the reset value is high, finite and infinite orbits can coexist, i.e., the system is bistable.

When the differential system has no stable fixed point, orbits are infinite, an infinite number of spikes are emitted, which is called *tonic spiking*. This is the most interesting aspect of the dynamics, where we must look at the properties of the adaptation map. When orbits converge to a fixed point of that map, spikes become regularly spaced, which corresponds electrophysiologically to the *regular spiking* behavior. Thus, theorem 3.3.2 provides conditions under which the neuron model has a regular spiking behavior. Periodic orbits translate to repeating spike patterns, which corresponds electrophysiologically to the *bursting* behavior, where the period is the number of spikes per burst. The existence of fixed points or periodic orbits depends in a complex way on the parameters. In particular, a period-adding bifurcation structure appears when increasing the reset parameter. It is particularly interesting to see that these two-dimensional models can exhibit chaos, whose electrophysiological signature is irregular spiking. Chaos has been observed in higher dimensional continuous neuron models such as the Hodgkin-Huxley model and variants (38; 49; 105). It has also been observed in real neurons in vitro, such as the Purkinje cell (36; 58; 88; 91), where period doubling was observed in experiments when increasing the temperature with a fixed input current.

3.5.2 Classifications

In (116), the authors defined electrophysiological classes for the subthreshold dynamics in the case of the adaptive exponential model[2]. These classes are sets of parameters such that the neuron has the same qualitative behavior in response to different levels of input currents. We know that when I is smaller than $-m(b)$ the neuron will be in a phasic spiking behavior and when I is large enough, it will fire regularly. Classes are therefore distinguished depending on what is happening between these two stages, and three cases are possible:

0. The neuron always fires regularly (no transition).

1. The neuron first bursts then fires regularly (1 transition, see e.g. figure 3.15(b)).

2. The neuron fires regularly, then bursts, then fires regularly again (2 transitions, see e.g. figure 3.15(a)).

Classes 0 and 1 are observed in general whatever v_r and d for given values of a and b. Class 2 exists less often, and is generally observed for large values of the spike triggered adaptation d. We numerically compute the transitions between regular spiking and bursting. In Figure 3.21 we represented the number of transitions (i.e. the class of neuron) as a function of the parameters a and b for different pairs (v_r, d).

---

[2]their classification readily generalizes to the whole class of models we study here
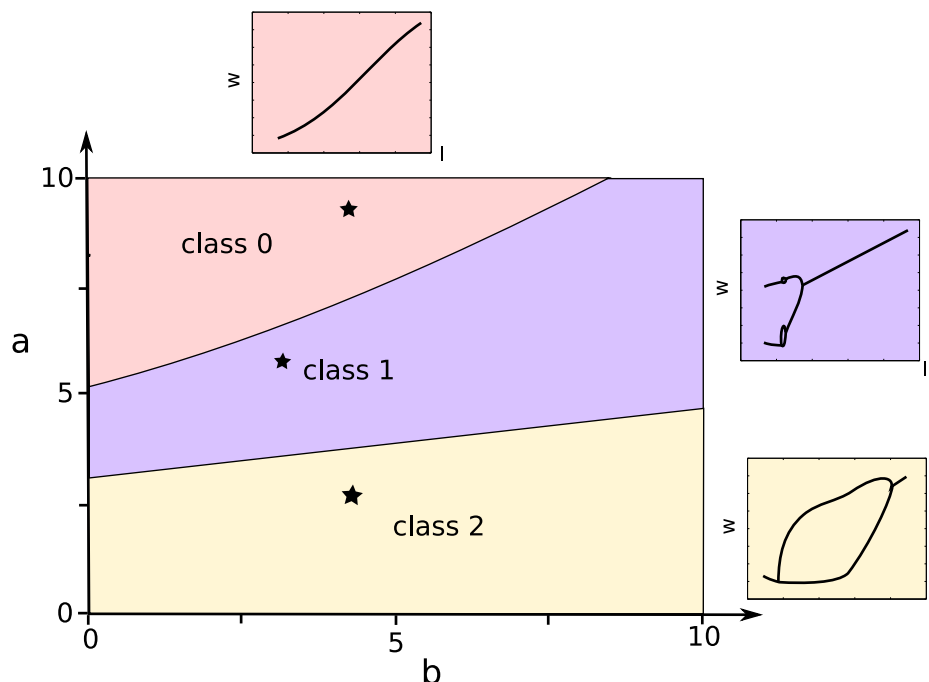
Figure 3.21. Electrophysiological classes for the quartic model with $d = 10$ and $v_r = 1$, as a function of the parameters a and b. Class 2 dissapears when d is small enough. Both classes 1 and 2 disappear when v_r is close to the minimum of F (or small enough in the case of the exponential model). Sample members of these classes have been represented in the small figures around the classification figure: we represented the adaptation sequence after a given elapsed time, as a function of the input current. Parameters are marked with stars: class 0: $a = 8.5$, $b = 4.5$, class 1: $a = 6$, $b = 3.2$, and class 2: $a = 2.5$, $b = 4.5$.

Let us now be more specific and define zones of parameters corresponding to a unique given behavior. The criteria for regular spiking given in theorems 3.3.2 and 3.3.3 rely on some very simple properties of the map Φ. We apply here the results of these theorems in order to define sets of parameters corresponding to different classes of behaviors: regular spiking with spike frequency adaptation, regular spiking with initial bursting, burst of period two, and a class of burst of unspecified period and chaotic spiking. The case where theorem 3.3.2 applies corresponds to the case of regular spiking with spike frequency adaptation. In the case where theorem 3.3.3 applies, we check the stability of the fixed point of Φ by computing the related multiplier: if it is smaller than one in absolute value, the system is in a regular spiking mode with intial bursting, and if not, the neuron fires bursts of period two. Eventually, in the cases where none of the theorems applies, the system is necessarily in a bursting or chaotic mode.

We have seen that when I is high enough or when d is high enough, the neuron fires regularly. Figure 3.22(c) helps us specify the parameter sets related to regular spiking (with initial bursting or spike frequency adaptation) and bursting. We observe in figure 3.22(c) that the input current has a stabilizing effect on the whole dynamics: we simulated a case where the map Φ is not globally contracting for input currents close to $-m(b)$. When increasing the current, we observe that the map becomes globally contracting when the input current is high enough, which results in a regular spiking behavior. Therefore the electrophysiological class depends on d.

Another pair of interesting parameters is the pair of reset parameters (v_r, d). The influence of these two parameters was numerically studied by Naud and collaborators in the case of the dimensioned adaptive exponential model (see (95)) for a current value twice the value of the saddle-node bifurcation current. They numerically simulated the spike trains and classified them as chaotic spiking, bursting, regular spiking with spike frequency adaptation and initial bursting. The mathematical criteria we have presented predict these zones, as shown on figure 3.22.

3.5.3 Perspectives

In this chapter we studied the spike patterns produced by neurons in the class of models introduced in (114) in the case where the spike is emitted when the membrane potential blows up. We introduced a discrete map called the adaptation map, which is a generalization of the usual Poincaré applications in dynamical

(a) Exponential Model

(b) Quartic Model
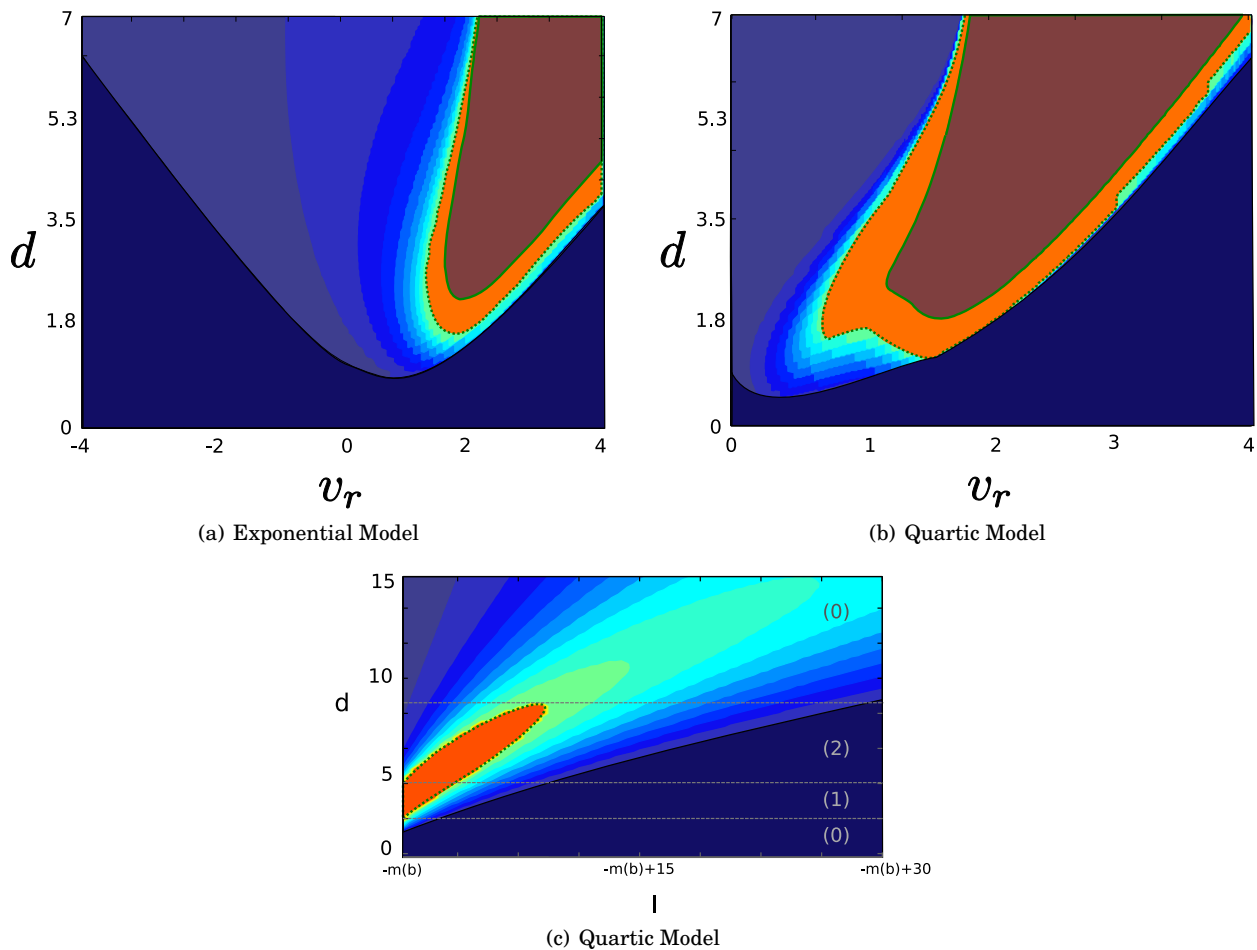
(c) Quartic Model

Figure 3.22. Parameter zones corresponding to different spiking behaviors. (a): Reduced adaptive exponential model with $a = 1$, $b = 2$ and $I = 3$. (b): Quartic model, $a = 1$, $b = 2$, $I = -m(b) + 2$. (c): $a = 1$, $b = 1$, $v_r = 1.5$. Regular spiking is indicated in blue. The dark blue zone corresponds to spike frequency adaptation, and the other blue regions correspond to initial bursting. The color intensity is proportional to the multiplier of the fixed point: the smaller the multiplier the darker the region. The separatrix we obtain in figure (a) is very close to the one found numerically by Naud and collaborators in (95). Bursts and chaotic spiking are indicated in red/orange. The orange region corresponds to bursts with two spikes per burst (according to theorem 3.3.3). The green dotted line corresponds to the period doubling bifurcation. The brown zone corresponds to burst and chaos and the green solid line corresponds the initiation of the cascade of period doubling at the transition from period two to period three. In (c) the electrophysiological classes are represented as a function of d.

systems corresponding to the case where the Poincaré section is set a infinity. The rigorous mathematical study of this map allowed us to distinguish between the different spike patterns fired, and to derive simple criteria to characterize different spiking regimes of the neuron. These criteria can be easily applied in order to derive classes of parameters corresponding to different kinds of behaviors. We also proved that the system presented bifurcations as a function of the reset value of the membrane potential.

This study of a hybrid dynamical system opens the way to the study of different spiking models, such as bidimensional compartment models or bidimensional spiking models with or without explosion. In particular, this study readily applies to the case of Izhikevich' quadratic integrate-and-fire model which is a bidimensional nonlinear spiking neuron model where spikes are emitted when the membrane potential reaches a finite threshold. This framework may also be interesting in other fields of applied mathematics, and in particular in mathematical biology, ecology, economy and generally in any nonlinear system where discrete events occur depending on the state of the variables of the system.

4

APPLICATION: DEFINING ELECTROPHYSIOLOGICA L CLASSES

ABSTRACT

In the last two sections we discussed the mathematical properties of a class of neuron models and explained briefly the reasons why they were able to reproduce the diversity of electrophysiological features displayed by real neurons while keeping a simple model, for simulation and analysis purposes. Among these models, the adaptive exponential integrate-and-fire model is physiologically relevant in that its parameters can be easily related to physiological quantities. The interaction of the differential equations with the reset results in a rich and complex dynamical structure. In this chapter we relate the subthreshold features of the model to the dynamical properties of the differential system and the spike patterns to the properties of a Poincaré map defined by the sequence of spikes. We build upon the results obtained in the chapters 2 and 3 an electrophysiological class description for the models of this class, i.e. the sets of parameters where the model responds qualitatively the same way to different current inputs. We are particularly interested in the Adaptive Exponential Model, for which we provide the closed-form equations in the parameter space of the separatrix we obtain between electrophysiological classes. This work is a collaboration with Romain Brette to be published in Biological Cybernetics (116).

4.1 INTRODUCTION

As reviewed in the previous two chapters, several authors recently studied two-variable spiking models (13; 63; 113) which, despite their simplicity, can reproduce a large number of electrophysiological signatures such as bursting or regular spiking. Different sets of parameter values correspond to different electrophysiological classes.

All these two-dimensional models are qualitatively similar, and we will be in this chapter especially interested in the adaptive exponential integrate-and-fire model (AdEx, (13)) because its parameters can be easily related to physiological quantities, and the model has been successfully fit to a biophysical model of a regular spiking pyramidal cell and to real recordings of pyramidal cells (23; 69). As already introduced, this model is described by two variables, the membrane potential V and an adaptation current w, whose dynamics are governed by the following differential equations:

$$\begin{cases} C\frac{dV}{dt} &= -g_L(V - E_L) + g_L\Delta_T \exp\left(\frac{V - V_T}{\Delta_T}\right) \\ & \quad -w + I \\ \tau_w\frac{dw}{dt} &= b(V - E_L) - w \end{cases} \tag{4.1}$$

When the membrane potential V is high enough, the trajectory quickly diverges because of the exponential term. This divergence to infinity models the spike (the shape of the action potential is ignored, as in the standard integrate-and-fire model). For displaying or simulation purposes, spikes are usually cut to some finite value (e.g. 0 mV). When a spike occurs, the membrane potential is instantaneously reset to some value V_r and the adaptation current is increased:

$$\begin{cases} V &\rightarrow V_r \\ w &\rightarrow w + d \end{cases} \tag{4.2}$$

Remark 10. The spike-triggered adaptation parameter denoted by d corresponds to the parameter denoted by b in the original article of Brette and Gerstner (13), and the parameter b of (4.1) corresponds to the parameter a of the original paper. We choose here to keep the same notations as in the previous chapters in order for the dissertation for the sake of consistency.

Although the differential system is only two-dimensional, the reset makes the resulting dynamical hybrid system very rich, as discussed in chapter 3.

The differential equations and the parameters have a physiological interpretation. The first equation is the membrane equation, which states that the capacitive current through the membrane (C is the membrane capacitance) is the sum of the injected current I and of the ionic currents. The first term is the leak current (g_L is the leak conductance and E_L is the leak reversal potential), the membrane time constant is $\tau_m = C/g_L$. The second (exponential) term approximates the sodium current, responsible for the generation of action potentials (41). The approximation results from neglecting the inactivation of the sodium channel and assuming that activation is infinitely fast (which is reasonable). Because activation curves are typically Boltzmann functions (6), the approximated current is exponential near spike initiation. The voltage threshold V_T is the maximum voltage that can be reached without generating a spike (without adaptation), and the slope factor Δ_T quantifies the sharpness of spikes. In the limit of zero slope factor, the model becomes an integrate-and-fire model with a fixed threshold V_T. Quantitatively, it is proportional to the slope constant k in the activation function of the sodium current. The second variable w is an adaptation current with time constant τ_w, which includes both spike-triggered adaptation, through the reset $w \rightarrow w + d$, and subthreshold adaptation, through the coupling (variable b). It may model ionic channels (e.g. potassium) or a dendritic compartment. Quantitatively, the coupling variable b can result from a linearization of the dynamics of a ionic channel, or from the axial conductance in the case of a dendritic compartment. We generally assume $b > 0$ in this chapter, although the analysis also applies for $b < 0$ when $|b|$ is not too large.

The interaction of the differential equations with the reset results in a rich dynamical structure. There are 9 parameters plus the injected current I, but these can be reduced to 4 variables plus the current I by changes of variables (e.g. setting V_T as the reference potential, Δ_T as the voltage unit, τ_m as the time unit, etc.). Thus, the electrophysiological class of the model, defined loosely here as the set of qualitative behaviors for different values of I, is parametrized in a 4-dimensional space. In this chapter, we will make this definition more precise by explaining different electrophysiological signatures in terms of dynamics of the model. Because we are dealing with a hybrid dynamical system, we shall study here two distinct dynamical aspects of the model: the subthreshold dynamics, defined by the differential equations (section 4.2), and the spiking dynamics, defined the sequence of resets (section 4.4). The former case was addressed in chapter 2 in a more general setting: we apply these results in order to derive new specific results, in

particular about oscillations, attraction basins and rebound properties, that are interesting from a biological point of view. In the latter case, we will see that the spike patterns of the model correspond to orbits under a Poincaré map, which we shall call the *adaptation map* Φ. Interestingly, we find that this map can have chaotic dynamics under certain circumstances, as studied in chapter 3.

All simulations shown in this chapter were done with the Brian software (45) The code is available on ModelDB at the following URL:
http://senselab.med.yale.edu/modeldb/ShowModel.asp?model=114242.

4.2 SUBTHRESHOLD BEHAVIOR

The equations of the AdExp model can be written in dimensionless units by expressing time in units of the membrane time constant $\tau_m = C/g_L$, voltage in units of the slope factor Δ_T and with reference potential V_T, and rewriting both the adaptation variable w and the input current I in voltage units. We already did this transformation in the chapter 2, but write it down here again for the sake of completeness, and for keeping interpreting a little bit more the results obtained.

We obtain the following equivalent model:

$$\begin{cases} \frac{d\bar{V}}{d\bar{t}} = -\bar{V} + e^{\bar{V}} - \bar{w} + \bar{I} \\ \bar{\tau}_w \frac{d\bar{w}}{d\bar{t}} = \bar{b}\bar{V} - \bar{w} \end{cases} \tag{4.3}$$

and when a spike is triggered:

$$\begin{cases} \bar{V} \quad \to \bar{V}_r \\ \bar{w} \quad \to \bar{w} + \bar{d} \end{cases} \tag{4.4}$$

where

$$\begin{cases} \bar{\tau}_w & := \frac{\tau_w}{\tau_m} = \frac{g_L \tau_w}{C} \\ \bar{b} & := \frac{b}{g_L} \\ \bar{I} & := \frac{I}{g_L \Delta_T} + (1 + \frac{b}{g_L}) \frac{E_L - V_T}{\Delta_T} \\ \bar{t} & := \frac{t}{\tau_m} \\ \bar{d} & := \frac{d}{g_L \Delta_T} \\ \bar{V}_r & := \frac{V_r - V_T}{\Delta_T} \\ \bar{V}(\bar{t}) & := \frac{V(t) - V_T}{\Delta_T} \\ \bar{w}(\bar{r}) & := \frac{w(t) + b(E_L - V_T)}{g_L \Delta_T} \end{cases} \tag{4.5}$$

Thus, as already mentioned in 2 only two parameters characterize the subthreshold dynamics: the ratio of time constants τ_w/τ_m and the ratio of conductances b/g_L (note: b can be seen as the stationary adaptation conductance), and the rescaled model belongs to the class studied in this chapter with $F(v) = e^v - v$, i.e., F is convex, three times continuously differentiable, has a negative derivative at $-\infty$ and an infinite derivative at $+\infty$. Therefore it has the same bifurcation structure, which is related as we develop here to electrophysiological properties, excitability type, rheobase current, voltage threshold, I-V curve. Besides, we give quantitative conditions for the occurrence of oscillations, along with a formula for their frequency. Finally, we examine the rebound properties of the model, in relationship with the attraction basin of the stable fixed point.

4.2.1 Excitability

The dynamics in the phase plane (V, w) are partly determined by the number and nature of fixed points, which are the intersections of the two nullclines (Fig. 4.1):

$$\begin{aligned} w &= F(v) + I \quad \text{(V-nullcline)} \\ w &= bv \quad \text{(w-nullcline)} \end{aligned}$$

and that read in the original parameters for the AdExp model:

$$\begin{aligned} w &= -g_L(V - E_L) + g_L \Delta_T \exp\left(\frac{V - V_T}{\Delta_T}\right) + I \quad \text{(V-nullcline)} \\ w &= b(V - E_L) \quad \text{(w-nullcline)} \end{aligned}$$

Because the membrane current (first equation) is a convex function of the membrane potential V, there can be no more than two fixed points. When the input current I increases, the V-nullcline goes up and the
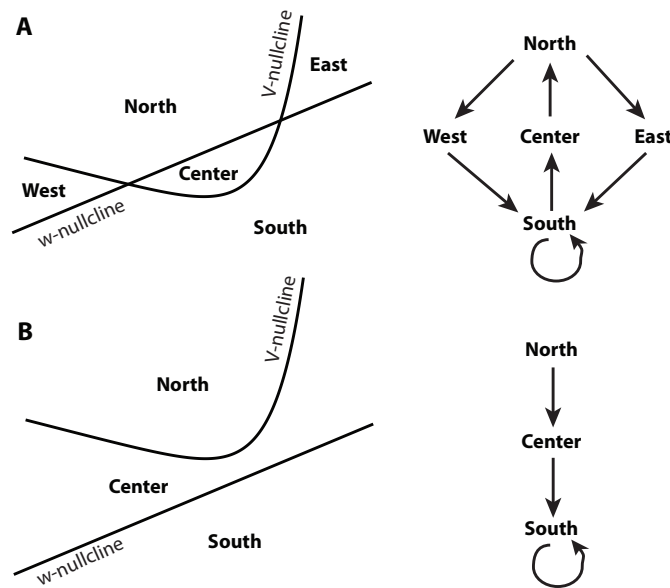
Figure 4.1. Nullclines of the dynamical system (horizontal axis: V; vertical axis: w). A. The nullclines intersect in two points, and divide the phase space into 5 regions. The potential V increases below the V-nullcline, w increases below the w-nullcline. The direction of the flow along each boundary gives the possible transitions between regions (right). Spiking can only occur in the South region. B. The nullclines do not intersect. All trajectories must enter the South region and spike.
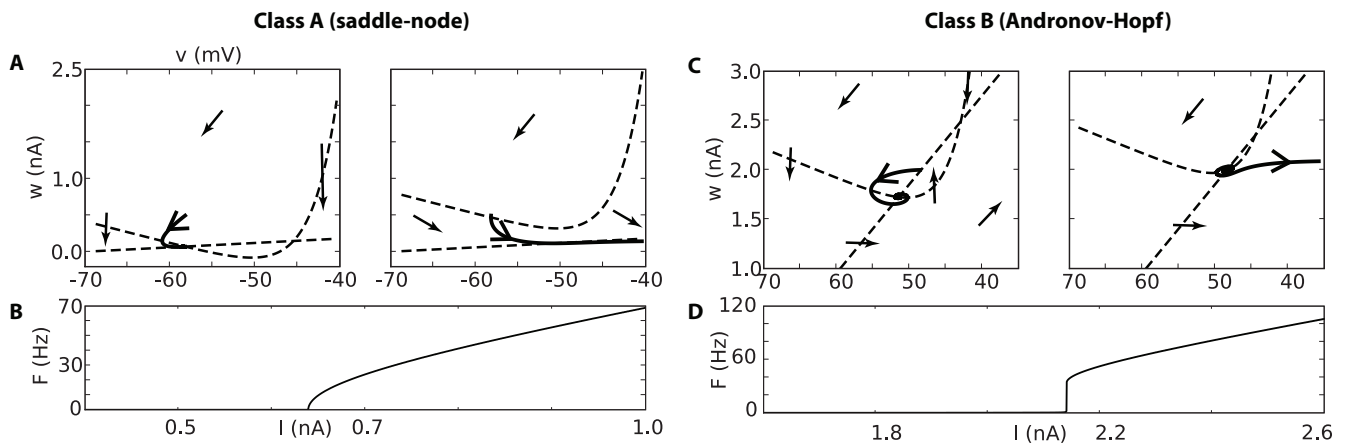
Figure 4.2. Excitability types. A,B. Type I: $\frac{b}{g_L} < \frac{\tau_m}{\tau_w}$ (here: $b = .2g_L$, $\tau_m = 3\tau_w$). When I is increased, the resting point disappears through a saddle-node bifurcation: the two fixed points merge and disappear. The current-frequency curve is continuous (B). C,D. Type II: $\frac{b}{g_L} > \frac{\tau_m}{\tau_w}$ (here: $b = 3g_L$, $\tau_m = .5\tau_w$). When I is increased, the resting point becomes unstable through an Andronov-Hopf bifurcation: the stable fixed point becomes unstable. The current-frequency curve is discontinuous, there is a non-zero minimum frequency (D).

number of fixed points goes from two to zero, while the trajectories go from resting to spiking. The excitability properties of the model depend on how the transition to spiking occurs, that is, on the bifurcation structure.

Excitability types

When I is very negative, there are two fixed points, one of which is stable (the resting potential). It appears that, when increasing I, two different situations can occur depending on ratio b/a, more precisely in the AdExp model, depending on the quantity $\frac{b\tau_w}{C} = \frac{b}{g_L}\frac{\tau_w}{\tau_m}$ (ratio of conductances times ratio of time constants).

If $b < a$ ($\frac{b}{g_L} < \frac{\tau_m}{\tau_w}$), then the system undergoes a saddle-node bifurcation when I is increased, i.e., the stable and unstable fixed points merge and disappear at the point $I = -m(b) = F(v^*(b))$. When the fixed points disappear, the vector field is almost null around the former fixed point (the *ghost* of the fixed point).

Since the vector field can be arbitrarily small close to the bifurcation, the trajectory can be trapped for an arbitrarily long time in the ghost of the fixed point, so that the firing rate can be arbitrary small when I is close to the bifurcation point (threshold). This property also explains the phenomenon of spike latency. This fact generally implies that the model has type I excitability, that is, the current-frequency curve is continuous (Fig. 4.2), but type II excitability may occur if the reset V_r is high (so that trajectories do not enter the ghost zone). However, we note that this latter case corresponds to bistable spiking before the bifurcation (4.4.3).

If $b > a$ (i.e. $\frac{b}{g_L} > \frac{\tau_m}{\tau_w}$), then the system undergoes a subcritical Andronov-Hopf bifurcation before the saddle-node one, meaning that the stable fixed point first becomes unstable before merging with the other fixed point. This fact implies generally that the model has type II excitability, that is, the current-frequency curve is discontinuous at threshold, the firing rate suddenly jumps from zero to a finite value when the bifurcation point is crossed (Fig. 4.2). It is however possible to have type I excitability in very specific cases, when the trajectory resets close to the stable manifold of the saddle fixed point.

In the following, we shall refer to the first case as class A and to the second one as class B. As noted above, excitability types I and II are related but not identical to classes A and B (for example, the model may belong to class A but have no well-defined excitability type when it is bistable).

For the limit case $b = a$ (i.e. $\frac{b}{g_L} = \frac{\tau_m}{\tau_w}$), the system undergoes a Bogdanov-Takens bifurcation. It has codimension two, i.e. it appears when simultaneously varying the two parameters $\bar{b}$ and $\bar{I}$. At this point, the family of unstable periodic orbits generated around the Andronov-Hopf bifurcation collides with the saddle fixed point and disappears via a saddle-homoclinic bifurcation. There is no other bifurcation in this model (as well as in Izhikevich model (63)). Other similar models such as the quartic model may also undergo a Bautin bifurcation, associated with stable oscillations (see chapter 2).

As already discussed, the system can have zero, one or two fixed points depending on the input current. When it has two fixed points, we denote by $x_+ < x_-$ the two fixed points for the general model and by V_+ and V_- in the AdExp model. The fixed points in the case of the original AdExp model are deduced from the expressions given in section 2.2.2 using the Lambert function W:

$$
\begin{cases}
V_- := E_L + \frac{I}{g_L+b} - \Delta_T W_0\left(-\frac{1}{1+b/g_L}e^{\frac{I}{\Delta_T(g_L+b)}+\frac{E_L-V_T}{\Delta_T}}\right) \\
V_+ := E_L + \frac{I}{g_L+b} - \Delta_T W_{-1}\left(-\frac{1}{1+b/g_L}e^{\frac{I}{\Delta_T(g_L+b)}+\frac{E_L-V_T}{\Delta_T}}\right)
\end{cases}
\tag{4.6}
$$

where W_0 is the principal branch of the Lambert function and W_{-1} the real branch of the Lambert function such that $W_{-1}(x) \leq -1$, defined for $-e^{-1} \leq x < 1$.

The fixed point x_+, or V_+, is always a saddle fixed point (hence unstable), i.e. its Jacobian matrix has an eigenvalue with positive real part and an eigenvalue with negative real part. The fixed point V_- is stable if the model has class A parameters, otherwise it depends on the current I, as we discuss below.

Rheobase current

The rheobase current is the minimum constant current required to elicit a spike. This electrophysiological definition could be ambiguous because it depends on the initial condition. If we consider that the current is slowly increased until a spike is elicited, then it corresponds to the first point when the stable fixed point becomes unstable, which depends on the parameter class (note that this is true only when the Andronov-Hopf bifurcation is subcritical).

For class A ($b < a$), it corresponds to the saddle-node bifurcation point:

$$
I_{\text{rh}}^A = -m(b)
\tag{4.7}
$$

which is obtained by calculating the intersection of the nullclines when these are tangent. It corresponds in the AdExp model for class A ($\frac{b}{g_L}\frac{\tau_w}{\tau_m} < 1$) to the curve:

$$
I_{\text{rh}}^A = (g_L+b)\left[V_T - E_L - \Delta_T + \Delta_T \log\left(1+\frac{b}{g_L}\right)\right].
\tag{4.8}
$$

For class B parameters ($b > a$), it corresponds to the Andronov-Hopf bifurcation point:

$$
I_{\text{rh}}^B = bv^*(a) - F(v^*(a))
\tag{4.9}
$$

that reads for the AdExp model in the case $\frac{b}{g_L}\frac{\tau_w}{\tau_m} > 1$ to the curve:

$$
I_{\text{rh}}^B = (g_L+b)\left[V_T - E_L - \Delta_T + \Delta_T \log(1+\frac{\tau_m}{\tau_w})\right] + \Delta_T g_L(\frac{b}{g_L} - \frac{\tau_m}{\tau_w})
\tag{4.10}
$$

It is important to note that the saddle-node bifurcation also occurs in the class B case at the point $I_{SN} = I_{rh}^I$ ($> I_{rh}^B$; for class B we use I_{SN} instead of I_{rh}^I to avoid ambiguities).

Voltage threshold for slow inputs

For a parametrized input $I_b(t)$, the threshold is the minimum value of the parameter b for which a spike is elicited. For example, the rheobase current is the threshold constant current. However, the notion of a spike threshold for neurons is often described as a *voltage threshold*, although the voltage is not a stimulation parameter (thus, it implicitly refers to an integrate-and-fire model). It is nevertheless possible to define a meaningful voltage threshold for the case of constant current inputs as follows: the voltage threshold is the maximum stationary voltage V for subthreshold constant current inputs ($I \leq I_{rh}$). For the exponential integrate-and-fire model (41), this is simply V_T. For the present model, it corresponds to the voltage V_- at the first bifurcation point, when the stable fixed point becomes unstable.

Not surprisingly, its value depends on the excitability type. In the general case, for class A parameters ($b < a$), the voltage threshold is

$$V_{\text{threshold}}^{\text{slow}} = v^*(b),$$

which reads for the AdExp model in the case $b/g_L < \tau_m/\tau_w$

$$V_{\text{threshold}}^{\text{slow}} = V_T + \Delta_T \log(1 + b/g_L)$$

and for class B parameters ($b > a$)

$$V_{\text{threshold}}^{\text{slow}} = v^*(a)$$

and for the AdExp model for $b/g_L < \tau_m/\tau_w$

$$V_{\text{threshold}}^{\text{slow}} = V_T + \Delta_T \log(1 + \tau_m/\tau_w)$$

Interestingly, the threshold for class A parameters depends on the ratio of conductances (b), while the threshold for class B parameters on the ratio of time constants (a).

Voltage threshold for fast inputs

For short current pulses ($I = q\delta(t)$, where q is the total charge and $\delta(t)$ is the Dirac function), the voltage threshold is different, but the same definition may be used: it is the maximum voltage V that can be reached without triggering a spike. Injecting short current pulses amounts to instantaneously changing the membrane potential V, i.e., in the phase space (V, w), to moving along an horizontal line. If, by doing so, the point (V, w) exits the attraction basin of the stable fixed point, then a spike is triggered. Therefore, the threshold is a curve in the phase space, defined as the boundary of the attraction basin of the stable fixed point (for which we have unfortunately no analytical expression, although it can be computed numerically). Therefore the model displays *threshold variability*: the voltage threshold depends on the value of the adaptation variable w, i.e., on the previous inputs. The boundary of the attraction basin of the stable fixed point is either the stable manifold of the saddle fixed point (separatrix) or a limit cycle.

4.2.2 I-V curve

The I-V curve of a neuron is the relationship between the opposite of the (constant) injected current and the stationary membrane potential (it may also be defined for non-constant input currents, see e.g. (8)). Experimentally, this curve can be measured with a voltage-clamp recording. We obtain a simple expression by calculating I at the intersection of the nullclines:

$$I(v) = bv - F(v)$$

that can be written for the AdExp model in the form:

$$I(V) = (b + g_L)(V - E_L) - g_L \Delta_T \exp\left(\frac{V - V_T}{\Delta_T}\right)$$

Thus, far from threshold, the $I - V$ curve is linear and its slope is the leak conductance plus the adaptation conductance.

4.2.3 Oscillations

Because of the coupling between the two variables V and w, there can be oscillations near the resting potential. For the AdExp model or the Izhikevich' model, only damped oscillations exist, and self-sustained oscillations are not possible, except via Bautin bifurcation that exists for instance in the quartic model. Oscillations occur when the eigenvalues associated with the stable fixed point are complex; when they are real, solutions converge (locally) exponentially to the stable fixed point.

Because of the nature of the bifurcations, near the rheobase current (section 4.2.1), the model is non-oscillating if it has class A parameters ($b < a$, or $b/g_L < \tau_m/\tau_w$) and oscillating if it has class B parameters. Far from threshold, these properties can change. In this section we give explicit expressions for the parameter zones corresponding to both regimes.

The parameter zones depend on the excitability types, on the finiteness of $F'_{-\infty} \overset{\text{def}}{=} \lim_{v \to -\infty} F'(v)$, the ratio $a = \tau_w/\tau_m$ and the following condition:

$$b < \frac{(F'_{-\infty} + a)^2}{4a} \tag{4.11}$$

translated for the AdExp model in:

$$\frac{b}{g_L} < \frac{\tau_m}{4\tau_w}\left(1 - \frac{\tau_w}{\tau_m}\right)^2 \tag{4.12}$$

These results are summarized in Fig. 4.3.

Identification of the oscillating regions

Oscillations around a stable equilibrium appear only when the systems has a stable fixed point, i.e. if $I < -m(b)$ for $b < a$ and $I < bv^*(a) - F(v^*(a))$ for $b > a$. Furthermore, the system will oscillate around the stable equilibrium v_- if and only if the imaginary part of the eigenvalues of the Jacobian matrix of the system at this point is non-null. This condition can be written at the stable equilibrium v_- via the discriminant δ defined by:

$$\delta = \left(F'(v_-) + a\right)^2 - 4ab.$$

The system will oscillate around the stable fixed point v_- if and only if $\delta < 0$. To invert this inequality, we compute the zones where we have

$$(x + a)^2 - 4ab < 0 \tag{4.13}$$

and check that a solution v_- exists. There exists a v_- such that $F'(v_-) = x$ if and only if $F'_{-\infty} := \lim_{u \to -\infty} F'(u) < x < F'(v^*(b)) = b$, since $v_- < v^*(b)$ and F' is increasing.

The solution of (4.13) is $x \in \{x_-, x_+\}$ where

$$x_\pm = -a \pm 2\sqrt{ab}$$

First of all we are interested in the apparition of oscillations in the class A case. We know that when the input current I is close to the rheobase current I_{rh}^l given by (4.7), the system returns monotonously to the resting potential. The system begins to oscillate when there exist solutions to the equation $F'(v_-) = x_+$. It is straightforward to check that x_+ is always lower than b, since this condition is equivalent to the condition $(a - b)^2 \geq 0$, which is always true.

If $F'_{-\infty} = -\infty$, as it is the case in the quadratic and quartic models, the condition $x_+ > F'_{-\infty}$ is trivial and always satisfied. If $F'_{-\infty} > -\infty$, then this condition can be written:

$$\{(a,b) \; ; \; a < -F'_{-\infty} \text{ or } 0 > F'_{-\infty} > -a \text{ and } b > \frac{(F'_{-\infty} + a)^2}{4a}\}$$

In this zone, oscillations occur when the current I is below I_+, where:

$$\bar{I}_+ = bv^*(x_+) - F(v^*(x_+))$$

Hence it appears for class A parameters. After the Bogdanov-Takens point, the equilibrium associated with x_+ is unstable, hence does not give rise to damped subthreshold oscillations.

In the case where $F'_{-\infty} > -\infty$ and $F'_{-\infty} > -a$, we always have $\frac{(F'_{-\infty} + a)^2}{4a} < a$. When $b = a$, we have $x_+ = a$ and hence $I_+ = I_v^-(v^*(a))$, which is the current at the Bogdanov-Takens bifurcation point. This result was predictable since around the saddle node bifurcation the system does not oscillate around the fixed point and around the Andronov-Hopf bifurcation the system does oscillate, and these two curves meet at the
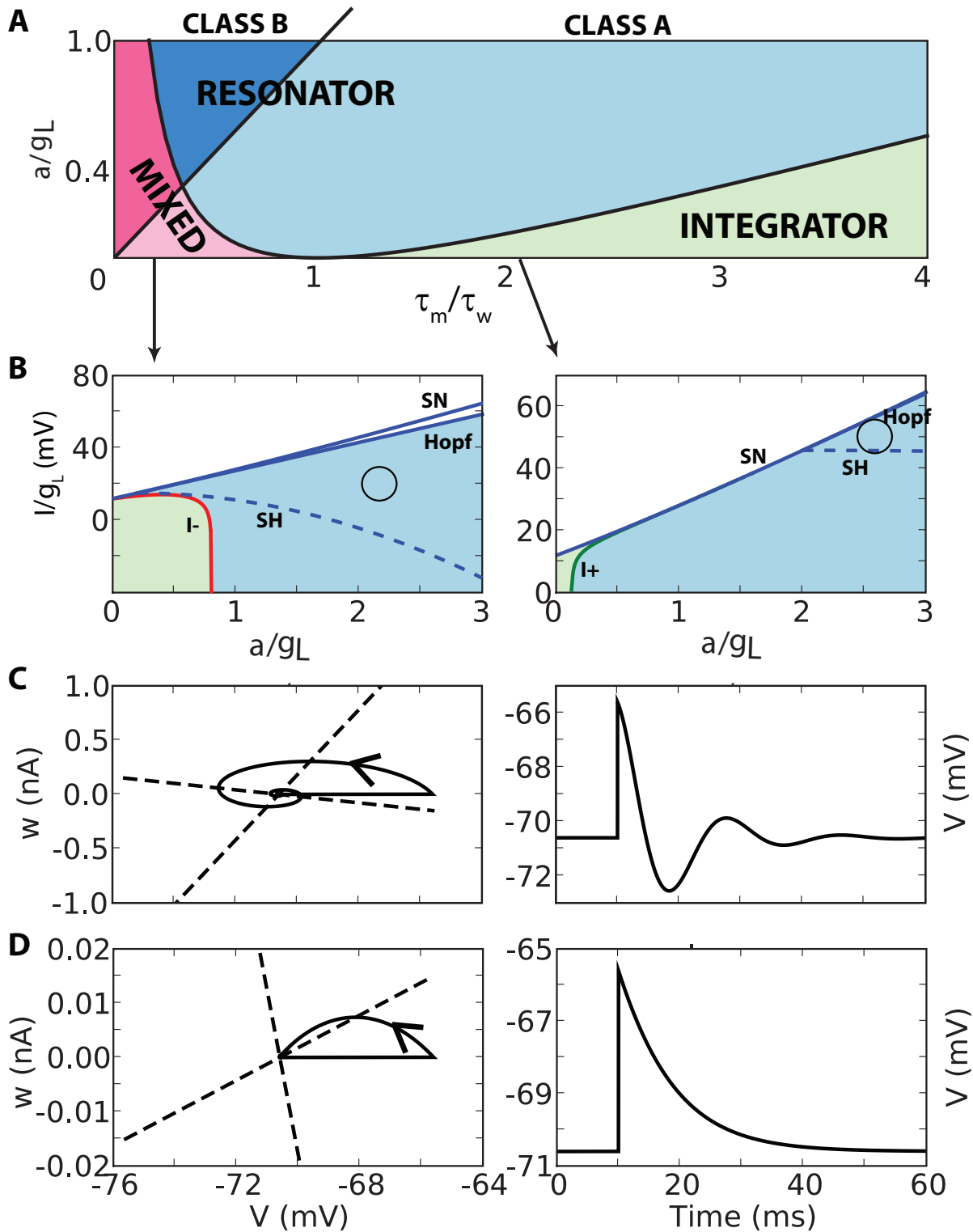
Figure 4.3. Oscillations. A. Behavior of the model as a function of a/g_L and τ_m/τ_w. Light (dark) colors indicate class A (class B) parameters. Blue: resonator mode (oscillations for any or almost any I). Green: integrator mode (oscillations for any I). Pink: mixed mode (resonator if I is large enough, otherwise integrator). B. Behavior of the model as a function of a/g_L and I/g_L for $\tau_m = .2\tau_w$ (left) and $\tau_m = 2\tau_w$ (right). White: spiking; blue: oscillations; green: no oscillation. Spiking occurs when I is above the saddle-node curve (SN) in the class A regime, and above the Hopf curve (Hopf) in the class B regime. A repulsive limit cycle (circle) exists when I is above the saddle-homoclinic curve (SH; only for class B). Oscillations occur when $I_- < I < I_+$ (on the left, $I_+ \geq I_{SN}$; on the right, $I_- = -\infty$). C,D. Response of the system to a short current pulse (Dirac) near the resting point, in the resonator regime (C; $a = 10g_L$, $\tau_m = \tau_w$) and in the integrator regime (D; $a = .1g_L$, $\tau_m = 2\tau_w$). Left: response in the phase space (V, w); right: voltage response in time.

Bogdanov-Takens point. Furthermore, after the Bogdanov-Takens point, the equilibrium associated with x_+ is no more stable, hence damped subthreshold oscillations associated with this separatrix only appear for class A parameters.

The oscillations possibly disappear when a solution to $F'(v_-) = x_-$ exists. Since $x_- = -a - 2\sqrt{ab} < 0$, the condition $x_- < b$ is always satisfied. The condition $x_- > F'_{-\infty}$ is always satisfied when $F'_{-\infty} = -\infty$. If $F'_{-\infty} > -\infty$, then the condition $x_- > F'_{-\infty}$ is equivalent to the set of conditions

$$a < -F'_{-\infty} \qquad \text{and} \qquad b < \frac{(a+F'_{-\infty})^2}{4a}.$$

In these cases, oscillations disappear when $\bar{I} < \bar{I}_-$, where:

$$\bar{I}_- = bv^*(x_-) - F(v^*(x_-))$$

In the case of the AdExp model with the original parameters, the expression of $I_\pm$ reads:

$$I_\pm = (g_L + a)\Delta_T \log\left(\frac{g_L\tau_w - C \pm 2\sqrt{aC\tau_w}}{g_L\tau_w}\right)$$

$$-\Delta_T \frac{g_L\tau_w - C \pm 2\sqrt{aC\tau_w}}{\tau_w} - (g_L + a)(E_L - V_T) \quad (4.14)$$

Hence there are two qualitatively different cases.

First of all, if $F'_{-\infty} = -\infty$, then the currents $I_\pm$ exist whatever the parameters of the model.

1. For class A parameters, the neuron oscillates around its stable equilibrium if and only if $I_- < I < I_+$.

2. For class B parameters, the neuron oscillates around the stable equilibrium if and only if $I_- < I < I_{rh}^B$.

If $F'_{-\infty} > -\infty$, then the behavior of the system depends on the parameters a and b and on the inequality

$$b > \frac{(F'_{-\infty}+a)^2}{4a} \tag{4.15}$$

1. For class A parameters, we have:

   (a) if $a < -F'_{-\infty}$, then I_+ always exists. If condition (4.15) is satisfied, then I_- does not exist and the system oscillates for $I < I_+$. If condition (4.15) is not satisfied, both I_+ and I_- are defined, and the system oscillates for $I_- < I < I_+$.

   (b) if $a > -F'_{-\infty}$, then I_- is undefined and I_+ only exists when condition (4.15) is satisfied. Hence if condition (4.15) is satisfied, the system oscillates for $I < I_+$ else it never oscillates.

2. For class B parameters, only the existence of I_- is important. When I_- is defined, then the system oscillates for any $I > I_-$. If I_- is not defined, the system always oscillates. In the class B regime, note that condition (4.15) is always satisfied. Hence we have:

   (a) if $a < -F'_{-\infty}$ and condition (4.15) is not satisfied then I_- exists and the system oscillates for any subthreshold current greater than I_-.

   (b) else it oscillates for any subthreshold current.

When the system oscillates, the oscillation (angular) frequency is given by $\bar{\omega} = -\delta$. If $F'_{-\infty} = -\infty$, then the frequency of the oscillations is bounded. If $F'_{-\infty} > -\infty$, then in the low-voltage approximation (far from $v_- << 0$), reads:

$$\bar{\omega} \approx 4ab - (F'_{-\infty}+a)^2$$

When the system oscillates, the time constant of the decay is the inverse of the opposite of the real part of the eigenvalues, which is $\frac{2}{a-F'(v_-)}$.

It becomes infinitely fast in the low voltage approximation if $F'_{-\infty} = -\infty$, else converges to

$$\frac{2}{a-F'_{-\infty}}$$

Oscillations for class A parameters in the AdExp model

Three cases appear:

- If inequality (4.12) is false, then the model oscillates when $I < I_+$, where the formula for I_+ is given in Appendix 4.2.3. In practice, we observe that I_+ is very close to the rheobase current, so that the model almost always oscillates below threshold.

- If inequality (4.12) is true and $\tau_m > \tau_w$, then the model never oscillates near the fixed point.

- If inequality (4.12) is true and $\tau_m < \tau_w$, then the model oscillates when $I_- < I < I_+$, where the formula for I_- is given in Appendix 4.2.3.

Oscillations for class B in the AdExp model

Two cases appear:

- If inequality (4.12) is false, then the model always oscillates near the fixed point, for any subthreshold input current I.

- If inequality (4.12) is true, then the model oscillates only when $I > I_-$.

We call the occurrence of oscillations the *resonator* regime and their absence the *integrator* regime (see 4.2.4). The model is called a resonator when it is always (for all I) or almost always (for $I < I_+$) in the resonator regime, i.e., when inequality (4.12) is false; it is called an integrator when it never oscillates, i.e., when $\tau_m > \tau_w$ and inequality (4.12) is true; it is said to be in a mixed mode when it oscillates only above some value I_- (see Fig. 4.3).

Frequency of oscillations in the AdExp model

When the model oscillates, the frequency of the oscillations is:

$$F = \frac{\omega}{2\pi} = \frac{2b}{\pi g_L \tau_w} - \frac{2}{\pi \tau_m} \left(e^{\frac{V_- - V_T}{\Delta_T}} - 1 + \frac{\tau_m}{\tau_w} \right)^2, \tag{4.16}$$

which can be approximated far from threshold ($V_- \ll V_T$) as follows:

$$F = \frac{\omega}{2\pi} \approx \frac{2b}{\pi g_L \tau_w} - \frac{2}{\pi \tau_m} \left(1 - \frac{\tau_m}{\tau_w} \right)^2. \tag{4.17}$$

4.2.4 Input integration

The way the model integrates its inputs derives from the results above.

Resonator vs. integrator

On the temporal axis, the integration mode can be defined locally (for a small input $I(t)$) as

$$V(t) = V_0 + (K \star I)(t)$$

where the kernel K is the linear impulse response of the model around V_0, and $K \star I$ is a convolution. This impulse response is determined by the eigenvalues of the stable fixed point. When these are complex, the kernel K oscillates (with an exponential decay), as discussed in section 4.2.3 (see Fig. 4.3C). In that case the model acts as a *resonator*: two inputs are most efficient when separated by the characteristic oscillation period of the model (given by eq. 4.16). The membrane time constant is $-1/\lambda$, where λ is the real part of the eigenvalues, that reads:

$$\tau = \frac{2}{a - F'(v_-)}.$$

Far from threshold ($v \ll -1$), this time constant tends to 0 when $F'_{-\infty} = -\infty$, else it tends to:

$$\tau \approx \frac{2}{a - F'_{-\infty}},$$

or, for the AdExp model in the case $V \ll V_T$:

$$\tau = 2\frac{\tau_m \tau_w}{\tau_m + \tau_w}$$

When the eigenvalues are real, the kernel K is a sum of two exponential functions, and the model acts as an integrator. In that case there are two time constants, given by the real part of the eigenvalues. It is interesting to note that there is a parameter region where both integration modes can exist, depending on the (stationary) input current I: oscillations arise only when the model is sufficiently depolarized ($I > I_-$).

Adaptation

There are two sorts of adaptation in the model: threshold adaptation and voltage adaptation. The former one comes from the orientation of the separatrix in the (V, w) plane, as we discussed in section 4.2.1. The latter one derives from the fact that in the integrator mode (no oscillation), the model kernel K is a sum of two exponential functions. If the slower one is negative, then the response to a step shows an overshoot (as in Fig. 4.4D for a negative current step), which is a form of adaptation (the voltage response is initially strong, then decays). That overshoot in the AdExp model can be seen when there is no oscillation and $\tau_m < \tau_w$ (see section 4.3), i.e., in the *mixed mode* shown in pink in Fig. 4.3, when the input current is low ($I < I_-$).

4.2.5 The attraction basin of the stable fixed point

Limit cycle

The existence of a repulsive limit cycle arises for class B parameters from the Andronov-Hopf bifurcation. The saddle-node and Andronov-Hopf bifurcations collide via a Bogdanov-Takens bifurcation. In the neighborhood of this bifurcation, the family of limit cycles disappears via a saddle-homoclinic bifurcation. The normal form of the Bogdanov-Takens bifurcation gives us a local approximation of this saddle-homoclinic bifurcation curve around the point in parameter space given by (4.18) (see (113)), and the full saddle-homoclinic curve can be computed numerically using a continuation algorithm. The current I above which a limit cycle exists is locally approximated at the second order around the Bogdanov-Takens point $b = a$, $I = I_{BT} \stackrel{\text{def}}{=} -m(a)$ by the following expression:

$$I_{\text{cycle}} = I_{BT} - \frac{12}{25}\frac{(b-a)^2}{a\,F''(v^*(a))} + o\left((b-a)^2\right), \tag{4.18}$$

for $b > a$, which has the expression for the AdExp model:

$$I_{\text{cycle}} = I_{BT} - \frac{12}{25}\frac{\Delta_T \tau_w^2}{C(\tau_m + \tau_w)}(b - \frac{C}{\tau_w})^2 + o(b_1^2) \tag{4.19}$$

for $b > \frac{C}{\tau_w}$, where I_{BT} is the rheobase current at the Bogdanov-Takens bifurcation:

$$I_{BT} = (g_L + \frac{C}{\tau_w})\left[V_T - E_L - \Delta_T + \Delta_T \log\left(1 + \frac{C}{g_L \tau_w}\right)\right]$$

Below the threshold current I_{cycle}, there is no limit cycle (see next section). Above the I_{cycle}, there is a family of limit cycles, which are repulsive in the case of the AdExp model or the quadratic adaptive model, and that depend on the location of the parameters with respect to the Bautin bifurcation in the cases where it exists, circling anti-clockwise around the stable fixed point (see Fig. 4.3B and 4.4A); the saddle fixed point is outside that cycle. Interestingly, it appears that one can exit the attraction basin of the stable fixed point (and thus generate a spike) not only by increasing V, but also by decreasing V or w (or increasing w). This phenomenon is sometimes called *rebound*, and we discuss it further in section 4.2.6.

Separatrix

Some information about the stable manifold of the saddle fixed point can be obtained from the nullclines (when these intersect). The nullclines cut the plane in 5 connected zones, which we call North, South, West, East and Center, as shown in figure 4.1. The stable manifold consists in two trajectories which converge to the saddle fixed point. Near the saddle point, these two trajectories must lie in the North and South zone, or in the Center and East zones.

First we remark that all the trajectories starting from the East zone must spike. Indeed, in that region, V increases and w decreases, until it crosses the w-nullcline horizontally and enters the South zone. From
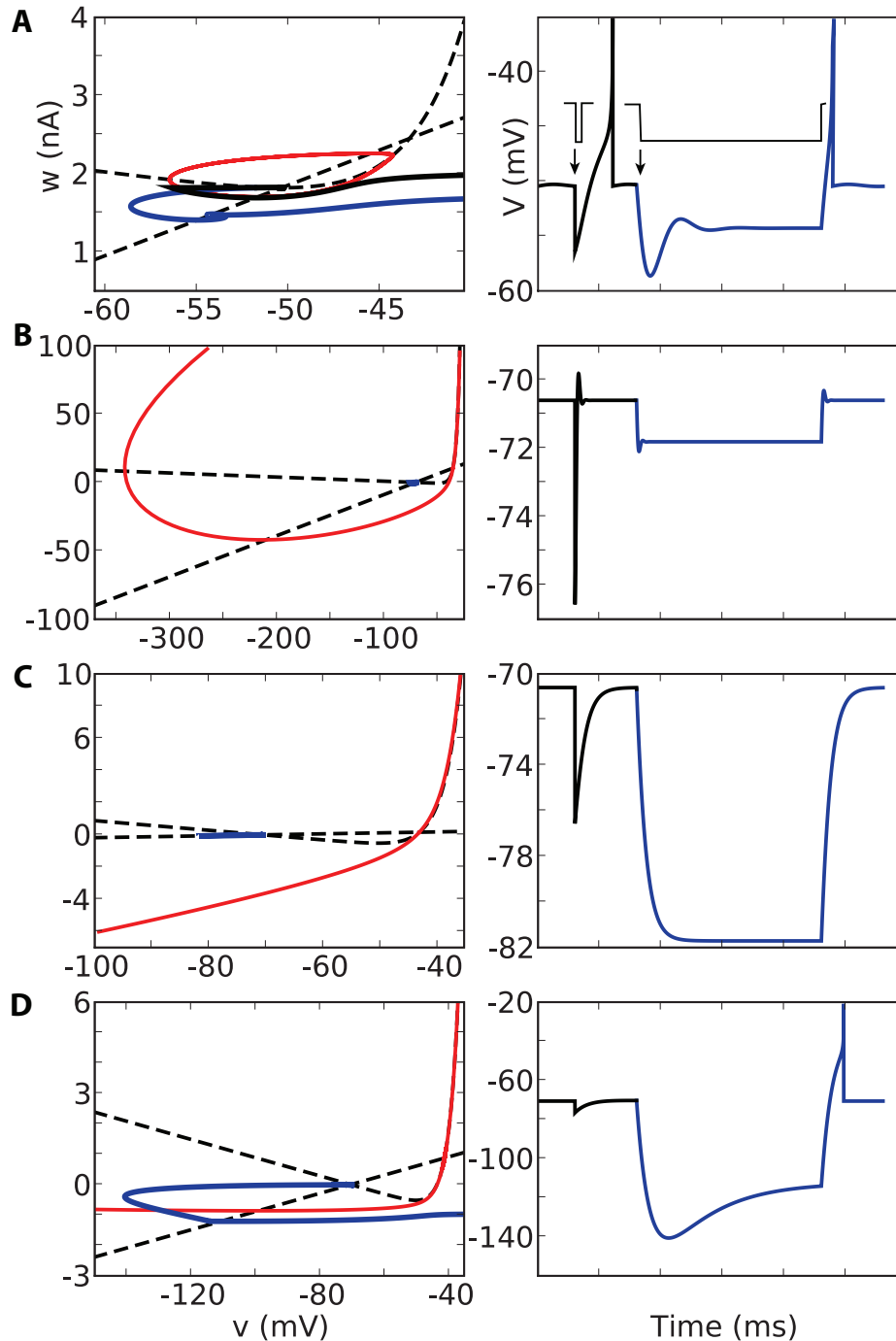
Figure 4.4. The attraction basin of the stable fixed point and rebound properties. Left column: the dashed lines represent the nullclines, each panel corresponds to a different set of parameter values; the red line delimits the attraction basin of the stable fixed point; the black line is the trajectory of the model in response to a short negative current pulse, while the blue line is the trajectory in response to a long negative current step. Right column: voltage response of the model to the a short pulse (black) and to a long step (blue). A. Class B resonator ($a = 3g_L$, $\tau_w = 2\tau_m$) close to the rheobase current. A repulsive limit cycle appears. Trajectories can escape the attraction basin and spike with fast or slow hyperpolarization. B. Class A resonator ($a = 10g_L$, $\tau_m = 12\tau_w$). The separatrix crosses both nullclines (for both branches, V and w go to $+\infty$). In theory trajectories can escape the attraction basin with hyperpolarization, but one would need to reach unrealistically low voltages (< -200 mV). C. Integrator ($a = .2g_L, \tau_m = 3\tau_w$). The separatrix does not cross the nullclines. No rebound is possible. D. Class B mixed mode ($a = g_L$, $\tau_w = 10\tau_m$). The separatrix crosses the w-nullcline. Rebound is possible with long hyperpolarization (short hyperpolarization can also induce rebounds, but with unrealistically low voltages).

that point, V keeps on increasing and w increases, which implies that the trajectory can only remain in the South zone or enter the East zone. However, the direction of the vector fields along the border does not allow crossing from South to East. Therefore, the trajectory will remain in the South zone and will spike. It follows that no part of the stable manifold can be in the East zone. Therefore it has to be locally in the North and South zones. By following the manifold from the saddle point to the North, we can see that V and w increase and, since the manifold cannot enter the East zone, it remains in the North zone and goes to infinity. In practice, it is in fact very close (but slightly to the left) of the V-nullcline, as shown in Fig. 4.4.

By following the manifold from the saddle point to the South, we can see that it has the same orientation as in the North zone, as long as it remains in the South zone. It may however cross the w-nullcline (Fig. 4.4D), and possibly the V-nullcline again (Fig. 4.4B).

For class A regime, or class B when $I < I_{\text{cycle}}$, there is no limit cycle. In that case the stable manifold of the saddle fixed point is an unbounded separatrix, i.e., it delimits the attraction basin of the stable fixed point. From the position of the nullclines, it appears that the stable manifold must cross the saddle fixed point from above both nullclines (North) to below both nullclines (South). It follows that the side above the nullclines is the graph of an increasing function of V (see Fig. 4.4). As for the other part of the manifold, several cases can occur: it may cross the w-nullcline, both nullclines or none. We can show that if condition (4.11) is false, then both nullclines are crossed, and if $\tau_m < \tau_w$, then at least the w-nullcline is crossed. These conditions cover all parameter regions except the zone where the model is always an integrator (no oscillations); in particular, it includes class B parameters. The position of the separatrix has important implications for the rebound property (section 4.2.6).

To understand whether the stable manifold can cross the w-nullcline and possibly the V-nullcline, we study the asymptotic behavior of the solutions when $t \to -\infty$. The idea is the following: if the manifold goes to $-\infty$ (for V), then the derivative of the nonlinear term vanishes tends to its limit $F'_{-\infty}$ which can either be finite, or $-\infty$. In the following we shall assume that the manifold does not cross the V-nullcline. In that case, the voltage $V(t)$ of the manifold, seen as a solution of the system, goes to $-\infty$ as $t \to -\infty$, and we will look for possible contradictions.

If we have $F'_{-\infty} = -\infty$, the trajectories are asymptotically horizontal and hence will necessarily cross the w-nullcline, but not necessarily the v-nullcline. In the case where $F'_{-\infty} > -\infty$, the approximated dynamics can be solved analytically. Asymptotically, the differential equations satisfied by a given solution (v, w) of the rescaled model can be approximated by:

$$\begin{cases} \dot{v} & = F'_{-\infty} v - w + I \\ \dot{w} & = a(bv - w) \end{cases} \tag{4.20}$$

When $t \to -\infty$, the solutions of the linear system either spiral around the fixed point (complex eigenvalues) or align asymptotically to the direction of eigenvector associated to the smallest negative eigenvalue of the matrix L governing the dynamics of the linear system (4.20):

$$L = \begin{pmatrix} F'_{-\infty} & -1 \\ ab & -a \end{pmatrix}$$

If the eigenvalues of this matrix are complex, i.e., when $b > \frac{(a + F'_{-\infty})^2}{4a}$, then the solutions spiral around the fixed point. Therefore the trajectories cross the V-nullcline, which contradicts our initial hypothesis. Thus when $b > \frac{(a + F'_{-\infty})^2}{4a}$ (resonator regime), the stable manifold crosses both nullclines.

If the eigenvalues are real, the trajectories of the linear system align asymptotically to the direction of the lower eigenvalue

$$\lambda_- = -\frac{1}{2} \left(a - F'_{-\infty} + \sqrt{(F'_{-\infty} + a)^2 - 4ab} \right)$$

This eigenvalue is always strictly negative hence solutions will diverge when $t \to -\infty$. The eigenvector associated with this eigenvalue is:

$$\begin{pmatrix} \frac{2}{a + F'_{-\infty} + \sqrt{(F'_{-\infty} + a)^2 - 4ab}} \\ 1 \end{pmatrix}$$

The slope of that eigenvector is always inferior to $F'_{-\infty}$, so that (linearized) trajectories do not cross the V-nullcline. However they can cross the w-nullcline when the slope of the eigenvector is smaller than b, i.e.:

$$\frac{a + F'_{-\infty} + \sqrt{(F'_{-\infty} + a)^2 - 4ab}}{2} < b$$

and this condition is satisfied when $b > \frac{1}{2}(a + F'_{-\infty})$. Assuming $\bar{a} > 0$, the inequality is always true if $\bar{\tau}_w > -F'_{-\infty}$; when when $\bar{\tau}_w < -F'_{-\infty}$, the inequality is never true given that the eigenvalues are real ($b > \frac{(a + F'_{-\infty})^2}{4a}$).

In summary, the stable manifold crosses both nullclines when $b > \frac{1}{2}(a + F'_{-\infty})$(resonator regime), and it crosses at least the w-nullcline when $\bar{\tau}_w > -F'_{-\infty}$ or $F'_{-\infty} = -\infty$.

4.2.6 Rebound

The term *rebound* refers to the property that a spike can be triggered by hyperpolarizing the membrane. This can be done either by sending a short negative current pulse, which amounts to moving the state vector (V, w) horizontally to the left, or by slowly hyperpolarizing the membrane with a long negative current step (or ramp) and releasing it, which amounts to moving the state vector along the w-nullcline.

For class A parameters, there is no limit cycle and there is an unbounded separatrix. If $\tau_m < \tau_w$ or if condition (4.11) is false, then the separatrix crosses the w-nullcline. It follows that both types of rebounds are possible. Otherwise the model is in the integrator regime, and the the separatrix may not cross the w-nullcline. In that case it is only possible to trigger a spike by increasing the voltage: there is no rebound.

For class B parameters, there is either a repulsive limit cycle which circles the stable fixed point when the input current is close enough to the rheobase current ($I > I_{\text{cycle}}$), or the separatrix crosses both the w-nullcline and the v-nullcline. In both cases, it is possible to exit the attraction basin of the stable fixed point and thus trigger a spike by changing any variable in any direction. Therefore, both types of rebound are possible. Note that with short current pulses, a more negative voltage must be reached in order to trigger a spike.

4.2.7 After-potential

After a spike, the state vector resets to a certain point in the state space. The subsequent trajectory is determined by this initial state. We will discuss the spike sequences in more details in section 4.4, but here we simply note that if the state vector is reset above the V-nullcline, then the membrane potential V will first decrease then increase (broad after-potential, or after-potential hyperpolarization); if the state vector is reset below the V-nullcline, V will increase (sharp after-potential).

The depolarizing after potential (figure 2.5.(xvii).) is linked with the position of the reset in the oscillatory case. In that case, if the neuron elicits a spike and is reset in the attraction basin of the stable fixed point, then the return to equilibrium will present oscillations around the fixed point. If the reset occurs on a point of a converging trajectory for which the voltage is increasing, the return to equilibrium will be characterized by a depolarizing afterpotential, i.e. the voltage will increase before returning to equilibrium.

4.3 OVERSHOOT

As discussed in section 4.2.4, the response of the neuron to a current step can present an overshoot when the coefficient of the slower exponential term is negative. In this section we show that in the low-voltage approximation ($V \ll V_T$), there is an overshoot if and only if $\tau_m < \tau_w$ and there is no oscillation, thus, in the mixed mode regime (Fig. 4.3).

Indeed, in the low voltage approximation, the dynamics is linear and is governed by the operator:

$$L = \begin{pmatrix} -1 & -1 \\ \frac{\bar{a}}{\bar{\tau}_w} & -\frac{1}{\bar{\tau}_w} \end{pmatrix}$$

which can be diagonalized. The overshoot appears only when the eigenvalues are real. In this case, the voltage response to a short pulse (Dirac) is a sum of two exponential functions $v(t) = \alpha e^{-t/\tau_1} + \beta exp^{-t/\tau_2}$ (we set the resting potential to 0) where $\frac{-1}{\tau_1}$ and $\frac{-1}{\tau_2}$ are the two real eigenvalues of L. The coefficient of the slower exponential term is

$$\frac{\varepsilon}{2\delta}(\sqrt{\delta}(1 - \bar{\tau}_w) + \delta)$$

with $\delta = (1 - \bar{\tau}_w)^2 - 4\bar{a}\bar{\tau}_w$. We now write the negativity condition of this coefficient:

$$\sqrt{\delta}(1 - \bar{\tau}_w) + \delta < 0 \Leftrightarrow 1 - \bar{\tau}_w < -\sqrt{\delta}$$

A necessary condition for this inequality to be satisfied is $\bar{\tau}_w > 1$. In this case, the condition reads:

$$(1 - \bar{\tau}_w)^2 > \delta = (1 - \bar{\tau}_w)^2 - 4\bar{a}\bar{\tau}_w$$
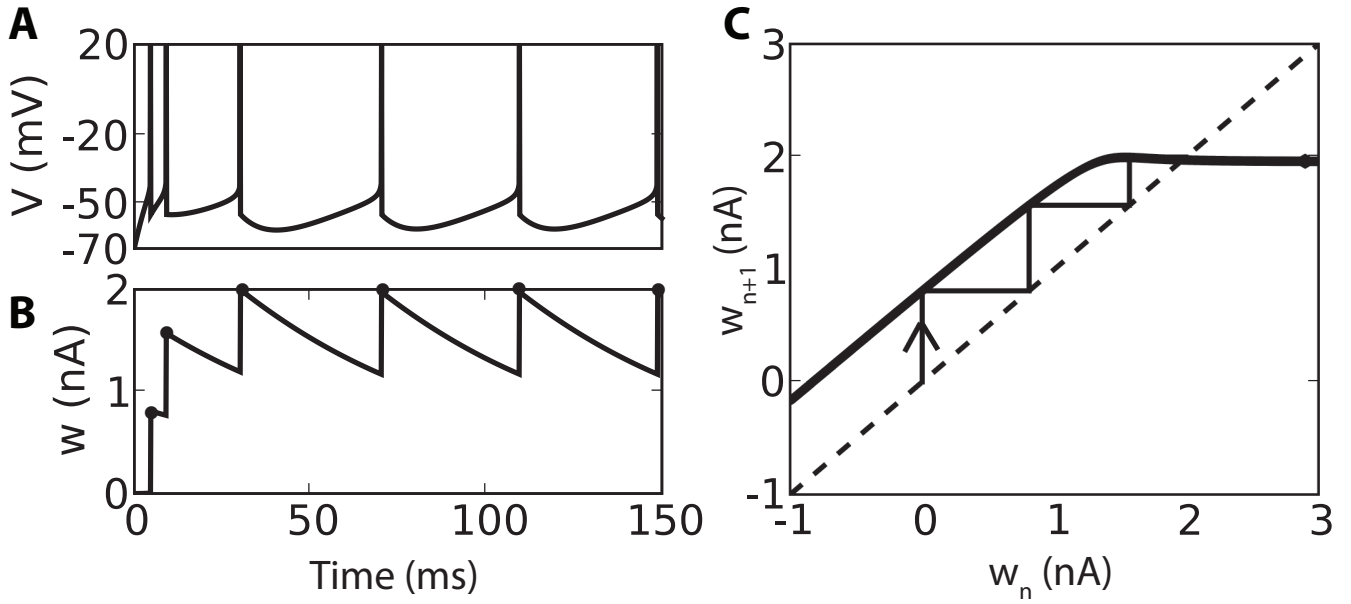
Figure 4.5. The adaptation map. A, B. Response of a class A model to a suprathreshold constant input (A: membrane potential V; B: adaptation variable w). The value of w after each spike defines a sequence (w_n). C. The adaptation map Φ maps the value of the adaptation variable from one spike to the next. The sequence (w_n) is the orbit of w_0 under Φ.

which is always true since $\bar{a}\bar{\tau}_w > 0$. Hence the overshoot appears in the low voltage approximation (far from threshold) when $\bar{\tau}_w > 1$, i.e., when $\tau_m < \tau_w$.

4.4   SPIKE PATTERNS

In the previous section, we analyzed the subthreshold dynamics of the model and found a rich structure, with the two parameters b and a, i.e. b/g_L and τ_m/τ_w for the AdExp model, controlling excitability, oscillations and rebound properties. Here we turn to the patterns of spikes, such as regular spiking, tonic/phasic bursting or irregular spiking, and explain them in terms of dynamics. Compared to the previous section, two additional parameters play an important role: the reset value V_r and the spike-triggered adaptation parameter d.

To study the spike sequences, use the Poincaré map (or adaptation map) introduced in chapter 3 which transforms the continuous time dynamics of the system into the discrete time dynamics of that map.

4.4.1   The adaptation map

In this section we recall the definition of this map and present some of its main features in the specific case of the AdExp model. v

We recall that after a spike emission, the potential V is always reset to the same value V_r, therefore the trajectory is entirely determined by the value of the adaptation variable w at spike time: the sequence of values (w_n), $w_n = t_n$ (t_n = time of spike number n) uniquely determines the trajectory after the first spike. The adaptation function Φ mapping w_n to w_{n+1} introduced in chapter 3 will therefore be used to characterize the spikes. We define again $\mathscr{D}$ as the domain of the adaptation variable w such that the solution of (4.1) with initial condition (V_r, w) spikes (blows up in finite time). Then the adaptation map Φ is

$$\Phi : \begin{cases} \mathscr{D} \mapsto \mathbb{R} \\ w_0 \mapsto w_\infty + d \end{cases} \tag{4.21}$$

where w_∞ is the value of w at divergence time (spike time) for the trajectory starting from (V_r, w_0), as illustrated in Fig. 4.5. The sequence (w_n) is the orbit of w_0 under Φ, as shown in Fig. 4.5C. Note that this sequence may be finite if for some n, $w_n \notin \mathscr{D}$. The property that the sequence is infinite (resp. finite) is called *tonic spiking* (resp. *phasic spiking*). The spike patterns are determined by the dynamical properties of Φ (fixed points, periodic orbits, etc.), as we show in next section. First, we examine the spiking domain $\mathscr{D}$.
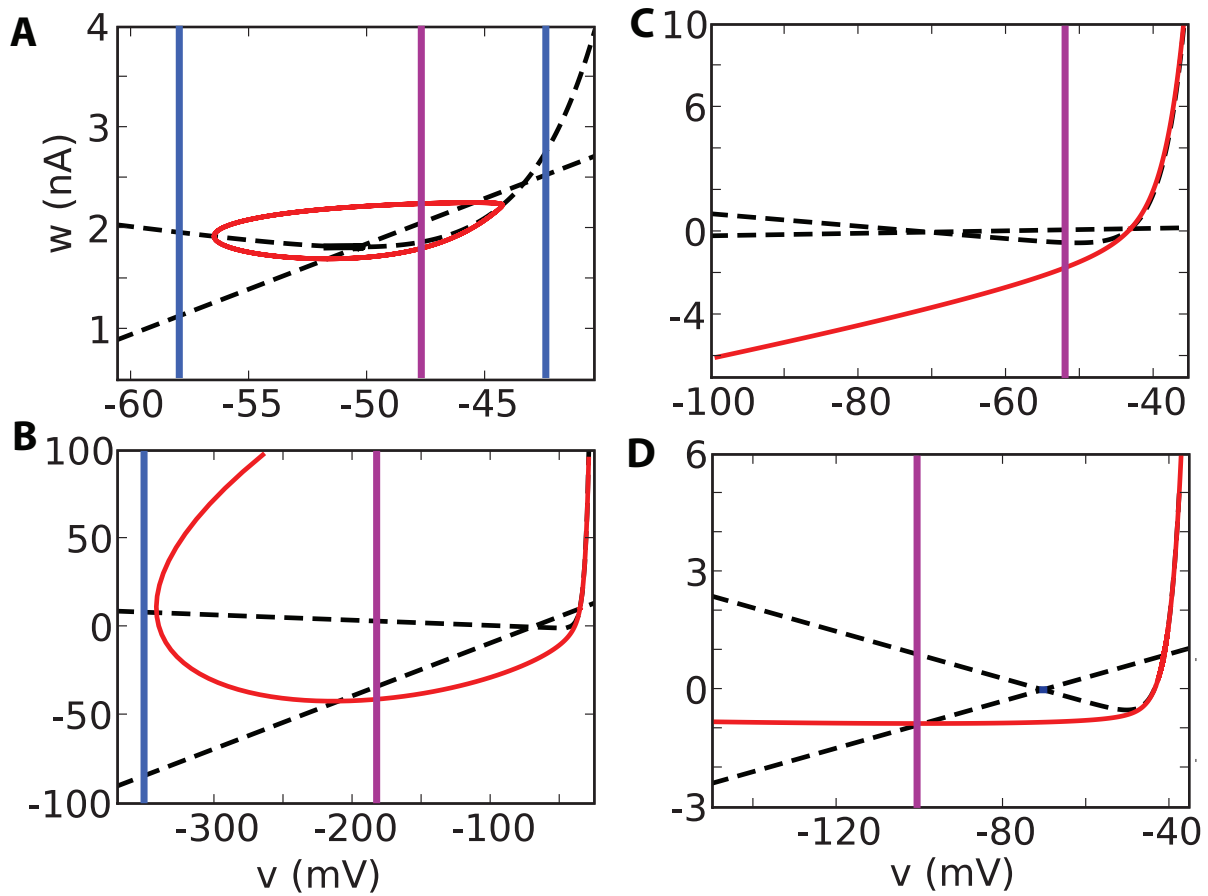
Figure 4.6. The spiking domain $\mathscr{D}$ for the same cases as in Fig. 4.4, when the nullclines (dashed lines) intersect. The attraction basin of the stable fixed point is bounded by the red curve. The blue and purple vertical lines indicate the reset line $V = V_r$. When that line is outside the attraction basin (blue), then $\mathscr{D} = \mathbb{R}$ and the model is bistable (tonic/resting). When the line intersects the attraction basin (purple), then $\mathscr{D}$ is an interval or the union of two intervals. In that case, the model is generally phasic (C,D) but may be bistable (A,B). In practice, with realistic values of d (spike-triggered adaptation), bistability essentially occurs when there is a limit cycle (A).

When there is no stable fixed point, i.e., when I is above the rheobase current (section 4.2.1), either I_{rh}^A or I_{rh}^B depending on the excitability type, then any trajectory spikes, except that starting at a countable number of points in the case $I_{\text{rh}}^B < I < I_{\text{rh}}^A$: the unstable fixed points or the intersections of the line $V = V_r$ with the stable manifold of the saddle fixed point.($\mathscr{D} = \mathbb{R} \setminus \{\text{these points}\}$. When there is a stable fixed point, all trajectories starting inside the attraction basin of that fixed point will not spike. The spiking domain $\mathscr{D}$ is then the complementary of the intersection of the reset line $V = V_r$ with the attraction basin of the stable fixed point (up to a projection onto the w axis), as shown in Fig. 4.6. We previously found (4.2.5) that the attraction basin of the stable fixed point is either a limit cycle or the stable manifold of the saddle fixed point. In the latter case, it may have a minimum voltage (resonator) or not (integrator or mixed). Fig. 4.6 shows how these different cases determine the spiking domain $\mathscr{D}$. We summarize these findings below, and describe the adaptation map Φ.

We first define two special values w^* and w^{**} as follows: the reset line $V = V_r$ intersects the V-nullcline and w-nullcline at the points (V_r, w^*) and (V_r, w^{**}), respectively, where

$$\begin{cases} w^* &= -g_L(V_r - E_L) + g_L \Delta_T \exp\left(\frac{V_r - V_T}{\Delta_T}\right) + I \\ w^{**} &= b(V_r - E_L) \end{cases}$$

Nearby spiking trajectories starting on the reset line $V = V_r$ above w^* (i.e., above the V-nullcline) may spike only after half a turn (since V initially decreases), or possibly an odd number of half-turns, which implies that the vertical order of the trajectories is reversed at spike time: Φ is locally decreasing above w^*. Spiking trajectories starting below w^* spike either directly or after an even number of half-turns, so that Φ is locally increasing below w^*. It follows that the sequences (w_n) are bounded.

We now describe the map Φ and the spiking domain $\mathscr{D}$ for the two excitability types, depending on the input current I.

1. Class A:

   (a) (subthreshold) if $I < I_{rh}^A$, then there is a stable fixed point and no limit cycle (see section 4.2.5). If the separatrix has no lower bound (typically: integrator or mixed regime), then the domain $\mathscr{D}$ is an interval $(-\infty, w_{\max})$ where $w_{\max}$ is the value of the adaptation variable on the separatrix for $V = V_r$. The map Φ is continuous on that set. We note that if $V_- < V_r < V_+$, then there can only be phasing spiking: indeed, $w_{n+1} > w_n + b$ for all n, therefore at some point the orbit exits $\mathscr{D}$.
   When the separatrix has a lower voltage bound $V_{\min}$ (typically: resonator), then there are two cases. If $V_r < V_{\min}$, then $\mathscr{D} = \mathbb{R}$ and Φ has the same properties as in case 1b. If $V_r > V_{\min}$, then $\mathscr{D} = (-\infty, w_{\min}) \cup (w_{\max}, +\infty)$. Besides, $\Phi((w_{\max}, +\infty)) \subset \Phi((-\infty, w_{\min}))$.

   (b) (suprathreshold) if $I > I_{rh}^A$, all trajectories spike. Therefore, $\mathscr{D} = \mathbb{R}$. The adaptation map is concave for $w < w^*$, regular, has a unique fixed point and an a horizontal asymptote when $w \to +\infty$.

2. Class B:

   (a) (subthreshold) if $I < I_{\text{cycle}}$, then there is a stable fixed point and no limit cycle, so that the situation is similar to case 1b.

   (b) (subthreshold) if $I_{\text{cycle}} < I < I_{rh}^B$, then there is a stable fixed point and a repulsive limit cycle bounding the attraction basin of the stable fixed point. Let $V_{\max}$ and $V_{\min}$ be the two extremal voltage values of the limit cycle. For $V_r < V_{\min}$ or $V_r > V_{\max}$, $\mathscr{D} = \mathbb{R}$ and Φ has the same properties as in case 1b.

   (c) (suprathreshold) if $I_{rh}^B < I < I_{SN}$, then there are two unstable fixed points and no limit cycle, hence all trajectories spike. Therefore $\mathscr{D} = \mathbb{R}$. When $V_r \in (V_-, V_+)$, the adaptation map is discontinuous at some point $w_{\max} < w^*$, and $\Phi(w_{\max}) < \Phi(w_{\max}^-)$ (when trajectories start circling around the fixed point). Thus Φ is locally but not globally increasing on $(-\infty, w^*)$. The map Φ also has a horizontal asymptote when $w \to +\infty$.

   (d) (suprathreshold) if $I > I_{SN}$, then $\mathscr{D} = \mathbb{R}$ and Φ has the same properties as in case 1b (class A).

Tonic spiking occurs for any initial w_0 if $\mathscr{D} = \mathbb{R}$ (in particular, in the suprathreshold regime). In other cases, spiking is generally phasic but there can be tonic spiking if the set $\bigcap_{n=0}^{\infty} \Phi^n(\mathscr{D})$ is not empty. When it occurs, the model is bistable.

The sequence $(w_n)_{n \geq 0}$ of values of the adaptation variable at spike times is the orbit of w_0 under Φ: $w_n = \Phi^n(w_0)$. Since there is a mapping from w to the interspike interval, the properties of Φ determine the spike patterns. In the following, we examine the relationship between the adaptation map Φ and the spike patterns.
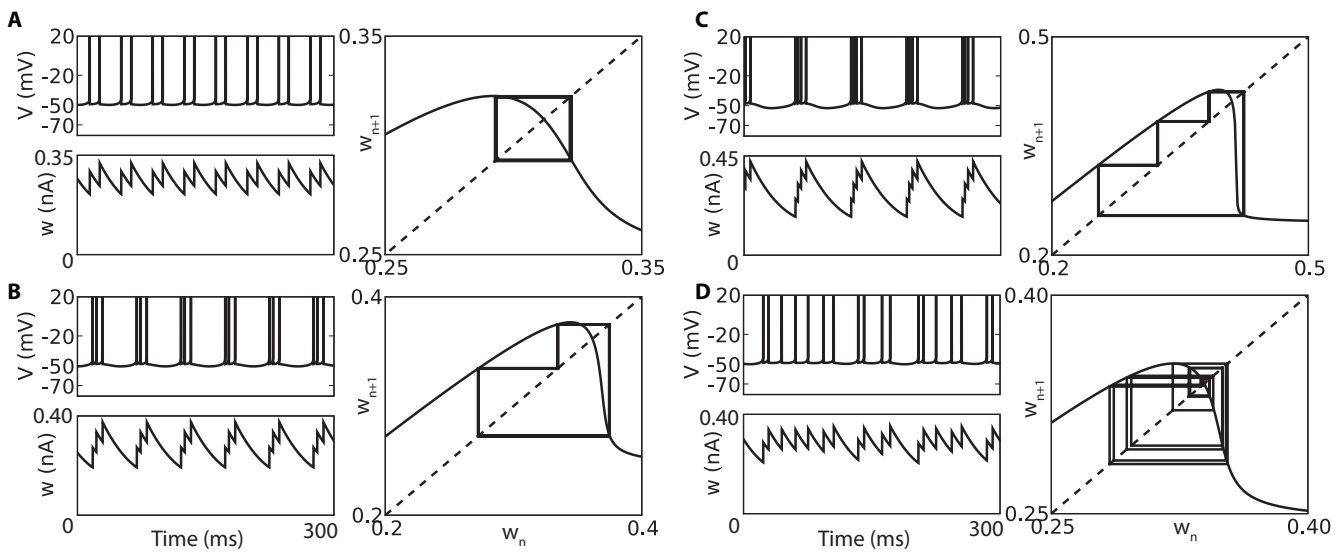
Figure 4.7. Bursting and chaos. Each panel shows a sample response (V and w) from the model, with different values of V_r (parameters: $C = 281$ pF, $g_L = 30$ nS, $E_L = -70.6$ mV, $V_T = -50.4$ mV, $\Delta_T = 2$ mV, $\tau_w = 40$ ms, $b = 4$ nS, $d = 0.08$ nA, $I = .8$ nA). A burst with n spikes corresponds to an n-periodic orbit under Φ. The last spike of each burst occurs in the decreasing part of Φ, inducing a slower trajectory. A. Bursting with 2 spikes ($V_r = -48.5$ mV). B. Bursting with 3 spikes ($V_r = -47.7$ mV). C. Bursting with 4 spikes ($V_r = -47.2$ mV). D. Chaotic spiking ($V_r = -48$ mV).

4.4.2 Tonic Spiking

Regular Spiking

Regular spiking means that interspike intervals are regular, possibly after a transient period of shorter intervals. For the adaptation variable, it means that the sequence (w_n) converges, i.e., Φ has a stable fixed point. This situation is shown in Fig. 4.5. For low initial values of the adaptation variable, Φ is increasing and $\Phi(w) > w$, so that the sequence (w_n) is increasing, implying that the duration of interspike intervals decreases (this implication is true for $w < w^*$, i.e., before the maximum of Φ).

The shape of after-potentials (broad or sharp) depends, as we previously saw, on whether (V_r, w) is above or below the V-nullcline, i.e., whether $w > w^*$ or $w < w^*$. Asymptotically, the condition for broad resets is thus $w_{\text{fp}} > w^*$, where w_{fp} is the fixed point of Φ. Given the properties of Φ, this means $\Phi(w^*) > w^*$. Since the parameter d (spike-triggered adaptation) shifts the curve of Φ vertically, there is a minimum d above which resets are (at least asymptotically) broad.

When Φ is continuous (cases 2d and 1b), it always has a fixed point (since $\Phi(w) > w + d$ for low w and Φ converges to a finite limit when $w \to +\infty$), but that fixed point may not be stable. That property depends on all parameter values; in particular, the fixed point is an attraction basin when d or I is large enough (for large d, the fixed point is on the plateau of Φ, which implies broad resets). If the fixed point is not stable, then the sequence (w_n) may converge to a periodic orbit or be irregular.

Bursting

A bursting response is a sequence of shortly spaced spikes, separated by longer intervals. For the adaptation variable w, it corresponds to a periodic orbit, where the period equals the number of spikes per burst. For the adaptation map, p-periodic orbits are associated with stable fixed points of Φ^p. This situation is illustrated in Fig. 4.7. Typically, bursting occurs for large reset values V_r: the first spike resets the trajectory to a high voltage value, which induces a fast spike, and the adaptation builds up after each spike, until the trajectory is reset above the V-nullcline (after the peak of Φ at w^*). At that point $dV/dt < 0$ and the trajectory must turn in phase space before it spikes, producing a long interspike interval. Thus, the number of spikes per burst increases when V_r increases (since w^* increases with V_r) and when d decreases. Thus the bifurcation diagram with respect to V_r (Fig. 4.8) shows a period adding structure. Interestingly, when zooming on a transition from n to $n+1$ spikes, a period doubling structure appears, revealing chaotic orbits.
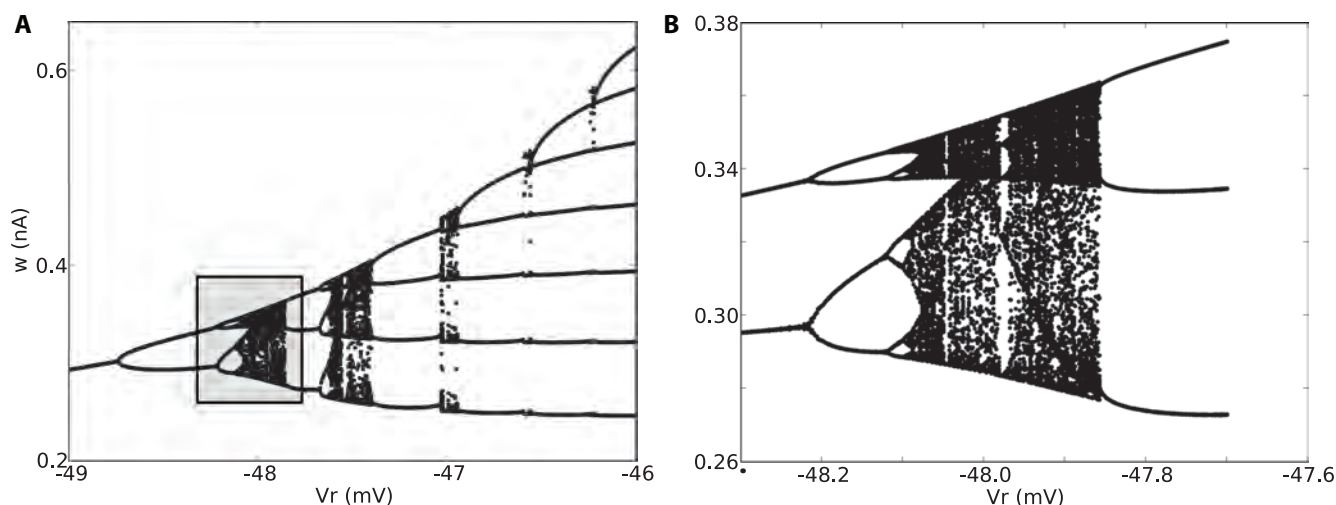
Figure 4.8. Bifurcation structure with increasing V_r (same parameters as in Fig. 4.7). A. Bifurcation diagram showing a period adding structure (orbits under the adaptation map Φ with varying values for V_r). Fixed points indicate regular spiking, periodic orbits indicate bursting, dense orbits indicate chaos. B. Zoom on the bifurcation diagram A (as indicated by the shaded box), showing a period doubling structure.

Chaotic spiking

The period doubling structure shown in Fig. 4.8B implies that orbits are chaotic for some parameter values. A sample response of the model for one of those values is shown in Fig. 4.7D. It results in irregular, unpredictable firing, in response to a constant input current.

4.4.3 Phasic spiking

Phasic spiking or (bursting) can occur in subthreshold regimes ($I < I_{\mathrm{rh}}^A$ for class A parameters, $I < I_{\mathrm{rh}}^B$ for class B), when there is a stable fixed point and $\mathscr{D} \neq \mathbb{R}$. In that case, the system needs to be destabilized (e.g. a short current pulse, which may be positive or negative, as explained section 4.2.6). The situation depends on the properties of the attraction basin of the stable fixed point, and can be understood from Fig. 4.6.

We can distinguish two cases:

1. If $\mathscr{D} = (-\infty, w_{\min})$ (C,D: integrator or mixed regime), then when $V_- < V_r < V_+$ there can only be phasic spiking, otherwise tonic spiking is possible. Indeed, if $V_- < V_r < V_+$, then the sequence (w_n) is such that $w_{n+1} > w_n + d$, so that it must exit $\mathscr{D}$ in finite time.

2. If $\mathscr{D} = (-\infty, w_{\min}) \cup (w_{\max}, +\infty)$ (A,B: resonator or mixed regime), then there can only be phasic spiking $\Phi(w_{\min}) > w_{\max}$, otherwise tonic spiking is possible.

When tonic spiking (or bursting) is possible, then the model is bistable (it can be turned on or off with current pulses).

4.5 DISCUSSION

The adaptive exponential integrate-and-fire model (13) is able to reproduce many electrophysiological features seen in real neurons, with only two variables and four free parameters. Besides, its parameters have a direct physiological interpretation. In the framework of this model, we can define an *electrophysiological class* as a set of dynamical properties for different values of the input I (for given parameter values). In this chapter, we tried to provide a classification of the parameter space as complete as possible, which is summarized for subthreshold dynamics in Fig. 4.3. The subthreshold dynamics depends only on the ratio of time constants (τ_m/τ_w) and on the ratio of conductances (b/g_L), but is already non-trivial. The model can have excitability type I or II depending whether it leaves the resting state through a saddle-node or an Andronov-Hopf bifurcation. It may act as an oscillator or an integrator depending on the eigenvalues associated to the resting point. It may spike in response to hyperpolarizing currents (rebound), depending on the properties of the attraction basin of the stable fixed point, which is bounded by either a limit cycle or a separatrix.

The spiking dynamics is even more rich, as it also depends on the reset parameters d and V_r. We related the spike patterns with orbits under a discrete Poincaré map Φ, and found a rich bifurcation structure including even chaos. Regular spiking corresponds to a stable fixed point of Φ, bursting corresponds to periodic orbits under Φ and irregular spiking corresponds to chaotic orbits under Φ.

Most of the results shown in this chapter generalize to two-dimensional spiking models in which the first (membrane) equation is $dV/dt = F(V) + I - w$, where F is a smooth convex function whose derivative is negative at $-\infty$ and infinite at $+\infty$ (in particular, Izhikevich model and the quartic model have these properties). We are currently working on the mathematical proofs of these results in that more general setting and on a more complete picture of the spiking dynamics (116). This work will provide both a dynamical system understanding of the the spiking properties of the model and analytical methods to relate the parameter values with electrophysiological classes. Another interesting line of research is the investigation of the responses of such bidimensional models to time-varying inputs, as was done in (11) for one-dimensional integrate-and-fire models.

5

SENSITIVITY TO THE CUTOFF VALUE IN THE QUADRATIC ADAPTIVE INTEGRATE-AND-FIRE MODEL

OVERVIEW

As already discussed, the quadratic adaptive integrate-and-fire model (62; 64) is recognized as very interesting for its computational efficiency and its ability to reproduce many behaviors observed in cortical neurons. For this reason it is currently widely used, in particular for large scale simulations of neural networks. This model is part of the general class of models studied in chapter 2: it emulates the dynamics of the membrane potential of a neuron together with an adaptation variable. The subthreshold dynamics is governed by a two-parameter differential equation, and a spike is emitted when the membrane potential variable reaches a given cutoff value. Subsequently the membrane potential is reset, and the adaptation variable is added a fixed value called the spike-triggered adaptation parameter. We show in this chapter that when the system does not converge to a resting state, both variables of the subthreshold dynamical system blow up in finite time. The cutoff is therefore essential for the model to be well defined and simulated. The divergence of the adaptation variable makes the system very sensitive to the cutoff: changing this parameter dramatically changes the spike patterns produced. Furthermore from a computational viewpoint, the fact that the adaptation variable blows up and the very sharp slope it has when the spike is emitted implies that the time step of the numerical simulation needs to be very small (or adaptive) in order to catch an accurate value of the adaptation at the time of the spike. It is not the case for the similar quartic (114) and exponential (13) models whose adaptation variable does not blow up in finite time, and which are therefore very robust to changes in the cutoff value.

5.1 INTRODUCTION

During the past few years, in the neuro-computing community, the problem of finding a computationally simple and biologically realistic model of neuron has been widely studied, in order to be able to compare experimental recordings with numerical simulations of large-scale brain models. The key problem is to find a model of neuron realizing a compromise between its simulation efficiency and its ability to reproduce what is observed at the cell level, often considering in-vitro experiments (63; 77; 104). Among the variety of computational neuron models, nonlinear spiking models with adaptation have recently been studied by several authors (13; 63; 114) and seem to stand out. They are relatively simple, i.e. mathematically tractable, efficiently implemented, and able to reproduce a large number of electrophysiological signatures such as bursting or regular spiking. These models satisfy the equations:

$$\begin{cases} \frac{dv}{dt} &= F(v) - w + I \\ \frac{dw}{dt} &= a\,(b-w) \end{cases} \tag{5.1}$$

where a and b are non-negative parameters and $F(v)$ is a regular strictly convex function satisfying assumption:

Assumption 5.1.1. There exists $\varepsilon > 0$ and $\alpha > 0$ for which $F(v) \geq \alpha v^{1+\varepsilon}$ when $v \to \infty$ (we will say that F grows faster than $v^{1+\varepsilon}$ when $v \to \infty$).

A spike is emitted at the time t^* when the membrane potential v reaches a cutoff value θ. At this time, the membrane potential is reset to a constant value c and the adaptation variable is updated to $w(t^*) + d$ where $w(t^*)$ is the value of the adaptation variable at the time of the spike and $d > 0$ is the spike-triggered adaptation parameter.

For these models we prove in section 5.2 that the membrane potential blows up in finite time. Among these models, the *quadratic adaptive* model (63) corresponds to the case where $F(v) = v^2$, and has been recently used by Eugene Izhikevich and coworkers (66) in very large scale simulations of neural networks. The *adaptive exponential* model (13) corresponds to the case where $F(v) = e^v$, has the interest that its parameters can be related to electrophysiological quantities, and has been successfully fit to intracellular recordings of pyramidal cells (23; 69). The *quartic* model (114) corresponds to the case where $F(v) = v^4 + 2av$ and has the advantage to of being able to reproduce all the behaviors featured by the other two and also self-sustained subthreshold oscillations which are of particular interest to model certain nerve cells.

In these models, the reset mechanism makes critical the value of the adaptation variable at the time of the spike. Indeed, when a spike is emitted at time t^*, the new initial condition of the system (5.1) is $(c, w(t^*) + d)$. Therefore, this value governs the subsequent evolution of the membrane potential, and hence the spike pattern produced. For instance in (116; 117), the authors show that the sequence of reset locations after each spike time shapes the spiking signature of the neuron.

Hence characterizing the reset location of the adaptation variable is essential to characterize the spiking properties of these models. To this end, we precisely study in this chapter the orbits of equation (5.1) in the phase plane (v,w) in order to characterize the value of the adaptation variable at the time of the spike. We prove in section 5.2 that the adaptation variable diverges when $v \to \infty$ in the case of the quadratic model and converges in the cases of the exponential and of the quartic model, and study in section 5.3 the consequences of this fact on the spiking signatures and on numerical simulation methods.

5.2 ADAPTATION VARIABLE AT THE TIMES OF THE SPIKES

As we can see in equation (5.1), the greater the membrane potential the greater the derivative of the adaptation variable. When the membrane potential blows up, the adaptation variable may either remain bounded or blow up, depending on the shape of the divergence of v. When this divergence is not fast enough, the adaptation variable simultaneously blows up.

We prove here that for the models satisfying assumption 5.1.1 the membrane potential blows up in finite time. We also prove that for quadratic adaptive model[1] the adaptation variable blows up at the same time as a logarithmic function of v, whereas if there exists $\varepsilon > 0$ such that $F(v)$ grows faster than $v^{2+\varepsilon}$ when $v \to \infty$, then the adaptation variable remains bounded when $v \to \infty$.

In (114), we have seen that there exists possibly one stable fixed point for system 5.1, which corresponds to a resting state. In (117), we prove that all the orbits of the system that do not converge to this stable fixed

---

[1] We can prove more generally that when $F(v)/v^2$ tends to a finite constant (possibly 0), the adaptation variable will blow up when the membrane potential blows up

point will be trapped after a finite time in a zone fully included in the half space $\{w < bv\}$ called the *spiking zone*[2]. Denote t_0 a time such that the orbit is inside the spiking zone. In this zone, we have

$$\frac{\mathrm{d}v}{\mathrm{d}t} \geq F(v) - bv + I$$

It is simple to prove that the solution of the equation

$$\begin{cases} \frac{\mathrm{d}u}{\mathrm{d}t} = F(u) - bu + I \\ u(t_0) = v(t_0) \end{cases}$$

blows up in finite time under the assumption 5.1.1[3]. Using Gronwall's theorem (47) we conclude that $v(t) \geq u(t)$ and hence v blows up in finite time.

To prove the divergence of the adaptation variable when the membrane potential blows up in the case of the quartic model, we study the orbit of a solution $(v(t), w(t))$ of the differential system (5.1) such that the membrane potential blows up at time t^*, and characterize the behavior of $w(t)$ in function of $v(t)$. In the spiking zone, we have seen that $w(t) \leq bv(t)$ and therefore $F(v) - w + I \geq F(v) - bv + I$ which tends to infinity when v tends to infinity. Since $v(t)$ blows up there exists a time $t_1 \in [t_0, t^*]$ such that we will have $F(v(t)) - w(t) + I \geq k > 0$ for all $t \in [t_1, t^*]$. We denote $(v_1 := v(t_1), w_1 := w(t_1))$. After time t_1, because of this inequality, the trajectory in the phase plane can be written as the graph of a function $W(v)$ that satisfies the equation:

$$\begin{cases} \frac{\mathrm{d}W}{\mathrm{d}v} = \frac{a(b-W)}{F(v)-W+I} \\ W(v_1) = w_1 \end{cases} \tag{5.2}$$

(i.e. $w(t) = W(v(t))$ for $t \in [t_1, t^*]$). Since $w(t)$ is increasing for $t \in [t_1, t^*]$, we necessarily have:

$$\frac{\mathrm{d}W}{\mathrm{d}v} \geq \frac{a(b-W)}{F(v)-w_1+I} \tag{5.3}$$

Therefore Gronwall's theorem (47) ensures us that the solution of equation (5.2) will be lowerbounded for $v \geq v_1$ by the solution of the linear ordinary differential equation:

$$\begin{cases} \frac{\mathrm{d}z}{\mathrm{d}v} = \frac{a(b-z)}{F(v)-w_1+I} \\ z(v_1) = w_1 \end{cases} \tag{5.4}$$

that reads:

$$z(v) = \left(\int_{v_1}^{v} \frac{abu}{F(u)-w_1+I} e^{-g(u)} \, du + w_1 \right) e^{g(v)}$$

where $g(v) = -\int_{v_1}^{v} \frac{a\,du}{F(u)-w_1+I}$. Because of assumption 5.1.1, the integrand is integrable, and the function g has a finite limit $g(\infty)$ when $v \to \infty$. The exponential terms will hence converge when $v \to \infty$. But the integral involved in the particular solution diverges in the quadratic case[4], since the integrand is equivalent when $u \to \infty$ to

$$\frac{ab}{u} e^{-g(\infty)}$$

Hence the solution of the linear differential equation (5.4) tends to infinity when $v \to \infty$ faster than a logarithmic function of v, and so does $W(v)$, and hence $w(t)$ blows up at the time when $v(t)$ blows up.

Let us now upperbound the adaptation variable on the orbits of the system. Using the same notations, since $w_1 \leq w(t) \leq bv(t)$ for $t \in [t_1, t^*]$, we have:

$$\frac{\mathrm{d}W}{\mathrm{d}v} \leq \frac{a(bv-w_1)}{F(v)-bv+I} \tag{5.5}$$

and hence

$$W(v) \leq w_1 + \int_{v_1}^{v} \frac{a(bu-w_1)}{F(u)-bu+I} \, du$$

---

[2]In the case where the subthreshold system has no fixed point this property can be derived from the shape of the vector field in the phase plane, as well as in the case where the initial condition (v, w) is such that v is greater than the largest v-value of the fixed points (the biggest solution of $F(v) - bv + I = 0$) and $w \leq bv$: in this case the vector field on the line $w = bv$ implies that the trajectory keeps trapped in this zone. In the case where there exist fixed points, the proof is slightly more complex and involves the description of the stable manifold of the saddle fixed point.

[3]For the quadratic model we can get analytic expressions of the solutions involving the tangent function, and therefore can derive an upperbound of the explosion time.

[4]or when $F(v)$ grows slower than v^2,

In the case where $F(u) = u^2$ this integral is bounded by a logarithmic function of v and in the case where $F(u)$ grows faster than $u^{2+\varepsilon}$, this integral converges when $v \to \infty$. Furthermore, since W is an increasing upperbounded function, it converges when $v \to \infty$.

We therefore conclude that in the case of the quadratic adaptive model, the adaptation variable blows up at the explosion time of the membrane potential variable v and this divergence is logarithmic in v, and in the case of the quartic and exponential models, the adaptation variable converges. The value of the adaptation variable at the cutoff θ is simply given by $W(\theta)$, that depends on the parameters of the system and of the initial condition. In the case of the quadratic model it is an unbounded increasing function of θ, and in the quartic and exponential models, a converging function of θ.

5.3 CONSEQUENCES

The divergence of the adaptation variable at the times of the spikes significantly impacts the theoretical, qualitative and computational analysis of the model.

We have seen that changing the cutoff value resulted in changing the value of the adaptation variable at the times of the spikes. Let (v_0, w_0) be an initial condition for the system (5.1). If the neuron fires, its membrane potential will reach the cutoff value θ at a given time. Since the membrane potential blows up in finite time, the time of the first spike emitted will not be very sensitive to changes in the cutoff value provided it is high enough. But the after-spike reset location $(c, W(\theta) + d)$ will significantly change when varying θ. The whole subsequent evolution of the system is therefore affected, as soon as the second spike is emitted. Thus the spike pattern produced depends on the cutoff value.

In the case of the quartic and exponential models, the adaptation variable converges when the cutoff tends to infinity. Therefore, the model defined by (5.1) with an infinite cutoff value is mathematically well defined. In that case, a spike is emitted when the membrane potential blows up and subsequently we reset the membrane potential to a fixed value c and add to the value of adaptation variable at the explosion time the spike-triggered adaptation parameter. We call this system the *intrinsic* system. The behavior of the system and the spike patterns it produces can be mathematically studied (see (116; 117)). Interestingly, these intrinsic spike patterns undergo bifurcations with respect to the parameters of the model. When considering a finite cutoff, the model (or the numerical simulation) will approximate these intrinsic behaviors provided that the cutoff threshold is high enough. The sensitivity to the cutoff in these cases will hence be very limited except in very small regions of the parameter space around the bifurcations of the intrinsic system. Unfortunately, for the quadratic model, no intrinsic behavior can be defined because of the divergence of the adaptation variable: the behaviors it produces will depend on the choice of the threshold.

First of all, we have seen that the dependency of this reset location in the quadratic model is a logarithmic function of θ, which makes the variations of the reset value in function of the cutoff unbounded but quite slow. Small changes in the cutoff slightly impact the value of the reset adaptation variable. For instance if we consider the firing rate of a neuron in the case where the system has no fixed point, increasing the cutoff value results in the case of the quadratic model in a a slow continuous decrease of the firing rate of the neuron that tends to zero as the cutoff increases, whereas the firing rate converges for the quartic model to the related intrinsic firing rate (see figure 5.1.(g)).

When considering the spike patterns produced, the effects of changes in the cutoff value for the quadratic model are much more dramatic. Indeed, the sequence of adaptation values at the times of spikes shapes the spike pattern produced: for instance, regular spiking corresponds to the convergence of this sequence, and bursting to cycles in this sequence. These properties are very sensitive to changes in the parameters of the model: bifurcations between different spike patterns, and even chaos appear when the model's parameters vary (see (96; 116; 117)). In the case of the quadratic model, we have seen that these adaptation values strongly depend on the cutoff. Therefore, since the dependency on the cutoff is unbounded, from a given initial condition and for fixed values of the parameters, increasing the cutoff may result in crossing many bifurcation lines, and hence in producing many different behaviors. We present in figure 5.1 a graph showing that bifurcations and chaos occur with respect to the cutoff value, in the usual range of simulation parameters. For instance, a period doubling bifurcation appears when varying the cutoff value (in figure 5.1(e) we give a graph of the stationary reset values in function of the threshold θ), that results in abruptly switching from a regular spiking behavior to a bursting behavior (figures 5.1(a) and 5.1(b)). More complex bifurcation structures involving chaotic patterns also appear, and in this case, infinitesimal changes in the cutoff value result in dramatic changes in the behavior. This raises the question of the meaning of the cutoff value in these ranges of parameters (see figure 5.1(f)). Changing the cutoff in that case makes the system switch between chaotic spiking, bursts with 8, 4 and eventually 2 spikes, for the cutoff values considered. And this behavior will not be observed only for very particular values of the parameters of the system. Depending on the extension of the interval where the cutoff value varies, quite a large set of parameters will present

bifurcations in the nature of the emitted spike train.

Because of this sensitivity, the cutoff value and the different parameters of the model have to be very carefully evaluated in order to quantitatively fit datasets. In this context the meaning of the threshold and therefore the problem of its accurate evaluation has to be specifically addressed in the case of the quadratic model, since it has no clear biophysical interpretation.

Eventually, from the numerical viewpoint, the unboundedness of the adaptation variable and of its time derivative at the explosion times of the membrane potential makes the accurate computation of this value very difficult. In particular, the time step necessary to accurately estimate this value has to be very small (or to be adaptive as a function of the value of the membrane potential variable) in order to obtain the right spike pattern. These remarks relativize the statement that this model can be efficiently simulated since very accurate methods have to be implemented in order to correctly evaluate the adaptation variable at the time of the spike.

These remarks do not apply for the models where the adaptation variable converges at the times of the spikes. In these cases, the system has intrinsic properties that make the times of the spike and the adaptation variable at these times robust to the choice of the cutoff value provided it is big enough and the numerical simulations less sensitive to the choice of the time step.

CONCLUSION

In this chapter we proved that the adaptation variable of the adaptive quadratic model blew up at the times of the spikes whereas it converged for the quartic and the adaptive exponential models. This property has some important implications that are discussed in the chapter. From a theoretical point of view, we showed that the nature of the spike patterns produced undergoes bifurcations with respect to the cutoff value, and this made the system very sensitive to this parameter: small changes in the value of this parameter can deeply affect the nature of the spiking pattern. From a quantitative viewpoint, it raises the question of how to evaluate this threshold in order to fit datasets, and from a numerical viewpoint, it has implications on the efficiency of the simulation algorithms to use. The convergence of this value for models having a faster blow up at the times of the spike, such as the quartic or the exponential adaptive models, implies that the system presents intrinsic spiking properties which can be mathematically studied, efficiently simulated and robust to changes in the cutoff value.
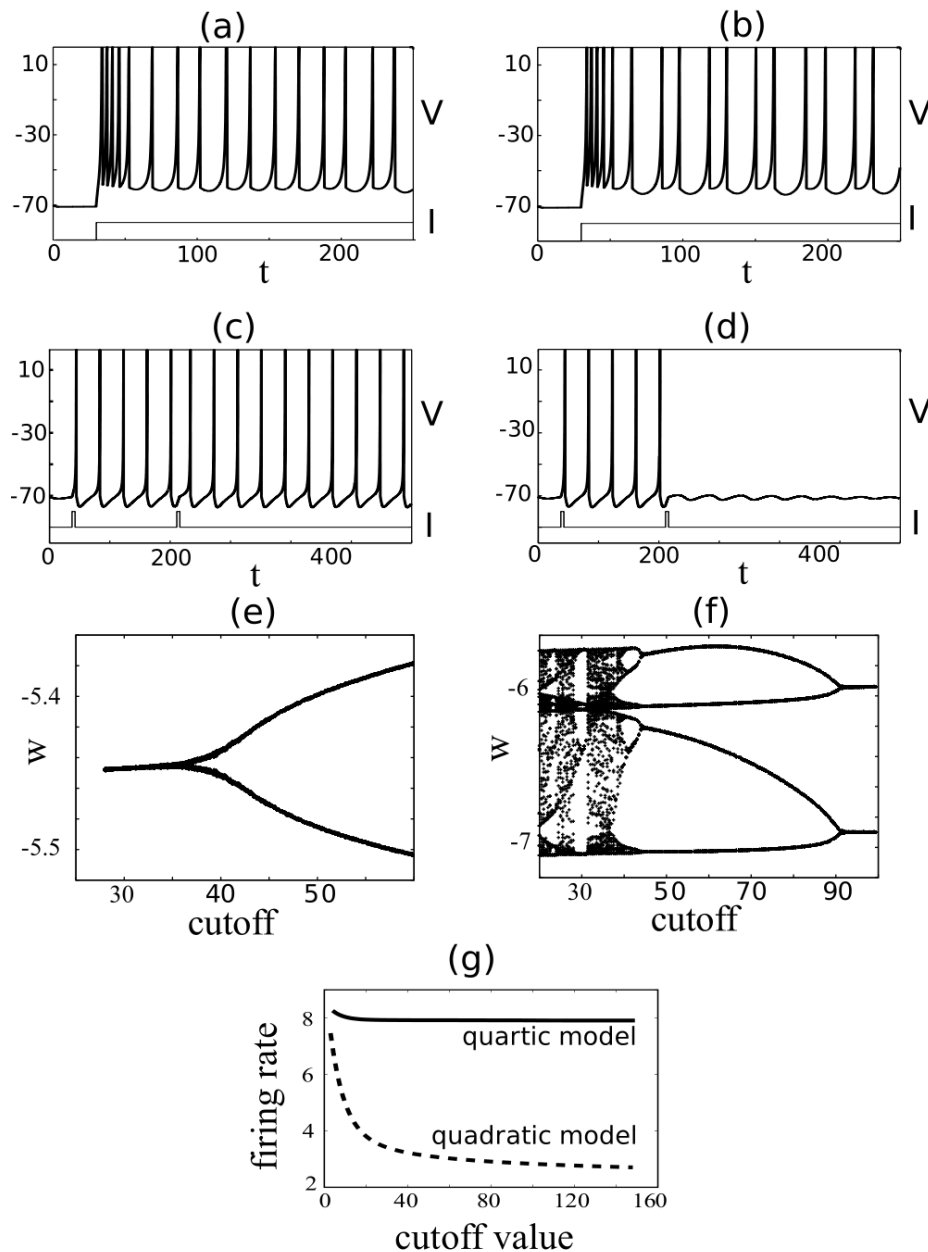
Figure 5.1. Sensitivity of the spike patterns with respect to the cutoff value for the quadratic model, for different set of parameters. Parameters used: $(A) = \{a = 0.02; b = 0.19; c = -60; d = 1.419\}$; $(B) = \{a = 0.1; b = 0.26; c = -60; d = 0; \}$, $(C) = \{a = 0.02, b = 0.19, c = -57.7, d = 1.15\}$. For figure (a) and (b) the parameters used are (A) with cutoff of 36 and 38 respectively: a small increase of the cutoff results in a sharp transition from spiking to bursting, linked with a period doubling bifurcation for the adaptation value at the reset represented in figure (e). Figures (c) and (d) corresponds to the parameters (B) with cutoffs value 32.9 and 33 respectively. Changing the cutoff results in two very different global behaviors. Fig. (e) and (f) represent the stationary sequence of reset values as functions of the threshold θ. Figure (f) corresponds to the set of parameters (C) for cutoff values ranging from 20 to 100: an intricate bifurcation structure appears. Figure (g) shows the convergence of the firing rate to the intrinsic firing rate in the case of the quartic model, while the firing rate of the quadratic model regularly decreases to 0.

CAUCHY PROBLEM

The Cauchy problem consists in proving that there exists a unique solution to the problem (3.1) and (3.2) defined for all $t \in \mathbb{R}$ for a given initial condition (v_0, w_0) at time t_0. It was adressed by Romain Brette in (12) in the case of spiking models defined by a one dimensional ODE with a finite spiking threshold and a reset condition. He found that the reset introduced a countable and ordered set of backward solutions for a given initial condition, and this that this structure of solutions had important implications in terms of neural coding.

The case of the system given by (3.1) and (3.2) is slightly more complex, but can be treated in the same fashion as done in (12). We have seen in section 3.2.6 that there exists a unique solution to the forward problem. Therefore in this appendix we are interested only in the backward solutions. The backward problem of equations (3.1) and (3.2) with initial conditions (v_0, w_0) at time t_0 corresponds to the forward solutions $v_b(t) = v(t_0 - t)$ and $w_b(t) = w(t_0 - t)$. of the system:

$$\begin{cases} \frac{\mathrm{d}v_b}{\mathrm{d}t} = -F(v) + w - I \\ \frac{\mathrm{d}w_b}{\mathrm{d}t} = -a(bv - w) \\ v_b(0) = v_0 \\ w_b(0) = w_0 \end{cases} \tag{A.1}$$

The nullclines for this system are the same as the nullclines of the forward problem, but the direction of the vector field changes. A new issue appears here: the membrane potential can may to $-\infty$ in finite time. In this case, the solution is not admissible. In the case of the adaptive exponential model, the backward membrane potential and the backward adaptation value will never blow up in finite time. Therefore, this solution is always an admissible solution. But in the case of the quartic model for instance, the membrane potential will always blow up in finite time when the backward solution do not cross the v-nullcline, and such solutions will exist, for instance in the case where there is no fixed point: in the proof of theorem 3.3.1, we show that there exist a spiking solution for which the backward solution tends to infinity. For initial conditions of the backward problem below this orbit, because of Gronwall's theorem, the membrane potential will tend to $-\infty$ in finite time.

- If the backward solution does not blow up in finite time and does not cross the line $\{v_b = v_r\}$, then the solution of the backward equation is unique, and there exists a unique solution of the problem which is defined on $\mathbb{R}$.

- If the backward membrane potential blows up at time t_1 and its orbit does not intersect the line $\{v_b = v_r\}$ there is no solution to the Cauchy problem for $t \leq t_1$.

- If the backward orbit intersects the line $\{v_b = v_r\}$ then the problem splits in two solutions, one of which corresponding to a reset, and the other corresponding to the solution of the system (A.1). The branch of solution corresponding to a regular subthreshold backward problem is treated as described above. For the solution corresponding to a reset, we check if the value of the membrane potential at this point is inside the image of the Poincaré application. If it is the case, the admissible solutions correspond to the different reciprocal images of this value under Φ. There can exist two possible values: one that is inferior or equal to w^* and another one greater than w^*, and these two possible points are on the same orbit (the orbit starting above w^* crosses the line $v = v_r$ at the point below w^*). To avoid the difficulty or resetting at an infinite value of the membrane potential, we directly jump to the reciprocal image of this point by Φ, and compute the same way the possible branches of backward solutions.

Figure A.1. Construction of the backward set of solutions. Description in the text.

Interestingly, in the case of the exponential model, since the backward solutions do not blow up in finite time, the backward solution is always an admissible solution. Therefore, we have a countable number of backward solution in this case.

In the case of the quartic model, the number admissible solutions is smaller. Indeed, the reciprocal images of Φ decrease, and when they are below the spiking trajectory diverging when $v \to -\infty$, the backward equation blows up in finite time. Therefore the only admissible solution is a spiking solution. Figure A.1 illustrates the construction of a backward solution and of the Cauchy problem. From a given initial condition (v_0, w_0), if the backward solution never crosses the reset line $\{v = v_r\}$ there is only one admissible solution provided it does not blow up in finite time. If the backward solution crosses the reset line (star (1) and (2) of figure A.1), the solution splits into two solutions, one of which corresponds to a spike when it exists (star (1)) and the other one corresponding to the regular solution of the backward equation (for star (2) no spiking solution correspond to the related adaptation value). Below the bold line corresponding to a diverging solution of the backward equation, in the case of models such as the quartic one, the only admissible solution is a spiking solution (star (3)).

Bibliography

[1] L. ABBOTT AND C. VAN VREESWIJK, *Asynchronous states in networks of pulse-coupled oscillators*, Physical Review E, 48 (1993), pp. 1483–1490.

[2] A. ALONSO AND R. KLINK, *Differential electroresponsiveness of stellate and pyramidal-like cells of medial entorhinal cortex layer II*, Journal of Neurophysiology, 70 (1993), pp. 128–143.

[3] A. ALONSO AND R. LLINÁS, *Subthreshold Na+-dependent theta-like rhythmicity in stellate cells of entorhinal cortex layer II*, Nature, 342 (1989), pp. 175–177.

[4] A. AMES, *CNS energy metabolism as related to function*, Brain Research Reviews, 34 (2000), pp. 42–68.

[5] R. AMIR, M. MICHAELIS, AND M. DEVOR, *Membrane potential oscillations in dorsal root ganglion neurons: Role in normal electrogenesis and neuropathic pain*, The Journal of Neuroscience, 19 (1999), pp. 8589–8596.

[6] E. ANGELINO AND M. P. BRENNER, *Excitability constraints on voltage-gated sodium channels*, PLoS Comput Biol, 3 (2007), p. e177.

[7] C. ARMSTRONG AND B. HILLE, *Voltage-Gated Ion Channels and Electrical Excitability*, Neuron(Cambridge, Mass.), 20 (1998), pp. 371–380.

[8] L. BADEL, S. LEFORT, R. BRETTE, C. C. H. PETERSEN, W. GERSTNER, AND M. J. E. RICHARDSON, *Dynamic i-v curves are reliable predictors of naturalistic pyramidal-neuron voltage traces*, Journal of Neurophysiology, 99 (2008), pp. 656–66. PMID: 18057107 doi: 01107.2007.

[9] L. BERNARDO AND R. FOSTER, *Oscillatory behavior in inferior olive neurons: mechanism, modulation, cell agregates*, Brain research Bulletin, 17 (1986), pp. 773–784.

[10] P. BILLINGSLEY, *Convergence of Probability Measures*, Wiley series in probability and statistics, 1999.

[11] R. BRETTE, *Dynamics of one-dimensional spiking neuron models*, Journal of Mathematical Biology, 48 (2004), pp. 38–56.

[12] ——, *The cauchy problem for one-dimensional spiking neuron models*, Cognitive Neurodynamics, 2 (2007), pp. 21–27.

[13] R. BRETTE AND W. GERSTNER, *Adaptive exponential integrate-and-fire model as an effective description of neuronal activity*, Journal of Neurophysiology, 94 (2005), pp. 3637–3642.

[14] K. BRODMANN, *Vergleichende Lokalisationslehre der Grobhirnrinde*, J.A.Barth, Leipzig, 1909.

[15] N. BRUNEL AND V. HAKIM, *Fast global oscillations in networks of integrate-and-fire neurons with low firing rates*, Neural Computation, 11 (1999), pp. 1621–1671.

[16] N. BRUNEL AND P. LATHAM, *Firing rate of noisy quadratic integrate-and-fire neurons*, Neural Computation, 15 (2003), pp. 2281–2306.

[17] H. BRYANT AND J. SEGUNDO, *Spike initiation by transmembrane current: a white-noise analysis*, The Journal of Physiology, 260 (1976), pp. 279–314.

[18] B. D. BURNS AND A. C. WEBB, *The spontaneous activity of neurones in the cat's cerebral cortex*, Proceedings of the Royal Society of London. Series B, Biological Sciences, 194 (1976), pp. 211–223.

[19] D. BUXHOEVEDEN AND M. CASANOVA, *The minicolumn hypothesis in neuroscience*, Brain, 125 (2002), pp. 935–951.

[20] W. CALVIN AND C. STEVENS, *Synaptic noise and other sources of randomness in motoneuron interspike intervals*, Journal of Neurophysiology, 31 (1968), pp. 574–587.

[21] B. CESSAC AND M. SAMUELIDES, *From neuron to neural networks dynamics.*, EPJ Special topics: Topics in Dynamical Neural Networks, 142 (2007), pp. 7–88.

[22] C. CHOW AND J. WHITE, *Spontaneous action potentials due to channel fluctuations.*, Biophysical Journal, 71 (1996), pp. 3013–3021.

[23] C. CLOPATH, R. JOLIVET, A. RAUCH, H. LÜSCHER, AND W. GERSTNER, *Predicting neuronal activity with simple models of the threshold type: Adaptive Exponential Integrate-and-Fire model with two compartments*, Neurocomputing, 70 (2007), pp. 1668–1673.

[24] K. COLE, *Membranes, Ions and Impulses*, A Chapter of Classical Biophysics, 1 (1968).

[25] K. COLE AND H. CURTIS, *Electric impedance of nerve and muscle*, Cold Spring Harbor symposia on quantitative biology, Cold Spring Harbor, Long Island Biological Association, 4 (1936).

[26] ——, *Electric impedance of the squid giant axon during activity*, The Journal of General Physiology, 22 (1939), pp. 649–670.

[27] P. DAYAN AND L. F. ABBOTT, *Theoretical Neuroscience : Computational and Mathematical Modeling of Neural Systems*, MIT Press, 2001.

[28] A. DESTEXHE, Z. F. MAINEN, AND T. J. SEJNOWSKI, *Methods in Neuronal Modeling*, in Koch and Segev (77), 1998, ch. Kinetic models of synaptic transmission, pp. 1–25.

[29] A. DESTEXHE AND D. PARÉ, *Impact of network activity on the integrative properties of neocortical pyramidal neurons in vivo.*, Journal of Neurophysiology, 81 (1999), pp. 1531–1547.

[30] R. DEVANEY, *An Introduction to Chaotic Dynamical Systems*, Westview Press, 2003.

[31] A. DHOOGE, W. GOVAERTS, AND Y. KUZNETSOV, *Numerical Continuation of Fold Bifurcations of Limit Cycles in MATCONT*, Proceedings of the ICCS, (2003), pp. 701–710.

[32] A. DHOOGE, W. GOVAERTS, AND Y. A. KUZNETSOV, *Matcont: A matlab package for numerical bifurcation analysis of odes*, ACM Trans. Math. Softw., 29 (2003), pp. 141–164.

[33] J. DIEUDONNÉ, *Éléments d'analyse - Tome I : Fondements de l'analyse moderne*, Gauthier-Villars, 1963.

[34] B. ERMENTROUT, M. PASCAL, AND B. GUTKIN, *The effects of spike frequency adaptation and negative feedback on the synchronization of neural oscillators.*, Neural Comput, 13 (2001), pp. 1285–1310.

[35] G. B. ERMENTROUT AND N. KOPELL, *Parabolic bursting in an excitable system coupled with a slow oscillation*, SIAM J. Appl. Math., 46 (1986), pp. 233–253.

[36] Y. ETZION AND Y. GROSSMAN, *Potassium currents modulation of calcium spike firing in dendrites of cerebellar Purkinje cells*, Experimental Brain Research, 122 (1998), pp. 283–294.

[37] L. EVANS, *Partial Differential Equations*, vol. 19 of Graduate Studies in Mathematics, Proceedings of the American Mathematical Society, 1998.

[38] U. FEUDEL, A. NEIMAN, X. PEI, W. WOJTENEK, H. BRAUN, M. HUBER, AND F. MOSS, *Homoclinic bifurcation in a Hodgkin–Huxley model of thermally sensitive neurons*, Chaos: An Interdisciplinary Journal of Nonlinear Science, 10 (2000), p. 231.

[39] R. FITZHUGH, *Mathematical models of excitation and propagation in nerve*, ch. 1.

[40] R. FITZHUGH, *Theoretical Effect of Temperature on Threshold in the Hodgkin-Huxley Nerve Model*, The Journal of General Physiology, 49 (1966), pp. 989–1005.

[41] N. FOURCAUD-TROCME, D. HANSEL, C. VAN VREESWIJK, AND N. BRUNEL, *How Spike Generation Mechanisms Determine the Neuronal Response to Fluctuating Inputs*, Journal of Neuroscience, 23 (2003), p. 11628.

[42] E. FURSHPAN AND D. POTTER, *Transmission at the giant motor synapses of the crayfish*, The Journal of Physiology, 145 (1959), p. 289.

[43] W. GERSTNER AND W. KISTLER, *Spiking Neuron Models*, Cambridge University Press, 2002.

[44] D. GOLDMAN, *Potential, Impedance, and Rectification in Membranes*, The Journal of General Physiology, 27 (1943), pp. 37–60.

[45] D. GOODMAN AND R. BRETTE, *Brian: a simulator for spiking neural networks in python*, Frontiers in Neuroinformatics (in preparation), (2008).

[46] F. GRIMBERT, *Mesoscopic models of cortical structures*, PhD thesis, University of Nice Sophia-Antipolis, feb 2008.

[47] T. H. GRONWALL, *Note on the derivative with respect to a parameter of the solutions of a system of differential equations*, Annals of Mathematics, 20 (1919), pp. 292–296.

[48] J. GUCKENHEIMER AND P. J. HOLMES, *Nonlinear Oscillations, Dynamical Systems and Bifurcations of Vector Fields*, vol. 42 of Applied mathematical sciences, Springer, 1983.

[49] J. GUCKENHEIMER AND R. OLIVA, *Chaos in the hodgkin–huxley model*, SIAM Journal on Applied Dynamical Systems, 1 (2002), p. 105.

[50] B. GUTKIN, B. ERMENTROUT, AND A. REYES, *Phase-response curves give the responses of neurons to transient inputs.*, J Neurophysiol, 94 (2005), pp. 1623–1635.

[51] B. HILLE, *Ion channels of excitable membranes*, Sinauer Sunderland, Mass, 2001.

[52] A. HODGKIN, *The local electric changes associated with repetitive action in a non-medullated axon*, The Journal of Physiology, 107 (1948), p. 165.

[53] A. HODGKIN AND A. HUXLEY, *Action potentials recorded from inside a nerve fibre*, Nature, 144 (1939), pp. 710–711.

[54] A. HODGKIN AND A. HUXLEY, *A quantitative description of membrane current and its application to conduction and excitation in nerve.*, Journal of Physiology, 117 (1952), pp. 500–544.

[55] A. HODGKIN AND B. KATZ, *The effect of sodium ions on the electrical activity of the giant axon of the squid*, The Journal of Physiology, 108 (1949), p. 37.

[56] A. HOLDEN, *Models of the Stochastic Activity of Neurones*, Lecture Notes in Biomathematics, 12 (1976), pp. 1–368.

[57] F. HOPPENSTEADT AND E. IZHIKEVICH, *Weakly connected neural networks*, Springer-Verlag New York, Inc., 1997.

[58] J. HOUNSGAARD AND J. MIDTGAARD, *Synaptic control of excitability in turtle cerebellar Purkinje cells.*, The Journal of Physiology, 409 (1989), p. 157.

[59] A. HUXLEY AND R. STÄMPFLI, *Evidence for saltatory conduction in peripheral myelinated nerve fibres*, The Journal of Physiology, 108 (1949), p. 315.

[60] E. IZHIKEVICH, *Neural excitability, spiking, and bursting*, International Journal of Bifurcation and Chaos, 10 (2000), pp. 1171–1266.

[61] ——, *Resonance and selective communication via bursts in neurons having subthreshold oscillations*, BioSystems, 67 (2002), pp. 95–102.

[62] E. IZHIKEVICH, *Simple model of spiking neurons*, IEEE Transactions on Neural Networks, 14 (2003), pp. 1569–1572.

[63] E. IZHIKEVICH, *Which model to use for cortical spiking neurons?*, IEEE Trans Neural Netw, 15 (2004), pp. 1063–1070.

[64] ——, *Dynamical Systems in Neuroscience: The Geometry of Excitability And Bursting*, MIT Press, 2007.

[65] E. M. IZHIKEVICH, *Dynamical Systems in Neuroscience: The Geometry of Excitability and Bursting*, The MIT Press, 2006. To appear.

[66] E. M. IZHIKEVICH AND G. M. EDELMAN, *Large-scale model of mammalian thalamocortical systems.*, Proc Natl Acad Sci U S A, 105 (2008), pp. 3593–3598.

[67] J. JACK, D. NOBLE, AND R. TSIEN, *Electric Current Flow in Excitable Cells*, Oxford University Press, USA, 1975.

[68] D. JOHNSTON AND S. WU, *Foundations of cellular neurophysiology*, MIT Press Cambridge, Mass, 1995.

[69] R. JOLIVET, R. KOBAYASHI, A. RAUCH, R. NAUD, S. SHINOMOTO, AND W. GERSTNER, *A benchmark test for a quantitative assessment of simple neuron models*, Journal of Neuroscience Methods, 169 (2008), pp. 417–424.

[70] E. JONES AND A. PETERS, eds., *Cerebral cortex, functional properties of cortical cells*, vol. 2, Plenum, New York, 1984.

[71] R. JONES, *Synaptic and intrinsic properties of neurones of origin of the perforant path in layer II of the rat entorhinal cortex in vitro*, Hippocampus ', 4 (1994), pp. 335–353.

[72] E. KANDEL, J. SCHWARTZ, AND T. JESSEL, *Principles of Neural Science*, McGraw-Hill, 4th ed., 2000.

[73] P. KARA, P. REINAGEL, AND R. C. REID, *Low response variability in simultaneously recorded retinal, thalamic, and cortical neurons*, Neuron, 27 (2000), pp. 635–646. Poisson, retina, spike variability.

[74] I. KARATZAS AND S. SHREVE, *Brownian motion and stochatic calculus*, Springer, 1987.

[75] B. W. KNIGHT, *Dynamics of encoding in a population of neurons*, J. Gen. Physiol., 59 (1972), pp. 734–766.

[76] C. KOCH, *Biophysics of Computation: Information Processing in Single Neurons*, Oxford University Press: New York, New York., 1999.

[77] C. KOCH AND I. SEGEV, eds., *Methods in Neuronal Modeling: From Ions to Networks*, The MIT Press, 1998.

[78] Y. A. KUZNETSOV, *Elements of Applied Bifurcation Theory*, Applied Mathematical Sciences, Springer, 2nd ed., 1998.

[79] L. LAPICQUE, *Recherches quantitatifs sur l'excitation des nerfs traitee comme une polarisation*, J. Physiol. Paris, 9 (1907), pp. 620–635.

[80] L. LAPICQUE, *L'excitabilite en fonction du temps*, Presses Universitaires de France, Paris, (1926).

[81] P. LATHAM, B. RICHMOND, P. NELSON, AND S. NIRENBERG, *Intrinsic dynamics in neuronal networks. I. Theory*, J. Neurophysiol., 83 (2000), pp. 828–835.

[82] ——, *Intrinsic dynamics in neuronal networks. II. Experiment*, J. Neurophysiol., 83 (2000), pp. 808–827.

[83] T. LI AND J. YORKE, *Period three implies chaos*, American Mathematical Monthly, 82 (1975), pp. 985–992.

[84] R. LILLIE, *Factors affecting transmission and recovery in the passive iron nerve model*, The Journal of General Physiology, 7 (1925), pp. 473–507.

[85] C. LIU, M. MICHAELIS, R. AMIR, AND M. DEVOR, *Spinal nerve injury enhances subthreshold membrane potential oscillations in drg neurons: Relation to neuropathic pain*, Journal of Neurophysiology, 84 (2000), pp. 205–215.

[86] R. LLINÁS, *The intrinsic electrophysiological properties of mammalian neurons: insights into central nervous system function*, Science, 242 (1988), pp. 1654–1664.

[87] R. LLINAS, A. GRACE, AND Y. YAROM, *In vitro neurons in mammalian cortical layer 4 exhibit intrinsic oscillatory activity in the 10-to 50-hz frequency range*, Proceedings of the National Academy of Sciences, 88 (1991), pp. 897–901.

[88] R. Llinas and M. Sugimori, *Electrophysiological properties of in vitro Purkinje cell somata in mammalian cerebellar slices*, The Journal of Physiology, 305 (1980), pp. 171–195.

[89] R. Llinás and Y. Yarom, *Electrophysiology of mammalian inferior olivary neurones in vitro. different types of voltage-dependent ionic conductances.*, J Physiol., 315 (1981), pp. 549–567.

[90] R. Llinás and Y. Yarom, *Oscillatory properties of guinea-pig inferior olivary neurones and their pharmacological modulation: an in vitro study*, Journal of physiology, 376 (1986), pp. 163–182.

[91] Y. Mandelblat, Y. Etzion, Y. Grossman, and D. Golomb, *Period Doubling of Calcium Spike Firing in a Model of a Purkinje Cell Dendrite*, Journal of Computational Neuroscience, 11 (2001), pp. 43–62.

[92] H. Markram, M. Toledo-Rodriguez, Y. Wang, A. Gupta, G. Silberberg, and C. Wu, *Interneurons of the neocortical inhibitory system*, Nature Reviews Neuroscience, 5 (2004), pp. 793–804.

[93] V. Mountcastle, *Modality and topographic properties of single neurons of cat's somatosensory cortex*, Journal of Neurophysiology, 20 (1957), pp. 408–434.

[94] ———, *The columnar organization of the neocortex*, Brain, 120 (1997), pp. 701–722.

[95] R. Naud, N. Macille, C. Clopath, and W. Gerstner, *Firing patterns in the adaptive exponential integrate-and-fire model*, Biological Cybernetics, 99 (2008), pp. 335–347.

[96] ———, *Firing patterns in the adaptive exponential integrate-and-fire model*, Biological Cybernetics (submitted), (2008).

[97] E. Newman, *Glial cell inhibition of neurons by release of ATP*, J Neurosci, 23 (2003), pp. 1659–1666.

[98] J. Nolte, *The Human Brain*, Mosby, 5th ed., 2001.

[99] A. Peters and E. Jones, eds., *Cerebral cortex, cellular components of the cerebral cortex*, vol. 1, Plenum, New York, 1984.

[100] D. Purves, G. J. Augustine, D. Fitzpatrick, L. C. Katz, A.-S. LaMantia, J. O. McNamara, and S. M. Williams, *Neuroscience*, Sinauer Associates, Inc., 2nd ed., 2001.

[101] S. Ramon y Cajal, *A new concept of the histology of the central nervous system*, pp. 7—29.

[102] S. Ramon y Cajal, *The stucture and connexions of neurons*, pp. 220–253.

[103] D. Reich, J. Victor, and B. Knight, *The power ratio and the interval map: Spiking models and extracellular recordings*, Journal of Neuroscience, 18 (1998), p. 10090.

[104] J. Rinzel and B. Ermentrout, *Analysis of neural excitability and oscillations*, MIT Press, 1989.

[105] J. Rinzel and R. Miller, *Numerical calculation of stable and unstable periodic solutions to the Hodgkin-Huxley equations*, Math. Biosci, 49 (1980), pp. 27–59.

[106] M. N. Shadlen and W. T. Newsome, *Noise, neural codes and cortical organization.*, Curr Opin Neurobiol, 4 (1994), pp. 569–579.

[107] W. R. Softky and C. Koch, *The highly irregular firing of cortical cells is inconsistent with temporal integration of random epsps*, Journal of Neuroscience, 13 (1993), pp. 334–350.

[108] R. Stein, *The Frequency of Nerve Action Potentials Generated by Applied Currents*, Proceedings of the Royal Society of London. Series B, Biological Sciences (1934-1990), 167 (1967), pp. 64–86.

[109] R. B. Stein, *Some models of neuronal variability*, Biophysical Journal, 7 (1967), pp. 37–68.

[110] I. Tasaki, *The Electro-Saltatory Transmission of the Nerve Impulse and the Effect of Narcosis upoon the Nerve Fiber*, American Journal of Physiology, 127 (1939), pp. 211–227.

[111] I. Tasaki and T. Takeuchi, *Der am Ranvierschen Knoten entstehende Aktionsstrom und seine Bedeutung für die Erregungsleitung*, Pflügers Archiv European Journal of Physiology, 244 (1941), pp. 696–711.

[112] ——, *Weitere Studien über den Aktionsstrom der markhaltigen Nervenfaser und über die elektrosalta-torische Übertragung des Nervenimpulses*, Pflügers Archiv European Journal of Physiology, 245 (1942), pp. 764–782.

[113] J. TOUBOUL, *Bifurcation analysis of a general class of nonlinear integrate-and-fire neurons*, SIAM Journal on Applied Mathematics, 68 (2008), pp. 1045–1079.

[114] J. TOUBOUL, *Nonlinear and stochastic models in neuroscience*, PhD thesis, Ecole Polytechnique, dec 2008.

[115] J. TOUBOUL, *Sensitivity to the cutoff value in the quadratic adaptive integrate-and-fire model*, Research Report 6634, INRIA, aug 2008.

[116] J. TOUBOUL AND R. BRETTE, *Dynamics and bifurcations of the adaptive exponential integrate-and-fire model*, Biological Cybernetics, 99 (2008), pp. 319–334. PMID: 19011921 DOI: 10.1007/s00422-008-0267-4.

[117] J. TOUBOUL AND R. BRETTE, *Spiking dynamics of bidimensional integrate-and-fire neurons*, Research Report 6531, INRIA, 05 2008.

[118] H. C. TUCKWELL, *Introduction to theoretical neurobiology*, Cambridge University Press, 1988.

[119] A. VAN ROTTERDAM, F. LOPES DA SILVA, J. VAN DEN ENDE, M. VIERGEVER, AND A. HERMANS, *A model of the spatial-temporal characteristics of the alpha rhythm*, Bulletin of Mathematical Biology, 44 (1982), pp. 283–305.

[120] U. WEHMEIER, D. DONG, C. KOCH, AND D. VAN ESSEN, *Modeling the visual system*, Methods in neuronal modeling (C. Koch, and I. Segev, Eds.), (1989), pp. 335–359.

[121] J. A. WHITE, T. BUDDE, AND A. R. KAY, *A bifurcation analysis of neuronal subthreshold oscillations.*, Biophys J, 69 (1995), pp. 1203–1217.

[122] A. WOHRER, *Model and large-scale simulator of a biological retina with contrast gain control*, PhD thesis, University of Nice Sophia-Antipolis, 2008.

[123] G. YOUNG, *Note on excitation theories*, Psychometrika, 2 (1937), pp. 103–106.